Dynamic Cell Rearrangements Shape the Cranial Vascular Network of Developing Zebrafish Embryos

Inauguraldissertation

zur
Erlangung der Würde eines Doktors der Philosophie
vorgelegt der
Philosophisch-Naturwissenschaftlichen Fakultät
der Universität Basel

von

Anna Lenard

aus

Warschau, Polen

Basel, 2013

Genehmigt von der Philosophisch-Naturwissenschaftlichen Fakultät

auf Antrag von

Prof. Dr. Markus Affolter

Prof. Dr. Anne Spang

Basel, den 13.11.2012

<div style="text-align: right;">

Prof. Dr. Jörg Schibler

Dekan

</div>

Content

Content

Content

1 List of abbreviations

aa	Amino acid(s)
ACeV	anterior (rostral) cerebral vein
AJs	Adherens junctions
aPKC	atypical protein kinase C
AMIS	apical membrane initiation site
bp	base pairs
Cdc42	cell division control protein 42 homologue
CMV	communicating vessel
COUP-TFII	chicken ovalbumin upstream promoter transcription factor 2
CrDI	cranial division of the internal carotid artery
DA	Dorsal aorta
DCV	dorsal ciliary vein
ddH2O	double deionized water (Quarz-Water)
DLAV	Dorsal longitudinal anastomotic vessel
DLL4	Delta-like-4
DLV	Dorsal longitudinal vein
DNA	Deoxyribonucleic acid
dpf	Days post fertilization
E. coli	Escherichia coli
ECs	Endothelial cells
EGFP	Enhanced GFP
ephrinB2	Ephrin receptor B2
ESAMa	Endothelial Cell Selective Adhesion Molecule a
ETS	transcription factors with E-twenty-six conserved DNA binding domain
Etsrp	ets1-related protein
Fli-1a	Friend leukemia integration 1 a
fliep	promoter fragment of *fli1a* gene driving endothelial specific expression
Flk-1 (Kdrl)	Fetal liver kinase 1 (VEGFR2)
Flt4	fms related tyrosin kinase 4 (VEGFR3)
GATA	transcription factors with ability to bind a GATA-DNA sequence
GFP	Green fluorescent protein
GFF/Gal4ff	DNA binding domain of Gal4 plus two 13 amino acid long modified transcriptional activation domains of VP16
hpf	Hours post fertilization
ICM	Intermediate cell mass
ISV	Intersegmental vessel

Abbreviations

JAM	Junctional adhesion molecule
Kdrl (flk-1)	Kinase insert domain receptor like
LCS	Leica confocal software
MCS	Multiple cloning site
MDCK	Madin-Darby canine kidney (cells)
MO	morpholino
NCA	nasal ciliary artery
PAP	pre-apical patch
PAR	Polarization complex including CDC42, PAR3, PAR6 and aPKC
PAR3	Partitioning defective 3 homolog
PAR6	Partitioning defective 6 homolog
PBS	Phosphate-buffered saline
PBST	Phosphate-buffered saline-Tween 20
PBSTX	Phosphate-buffered saline-Tween 20- Triton-X 100
PCeV	Posterior (caudal) cerebral vein
PCR	Polymerase chain reaction
PCV	Posterior cardinal vein
Pdxl2	Podocalyxin 2
PFA	Paraformaldehyde
PHS	Primary head sinus
PLA	palatocerebral artery
PLAJ	junction of the palatocerebral arteries
PMBC	primordial midbrain channel
polyA	polyadenylation signal (SV40)
PrA	prosencephalic artery
PTU	Propylthiouracil
RAC1	GTPase: Ras-related C3 botulinum substrate 1
Shh	sonic hedgehog
SAP	Shrimp Alkaline Phosphatase
SV40	Simian virus 40 (polyA signal)
TJs	Tight junctions
UAS	Upstream activating sequence/site
VE-cadherin	Vascular endothelial cadherin
VEGF	Vascular endothelial growth factor
VEGFR	Vascular endothelial growth factor receptor
ZO1	Zonula occuldens-1 protein

2 Abstract

To form the complex network of endothelial tubes making up the vasculature, a number of vessels have to interact and connect to each other during development. This involves the transformation of blunt-ended angiogenic sprouts into interconnected functional tubes, a process called vessel fusion or anastomosis. While much is known about vessel sprouting, little is known about vessel fusion at the cellular and molecular levels. Most of the vessels in the developing vertebrate embryo form in the presence of stable blood flow in adjacent tubes, suggesting the importance of flow and/or blood pressure for angiogenic sprouting and anastomosis. For this reason, my analyses focused on the head vasculature where many vessels form in the presence of stable blood flow in the zebrafish embryo.

In this study I performed detailed analyses of different fusion events in cranial vessels of the developing zebrafish embryo. Using novel transgenic tools and high resolution live imaging I defined a multistep model of vessel fusion and showed that it is conserved in various vascular beds, regardless of vessel shape and the age of the embryo. I also showed that in all the cranial vessels I studied, the initial fusion steps are the same and involve *de novo* deposition of junctional proteins, ZO-1 and VE-cadherin, in a form of a junctional spot, which subsequently elaborates into a ring, followed by *de novo* apical membrane insertion. Lumen formation in the newly formed vessel takes place through blood pressure-dependent luminal/apical cell membrane invagination and fusion of apical membranes, leading to a continuous lumen. During this process, the tip cells become unicellular/seamless tubes with transcellular lumen. I found that such newly connected vessels subsequently undergo dynamic cellular rearrangements that lead to the transformation of the unicellular tubes into multicellular ones. This transformation involves cell splitting, a novel cellular mechanism that, to our knowledge, has not been described before in branching morphogenesis of any organ. Additionally, I analyzed the fusion process in VE-cadherin deficient embryos and showed that this adhesion molecule is necessary for formation of a single contact surface between the fusing vessel sprouts and thus, has an important role in coordinating anastomosis.

I have also analyzed vessel regression during vascular pruning and I showed that it follows a multistep process involving dynamic cell rearrangements that resemble "reversed" vessel fusion. These analyses represent the first studies of vessel remodeling at the cellular level in an *in vivo* system.

3 Introduction

3.1 Vascular morphogenesis

3.1.1 Tubular organs in multicellular organisms

Tubular organs are crucial for the survival of multicellular organisms, enabling transport and exchange of vital components, such as gas and nutrients, between different tissues. They form complex networks that allow maximizing the surface of the organ to assure more efficient performance, like in the case of the lung or the kidney. They also allow reaching the most distant regions of the body, which is necessary for transporting nutrients and metabolites, e.g. by the vascular and lymphatic system. Tubular organs consist of numerous cells that are specialized to keep the shape and function of the tubes. All tubular organs have a space within the tubes – the lumen – that is lined with a single layer of epithelial cells, which are very flat, polarized cells connected to each other by junctional complexes. The apical membrane of the cells is facing the lumen whereas the basal membrane faces and interacts with the extracellular matrix (ECM) and the surrounding cells.

In a developing embryo one way to form tubes is the process called branching morphogenesis. The initial tubes are usually assembled from precursor cells and further parts of the network are formed by branching of new tubes from existing ones, which is strictly controlled by genetic cues (Affolter et al., 2009).

3.1.2 The vascular system

The vasculature is one of the largest organs in the vertebrate body. It is made up of vessels of different sizes and shapes that form a complex network of tubes serving to transport gas, liquid, nutrients and metabolites to and from all places and organs in the body. The circulation initiated by the beating heart goes through large arteries to smaller arterioles to finally reach the capillary beds that infiltrate the tissues and directly participate in gas and metabolites exchange (Fig. I). The blood returns through venules
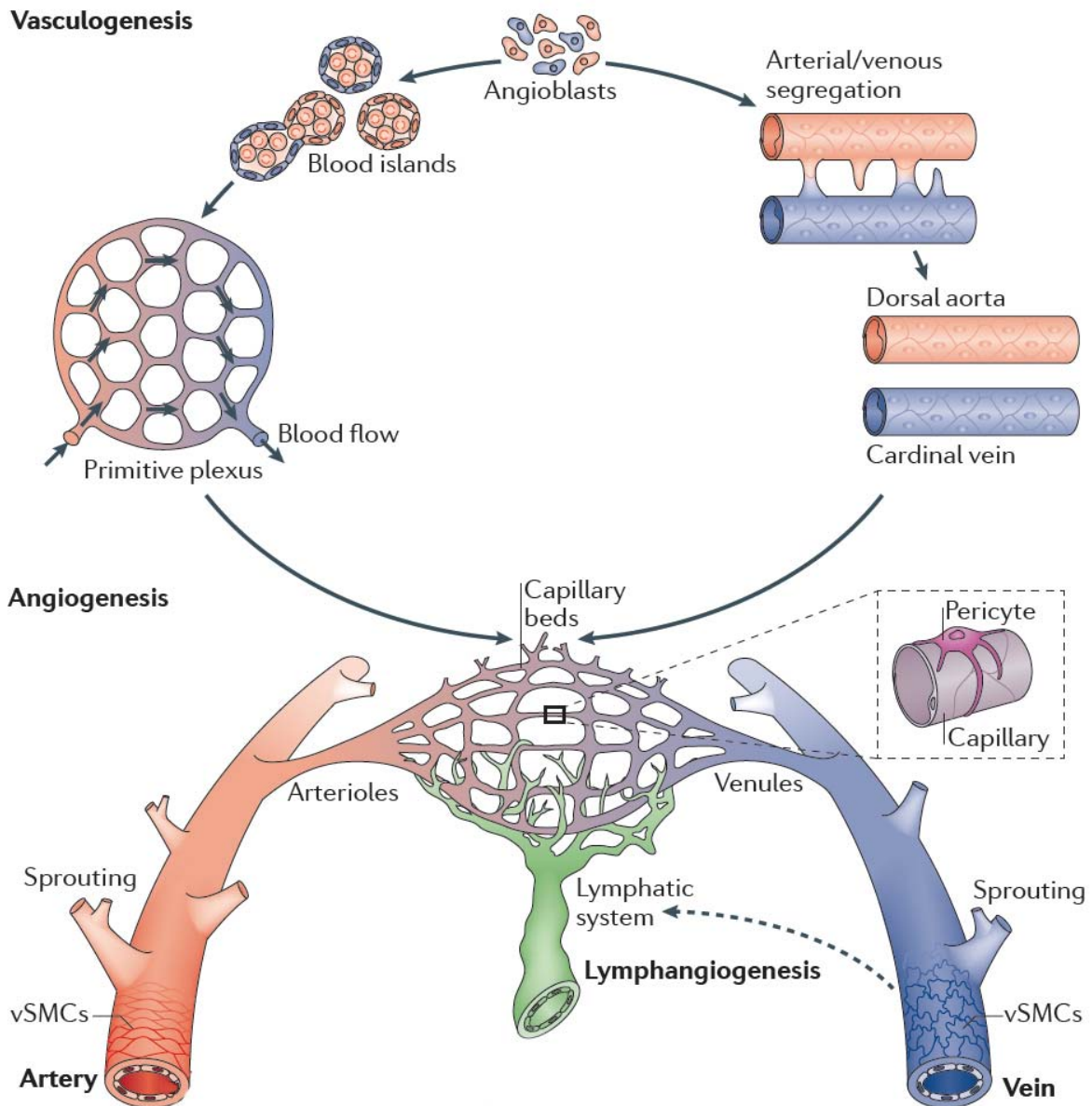
Figure I. Blood vessel network develops through vasculogenesis and angiogenesis

The endothelial progenitor cells (angioblast), forming the first blood vessels, arise from the mesoderm. They aggregate and acquire arterial (red) or venous (blue) fates by expression of specific genes and form the first embryonic blood vessels – the dorsal aorta and the posterior cardinal vein. Blood islands, also formed from angioblasts, generate primitive vascular plexi. Subsequent new vessels form through angiogenesis – the sprouting of new vessels from existing ones – to finally form a hierarchical network of vessels, consisting of arteries, arterioles, capillary beds, veins and venules. Mural cells (pericytes and smooth muscle cells - SMCs) stabilize the vessels and promote maturation. Lymphatic endothelial cells sprout from the venous vessels to form the lymphatic network. (Adapted from Herbert et al., 2011)

and veins into the heart and then to the lungs where it gets replenished with oxygen (reviewed in: Adams and Alitalo, 2007; Carmeliet, 2003; Risau and Flamme, 1995).

Both arteries and veins are lined with a single layer of endothelial cells (ECs), surrounded by elastic tissue, a smooth muscle cell layer and fibrous connective tissue (Fig. I). The smooth muscle layer is thicker in large arteries that have to cope with stronger blood pressure. Larger veins contain valves, which are specialized structures facilitating blood transport back to the heart (reviewed in Torres-Vazquez et al., 2003).

The vasculature is the first functional organ emerging in a developing vertebrate embryo and many subsequent morphogenetic processes depend on its proper formation (Risau and Flamme, 1995). Therefore a dysfunctional or aberrant vasculature is associated with many diseases, including cancer, arthritis, atherosclerosis, blindness and others (reviewed in Carmeliet, 2003). Studies on vascular formation and function play an important role in developing new disease therapies and prevention.

3.2 Vascular development of the zebrafish

3.2.1 Blood vessel formation is conserved among species

The mechanisms and genetic control of vascular development are highly conserved among a number of species that serve as model systems to study this process, including the mouse, chicken, frog and zebrafish (Fig. II). Vertebrate 2D and 3D cell culture systems have been used extensively to study cell migration and multiple genetic components necessary for cell-cell contact formation and cell polarization (Davis et al., 2002). However, even modern *in vitro* techniques fail to reproduce the complex three dimensional structures of blood vessels. This is especially true in the study of their interactions with the surrounding cells and the role of blood flow in the vessel formation and remodeling. Therefore *in vivo* systems, such as mouse, chicken, frog and zebrafish, are indispensable for research in the vascular field.
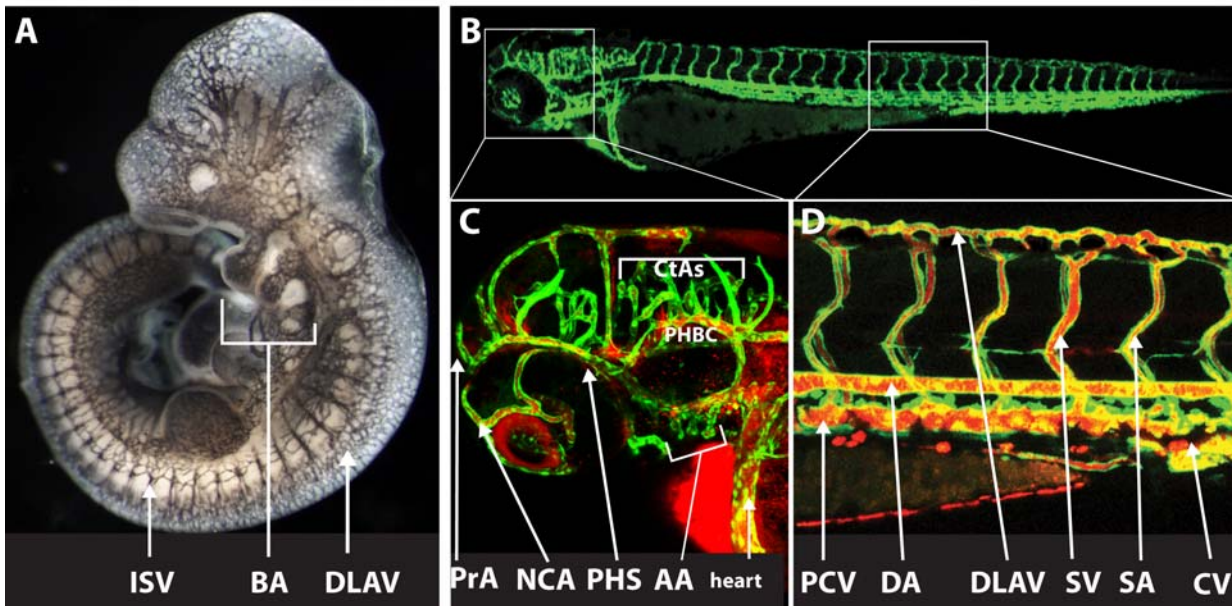
Figure II. The vascular system of the mouse and the zebrafish embryo
The vascular networks of different species show common characteristics. **A)** Immunostaining for PECAM-1 marking the vascular system of a mouse embryo in embryonic day 10. BA-branchial arches, ISV-intersegmental vessels, DLAV – dorsal longitudinal anastomotic vessel. **B-D)** Vascular system in a zebrafish embryo at ~48 hpf visualized in a transgenic fish Tg(*kdrl:*EGFP) in green and by angiography using a fluorescent dye, marking perfused vessels (red) **B)** An overview of the zebrafish embryo blood vessel system. **C-D)** Close up images of the head (C) and the tail (D) regions of the embryo with indicated vessels: PrA - prosencephalic artery, NCA - nasal ciliary artery, PHS - primary head sinus, AA - aortic arches, PCV - posterior (caudal) cardinal vein, DA - dorsal aorta, DLAV - dorsal longitudinal anastomotic vessel, SV – segmental vein, SA – segmental aorta, CV – caudal vein. (adapted from (Ellertsdottir et al., 2010)).

In all studied model organisms the cells that form the first vascular tubes originate from mesodermal tissue and are called endothelial cells (ECs). Small capillaries, including the newly formed vessels, are made just of ECs whereas larger vessels include an additional layer of mural cells, which are either pericytes or smooth muscle cells.

Initially blood vessels form by the assembly of precursor cells (angioblasts) in a process known as vasculogenesis. In this process the primordial vessels – the dorsal aorta (DA) and the posterior cardinal Vein (PCV) – form within the first days of embryonic life (see Fig. I and II). Subsequently new capillaries sprout out of the existing vessels to infiltrate all tissues and form a complex network, in the process of angiogenesis. The first vessels formed this way are the intersegmental vessels (ISVs) and the dorsal longitudinal anastomotic vessel (DLAV) in the embryo trunk (Fig. II)

(Risau and Flamme, 1995). Additionally, newly formed vascular networks are further remodeled through alternative processes that change the number and shape of tubes, such as intussusceptive angiogenesis and vessel pruning.

3.2.2 Different animal models serve to study vascular development

Genetic factors that control vasculogenesis and angiogenesis, such as the VEGF signaling and ETS transcription factors, are conserved in all mentioned model systems. However, different features such as accessibility and availability of genetic tools, favor some of the models for specific research areas in the angiogenesis field.

The chick embryo is a favored model for tumor angiogenesis. The capillary bed of the chorioallantoic membrane is easily accessible and serves to study proangiogenic and antiangiogenic factors (Ausprunk et al., 1974, reviewed in Ribatti, 2012).

The retina vasculature is a favored model to study angiogenesis in the mouse. It develops after birth and forms a flat, two dimensional network with new vessels in the periphery and more mature ones in the center. This arrangement allows the easy identification of sprouting, mature and remodeling vessels (Uemura et al., 2006). Studies in the retina uncovered many genetic factors involved in vessel sprouting and network formation. However, this system is unsuitable for live observations and therefore the dynamics of vessel formation cannot be followed.

Zebrafish is the only model organism easily accessible for long-term live imaging allowing observation of angiogenesis in developing embryos over time. The easy manipulation and growing number of available molecular tools make the fish a very popular model system that allows not only "static" studies but also can be used to understand the dynamic features of vascular development (Fig. II. B-D, the zebrafish vascular system).

3.2.3 Zebrafish embryos as a model to study development

Zebrafish are small tropical freshwater teleosts originating from India and Southeast Asia, where they inhabit shallow rivers (Hamilton-Buchanan, 1822). The size of an adult animal is 4-5 cm and they live 2-3 years. The fish reach adulthood at around 3 months of age (Westerfield, 1993). The females can produce eggs every week and lay

50-100 at a time. The eggs are fertilized externally within 10-15 minutes after egg laying, when males spawn sperm over them. The embryos develop externally, rapidly and synchronously; this makes them very attractive for biological studies. Detailed knowledge on early development of the fish allows to assign a developmental stage with up to 0.5-1 h precision (Kimmel et al., 1995). Additionally the embryos are transparent, which allows live observation of development over time, making the fish one of the few vertebrate models where long time live imaging is possible. These characteristics, among others, made the zebrafish a very attractive new genetic model animal that was first used in the 80's to study early embryonic development (Streisinger et al., 1981). Since then the zebrafish field grew rapidly and created a large number of new tools and methods.

3.2.4 The zebrafish in vascular research

Zebrafish quickly emerged as a useful vertebrate model to study vascular development. The vasculature develops early in the embryo and already at 24 hpf (hours post fertilization) heart beat begins and the first blood cells can be seen travelling along the anterior-posterior axis. Optical clarity of the embryo allowed identification of mutants with vascular defects without the need of any other markers (Stainier et al., 1996). To analyze mutants in more detail, in addition to previously used tools such as in situ hybridization and antibody staining, new tools were developed to allow live observation of development. One of the first techniques was microangiography introduced by injection of fluorescent dyes into the heart of the fish and observation of perfused vessels and blood flow over time with confocal microscopy (Weinstein et al., 1995). The same method was later used by Isogai et al. (Isogai et al., 2001) to create an anatomical atlas of zebrafish vascular development which shows in great detail and names all vessels in the embryo between 0-7 days. The drawback of this method, however, is its inability to see non perfused vessels, which makes it unsuitable for studying vasculature before the onset of circulation or looking at immature, developing branches. In addition, many mutants have circulation problems and cannot be analyzed this way. To overcome this limitation, new molecular tools were developed, namely transgenic zebrafish lines expressing fluorescent proteins under the control of

endothelial specific promoter region (Jin et al., 2005; Lawson and Weinstein, 2002; Zhu et al., 2005). The two transgenic lines used in most vascular research are Tg(*fli1a*:EGFP*)* (Lawson and Weinstein, 2002) and Tg(*kdrl*:EGFP) (Jin et al., 2005). In these lines GFP specifically labels endothelial cells as early as 3 somite stage (~11 hpf) allowing the observation of the axial vessel assembly (vasculogenesis) and the following vascular development all the way till adulthood. These live transgenic tools have opened a new chapter in vascular research shedding light on the dynamics of the process of vessel formation.

3.2.5 The anatomy and development of zebrafish trunk/tail vasculature

In most studies that use zebrafish as a model for vasculogenesis and angiogenesis the trunk/tail vasculature is analyzed. The tail vasculature is simple, yet stereotypically patterned, and it forms a complete circulatory network at a very early embryonic stage, before 48 hpf (Fig. II. B). Importantly, the tail is flat and easily accessible for imaging.

The two main axial vessels - the dorsal aorta (DA) and the posterior cardinal vein (PCV) - arise through vasculogenesis starting ~16 hpf and lumenizing at ~23 hpf (Fouquet et al., 1997). This process will be described in more detail in chapter 3.3.4 on vasculogenesis. The assembly of the axial vessels is followed by the formation of intersegmental vessels (ISVs) of the trunk through angiogenesis. ISVs branch dorsally from the DA in every body segment of the tail, making an evenly distributed ladder-like network of parallel vessels connected at the top of the tail into a dorsal longitudinal anastomotic vessel (DLAV). A row of ISVs is present at either side of the notochord and neural tube. The DLAV forms when ISV sprouts reach the dorsal region of the tail and extend to the posterior and the anterior to finally connect to each other (Childs et al., 2002; Isogai et al., 2003). Subsequently, so called secondary sprouts appear from the PCV and connect to ~50% of the ISVs, transforming them into segmental veins that lose their connection to the aorta and are meant to bring the circulating blood back to the vein (Fig. II D, Fig. III). Random distribution of segmental arteries and veins within the tail leads to the formation of small circulatory loops delivering blood to and from the body segments. The ISVs start growing out at ~18 hpf and fuse to each other from ~22-30

15

hpf, starting with the most anterior segments and continuing towards the tail region. Fusion is followed by lumen formation, but blood flow only starts after the venous connections are made. Secondary sprouts start coming ~30 hpf anteriorly and the tail network is completely developed and perfused by 46-48 hpf (Isogai et al., 2003, own data). ISVs are among the first vessels to carry blood in the developing fish (Isogai et al., 2003). The patterned character of ISVs makes them a very useful model to study angiogenic sprouting, as it allows the observation of the same event repeated multiple times in one embryo.
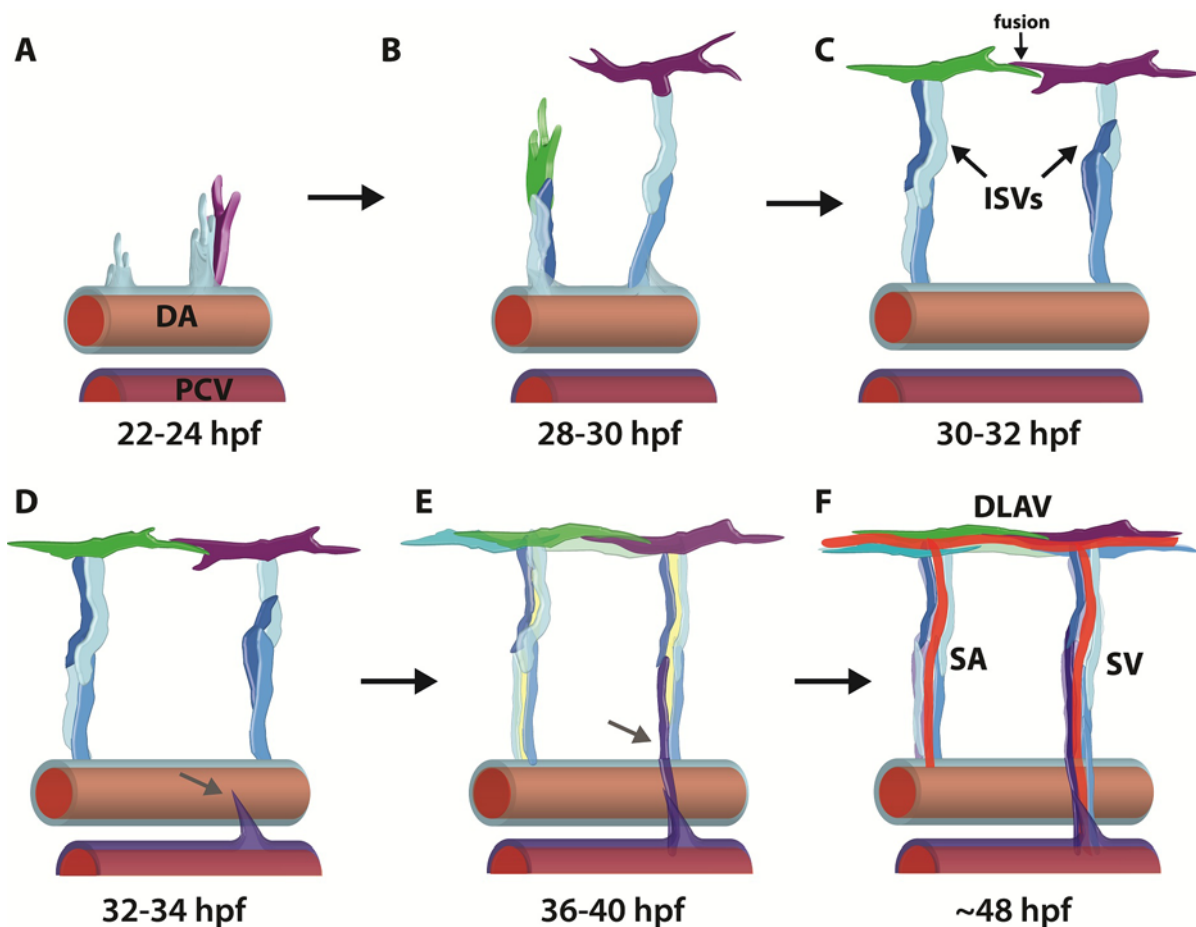
Figure III. Formation of intersegmental vessels in the zebrafish trunk
A) The ISVs sprout out of the dorsal aorta (DA) following the VEGF gradient in the somites. **B)** The cells in the sprout establish a hierarchy and one tip cell is selected in each sprout (green and purple cells). The following cells in the sprout become stalk cells (blue). **C)** When the ISVs reach the dorsal part of the tail, they produce anterior and posterior extensions that connect to neighboring sprouts in the process of vessel fusion/anastomosis. **D-F)** At ~32 hpf the secondary sprouts (arrows) grow out of the posterior cardinal vein (PCV) and connect to ~50 % of the ISVs transforming them into segmental veins (SV). These vessels lose their connection to the aorta. The remaining ISVs become segmental arteries (SA). (Adapted from (Ellertsdottir et al., 2010)).

3.2.6 The zebrafish head vasculature as an emerging model system to study vascular development

Despite the experimental advantages of ISVs, some characteristics of these vessels are unique, making it difficult to extrapolate the insights gained in their study to other vessel types. First, each ISV fuses with two other sprouts, on the left and right side (see Fig. III B-C). This gives the tip of the sprout a T-shape, which is not observed in other sprouts in the fish (own data) nor in the mouse retina (Gerhardt et al., 2003). Second, the ISVs sprout and fuse very early on, almost simultaneously with the onset of blood circulation, meaning the fusion process and initial lumen formation take place in the presence of a very weak or no blood pressure, whereas all vessels forming at later stages are subjected to relatively strong flow which influences the formation of the network. After the ISVs have fused at around 32 hpf, the tail vasculature grows in size together with the embryo, without forming additional angiogenic branches. Therefore it became necessary to look at different vessel types to follow the influence of blood pressure on vessel formation. The recent findings regarding the head vasculature will be presented at the end of the introduction, in chapter 3.5.

3.3 Vasculogenesis and angiogenesis

Vasculogenesis and angiogenesis are the two processes that form vascular networks in developing embryos. They represent two distinct mechanisms of tube formation: by *de novo* cell assembly (vasculogenesis) and branching of new tubes from existing ones (angiogenesis) (see Fig. I). Both mechanisms are multistep processes that have a lot of common features. In both of them cell migration in response to extracellular cues is very important. VEGF (vascular endothelial growth factor) is the major attractant inducing endothelial cell migration, acting through VEGF receptors on the ECs (see chapter 3.3.1.1 below). Repulsive signals play a role in vessel guidance, which will be introduced with the example of Plexin/Semaphorin signaling (chapter 3.3.1.2). Interaction of cells with each other is crucial for the formation of a multicellular organ. In the vasculature a key role is attributed to junctional proteins that connect endothelial cells to make a sealed vessel wall and mediate signals inducing changes in cell shape

and behavior (chapter 3.3.2.1). To expand existing networks, vessels have to form new branches and connect them to each other, in the processes of angiogenic sprouting and anastomosis (chapter 3.3.5). Finally, the developing vessels have to form hollow tubes, which takes place through a process called lumen formation, which involves changes in cell polarity and specific cell behaviors (chapter 3.3.3).

All of the mentioned processes and molecular components interact with each other and intermingle during the various steps of vascular network formation. Therefore, the key factors and concepts will be briefly introduced at the beginning of the chapter, and will be described in more detail in the following sections in the context of specific processes.

3.3.1 Extracellular cues - initiation and guidance of new vessels

3.3.1.1 VEGF signaling

Vascular Endothelial Growth Factor (VEGF) is a soluble molecule crucial for initiation and development of the vascular system. VEGFA, B, C, D and PlGF (Placental growth factor) belong to the VEGF superfamily of signaling molecules. VEGFA plays a key role in vascular development. VEGFA signals through its tyrosine kinase receptors and thereby promotes endothelial differentiation through activation of EC specific gene expression. VEGFA also plays a key role in the vascular network formation through vasculogenesis and angiogenesis (Carmeliet et al., 1996; Ferrara and Davis-Smyth, 1997). The two main receptors activated by VEGF are VEGF receptor 1 (VEGFR-1, Flt1) and VEGF receptor 2 (VEGFR-2, Kdrl, Flk1). VEGFR-2 signaling promotes cell migration, proliferation and survival. Mice lacking this gene die in early embryonic stages due to loss of vascular development (Shalaby et al., 1995). VEGFR-1 has high affinity for VEGF but low kinase activity and is thought to act as a sink for the ligand, to control the mechanism of sprout formation and prevent hyper sprouting. Loss of function of this protein leads to extensive sprouting and vasculature disorganization and is also embryonic lethal (Fong et al., 1995). This suggests that the two receptors control vessel outgrowth through antagonistic interactions.

VEGFR-3 (Flt-4) is responsible for lymphatic development through its interactions with VEGFC (Dumont et al., 1998) but has also been shown to play a role in vascular development, as it is present in the tip cell of angiogenic sprouts (Covassin et al., 2006). Its down regulation leads to impaired vessel sprouting resulting in decreased branching (Tammela et al., 2008).

3.3.1.2 Guidance signals for angiogenic sprouts

Studies in zebrafish revealed that the outgrowing angiogenic sprouts are guided in the right direction by repulsive interactions of Semaphorin - Plexin signaling. PlexinD1 is a receptor expressed in ECs, which responds to Semaphorin 3a ligand present in the somites of the fish. This interaction provides guidance for the outgrowing intersegmental vessels between the somites in the tail of the embryo. PlexinD1 mutant - *out of bounds* (*obd*) (Childs et al., 2002) and morpholino knock down experiments (Torres-Vazquez et al., 2004) show unorganized sprouting patterns with ISVs randomly distributed over the tail, often crossing the somite borders and connecting to neighboring sprouts in their middle parts. This mechanism resembles the control of axonal outgrowth by Semaphorin signaling (reviewed in Tamagnone and Comoglio, 2000).

3.3.2 Signaling between and within endothelial cells: Cell-cell contacts and cell polarization

3.3.2.1 Junctional molecules

In the vascular system junctional proteins connect cells to each other allowing formation of well-sealed tubes and play a key role in the formation of new vessels and maintaining their integrity. Since endothelial cells are very thin, the junctional complexes occupy most of the lateral cell membrane and define the borders and shapes of the ECs. Junctional proteins contain transmembrane and intracellular proteins that connect endothelial cells to each-other, to surrounding cells and to the extracellular matrix. They also interact with intracellular components, such as the cytoskeleton, to induce changes in cell shape and behavior and take part in regulating gene expression in response to extracellular signals provided by cell-cell contacts. The two main types of junctions

present in blood vessels are adherens junctions (AJs) and tight junctions (TJs) (reviewed in Xu and Cleaver, 2011).

3.3.2.2 AJs

Adherens junctions are responsible for cell-cell adhesion. AJs are multiprotein complexes containing Cadherins and Catenins that are attached to cytoplasmic actin filaments. A number of adhesion molecules are present in the vascular system (reviewed in Xu and Cleaver, 2011). Among these, vascular endothelial cadherin (VE-cadherin) is expressed specifically in endothelial cells and was shown to be extremely important for vessel stability and function, as described in more detail in the following section.

Another adhesion molecule expressed in endothelial cells is N-cadherin. N-cadherin is thought to mediate EC contact with the surrounding ECM and mural cells, as well as influencing VE-cadherin levels in ECs (reviewed in: Xu and Cleaver, 2011; Luo and Radice, 2005; Navarro et al., 1998).

PECAM-1 (platelet/endothelial cell adhesion molecule 1) and VCAM-1 (vascular cell adhesion molecule) are also expressed in the ECs, but do not appear to be strictly required for lumen formation, although PECAM is a part of a mechanosensory complex involved in EC sprouting initiation (Tzima et al., 2005).

3.3.2.3 TJs

TJs form a continuous, impermeable seal between the adjacent cells. TJs are protein complexes containing Claudins, Occludins and JAMs. Among these, Claudin5b and ESAM (one of the JAMs) show vascular specific expression. Zona occludens 1 and 2 (ZO-1 and 2) are intracellular components associated with TJs, also localizing to the cell-cell contacts. TJs participate in the formation of blood brain barrier, but their role in early vascular development is not known (reviewed in Xu and Cleaver, 2011 and Zeeb et al., 2010).

3.3.2.4 VE-cadherin as a key adhesion molecule of the vascular system

Vascular endothelial cadherin (VE-cadherin) is an adhesion molecule expressed specifically in ECs. VE-cadherin is a transmembrane protein that connects ECs to each other by forming a zipper-like structure through homophilic interactions of extracellular domains on opposing cells (reviewed in Dejana and Giampietro, 2012; Vestweber, 2008).

VE-cadherin was shown to be present along the contact area between EC plasma membranes in the vascular cords (at early stages of vessel formation) and on lateral cell membranes in lumenized vessels, where it flanks the apical/luminal membranes. Through homotypic interactions, VE-cadherin influences ECs polarization and lumen formation. VE-cadherin is present at all EC cell-cell contacts but, surprisingly, it is not strictly required for cell-cell adhesion (Carmeliet et al., 1999; Strilic et al., 2009). On the intracellular site, VE-cadherin binds to β-catenin and plakoglobin which mediate its connection to F-actin and allow it to trigger cell shape changes through cytoskeletal rearrangements (Cattelino et al., 2003). Cytoskeletal rearrangements are necessary for VE-cadherin mediated contact inhibition, which stops the sprouting behavior of EC after a connection to another vascular sprout has been made (Abraham et al., 2009). VE-cadherin was also shown to interact with VEGFR-2 to inhibit its activation and limit angiogenic cell behavior, leading to vessel stabilization (Lampugnani et al., 2006).

Mouse embryos null for VE-cadherin show severe vascular defects and die around stage E10. The initial primitive vessels form, but further development of the network does not proceed correctly and eventually the vasculature regresses (Carmeliet et al., 1999; Gory-Faure et al., 1999). Due to early lethality, studies in the mouse do not reveal the role for VE-cadherin in angiogenesis.

Studies in the zebrafish embryos using morpholino knock-down experiments have shown the role of this adhesion molecule in the dynamics of vascular network formation. VE-cadherin knock-down embryos develop normally until ~30 hpf and their vascular pattern does not differ from the wild type. However, due to malformation in the heart, normal blood flow is not established. Lumen fails to form in the cranial vessels and in ISVs. Mosaic transplantation analyses showed that this defect is independent of the missing circulation and rather is a result of reduced adhesion of the morphant cells that

fail to correctly incorporate in the vascular network and do not interact properly with neighboring cells. Furthermore, the process of blood vessel fusion observed in the ISVs was affected in the morphants. The tip cells extended filopodia but took much longer to establish a connection and seem to touch and retract multiple times before finally fusing. Additionally, the tip cells continued the filipodial activity after the contact was made, whereas in wild type embryos VE-cadherin activity lead to the inhibition of sprouting activity upon contact. Partial knock-down of VE-cadherin resulted in fragile vessels with a tendency to hemorrhages, especially in the head (Montero-Balaguer et al., 2009).

Abraham and colleagues (Abraham et al., 2009) also observed increased sprouting in the zebrafish ISVs upon VE-cadherin inactivation and further investigated the mechanism of this process in 3D cell culture of HUVEC cells. This study showed that ectopic sprouting present in VE-cadherin deficient vessels is Rac1 dependent, and is a result of VEGF activity, which in a normal situation is blocked by VE-cadherin antagonizing VEGFR2. This blocking is only possible with the correct VE-cadherin distribution at cell-cell junctions, regulated by actomyosin contractility, which is a result of myosin light chain 2 (MLC2) phosphorylation through VE-cadherin mediated Rho-kinase activity.

VE-cadherin also plays a role in contact inhibition of cell growth by modifying VEGF signaling. In cell culture experiments VE-cadherin, through β-catenin, interacts with VEGFR2 limiting its responsiveness to VEGF and therefore inhibiting cell growth and proliferation of confluent cells (Lampugnani et al., 2006).

I characterized the role of VE-cadherin in early steps of blood vessel anastomosis, analyzing *ve-cadherin* mutant zebrafish generated in our lab. The results of these studies will be presented in chapter 5.6.

3.3.3 General features of cell polarization and lumen formation

Endothelial cells lining the blood vessels are polarized, with the apical membrane facing the lumen and the basal membrane facing the surrounding tissue. The polarization of the ECs is crucial for proper vessel development. During vasculogenesis, *de novo* establishment of polarity starts right after the assembly of primitive angioblasts and is necessary for the first lumen formation. In vessels formed through angiogenesis,

cells in a new outgrowing branch keep the polarized state, but have to redefine their polarity when they form a new contact with another sprout. Polarization and lumen formation processes are strictly dependent on each other and can differ depending on tube type and the mechanism of its formation. Therefore the general concept of cell polarization and lumen formation mechanisms will be introduced briefly here and described in more detail in specific chapters on particular tube formation mechanisms (3.3.4.3 and 3.3.5.7).

3.3.3.1 Lumen formation

The process of lumen formation has been described in great detail for epithelial tubes, based on studies in cell culture, drosophila, zebrafish and mouse in a number of tubular organs, such as the gut, the kidney, the respiratory system and vasculature. The 5 main cellular mechanisms of tube formation are: wrapping, budding, cavitation, cord hollowing and cell hollowing (Lubarsky and Krasnow, 2003). Three of these are thought to occur during blood vessel formation from endothelial cells. 1) Budding is the formation of new tubes by branching from existing ones, this can happen by sprouting of a multicellular cord with lumen forming inside as a continuation of the existing lumen in the initial tube. In the vasculature, budding can be present during angiogenesis (Fig. IV. B). 2) During cord hollowing, lumen is made de novo in-between cells assembled in a cluster. Cord hollowing requires cell polarization and involves junctional rearrangements. The first blood vessels, formed through vasculogenesis, lumenize this way (Fig. IV. B'). 3) Cell hollowing involves lumen formation within a single cell initiated by vesicle formation and assembly in large vacuoles, that later fuse together to form intracellular lumen and eventually a hollow cell. Cell hollowing can also occur through cell membrane invagination resulting in cell perfusion. This last process is thought to accompany lumen formation during anastomosis (Fig. IV. B'').
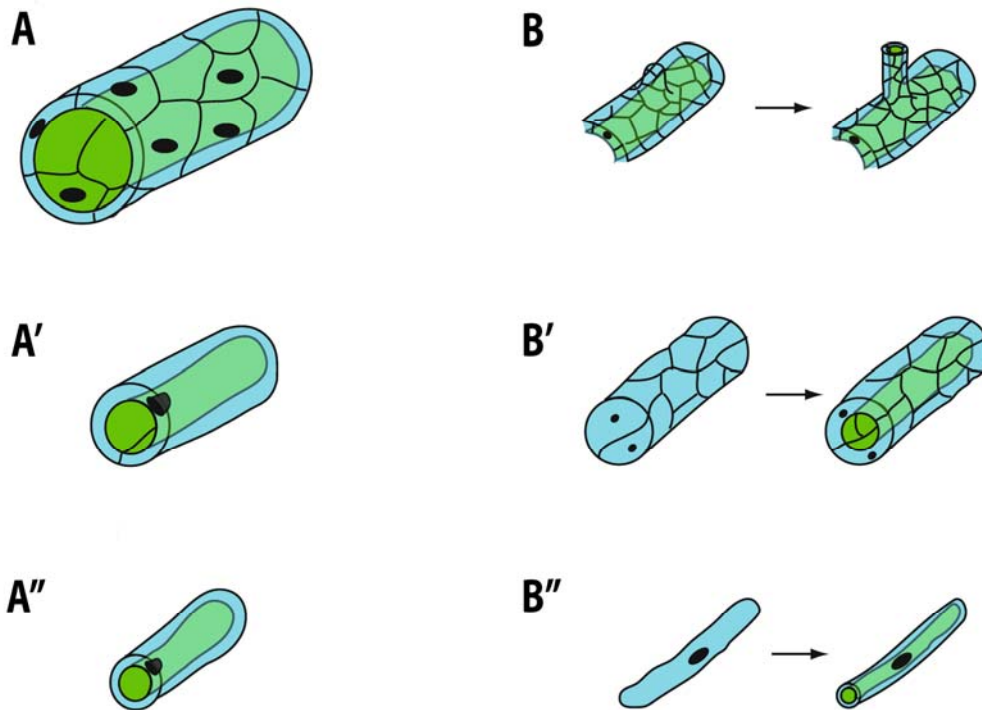
Figure IV. Types of tubes and mechanisms of lumen formation
A-A''). Three main types of tubes present in tubular organs. **A)** Multicellular tubes are formed by many cells connected to each other by junctional complexes (black), forming continuous lines of junctions along the tube. The lumen is extracellular. **A')** unicellular tubes are formed by single cells wrapped around the lumen. Each of the cells makes an autocellular junction, visible as a line along the tube, and connects to neighboring cells by ring-shaped junctions. **A'')** a unicellular/seamless tube forms transcellular lumen through cell hollowing or cell membrane invagination. The cell connects to the neighboring cells by ring-shaped junctions. No junctions are present along the cell.
B-B'') Three mechanisms of lumen formation observed in the vascular system. **B)** Budding - a number of cells grow out of an existing, multicellular tube to form a new branch. The lumen forms as continuation of the lumen existing in the parental tube. **B')** cord hollowing – extracellular lumen opens between cells in a multicellular cord. **B'')** cell hollowing - formation of seamless tubes with transcellular lumen. That process can involve vesicular delivery of new apical membrane. (Adapted from Baer et al., 2009).

3.3.3.2 Types of tubes

Different mechanisms of lumen formation result in tubes of various shapes and cellular architectures (reviewed in Baer et al., 2009). Several types of tubes have been described so far in living organisms: 1) Multicellular tubes, where the tube is made of multiple cells connected to each other with intercellular junctions (Fig. IV. A). The lumen of multicellular tubes is extracellular and forms by cord hollowing, cell sheet wrapping,

cavitation or as shown recently (Herwig et al., 2011; Dong et al., 2009) by cell rearrangements. 2) Unicellular tubes consist of a single cell with an autocellular junction (Fig. IV. A'). The lumen is extracellular and forms by single cell wrapping around the lumen. The junctions in this kind of tube appear as a single line running along the cell where its two edges connect (Ribeiro et al., 2004; Caussinus et al., 2008). 3) Seamless tubes are single cells with lumen going through them (a transcellular lumen), with no autocellular junctions, giving them a doughnut shape with a continuous, toroid membrane (Fig. IV. A''). These tubes can form through cell hollowing (Kamei et al., 2006; Samakovlis et al., 1996b) or cell membrane invagination (Herwig et al., 2011). In the vasculature, all these types of tubes are present and their occurrence depends on the type of vessel and its developmental stage. Detailed descriptions of mechanisms underlying different tube type formation in blood vessels will be provided in further chapters.

3.3.3.3 Key molecules involved in endothelial cell polarization

A number of molecules involved in epithelial cell polarization have been shown to play a key role in this process also in endothelial cells, where polarization is necessary for subsequent lumen formation. Most of the known factors and pathways involved in EC polarization have been identified in cell culture studies. The role of some of them has been verified *in vivo*, mostly in studies of the mouse aorta formation and more recently in the zebrafish.

Apical components are found on the luminal side of the cell. In cell culture and the mouse aorta, the Par3 complex, which includes Par3, Par6 and atypical Protein kinase C (aPKC), was found at the apical membrane of the ECs. Signaling from the Par 3 complex through a number of intracellular components, e.g. PIP, recruits cdc42 and Podocalyxin 2 to the apical cell membrane defining the EC polarity (Bryant et al., 2010; Koh et al., 2009). Podocalyxin 2 is a member of CD34-sialomucins, which have de-adhesive properties that are thought to facilitate lumen formation through mutual repulsion of negatively charged extracellular domains (Strilic et al., 2010). Basal proteins mediate EC contact with extracellular matrix and surrounding cells. Laminins, collagens, integrins and fibronectin belong to these components (reviewed in Xu and Cleaver,

2011). Through their interactions with the ECM, endothelial cells are anchored to the surrounding tissue which allows them to define the polarity. For example integrins in mouse aorta were shown to act upstream of the Par3 complex, and therefore play an important role in the initiation of cell polarization and subsequent lumen formation (Drake et al., 1992; Zovein et al., 2010).

3.3.3.4 New apical membrane insertion initiates lumen formation

As mentioned before, establishment of cell polarity is crucial for the lumen formation process. As the luminal membrane is of apical nature, *de novo* lumen formation between adjacent endothelial cells involves generation of new apical membrane compartments in each of the ECs, which marks the site of the future lumen. This process was described in great detail in epithelial cell culture experiments and the following steps were defined. Luminal membrane generation between two adjacent ECs starts with the formation of an Apical Membrane Initiation Site (AMIS), where apical and junctional components are deposited together. Subsequent segregation of these components leads to formation of a more mature pre-apical patch (PAP) and this is thought to occur either through VE-cadherin endocytosis from the apical surface or its lateral displacement by e.g. CD34-sialomucins (Bryant et al., 2010; Zeeb et al., 2010). Lumen opening is thought to be triggered by VEGF signaling through VEGFR-2 (Strilic et al., 2009).

In vivo studies in our lab have shown that similar steps, including AMIS and PAP formation, take place during new contact establishment in zebrafish blood vessels (described in detail in chapter 3.3.5.5)

3.3.4 Cellular and molecular mechanisms of Vasculogenesis

3.3.4.1 Angioblasts specification and assembly

The first embryonic blood vessels arise through a process called vasculogenesis – the *de novo* assembly of endothelial cell precursors (angioblasts) into a tube (see Fig. I).

In mammals, endothelial and hematopoetic cells differentiate from embryonic mesoderm and form so called blood islands in the extraembryonic yolk sack, with endothelial precursors in the outer part and blood cell precursors inside. These cells eventually assemble forming the first vascular plexus (Fig. I, Flamme et al., 1997; Risau and Flamme, 1995).

In zebrafish, angioblasts develop from the ventral mesoderm in the intermediate cell mass (Detrich et al., 1995). The endothelial cells are spatially separated from the hematopoetic cells, but they are thought to have a common precursor (Vogeli et al., 2006). The angioblasts start to express endothelial specific genes around early somitegenesis ~12 hpf (Kimmel et al., 1990), (Fouquet et al., 1997). Some of these earliest genes belong to the ETS family of transcription factors (reviewed in Lelievre et al., 2001) and include *friend leukemia integration* 1 (*fli1*) and *ets1-related protein* (*etsrp*) and several others. ETS genes act in a synergistic fashion with each other and additional genes, e.g. from the FOX family, and are important for early specification of endothelial cells, since they activate the expression of numerous endothelial specific genes, such as *vegfr2* and *ve-cadherin*.

The specified angioblasts migrate from the ventral mesoderm to the embryonic midline and coalesce to form the primordia of the two first axial vessels in the embryo: the dorsal aorta (DA) and the posterior cardinal vein (PCV) (Jin et al., 2005; Torres-Vazquez et al., 2003). Two waves of angioblast migration are observed in zebrafish. The first one starts at ~14 hpf with angioblasts migrating towards the midline to aggregate above the endodermal layer and under the hypochord, forming a vascular cord that will give rise to the DA. The second wave starts around 16 hpf and these cells are thought to mostly contribute to the PCV. Knock down of VEGF or lack of endoderm does not stop the migration (Jin et al., 2005) and the signal that guides the cells remains unknown.

Angioblast formation is followed by fibronectin deposition between the cells and formation of cell-cell junctions containing e.g. ZO-1 and β-catenin. The DA cord lumenizes around 22 hpf, in a process which will be described in more detail in chapter 3.3.4.3 on lumen formation. Angiogenic ISVs start to sprout dorsally around the same time.

3.3.4.2 Cell segregation after the assembly of primordial vessels

Recent live imaging studies in zebrafish showed that formation of the first vessels – the DA and the PCV- involves an additional mechanism, namely ventral sprouting of angioblasts. These studies showed that the DA assembles first from the migrating angioblasts and subsequently a subset of cells in the DA migrates ventrally to form the cardinal vein around erythrocytes that at this stage (~20-22 hpf) accumulate in the tail region of the embryo. This is contradictory to previous reports saying that the PCV arises from the second wave of migrating angioblasts and forms independantly of the DA (Jin et al., 2005; Torres-Vazquez et al., 2003). The process of ventral sprouting is regulated by repulsive interactions of arterial EphrinB2 and venous EphB4 that direct the venous cells ventrally and arterial cells dorsally. Since VEGF/Notch signaling is crucial for activation of arterial identity, disruption of this signaling pathway disturbs the ventral migration and segregation process. (Herbert et al., 2009).

3.3.4.3 Cord hollowing in vasculogenesis

The lumen of the Dorsal Aorta (DA) is the first vascular lumen that forms in the developing embryo. Studies in mouse (Strilic et al., 2009) and zebrafish (Jin et al., 2005) have shown that the lumen in the DA forms extracellularly through cell cord hollowing. Cord hollowing is achieved through addition of new apical membrane and redistribution of junctions that move away from the cord center (reviewed in Xu and Cleaver, 2011). Apical membrane associated components, such as Podocalyxin, Moesin and F-actin were found to localize to the cell-cell contacts in the cord and subsequently to the apical (luminal) membrane in a lumenized mouse aorta (Fig. V). Podocalyxin is linked to F-actin, which interacts with Non-muscle myosin II to induce cell shape changes necessary for lumen opening. VEGF-A signaling is required for this process to take place. Additionally, in VE-cadherin mutant mice these proteins are not enriched at the apical membrane and lumen fails to form, suggesting a role of this adhesion molecule in EC polarization (Strilic et al., 2009).
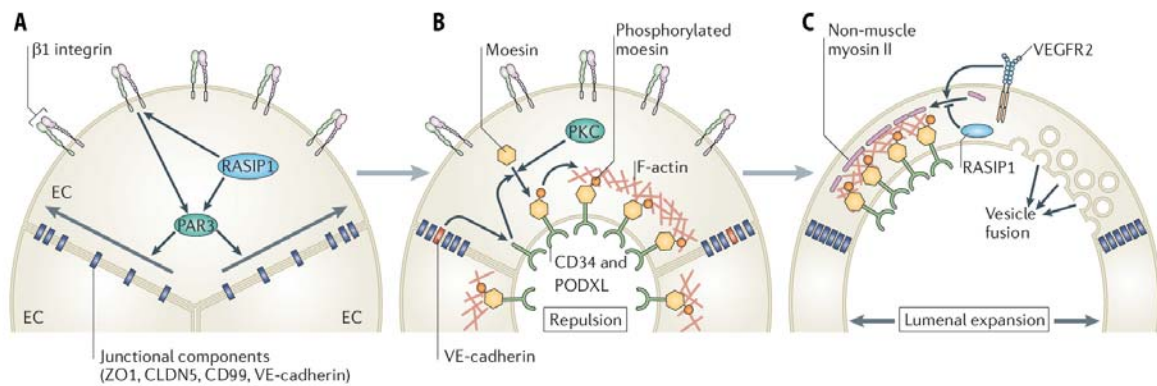
Figure V. Molecular mechanisms of lumen formation in vasculogenesis
A) Initially endothelial cells (ECs) form a cord of cells connected to each other by junctional complexes (VE-cadherin, ZO-1, Claudin5). Signals mediated by β1-integrin (connected to the ECM) through RAS interacting protein 1 (RASIP1) and PAR3 lead to lateral redistribution of junctional complexes to the periphery of EC-EC contacts, defining the apical compartment in the inner part of the cord. **B)** Lumen formation starts after the apicobasal polarity is established. Podocalyxin is redistributed to the apical membrane; a process partially mediated VE-cadherin and β1-integrin. Moesin phosphorylated by aPKC localizes to the apical membrane and promotes the deposition of F-actin. Podocalyxin is thought to initiate lumen formation by repulsive interactions. **C)** Lumen expansion can be mediated by a number of factors. Among these, VEGF can induce association of Non-muscle myosin 2 with apical F-actin to drive cell shape changes. In contrast, RASIP1 can repress actomyosin contractility. Additionally, small vesicles can contribute to expansion of the apical membrane. (Adapted from Herbert et al., 2011)

3.3.4.4 Arterial-venous specification

Arterial-venous specification of the blood vessels starts as soon as the first vessels assemble from the precursor angioblasts and a number of genes have been shown to take part in this process. Sonic hedgehog (Shh) signaling from the notochord induces *vegf* expression in the somites of the embryo. VEGF acts through VEGFR-2 and activates the Notch pathway in the ECs, which promotes arterial differentiation and activation of arterial genes, such as *ephrinB2*. It has been shown in zebrafish that embryos lacking Shh, Notch or Vegf do not express *ephrin B2* in blood vessels anymore (Lawson et al., 2001). Overexpression of these genes causes ectopic expression of arterial markers.

EphrinB2 is a ligand belonging to the ephrin family of proteins involved in repulsive-adhesive signaling. *EphrinB2* is expressed specifically in endothelial cells of arterial character. It is absent in the venous cells that express another protein, receptor

EphB4 (Wang et al., 1998). These genes are expressed very early in development which means that the arterial-venous specification is independent of blood flow. As described before, EphrinB2-EphB4 signaling is involved in arterial-venous cell segregation in the first embryonic vessels where they act through repulsive interactions (Herbert et al., 2009).

Originally, it was thought that venous identity was a default state of angioblasts and only activation of arterial genes by Shh/Vegf/Notch signaling could induce arterial fate. Recently, however, venous specific transcription factors were shown to be necessary to induce venous fate. Work in mice showed that the transcription factor COUP-TFII acts upstream of Neuropilin 1 (NRP1) to suppress Notch signaling, and therefore arterial-specific genes, in the venous cells (You et al., 2005).

Although arterial-venous identity is determined at very early stages, it can still be modified at later stages by a number of factors, including blood flow direction, oxygen levels and genetic signals from neighboring tissues.

3.3.5 Cellular and molecular mechanisms of Angiogenesis

After the first vessels in the embryo have formed by vasculogenesis, subsequent new vessels form by active sprouting of endothelial cells from the existing vessels, in the process called angiogenesis. In response to proangiogenic signals, ECs embedded in an existing vessel differentiate into active angiogenic sprouts that extend filopodia to sense the signals and directionally migrate making a new vascular branch. This process is tightly regulated and consists of defined steps: 1) sprout formation and migration, which involves tip cell/stalk cell selection (chapter 3.3.5.1-3), 2) anastomosis/fusion of the sprouts (chapter 3.3.5.4-6) and 3) lumen formation (chapter 3.3.5.7-12).

3.3.5.1 Sprout formation and tip cell/stalk cell selection

Formation of a new vascular branch from an existing vessel requires a group of cells embedded in a tube to exit their quiescent state and migrate out towards the attracting signals, such as VEGF or Angiopoietin 2. To move out of the vascular bed the cells undergo substantial changes, involving redefinition of polarity and loosening of

junctions, digestion of the surrounding ECM and extension of filopodia that enable cell migration (reviewed in Adams and Alitalo, 2007; Carmeliet and Jain, 2011). Since the mother vessel is usually a functional one, the process of branching has to be strictly controlled to prevent vessel breakage and hemorrhage. Therefore, the architecture of the sprout is highly organized and this is controlled by a number of molecular factors.

A typical sprout consists of a leading tip cell and following stalk cells that have a common lumen with the mother vessel. Tip cells are actively migrating cells leading the outgrowing angiogenic sprout and extending long filopodia to sense signaling cues from the environment (Fig. VI). In the mouse retina, the filopodia are ~100 nm thick and up to 100 um long. The tip cell is morphologically distinct from the stalk cells and it shows different expression levels of several genes. Tip cells respond to VEGF-A signaling through VEGFR-2. Removal of any of these factors inhibits tip cell sprouting behavior and vessel plexus formation in the retina. A VEGF gradient in the retinal extracellular matrix is responsible for the guidance and directional sprouting of the tip cells' filopodia. It has also been shown that in the mouse retina tip cells often extend filopodia along the VEGF-A producing astrocytes (Gerhardt et al., 2003).

In zebrafish, angiogenic sprouts were also shown to extend filopodia and move out of the existing vessels; the dynamics of this process could be observed in transgenic embryos using time lapse confocal imaging (Isogai et al., 2003; Lawson and Weinstein, 2002). Angiogenic sprouts in the fish embryo have been best described in the tail region where the intesegmental vessels (ISVs) grow dorsally from the DA following VEGF signaling from the somites (Habeck et al., 2002).

3.3.5.2 Tip cell selection

All the outgrowing ECs are subjected to the stimulating VEGF-A signaling, but only one of the ECs in a sprout becomes a tip cell at a given time. Recent studies of the process of tip cell selection in zebrafish and mouse have revealed a key role of Notch signaling in this process. VEGF-A acts through VEGFR-2 to induce expression of the Notch ligand Dll4 in endothelial cells. Presence of Dll4 in one endothelial cell induces Notch signaling in the neighboring cells, which inhibits their tip cell behavior and promotes stalk cell differentiation. Hence, cells with the highest Dll4 levels become tip

Figure VI. Molecular control of endothelial tip cell selection
Endothelial cells forming an angiogenic sprout are organized in a hierarchy, with one leading tip cell and following stalk cells. The sprout forms in response to VEGF gradient in the surrounding tissue. VEGF signaling through VEGFR2 activates Dll4 in the tip cell, which activates Notch signaling in adjacent stalk cells limiting their responsiveness to further VEGF signals. This triggers morphological changes in the two cell types (see table in the figure). (Adapted from Herbert et al., 2011).
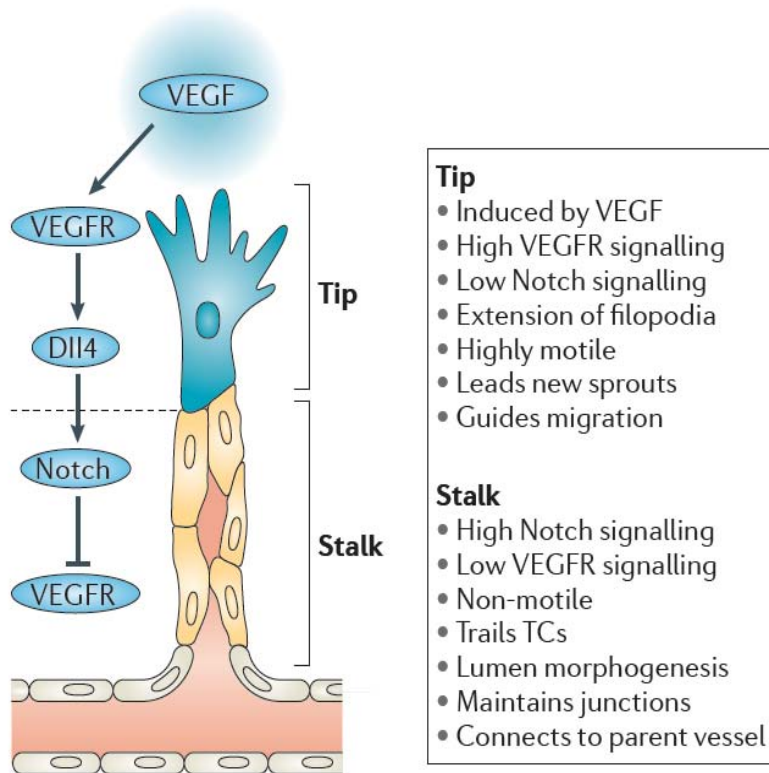
cells, characterized by enhanced sprouting behavior and expression of tip cell specific genes, such as Flt4. Activation of Notch signaling in stalk cells inhibits VEGFR-2, making them insensitive to further VEGF stimulation (Fig. VI). It also induces VEGFR-1 that inhibits tip cell differentiation even more, due to its high affinity to VEGF but low kinase activity. Depletion of Dll4 or Notch signaling in mice and zebrafish results in increased tip cell numbers and causes a hyper-sprouting phenotype. In mosaic analyses, *dll4* overexpressing ECs as well as Notch deficient cells ended up much more frequently in a tip cell position, confirming the importance of Notch signaling for the establishment of cell hierarchy in the sprout (Hellstrom et al., 2007; Lobov et al., 2007; Siekmann and Lawson, 2007; Suchting et al., 2007).

The VEGFR-Dll4-Notch dependent process of tip cell selection is very dynamic. Studies in the retina and in 3D cell culture have shown that ECs actively compete for the tip cell position and support the key role played by relative levels of VEGFR-1 and -2 that change dynamically as the cells move around and change neighbors. Mosaic analyses *in vivo* and *in vitro* showed that cells heterozygous for VEGFR-2 contributed more to the stalk, whereas cells with lower levels of VEGFR-1 more likely became tip cells. Live imaging of 3D EC cell culture revealed dynamic cell rearrangements within

sprouts where cells with higher VEGFR-2 and lower VEGFR-1 overtake neighboring cells more frequently (Jakobsson et al., 2010). Accordingly, if Notch is inhibited, cells with high VEGFR-2 levels do not have the advantage to become tip cells anymore.

An additional player influencing the tip cell selection process turned out to be VEGFR-3, activated by VEGF-C produced in macrophages. VEGF3 signaling can also induce Notch signaling, thus promoting stalk cell differentiation, which in this case happens in newly formed vessels where sprouting behavior is not needed anymore (Tammela et al., 2011).

3.3.5.3 Sprout formation in the *Drosophila* tracheal system

Many parallels can be drawn from the development of the fly tracheal system and the vertebrate vasculature. For instance, epithelial cells from the lumenized trachea start extending filopodia and produce sprouts after activation of their FGF receptor Breathless, in response to the ligand Branchless expressed in surrounding cells (Sutherland et al., 1996, reviewed in Ochoa-Espinosa and Affolter, 2012), Tracheal branches, in particular dorsal branches (DB), which have been the most studied, also contain tip cells and it has been shown that the migration of these cells drives dorsal branch elongation, which takes place through stalk cell rearrangements involving cell intercalation (Ghabrial and Krasnow, 2006; Ribeiro et al., 2004), Ablation of the tip cell results in a new tip cell selection from the stalk cells (Caussinus et al., 2008), meaning that all the cells have the potential to become tip cells, similarly to the vascular sprouts described before.

3.3.5.4 Anastomosis

To form a functional network of tubes, the outgrowing angiogenic sprouts have to connect to each other and form a continuous lumen. This requires significant changes in cell shape and polarization. A blunt ended sprout, led by an actively migrating tip cell with filopodial extensions and defined apico-basal polarization, has to redefine its junction and membrane compartments and adapt to the new situation upon contact with another sprout. This involves remodeling of cell-cell contacts and changes in cell

polarity. This process, called vessel anastomosis or vessel fusion, is the main focus of the work in our lab and of my project.

3.3.5.5 Blood vessel fusion in the zebrafish vasculature

In a developing zebrafish embryo, multiple angiogenic sprouts are present and through dynamic migration find each other and connect to form a new, functional vascular branch. The use of live imaging techniques allowed observing this dynamic process in the developing embryo over time. However, the cellular mechanism of vessel fusion was not described and the cellular behaviors involved in this process were unknown. Studies in our lab have revealed the initial steps of blood vessel fusion at single cell resolution in intersegmental vessels in the zebrafish tail. The ISVs are among the first vessels in the fish embryo to be formed by angiogenesis, as described in the previous chapter 3.2.5. They form T-shaped sprouts that connect to each other after reaching the dorsal edge of the tail (Fig. III). Blum et al. (Blum et al., 2008) analyzed the connection of ISV tip cells using antibody staining for junctional proteins, VE-cadherin and ZO-1, that mark the cell-cell contacts. These studies showed that upon contact of filopodial extensions, junctional proteins are deposited in a form of a spot at the contact site and subsequently elaborate into a ring-like structure as the cell contact surface expands.

The process of new contact formation was further investigated in the lab using transgenic junctional reporter, ZO-1-EGFP, which allows live observation of the process over time with confocal time lapse microscopy. Herwig et al. (Herwig et al., 2011) showed that the new contact formation between filopodia of endothelial tip cells involves de novo deposition of ZO-1-EGFP in a form of a spot that is transformed into a ring within minutes, confirming previous analyses on still images. Additionally it was shown that the cell membrane within the junctional ring is of apical character, as marked by *de novo* deposition of an apically localized protein Podocalyxin 2 (Pdxl2).

3.3.5.6 Fusion process in the *Drosophila* trachea resembles new contact formation in blood vessels

The connection of newly grown branches also takes place in the tracheal system of *Drosophila*. Also here the fusion process is initiated by long filopodial extensions coming from the tip cells of each branch. Upon touching of filopodia, a new contact has to be elaborated, and this involves *de novo* deposition of junctional protein E-cadherin (DE-cad) and the formation of a new apical membrane compartment (Gervais et al., 2012; Lee et al., 2003; Lee and Kolodziej, 2002). At the same time, a cytoskeletal track consisting of F-actin, microtubules and plakin Short Stop (Shot) forms within the cell body. This track helps to stabilize the new junctional connection and takes part in the following step of lumen formation.

3.3.5.7 Lumen formation during anastomosis

Angiogenic sprouts form cords or tubes ended with a tip cell. When two sprouts connect, the fusion process not only has to seal the two cells to each other but also has to form a continuous lumen that will provide a new route for the blood flow. The process of lumen formation has been studied extensively in cell culture and during vasculogenesis in the mouse aorta. However, not much was known about lumen formation during angiogenesis in the living organism. Recent studies in the zebrafish have addressed this question and through observation of vessel development over time described cellular mechanisms involved in the lumen formation process. All of these studies so far were performed in the intersegmental vessels of the zebrafish embryo.

3.3.5.8 Cell hollowing during anastomosis

The initial question that the researchers asked concerned the type of tubes the ISVs form. Early studies have suggested that these vessels are of uniform architecture, each consisting of 3 cells connected head to tail, forming transcellular lumen (Childs et al., 2002; Kamei et al., 2006). Following this architecture, the formation of lumen was proposed to occur through cell hollowing preceded by formation of large intracellular vacuoles. This idea was supported by studies in 3D endothelial cell culture, where

assembly of intracellular vacuoles led to lumen formation (Bayless and Davis, 2002; Davis and Camarillo, 1996). In these *in vitro* studies, cytoskeleton and polarity changes where shown to be mediated by Rac1 and Cdc42 signaling. Intracellular pinocytic vacuoles were observed in 3D EC cell culture, by uptake of carboxyrodamine and presence of cdc42-EGFP. Lumen was shown to form by fusion of the vacuoles and subsequent exocytosis to the intercellular luminal space. Similar experiments in zebrafish showed the presence of vacuole-like structures in the ISVs. These apparent vacuoles dynamically moved and fused together leading to the formation of a continuous lumen. Evidence for the presence of vacuoles was gathered using a transgenic line expressing apically localized cdc42-EGFP and by intravascular injections of fluorescent rhodamine-dextran that gradually filled the luminal spaces (Kamei et al., 2006).

Work in our lab has shown that the cellular architecture of the ISVs is much more complex and that dynamic cell rearrangements are involved in the process of ISV lumen formation. Blum et al. used antibody staining of the junctional proteins VE-cadherin and ZO-1 that mark the cell-cell contacts. In the case of very thin endothelial cells the junctions correspond to the lateral surface of the cells and outline the cell borders. These analyses revealed extensive overlap of cells within the ISVs, showing that at most parts the lumen of these vessels is made up of 2 or more cells and hence is extracellular. In this case, the contribution of large intracellular vacuoles to the formation of extracellular lumen between the cells is unlikely (Blum et al., 2008).

In further studies on the zebrafish ISVs, Wang et al. propose that small intracellular vacuoles participate in the extracellular lumen formation between endothelial cells. The small vacuoles would accumulate near the luminal space and contribute to lumen expansion by fusing to the apical membrane. Additionally these studies reveal a role for Moesin 1 and VE-cadherin in lumen formation in the zebrafish ISVs. In these studies Moesin 1-EGFP was enriched on the apical side of cells, within regions defined by junctions connecting two or more ECs that make extracellular lumen (Wang et al., 2010). In contrast to Kamei et al, Wang et al. did not observe large vacuoles, but smaller ones (~1 um) that accumulate at the luminal side and fuse to the lumen. Vacuoles were also not observed during lumen formation in the dorsal aorta, in agreement with previous reports (Jin et al., 2005; Strilic et al., 2009). Therefore, the

authors suggest that different mechanisms are involved in lumen formation in different vascular beds.

3.3.5.9 Two distinct mechanisms lead to lumen formation in the zebrafish ISVs

Recent studies in our lab used live junctional markers and high resolution live imaging experiments to provide in depth analyses of cell behavior during the lumen formation process. Based on this studies we proposed two distinct mechanisms that can lead to lumen formation in the developing ISVs: 1) dynamic cell rearrangements leading to formation of a multicellular tube with extracellular lumen, 2) transcellular lumen formation through membrane invagination leading to formation of unicellular tubes. These two mechanisms occurred in the ISVs with approximately equal frequency and will be described in detail below.

3.3.5.10   Dynamic cell rearrangements lead to formation of multicellular ISVs

The first contact of the ISV sprouts formed always the same way, with deposition of new junctional material at the contact site in a form of a spot subsequently transformed into a ring with new apical membrane within (see chapter 3.3.5.5). In the first lumen formation mechanism, the contact formation was followed by dynamic cell rearrangements. The cells moved over each other, thereby extending contact surfaces with their neighbors and finally forming a multicellular cord with continuous apical surface within, confirmed by staining for Podocalyxin 2. At the end of this process the lumen inflated through filling of the cord with blood plasma, which resulted in the formation of a multicellular tube with extracellular lumen (Fig. VII. A).

This process highly resembled lumen formation in the notochord of *Ciona intestinalis*, recently described by Dong and colleagues (Dong et al., 2009) (Fig. VII. B). In this case the coin shaped cells first assembled in a row 1 cell wide and 40 cell long. Lumen formation started by small apical membrane patches appearing in the middle of the contact surfaces between adjacent cells, meaning that each cell has two of them, one on each side, making small, spherical luminal pockets between neighboring cells. These apical pockets grow to finally extend all the way dorsally and ventrally taking a big spherical shape and leaving the cells in an hourglass shape with only narrow connection

points to their anterior and posterior neighbors. The multiple luminal pockets finally connect to each other through dynamic rearrangements of the cells. Each of the cells contracts its two edges on dorsal (or ventral) side and simultaneously expands its surface on the opposite edge. Neighboring cells undergo this process in a mirrored fashion meaning that an extending edge of one cell pasts a retracting edge of its direct neighbor and meets an extending edge of the following (third in a row) cell. This makes the luminal pockets tilt towards each other and finally connect in the points of cell edge retraction to make a continuous extracellular lumen between multiple cells (Fig. VII. B).

3.3.5.11 Transcellular lumen formation

The second mechanism of lumen formation in the ISVs was quite different. After new contact formation, the two newly connected cells did not move over each other but instead maintained the ring shaped connections and a head-to-tail arrangement until the blood plasma entered the ISV. These cells subsequently formed transcellular lumen, shown by presence of quantum dots and blood cells within a single cell, proving that the vessel was open and connected to the flow. Additionally, antibody stainig for an apical membrane marker Podocalyxin 2 was observed within single cells. Based on these results a model of lumen formation was proposed, where the apical/luminal membrane of a single cell invaginates pushed by the blood plasma coming from the DA and entering the ISV. The invagination proceeds throughout the cell length and eventually a transcellular lumen opens forming a unicellular tube. It was proposed that opening of this type of lumen requires apical membrane fusion at the proximal cell end, which allows perfusion of the cell (Fig. VII. C).

3.3.5.12 Transcellular lumen formation in the *Drosophila* trachea

A mechanism of transcellular lumen formation was first described in the tracheal system, where fusion cells of two connecting tracheal branches transform into doughnut shaped cells with a continuous transcellular lumen (Lee et al., 2003; Lee and Kolodziej, 2002; Samakovlis et al., 1996b). In this case, tip cell contact establishment through E-cadherin lead to activation of cytoskeleton components and formation of an intracellular

track connecting the two apical compartments of the cell –the new one at the contact site and the old one where the stalk cells connect. This facilitates subsequent lumen formation through invagination of the old apical membrane towards the new contact point. During this step the track shrinks, bringing the two apical membranes closer together. Subsequently, the two apical membranes fuse to allow lumen perfusion and transform the two fusion cells into doughnut shaped cells (Lee et al., 2003; Lee and Kolodziej, 2002; Ribeiro et al., 2004). Arl3 (Arf-like 3) and Sec 5 were shown to be involved in vesicle trafficking that mediates exocytosis necessary for lumen expansion and finally fusion of the two apical membranes to form continuous lumen (Jiang et al., 2007; Kakihara et al., 2008), (Fig. VII. D).
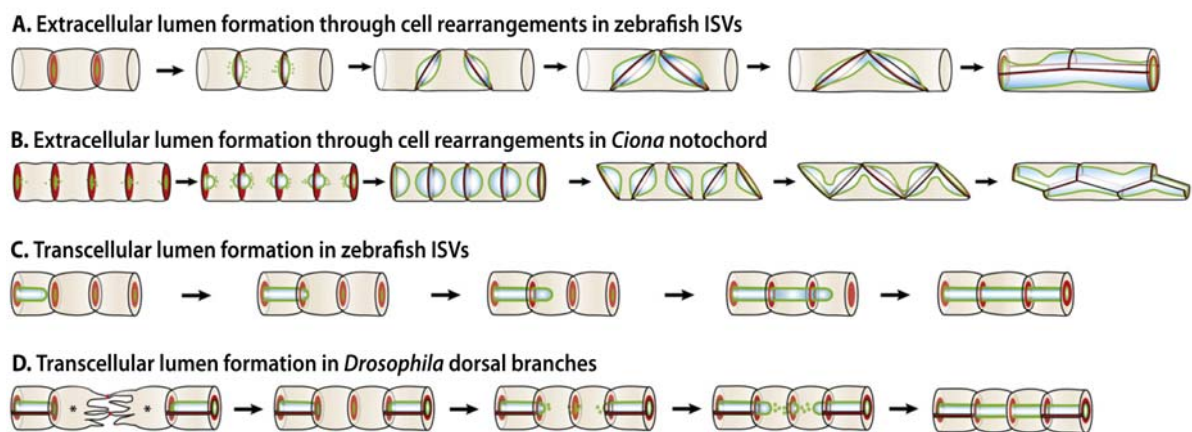
Figure VII. Diverse cellular mechanisms of lumen formation
A) The process of lumen formation through cell rearrangements observed in the zebrafish ISVs. The newly connected cells form junctional rings (red) with apical membrane insertions (green) at the contact site. These new apical compartments move towards each other as the cells migrate over one another within the vascular cord. Eventually the most outer cells meet on top of the middle one leading to connection of all luminal compartments into a continuous one, and making a multicellular cord. The lumen inflates in the cord forming a multicellular tube with extracellular lumen. **B)** A similar mechanism was observed in the *Ciona intestinalis* notochord, where cells initially aligned in a row form small apical pockets at the contact sites to neighboring cells. These luminal compartments grow in size to extend along the dorso-ventral axis. Subsequently, dynamic cell rearrangements lead to connection of all the luminal spaces and to the formation of a continuous extracellular lumen. **C)** An alternative process of lumen formation in the zebrafish ISVs involves seamless tube formation. Luminal apical membrane invaginates towards a new contact point and leads to cell perfusion and formation of transcellular lumen. Invagination usually proceeds in one direction. **D)** Similarly, the tracheal branches of *Drosophila* undergo a fusion process followed by transcellular lumen formation in the two fusion cells. New apical membrane compartment forms at the contact site within a new junctional ring. The previously existing apical membrane on the luminal site invaginates towards the new contact. Intracellular vesicles participate in the apical membranes fusion that leads to transformation of the fusion cells into unicellular tubes with transcellular lumen. (Adapted from Denker and Jiang, 2012).

3.4 Vascular remodeling

After the assembly of the first vascular networks through vasculogenesis and angiogenesis the network is shaped by processes of vascular remodeling leading to changes in shape and pattern of the tubes. This takes place through a number of processes, among which vessel splitting (intussusception) and vessel pruning have been described in some detail.

3.4.1 Intussusception

Intussusceptive angiogenesis is a process in which vascular tubes undergo rearrangements leading to splitting of a larger vessel into a number of smaller diameter capillaries. Intussusception was first described in the pulmonary capillaries of neonatal rats (Caduff et al., 1986) and by now has been associated with remodeling in many other systems, e.g. the chick chorioallantoic membrane (Patan et al., 1993), skeletal muscle (Zhou et al., 1998), myocardium (van Groningen et al., 1991), eye (Djonov et al., 2000) and others (reviewed in Djonov et al., 2003). Intussusception is a stepwise process that involves EC rearrangements but does not require cell division or drastic changes of the surrounding tissue. First, the opposing walls of the remodeling capillary move closer together and establish a contact. Next, the junctional connections between the ECs rearrange to form a vertical perforation in the vessel that later transforms into a pillar that splits the vessel lumen in two. The pillar enlarges as pericytes and myofibroblasts invade and deposit ECM components in the newly formed perivascular space, to finally form two separate capillaries (Burri and Tarek, 1990; Caduff et al., 1986). Intussusception is thought to be a dominant process of growth of capillary beds after the initial network is formed through vasculogenesis and angiogenesis. This mechanism is considered a faster and energetically less demanding way to form new vessels without the need for cell proliferation or invasion of new regions in the tissue, which gives an advantage over sprouting angiogenesis.

Formation of an intussusceptive pillar can change the geometry and hemodynamic properties of the remodeling vessel, leading to formation of additional branches (Djonov et al., 2002). Vessel splitting can also result in detachment of

fragments of vessels through narrowing of the lumen on one side of the pillar resulting in disconnection of the branch, also known as vessel pruning.

In the zebrafish mechanisms of intussusception have not been described so far, but it is thought to take part in the formation of posterior cardinal vein plexus and the eye vasculature (our own observations).

3.4.2 Pruning

Remodeling of the developing vasculature also involves removing of branches resulting in a simplified or reshaped network. This process, called vessel pruning, was first described in the mouse retina, where regression of capillaries was shown to shape the vascular plexus (Ashton, 1966). Further analyses revealed a role of VEGF in this process. In the presence of high oxygen levels the production of VEGF in the vessel surrounding tissues is shut off, leading to vessel pruning (Alon et al., 1995). Similar experiments in the chicken confirmed the role of VEGF in the pruning process (Hlushchuk et al., 2011). In the above mentioned studies apoptosis was thought to play a key role in the pruning process. Studies in *in vitro* cell culture and in the mouse retina show a novel role of a member of Rho guanine-nucleotide exchange factor – FGD5 - in vessel regression. This endothelial-specific factor induces vascular regression through activation of cdc42 that promotes p53 mediated apoptosis (Cheng et al., 2012).

However, it has recently been observed that apoptosis, although present, is not a dominating mechanism of vessel pruning. *In vivo* time lapse analyses in the zebrafish brain show that pruning mostly occurs through dynamic cell rearrangements ((Chen et al., 2012), own data, unpublished). Chen et al (2012) describe the dynamics of vessel pruning in the developing brain of zebrafish embryos. They have shown that pruning occurs through endothelial cell migration from the pruning to the adjacent vessel segment. Hemodynamic forces are involved in the process as blood flow is reduced and finally stopped in the segments that are about to prune. Increased blood pressure results in lower numbers of pruned vessels, whereas blocking flow in certain segments causes their regression.

Further analyses of cell behavior during vessel pruning were performed in our lab and will be described in the Results (chapter 5.7).

3.5 The cranial vasculature of developing zebrafish embryos

The cranial vasculature of the zebrafish embryo is a complex network of tubes built around and within the brain structures (Isogai et al., 2001). The first reports on angiogenesis in the cranial vessels of the fish embryo were published some years ago (Lawson and Weinstein, 2002), but only recently it became of interest for many research groups; in the last couple of years this model system emerged as a useful alternative to ISVs. The following chapter provides insight into these recent findings.

3.5.1 Early development of the head vasculature

The cranial vasculature forms from the Anterior Lateral Plate Mesoderm (ALPM) whereas the trunk vessels arise from the Posterior Lateral Plate Mesoderm (PLPM) (Lieschke et al., 2002; Warga et al., 2009). Proulx and colleagues (Proulx et al., 2010) have shown that the cranial vasculature forms through a combination of vasculogenesis and angiogenesis, which they describe using an early vascular progenitor cell marker etsrp/etv2, an ETS domain transcription factor that is crucial for the expression of many vascular specific genes, such as *fli1, flk1, scl* and *pu.1*. The ALPM angioblasts form two pairs of clusters: one bilateral pair in the midbrain (MOC – midbrain organizing center) and one bilateral pair in the rostral region (ROC – rostral organizing center). These clusters of endothelial progenitor cells form by vasculogenesis at around 7-somite stage (~12 hpf). At around 15-18 somite stage (~17-19 hpf), the clusters start to extend angiogenic sprouts, which lead to formation of most of the cranial vessels. In certain cases, single cells migrate away from the clusters to contribute to vessel formation in a vasculogenic manner. Based on these findings and the fact that the original clusters also contribute to future vessels, the first cranial vessels form through the combination of vasculogenesis and angiogenesis.

The development of the cranial vasculature and of the brain is coupled, as shown in zebrafish by Ulrich and colleagues (Ulrich et al., 2011) in a detailed analysis of the neurovascular hindbrain development. The first step of this process is the formation of perineural vessels along the neuroectoderm surface. Subsequently, angiogenic sprouts migrate into the hindbrain tissue from the primary vessels. The sprouts migrate via the rhombomere centers and their pattern is not identical in every embryo, but certain connections are conserved. A number of these vessels align to neuron clusters and axon tracts, but endothelial cells are not necessary for these neurons to form in the right place.

Detailed studies on the hindbrain vasculature showed that the network of central arteries (CtAs), which penetrate the brain tissue, forms by angiogenic sprouting from the bilateral primordial hindbrain channels (PHBCs) of a venous character (Fig. II C). The arch-shaped sprouts connect to the centrally localized basilar artery (BA) in a semi-organized fashion (Bussmann et al., 2011; Fujita et al., 2011). Similarly to the ISVs (Siekmann and Lawson, 2007), sprouting is controlled by proangiogenic VEGF and antiangiogenic Notch signaling. However, additional signaling molecules were shown to play an important role in the CtA but not ISV development. Chemokine Cxcl12b is expressed right above the BA, whereas its receptor Cxcr4a was shown in the tips of sprouting CtAs. Cxcr4a was down-regulated after the CtA sprouts have established a connection to the BA and perfused. Embryos mutant for either of these factors showed reduced CtA-BA contact formation and elevated angiogenic activity in connected sprouts, which in wild type embryos would stop within minutes after vessel fusion. Additionally, *cxcr4a* expression and EC filopodial activity was down-regulated by blood flow presence in connected, perfused CtAs, pointing at the role of hemodynamic forces in the angiogenic network formation in the brain of the zebrafish embryo.

The process of blood vessel fusion in the complex network of the head vasculature (see Fig. VIII) has not been analyzed so far and therefore became the main focus of my project.
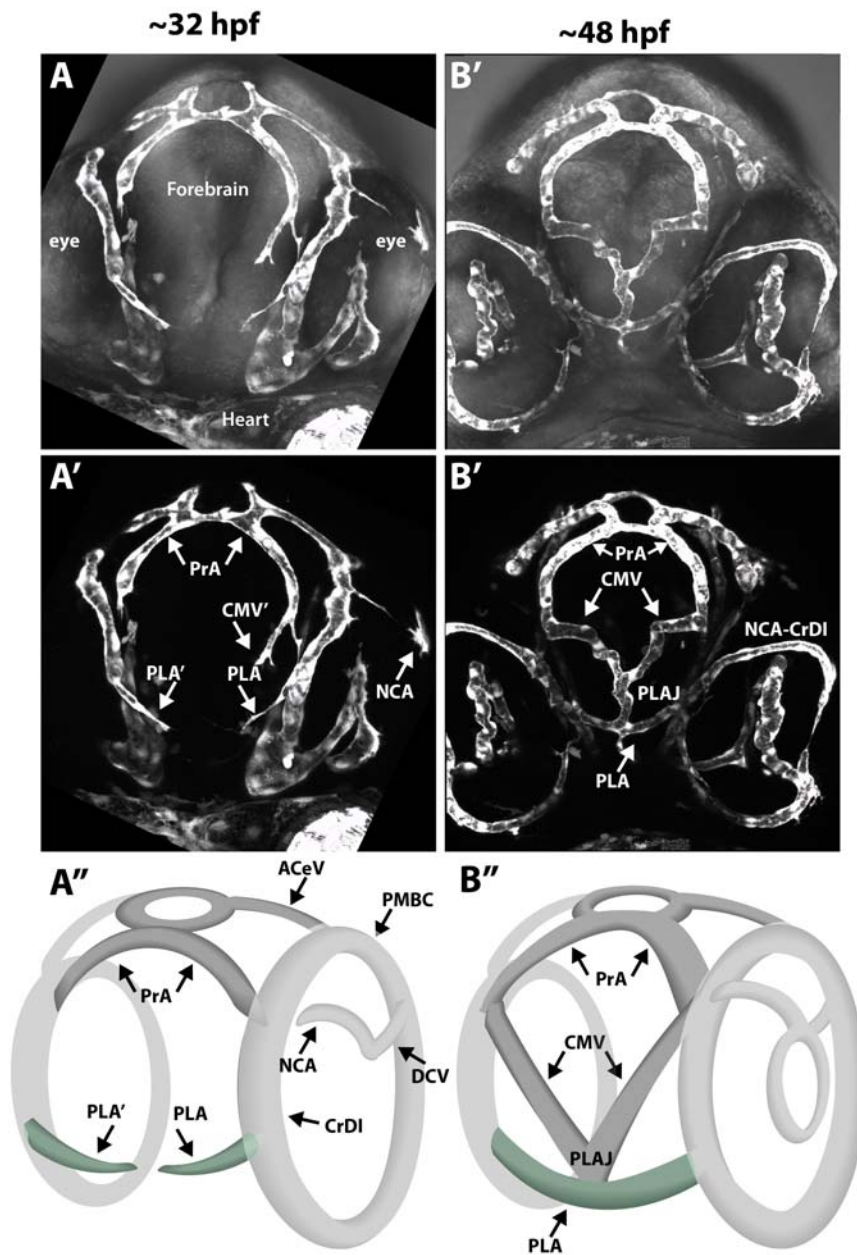
Figure VIII. The zebrafish cranial vasculature
A-B') Confocal images of the front head view of a transgenic zebrafish embryo Tg(kdrl:EGFP) (white) showing the most rostral head vasculature at two developmental stages. **A-A')** the head vessels at ~32 hpf (white) together with the bright field image, showing the surrounding head tissue (A). A' shows the vessels alone with the corresponding names. **B-B')** the head vasculature of the same embryo at 48 hpf showing the vessels formed over time by angiogenesis and blood vessel fusion. **A''-B'')** The models show a simplified view of the network at corresponding times and name the major vessels: PLA - palatocerebral artery, PLAJ - junction of the palatocerebral arteries, CrDI - cranial division of the internal carotid artery, DCV - dorsal ciliary vein, PrA - prosencephalic artery, PMBC - primordial midbrain channel, ACeV - anterior (rostral) cerebral vein, CMV - communicating vessel, NCA - nasal ciliary artery.

3.6 The aim of this study

Transformation of two blunt-ended angiogenic sprouts through vessel anastomosis into a functional, open tube is a key step in the development of vascular networks. Most of the blood vessels in the embryo form in the presence of stable blood flow in adjacent tubes, suggesting the importance of this factor for angiogenic sprouting and anastomosis. Therefore, I have decided to follow the development of blood vessels in the head of the zebrafish, which form when blood flow is fully established. Since data on angiogenic sprouting in the head were not available when I started the project, I first created a map of the cranial vascular network using transgenic lines marking endothelial cells, with the aim to identify the place and the timing of fusion events. For my purpose the most interesting vessels were the ones placed close to the surface of the embryo, since this allows high resolution live imaging. Therefore I have focused on the most rostral part of the head where I identified numerous vessels undergoing angiogenic activity within the first 3 days of embryonic development.

The main aim of my project was to describe the stepwise process of vessel fusion and lumen formation in the cranial vasculature and to determine the influence of blood flow on the observed cellular mechanisms. Analyses of multiple vessels of different shapes, positions and at various developmental stages served to generalize the model and prove its recurrence in various vessel types. To identify molecular players involved in particular steps of vessel fusion I analyzed this process in *ve-cadherin* mutant zebrafish generated in our lab. Additionally, I analyzed the process of vessel pruning in the tail and the eye vasculature to describe cellular rearrangements involved in vessel regression.

4 Materials and Methods

4.1 Companies

All chemicals were obtained from the following companies:

Applichem	BD Biosciences
BioRad	Difco laboratories
Eurogentec	Fluka
Invitrogen	Machery-Nagel
Merck	Roche
Schwartz	Sigma-Aldrich

4.2 Buffers, solutions and media

Solution	contains
1 % Agarose	Agarose in 1xTAE/TBE
10 % (2 mM) PTU (Phenylthiourea)	304 mg PTU (RT) in 1 l egg water, stir on a heated plate, store at 4 °C
2 % Paraformaldehyde (PFA)	Dilute 4 % PFA with 1x PBST
20 mg/ml Proteinase K	Lyophilized powder is dissolved 20 mg/ml in sterile 50 mM Tris (pH 8.0), 1.5mM calcium acetate. Divide stock solution into small aliquots and store at -20 °C.
25x Tricaine	2 g tricaine in 350 ml set to pH 7.0 w TrisHCL (1 M pH 8.0). Fill up to 500 ml. Aliquot. Store at -20 °C.
4 % PFA	550 ml ddH$_2$O, warm under the hood to 60 °C. Add 40 g PFA; wear gloves, protection glasses, lab coat. Stir 5 – 40

	min at 60 °C. Add three to four drops of 2 M NaOH, wait until cleared; if not, repeat. Take from heater, add 333,3 ml 10x PBS (pH 7.22). Fill up to 1 l; filtrate
5 % Bakto-Agar	5 % Bakto-Agar in 0,3 M Sucrose/PBS
50-70 % glycerol	50-70 % glycerol in ddH$_2$O
Blocking solution antibody staining	5 % goat serum and 1 % BSA in PBST + 1:1000 NaAzid
Chloramphenicol stock solution (34 mg/ml)	340 mg Chloramphenicol dissolved in 10 ml 100% EtOH. Aliquot and store at -20 °C.
DNA loading buffer (10x)	Dissolve 15 ml glycerol in 40 ml ddH$_2$O. Dissolve 100 mg Orange G. Fill up to 50 ml with water. Store at -20 °C.
0.5 M EDTA pH 8.0	Dissolve 93.05 g EDTA disodium salt in 400 ml ddH$_2$O. Adjust pH to 8.0 with NaOH. Adjust the volume to 500 ml.
Genomic DNA extraction buffer	10 mM Tris pH 8 2 mM EDTA 0.2 % TritonX-100 0.5 % SDS 200 µg/ml Proteinase K (keep on ice)
Kanamycin stock solution (10 mg/ml)	100 mg Kanamycin dissolved in 10ml ddH$_2$O. Filter sterilize. Aliquot and store at -20 °C.
LB (Lysogeny-broth) medium	10 g peptone, 5 g yeast extract, 10 g NaCl in 950 ml ddH$_2$O. Shake until dissolved. Adjust to pH 7.0 with 5 M NaOH. Adjust to 1 l with ddH$_2$O. Autoclave.

LB agar plates	Add 15 g Bacto agar per liter LB medium. Autoclave and add antibiotics at 50 °C. Pour into Petri dishes.
NaAzid	10 % solution in ddH$_2$O. Store at -20°C.
PBS	NaCl 8 g
	KCl 0.2 g
	Na$_2$HPO$_4$(2H$_2$0) 1.8 g
	KH$_2$PO$_4$ 0.24 g
	Add H$_2$O to 1l
	Adjust to pH 7,2
PBST	1x PBS, 0.1 % Tween 20
PBSTX	0.5 % TritonX-100 in PBST
50x TAE (Tris-acetate-EDTA electrophoresis buffer)	Dissolve 242 g Tris base in ~750 ml ddH$_2$O. Carefully add 57.1 ml glacial acetic acid and 100 ml of 0.5 M EDTA (pH 8.0). Adjust the solution to a final volume of 1 l.
5x TBE (Tris-borate-EDTA electrophoresis buffer)	54 g Tris, 27.5 g boric acid, dissolve in ~900 ml ddH$_2$O, add 20 ml of 0.5 M EDTA (pH 8.0) and adjust the solution to a final volume of 1 l
TE (tris-EDTA) -buffer	10 mM Tris HCl, 1 mM EDTA in ddH$_2$O. Adjust to pH 8.0.

4.3 Molecular biology protocols

4.3.1 BAC recombineering (recombination-mediated genetic engineering)

BAC (Bacterial Artificial Chromosome) recombineering serves to modify large DNA constructs, containing 150-250 kb fragments of genomic DNA: It allows insertion and deletion of DNA fragments from a chosen clone that can contain a full gene

48

sequence with large upstream and downstream genomic fragments, limiting the possibility of losing important enhancer regions. This method uses a lambda (λ) Red-mediated homologous recombination in modified *Escherichia coli* bacterial strains. Recombineering was performed following the published protocol (Warming et al., 2005).

4.3.1.1 Recombineering bacteria strains

Bacteria strain SW 102 was obtained from NCI BRB Preclinical Repository. The strain was derived from DY380 bacteria and contains the λ prophage recombineering system and lacks the *GalK* cassette.

4.3.1.2 Recombineering media and solutions

Solution	contains
M9 medium (washing solution)	Per 1 liter: 6 g Na_2HPO_4; 3 g KH_2PO_4; 1 g NH_4Cl; 0.5 g NaCl autoclave
5x M63 solution (for minimal plates)	Per 1 liter: 10 g $(NH_4)_2SO_4$; 68 g KH_2PO_4; 2.5 mg; $FeSO_4 \cdot 7H_2O$ adjust to pH 7 with KOH, autoclave
0.2 mg/ml d-biotin (1:5000)	2 mg d-biotin powder in 10 ml H_2O, sterile filtered
20 % galactose (1:100)	10 g galactose powder in 50 ml H_2O, autoclave
20 % 2-deoxy-galactose (1:100)	1 g 2-deoxy galactose powder in 5 ml H_2O, autoclave
20 % glycerol (autoclaved) (1:100)	Dilute 100% glycerol in H_2O (1:5), autoclave
10 mg/ml L-leucine (1%)	1 g of L-leucine in 100 ml H_2O, heat to dissolve, cool down, filter sterilized
12.5 mg/ml Chloramphenicol in EtOH (1:1000)	2.5 g Chloramphenicol dissolved in 200 ml, stored at -20 °C
1 M MgSO4·$7H_2O$ (1:1000)	12.32 g $MgSO_4 \cdot 7H_2O$ in 50 ml H_2O

Galactose positive minimal selection plates	Autoclave 15 g agar in 800 ml H_2O, cool down a little, add 200 ml 5xM63 and 1 ml 1 M $MgSO_4 \cdot 7H_2O$, let cool down to 50 °C, add 10 ml of 20% galactose, 5 ml of 0.2 mg/ml d-biotin, 4.5 ml of L-leucine (1%) and 100 µl of 12.5 mg/ml Chloramphenicol. Poor the plates into Petri dishes, let solidify, store in 4 °C
2-deoxy-galactose positive minimal selection plates	Autoclave 15 g agar in 800 ml H_2O, cool down a little, add 200 ml 5xM63 and 1 ml 1 M $MgSO_4 \cdot 7H_2O$, let cool down to 50 °C, add 10 ml of 20% 2-deoxy-galactose, 5 ml of 0.2 mg/ml d-biotin, 4.5 ml of L-leucine (1%), 10 ml of 20% glycerol and 100 µl of 12.5 mg/ml Chloramphenicol. Poor the plates into Petri dishes, let solidify, store in 4 °C
MacKonkey indicator plates with galactose	Dissolve 25 g MacKonkey agar powder (Sigma) in 500 ml H_2O. Autoclave, cool down to 50 °C, add 5 ml of 20% galactose and 500 µl of 12.5 mg/ml of Chloramphenicol.

4.3.1.3 Primers and vectors for recombineering

Primer/vector name	description	Source
Kdrl_GalK_F and R	To amplify *GalK* cassette; include	*GalK* sequence: (Warming et al. 2005) *Kdrl* sequence obtained by sequencing

	homologous sites for *kdrl* gene, 50 bp upstream and downstream of the ATG codon	the BAC F:5'aaaagcacgtgaagagtgaagaaggctttgact gaggttttaagaggagtCCTGTTGACAATTA ATCATCGGCA R:5'cgtgaagtgacatacggagtatcattcgggacgt tattttaacagacaaaTCAGCACTGTCCTGC TCCTT
Vector GalK-cassette	Containes the *GalK* cassette	(Warming et al. 2005)
Kdrl_KateRAS_F and R	To amplify mKate-CAAX cassette, include homologous sites for *kdrl* gene	F:5'aaaagcacgtgaagagtgaagaaggctttgact gaggttttaagaggagtTTAACCCTCACTAAA GG R:5'cgtgaagtgacatacggagtatcattcgggacgt tattttaacagacaaaATGGTGAGCGAGCTG ATTAA
Kdrl_G21_F and R	Primers to screen the BAC-containing colonies	F:5'CGGGACGTTATTTTAACAG R:5'ACCCCATAACCAAACGTCAG
mKAte_F and R primers	To screen recombined BAC colonies	F:5'ATGGTGAGCGAGCTGATTAAGG R:5'CATCTGTGCCCCAGTTTGCTAGG
pBSII_mKate2-CAAX	mKate2 fluorescent protein with a membrane tagging sequence (Ras, CAAX)	courtesy of Dr. Oguz Kanca
BAC CH211-276G21 with kdrl gene (BAC:kdrl)	BAC clone with full *kdrl* gene sequence	BACPAC Resources
BAC:kdrl: GalK	BAC construct with the	This study, courtesy of Dr. Elin

	GalK cassette inserted at the ATG start codon	Ellertsdottir
BAC:kdrl: mKate-CAAX	BAC construct with the *mKate2-CAAX* sequence insterted at the ATG, ended with a STOP codon	This study

4.3.1.4 Preparing glycerol stocks of BAC clones

LB agar stab cultures of BAC clones in DH10B bacteria (BACPAC Resources) were purchased. Bacteria were streaked on LB agar plates with 12.5 µg/ml Chloramphenicol. Bacteria were grown overnight at 37 °C and colonies were screened with PCR for positives containing the BAC. PCR products of chosen colonies were sequenced.

Positive clones were inoculated into 5 ml LB medium with 12.5 µg/ml Chloramphenicol and grown overnight at 37 °C. 0.5 ml of the culture was used for glycerol stock (1:1 with 70 % autoclaved glycerol) and kept in -80 °C.

4.3.1.5 Transformation of SW102 recombineering bacteria with the BAC DNA

Preparation of fresh competent recombineering bacteria

5 ml of LB medium was inoculated from a glycerol stock with recombineering bacteria SW102 and grown overnight at 32 °C. 0.5 ml of the culture was inoculated into 24.5 ml of LB medium and grown in a shaker incubator at 32 °C with 220 rpm till OD_{600}=0.6. After reaching the OD, 10 ml of the culture was spun down at 0 °C for 10 min with 4 000 rpm in a 15 ml falcon tube with a round bottom. The supernatant was removed and bacteria were resuspended in 1 ml of ice-cold water by gently swirling the tubes in ice/water slurry. After full resuspension the tube was filled up to 10 ml with ice-cold water and centrifuged as before. The washing step was repeated 2 times. The last

time after removing the supernatant, the becteria were resuspended in the left over water and used for electroporation.

Preparation of BAC DNA for electroporation

BAC carrying bacteria form the glycerol stock were inoculated into 5 ml ml LB medium with 12.5 µg/ml Chloramphenicol and grown overnight at 37 °C. The culture was spun down 5 min with 4000 rpm. The pellet was resuspended using 250 µl Resuspention Buffer from a Mini Plasmid isolation KIT (Sigma or NucleoSpin). 250 µl of Lysis buffer was added and the samples were mixed and incubated at RT for 3-5 min. 420 µl of Neutralization Buffer was added and the samples were mixed gently and incubated on ice for 5 min. The samples were centrifuged for 5 min at 14 000 rpm. The supernatant was carefully transferred in a new tube and centrifuged again for 5 min. The supernatant was carefully transferred in a new tube and 750 µl of Isopropanol was added for DNA precipitation. The tubes were incubated on ice for 30 min and centrifuged at 4 °C for 15 min with 14 000 rpm. The supernatant was carefully removed and 1 ml of 70 % ethanol was added to wash the DNA. The tubes were centrifuged again for 10 min. The supernatant was removed and the DNA was dried at 50 °C till no ethanol remained. The DNA was dissolved in 50 µl of water in a shaker at 50 °C.

Transformation of SW102 bacteria with BAC DNA

1 µl of the freshly prepared BAC DNA was used for electrotransformation of 25 µl of freshly prepared competent SW 102 bacteria. Bacteria were put into a Gene Pulser Cuvette with 0.1 cm electrode gap (Bio-Rad) and electroporated in Gene Pulser II with 1.8 kV pulse.

Bacteria were recovered in 1 ml of LB in 15 ml tube at 32 °C in a shaker incubator. The bacteria were plated in following volumes: 10 µl, 100 µl and rest of the culture on LB plates with 12.5 µg/ml Chloramphenicol and incubated overnight at 32 °C.

Colonies were screened with PCR and positive clones were used to prepare glycerol stock for further use.

4.3.1.6 GalK cassette insertion

5 ml LB 12.5 µg/ml Chloramphenicol was inoculated with SW102 recombineering bacteria carrying the BAC clone BAC CH211-276G21 with *kdrl* gene (BAC:kdrl). The bacteria were grown overnight at 32 °C OD_{600}=0.6 and transferred in a 42 °C water bath to incubate for 15 min with shaking (heat shock to activate recombineering gene expression). The bacteria were made competent as described before in point 4.3.1.5.

Primers kdrl_GalK_F and R were used to amplify the GalK cassette from the GalK plasmid using Phusion Polymerase PCR. The PCR product was separated on a 1 % agarose gel and the right band was extracted to isolate the DNA using the Gel Clean-Up KIT (Sigma or NucleoSpin). The DNA was shortly dialyzed on 0.25 µm nitrocellulose filters over H_2O (Millippore) and up to 5 µl (up to 200 ng) was used to transform the competent cells, as described before.

Bacteria were recovered for 1 h in 1 ml of LB in 15 ml tube at 32 °C in a shaker incubator. The bacteria were washed with the M9 medium in a flollowig way: The cultures were centrifuged for 30 sec at 14 000 rpm. The supernatant was removed and the pellet was resuspended in 1 ml M9. The washing was repeated 2 times. After the last wash, the cells were resuspended in 1 ml M9 and the bacteria were plated on Galactose minimal selection plates in following volumes: 10 µl, 100 µl and rest of the culture, and incubated for 3 days at 32 °C.

The obtained colonies were streaked on the MacKonkey indicator plates with Galactose and incubated overnight at 32 °C. The colonies containing the galactose cassette turn red. The positive clones were used to prepare glycerol stocks.

4.3.1.7 Target gene insertion

Generation of Kate-CAAX construct

pmKate2-N (Evrogen) was used to amplify mKate2 red fluorescent protein coding sequence, which was inserted into pBS_II vector with a CAAX tag added at the C terminus (courtesy of Dr. Oguz Kanca). mKate2-CAAX was inserted into pG1 vector using BamHI/XhoI. This construct was used as a template to generate the PCR product used for recombineering.

Insertion of mKate-CAAX cassette into BAC:kdrl:GalK

The glycerol stock of SW102 bacteria carrying BAC:kdrl:GalK was used to inoculate 5 ml LB 12.5 µg/ml Chloramphenicol. The culture was used to prepare recombineering competent bacteria and heat shock, as described before.

Plasmid mKate_CAAX was used for Phusion Polymerase PCR with primers Kdrl_KateRAS_F and R to amplify the Kate-CAAX cassette. The PCR product was purified as described before and used for electrotransformation.

After the electrotransformation the cells were recovered in 10 ml LB for 3-4 h at 32 °C in a shaker incubator. The culture was centrifuged for 5 min at 4 000 rpm and washed with the M9 solution, as described before. The cells were plated on 2-deoxy-galactose positive minimal selection plates in the following volumes: 10 µl, 100 µl and rest of the culture and incubated for 3 days at 32 °C.

The colonies were screened with colony PCR using primers amplifying mKate2 sequence (mKate_F and R). Positive clones were tested with additional PCR using the kdrl_G21_F and R primers. The positive clones were used to prepare glycerol stocks.

4.3.1.8 BAC DNA isolation

To isolate BAC DNA for injections of the zebrafish embryos, 150 ml of LB with 12.5 µg/ml Chloramphenicol was inoculated with the glycerol stock of SW102 bacteria containing BAC:kdrl:mKate_CAAX. The culture was grown overninght at 32 °C. NucleoBond BAC 100 KIT was used to isolate the BAC DNA according to the manual.

Before injection, the DNA was dialyzed on 0.25 µm nitrocellulose filters over H2O (Millippore) for ~ 20-30 min. 15-50 ng/µl of DNA was used for injections.

4.3.2 Plasmids and cloning

4.3.2.1 Bacteria strains

Strain	source
E.coli DH5α	Invitrogen
E.coli TOP10 electrocompetent cells	Invitrogen
E.coli OneShot®TOP10chemically competent cells	Invitrogen

4.3.2.2 Plasmids

Plasmid	description	source
pmKate2-N	mKate2 expression, N-fusion	Evrogen
pG1mmGFP	Expression vector used to clone mKate-CAAX with polyA and SV40 as template for recombineering	Elin Ellertsdottir
pBS_II_tdEos2	Tandem of 2 copies of Eos2 photoconvertible fluorescent protein	Alexandru Denes
pG1 flk1MCS_tol2_tdEos2	The vector drives expression of photoconvertible Eos2 protein in the	This study

	endothelial cells	
pCS2+ mKate	MKate2 fluorescent protein with a STOP codon, PolyA and SV40 sequences	Alice Krudewig
pG1 flk1MCS_tol2_mKate2-3NLS	The vector drives expression of red fluorescent mKate2 protein in the nuclei of endothelial cells	This study

4.3.2.3 PCR amplification

PCR with Taq DNA Polymerase

PCR mix:

Thermopol 10x buffer NEB	5 µl
dNTPs MIX 10mM	1 µl
Primer Forward 10 µM	1 µl
Primer Reverse 10 µM	1 µl
Template DNA (10-20 ng/ µl)	1 µl
Taq polymerase (5 U/ µl) NEB	0.5 µl
H_2O	41.5 µl

Thermocycler program used for PCR:

Materials and Methods

1	Initial denaturation	98 °C	5 min	
2	Denaturation in cycle	98 °C	20 sec	Repeat in cycle 35 times
3	Primer anniling	58-60 °C	30 sec	
4	Elongation	72 °C	40-60 sec (60 sec/1 Kb)	
5	Final elongation	72 °C	10 min	

PCR with high fidelity Phusion Polymerase

PCR mix:

5x Phusion HF Reaction buffer NEB	10 µl
dNTPs MIX 10mM	1 µl
Primer Forward 10 µM	1 µl
Primer Reverse 10 µM	1 µl
Template DNA (10-20 ng/ µl)	1 µl
Phusion High-Fidelity Polymerase (2 U/ µl) NEB	0.5 µl
H_2O	31.5 µl

Thermocycler program used for PCR:

1	Initial denaturation	98 °C	30 sec	
2	Denaturation in cycle	98 °C	10 sec	Repeat in

58

3	Primer anniling	58-60 °C	30 sec	cycle 35 times
4	Elongation	72 °C	40-60 sec (60 sec/1 Kb)	
5	Final elongation	72 °C	10 min	

4.3.2.4 Restriction enzyme digestion

Digestion mix:

10x Reaction buffer NEB (1-4, depending on the enzyme)	4 µl
10 % BSA in H_2O	4 µl
DNA to digest (1-1.5 µg)	5 µl
Enzyme 1 (5-20 U/µl) NEB or Roche	0.5 µl
Enzyme 2 (5-20 U/µl) NEB or Roche	0.5 µl
H_2O	11 µl

Thermocycler program used to digest:

1	Digestion	37 °C	1-3 h
2	Enzyme denaturation	60 °C	10 min

4.3.2.5 Ligation and bacteria transformation

10x Ligation buffer Roche	2 µl
Linearized vector (10-50 ng/ µl)	Up to 10 µl
Digested insert (10-50 ng/ µl)	Up to 10 µl
DNA Ligase (5-20 U/µl) NEB or Roche	1 µl
H_2O	To 20 µl

DNA fragments for ligation were purified from 1 % agarose gel using Gel and PCR Clean-up KIT (Sigma or NucleoSpin) according to the manual. Obtained clean DNA of concentration ranging from 10 to 50 ng/µl was used for ligation. The reactions were prepared to obtain molar ratio of insert to vector of 1:1, 3:1 or 6:1. The ligation mix was incubated in 20 °C for 2 hours and then in 16 °C for 16 hours. Chemically competent cells were transformed with 10 µl per 100 µl bacteria. Bacteria were incubated on ice for 10 minutes alone, then 15 minutes with the DNA. Bacteria were heat shocked for 45 sec in 42 °C, then put on ice for 2 minutes and recovered in 500 µl LB medium for 1 hour in a 37 °C shaker incubator. Bacteria were plated on LB plates with a respective antibiotic, 50 µl on one plate and 250-450 µl on the other and incubated overnight at 37 °C. Obtained colonies were tested by colony PCR. A part of each colony was picked and dissolved in 20 µl of H_2O, then heated for 10 min in 95 °C and spinned down shortly. 1 µl was used as PCR template. The positive colonies were picked and grown in 5 ml LB with antibiotic overnight for plasmid isolation. Plasmid mini purification KIT (Sigma or NucleoSpin) was used to isolate the plasmid DNA that was used for restriction digestion to analyze the ligated DNA. Positive clones were sent for sequencing (Sigma-Aldrich Bar Code Economy Run) and the obtained sequence was verified using ApE computer program.

4.3.2.6 DNA preparation for injection

To prepare plasmid DNA for injection into zebrafish embryos, Midi plasmid purification KIT was used (Sigma or NucleoBond). 30 min before the injection DNA was dialyzed on 0.25 µm nitrocellulose filters over H_2O. 20-100 ng/µl DNA concentration was used for injections.

4.3.2.7 Plasmids used for transgenic fish generation in this study

pG1 flk1MCS_tol2_tdEos2

Eos2 fluorescent photoconvertible protein sequence (McKinney 2009) was inserted in 2 copies (tandem Eos2, tdEos2) into pBS_II vector (Alexandru Denes). The pBS_II_tdEos2 was used to amplify the tdEos2 and inserted with EcoRI/NotI into pG1flk1MCS_tol2 expression vector. 7.5 ng/µl of the vector together with 6 ng/µl Tol2 Transposase was injected into 1-cell-stage zebrafish embryos that were screened for transient expression at 24-48 hpf. Positive embryos were grown separately and screened for germ line transmission.

pG1 flk1MCS_tol2_mKate2-3NLS

pmKate2-N (Evrogen) was used to amplify the mKate2 sequence that was ligated with the 3NLS synthesized sequence and inserted into the pBSII vector using PstI/BamHI/XbaI restriction sites. The mKate-3NLS sequence was subsequently inserted into the pG1flk1_tol2 vector. 7.5 ng/µl of the vector together with 6 ng/µl Tol2 Transposase was injected into 1-cell-stage zebrafish embryos that were screened for transient expression at 24-48 hpf. Positive embryos were grown separately and screened for germ line transmission.

4.4 Genotyping of *ve-cadherin* mutant fish and embryos

4.4.1 Fin clips

Adult fish were genotyped using a clip of fin tissue as the DNA source. A fish was anesthetized in 1 x tricaine solution in egg water. The fish was put on a sterile plastic dish and the tip of the tail was cut using ethanol (70 %) sterilized razor blades. The tissue was immediately put in 200 µl of DNA extraction buffer with proteinase K and kept on ice. The fish was kept in egg water with methylene blue for recovery.

The fins were digested over 12 h in 50 °C heated shaker, and then heated for 10 min in 95 °C to deactivate the enzyme. 1 µl of the solution was used for PCR.

4.4.2 Single embryo PCR

Single embryos were digested in 50 µl DNA extraction buffer for 4-12 h, following the protocol above.

4.4.3 PCR protocol and primers

The PCR was designed to distinguish the VE-cadherin mutant and wild type embryos. 4 primers used in one reaction result in products of different size for the mutant and the wild type embryos (Krudewig et al. in preparation).

PCR mix:

10x Titanium Taq DNA Polymerase Buffer	5 µl
dNTPs MIX 10mM	1 µl
Primer Forward 1 10 µM	1 µl
Primer Forward 2 10 µM	1 µl
Primer Reverse 1 10 µM	1 µl

Primer Reverse 2 10 µM	1 µl
Template genomic DNA (see above)	1 µl
Titanium Taq DNA Polymerase (50x)	0.5 µl
H_2O	38.5 µl

Primers:

VE-CAD-EX3-FWD''2b	TTGGTGTAACTGACAATGGGG
VE-CAD-WT-FWD''2	ATCCCCGTTTTCGATTCTGAC
VE-CAD-UBS8-REV''1	CTGATGGATCCAGATTGGAAT
VE-CAD-EX4-REV''1b	ACAGTCTTGGTGTTACCATTGGG

PCR program

1	Initial denaturation	96 °C	2 min	
2	Denaturation in cycle	96 °C	30 sec	Repeat in cycle 35 times
3	Primer anniling	66 °C	30 sec	
4	Elongation	70 °C	20 sec	

Data analyses

The PCR relies on competition of primers that bind to the wild type (VE-CAD-WT-FWD''2) or mutated (VE-CAD-UBS8-REV''1) *ve-cadherin* genomic sequence, resulting in the product of different sizes (~300 bp for the mutant and ~500 bp for the wild type).

This allows differentiation between wild type, homozygous mutant and heterozygous fish. The method is described in detail in Krudewig et al. (in preparation).

4.5 Immunostaining of fish embryos

4.5.1 Embryo fixation

Zebrafish embryos of the chosen developmental stage (24-48 hpf) were decorionated and fixed in 2% PFA (4% PFA stock mixed 1:1 with 1xPBST 0.1 % Tween) at 4 °C overnight in 2 ml Eppendorf plastic tubes (10-30 embryos per tube). After fixation, embryos were washed minimum 4 times for 5 minutes in 1x PBST in RT with intensive shaking.

4.5.2 Staining protocol

4.5.2.1 Permeabilization and blocking

Embryos were incubated in 1 ml 0.5 % Triton-X-100 in PBST for 15-30 min in RT with shaking. Embryos were incubated in 1 ml of Blocking Buffer at 4 °C overnight with shaking.

4.5.2.2 Primary antibodies

Embryos were incubated in 300 µl of the primary antibody solution (in Blocking Buffer) at 4 °C overnight. Embryos were washed in 1xPBST minimum 6 times over 3 hours.

Primary antibodies concentrations:

Specificity	Dilution	Host	Source
VE-cadherin	1:200	rabbit αzebrafish	H. G. Belting
ZO-1	1:1000	mouse αhuman	Zymed
Podocalyxin 2	1:200	rabbit αzebrafish	H. G. Belting
ESAM-a	1:200	rabbit αzebrafish	H. G. Belting

4.5.2.3 Secondary antibodies

Embryos were incubated in 300 µl of the secondary antibody solution (in Blocking Buffer) at 4 °C overnight. Embryos were washed in 1xPBST minimum 6 times over 4 hours.

Conjugate	Dilution	Host	Source
Alexa568	1:1000	goat αrabbit IgG	Invitrogen
Alexa633	1:1000	goat αrabbit IgG	Invitrogen
Alexa568	1:1000	goat αmouse IgG	Invitrogen
Alexa633	1:1000	goat αmouse IgG	Invitrogen

4.6 Confocal microscopy

4.6.1 Fixed embryo confocal imaging

After completion of the immunostaining procedure, the embryos were kept in 1xPBST at 4 °C. To mount the embryos for confocal imaging of the head vasculature the heads were detached with forceps and put on a glass slide in a drop of Vectashield mounting medium for fluorescence H-1000 (Reactolab S.A.) a cover glass was put on top with thick grease spacers.

4.6.2 Live embryo confocal imaging

For time lapse imaging of living embryos, the embryos older than 24 hpf were kept in 1xPTU solution to inhibit pigmentation. The fluorescence positive embryos were selected using a Leica MZ FLIII fluorescent stereomicroscope for presence of red and green fluorescence. Selected embryos were anaesthetized using tricaine and mounted in a 35 mm glass bottom petri dish (0.17 mm, MatTek), using 0.7% low melting agarose (Sigma) containing 0.01% tricaine and 0,003% PTU. The time lapse movies have the frame size of 512x512 or 1024x512 pixels. A standard z-stack consisted of 50-90 slices

with a step size of 0.7-1 µm. Stacks were taken every 5-12 minutes. All images are maximal z-stack projections. Leica TCS SP5 confocal microscope was used. Images were taken with objectives: 20x air, 40x water and 63x glycerol immersion.

4.6.2.1 Spinning disc microscope imaging

A 3i Spinning Disc microscope was used to perform high time resolution imaging. The embryos were mounted like before. The embryos were imaged using a 63x oil immersion objective. A standard z-stack consisted of 25-35 slices of 0.5 µm. Stacks were taken every 15 seconds.

4.7 Fish

4.7.1 Zebrafish husbandry and handling

Fish were maintained and bred according to standard protocols (Westerfield, 2000).

4.7.2 Zebrafish lines

Wild type lines:

Genotype	Source
AB/EK	W. Driever, Freiburg
EK/TL	W. Driever, Freiburg

Transgenic lines

Genotype	Source
Tg(*fliep*:GFF)[UBS2-4]	(Totong et al., 2011; Zygmunt et al., 2011)
Tg(*fli1a*:EGFP)[y1]	(Lawson and Weinstein, 2002)
Tg(*gata1a*:dsRed)[sd2]	(Chico et al., 2008)
Tg(*kdrl*:EGFP)[s843]	(Jin et al., 2005)

Tg(UAS:EGFP-ZO-1)[UBS5-6]	(Herwig et al., 2011)
Tg(UAS:VE.cadherinΔC-EGFP)[UBS12]	Lukas Herwig, this study
Tg(UAS:mRFP)	(Totong et al., 2011; Zygmunt et al., 2011)
Tg(*kdrl*:msna-EGFP)[is1]	(Wang et al., 2010)
Tg(UAS:KAEDE)[rk8]	(Hatta et al., 2006)
Tg(*kdrl*:tdEos2)[ubs15]	This study
Tg(*kdrl*:mKate2-3NLS)[ubs13]	This study
Tg(BAC:*kdrl*:mKate2-CAAX)[ubs16]	This study

4.7.3 Injection of DNA/RNA and Morpholino into zebrafish embryos

Plates for injections were prepared using 1 % Agarose solution in egg water. Hot Agarose solution was poured into Petri dish plates and a striated mold was inserted to create slots. After solidification of the Agarose, the molds were removed and plates were stored at 4 °C with egg water on top to prevent from drying.

The microinjection needles were pooled using Sutter Instrument Co. The needles were filled using a microloader (Eppendorf) and the end of the needle was broken with forceps. 0.5 – 5 nl drops were injected into 1-cell-stage zebrafish embryos.

Tnnt2 Morpholino sequence: 5′-CATGTTTGCTCTGATCTGACACGCA-3′

4.7.4 Generation of transgenic reporter lines

30-100 ng/µl of DNA was injected into the cell of 1-cell-stage embryos. 15-30 ng/µl of TOL2 RNA was co-injected, if needed. The embryos were screened for transient expression at 24-48 hpf. 100-200 positive fish were grown till adulthood and screened for germ line transmission.

5 Results

Contribution to publications
(chronological)

5.1 Vascular morphogenesis in the zebrafish embryo

Ellertsdóttir E, Lenard A, Blum Y, Krudewig A, Herwig L, Affolter M, Belting HG.

Developmental Biology;341(1), 56-65, Published online November 3, 2009.

Contribution:

I prepared all the figures in the review and contributed to discussions during writing of the manuscript.

Review

Vascular morphogenesis in the zebrafish embryo

Elín Ellertsdóttir, Anna Lenard, Yannick Blum, Alice Krudewig, Lukas Herwig,
Markus Affolter, Heinz-Georg Belting *

Department of Cell Biology, Biozentrum der Universität Basel, Klingelbergstrasse 70, CH-4056 Basel, Switzerland

ABSTRACT

During embryonic development, the vertebrate vasculature is undergoing vast growth and remodeling. Blood vessels can be formed by a wide spectrum of different morphogenetic mechanisms, such as budding, cord hollowing, cell hollowing, cell wrapping and intussusception. Here, we describe the vascular morphogenesis that occurs in the early zebrafish embryo. We discuss the diversity of morphogenetic mechanisms that contribute to vessel assembly, angiogenic sprouting and tube formation in different blood vessels and how some of these complex cell behaviors are regulated by molecular pathways.

© 2009 Elsevier Inc. All rights reserved.

Introduction

Branched tubular organs, such as the insect tracheal system or the vertebrate cardiovascular system, kidney or lung, are found throughout the animal kingdom. Formation of such tubular networks from precursor cells or tissues involves a variety of morphogenetic processes, such as tube formation, elongation, branching and fusion. These processes are brought about by complex cellular behaviors, which include cell polarization, cell migration, cell rearrangements, cell shape changes and cell division. Although tubular organs are extremely diverse in anatomy and function, the cellular activities that govern tube formation and branching morphogenesis appear to be quite similar (Baer et al., 2009; Andrew and Ewald, 2010). In this review, we describe the current understanding of blood vessel formation in the early zebrafish embryo. We are placing special emphasis on the morphogenetic processes that contribute to vascular development and discuss the regulatory components that accompany these events.

In vertebrates, the cardiovascular system constitutes a highly ramified network of tubes that transports gas, nutrients, hormones and metabolites throughout the body. It also has important roles in the regulation of homeostasis and wound healing and is involved in the pathology of numerous diseases including cancer and inflammation (Carmeliet, 2003). The cardiovascular system emerges as one of the first organs during embryonic development and retains morpho-

genetic plasticity in adult life. Blood vessels are an integral component of all organs and are vital not only for their function but also for their formation during embryonic development (Nikolova and Lammert, 2003; Red-Horse et al., 2007; Sakaguchi et al., 2008). Blood vessels are highly diverse: they differ in size and are specialized depending on their function and the tissue or organ they are embedded in (Aird, 2007; Rocha and Adams, 2009). In general, they consist of an inner epithelium (endothelium) lining the lumen; depending on the type of vessel, this endothelium is surrounded by a basal lamina and by mural cells, such as pericytes and smooth muscle cells, which both support and regulate the function of the endothelium (Armulik et al., 2005).

Over the last decade, the molecular pathways controlling vascular development have attracted much attention, and a large number of key molecules has been identified that regulate different aspects of blood vessel morphogenesis. The basic frameworks of the vascular anatomy are conserved among vertebrates, which makes it possible to assign homologies between distinct blood vessels and to directly compare the formation of these vessels in different vertebrate species (Isogai et al., 2001; see Fig. 1). The zebrafish embryo has proven to be a useful model to study vascular morphogenesis in vivo. The vasculature can be easily visualized using a variety of labeling techniques, such as endothelial specific expression of fluorescent protein or by microangiography (Fig. 1). Its small size, experimental accessibility, optical clarity and rapid development allow to observe cellular activities, such as cell migration, cellular rearrangements and cell divisions, as they occur during blood vessel formation in the embryo. It is also possible to follow cardiovascular mutant phenotypes for several days because oxygenation of the early zebrafish embryo does

* Corresponding author.
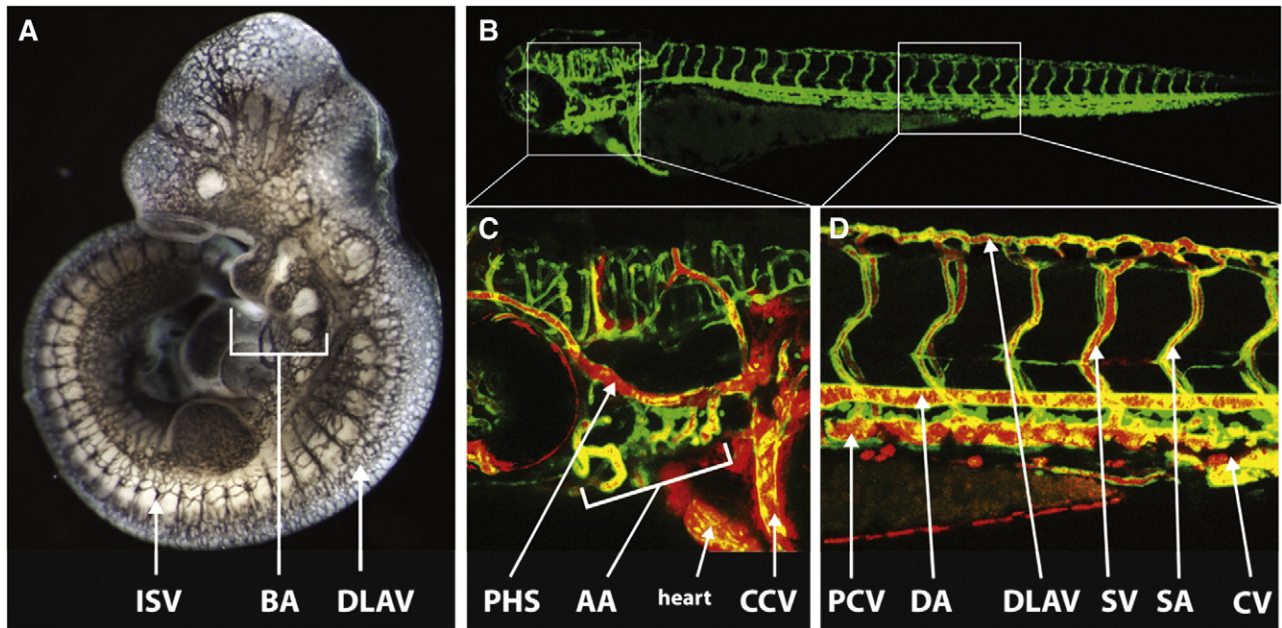*E-mail address:* heinz-georg.belting@unibas.ch (H.-G. Belting).

Fig. 1. The vascular system in mouse and fish embryos. (A) Visualization of the vascular system by immunohistochemical localization of PECAM-1 in a day 10 mouse embryo (photo courtesy of Ralf Adams, MPI, Münster, Germany). Owing to the opacity of the mouse embryo, only superficial blood vessels can be seen. BA: branchial arches (1st and 2nd); ISV: intersegmental vessel; DLAV: dorsal longitudinal anastomotic vessel. (B–D) The vascular system in a 3-day-old zebrafish embryo visualized by reporter gene analysis (*TG:flk1:EGFP* in green) and by microangiography using quantum dots (red in panels C and D). Some blood vessels are indicated according to Isogai et al. (2001). AA: aortic arches (1–6); CV: caudal vein; CCV: common cardinal vein; DA: dorsal aorta; PCV: posterior cardinal vein; PHS: primary head sinus; SA: segmental artery; SV segmental vein. At these stages, anatomical similarities between the two species are best observed in the branchial arches and in the ISV of the trunk. ISV and DLAV form quite similarly in both species (Isogai et al., 2003; Walls et al., 2008).

not rely on blood circulation. Furthermore, functional studies by forward and reverse genetics have shown that the molecular components that regulate vascular development are conserved between mammals and fish (Beis and Stainier, 2006; Lawson and Weinstein, 2002b; Thisse, 2002). Thus, the zebrafish embryo presents a unique system in which live imaging can be combined with functional studies to gain a more complete insight into how the molecular and morphogenetic mechanisms are integrated at the (sub)cellular level to shape the vascular tree.

Vasculogenesis

The formation of vertebrate blood vessels is commonly subdivided into two distinct morphogenetic processes, called vasculogenesis and angiogenesis. Vasculogenesis is defined by in situ aggregation of angioblasts into a blood vessel (Coffin and Poole, 1988; Poole and Coffin, 1989; Risau, 1995; Risau et al., 1988), while further sprouting of vessels from existing vessels occurs via a process called angiogenesis (Risau, 1995).

Origin and specification of endothelial cells

Angioblasts are precursors of endothelial cells not yet incorporated into blood vessels. They originate from the ventrolateral mesoderm (Kimmel et al., 1995; Stainier et al., 1995). Analyses of genes expressed in the hematopoietic and endothelial cell lineages have revealed a remarkable conservation between vertebrate species. In particular, transcription factors belonging to the ETS, GATA and LMO families have been shown to control specification of these lineages in mammals as well as fish (De Val et al., 2008; Detrich et al., 1995; Liu and Patient, 2008; Thompson et al., 1998; Zon et al., 1991). At the beginning of somitogenesis, transcription factors, such as *scl*/*tal1* and *lmo2*, which specify angioblasts and hematopoietic cells, are expressed in two domains along the body axis, the anterior and the posterior lateral mesoderm (Dooley et al., 2005; Liao et al., 1998; Patterson et al., 2007). During somitogenesis these cell populations

acquire unique gene expression profiles. For example, *flk1*-positive/*scl*-positive precursor cells differentiate into *flk1*-positive/scl-negative and *flk1*-negative/*scl*-positive cells, which will give rise to endothelial and hematopoietic cells, respectively (Gering et al., 1998). There seems to be no transcriptional factor regulating exclusively the endothelial specification but a combination of multiple factors with overlapping expression patterns (reviewed by De Val and Black, 2009).

Formation of the dorsal aorta and the cardinal vein

The basic anatomy of the initial embryonic circulatory system is quite similar among vertebrates. In addition, the first embryonic vessels to appear, the dorsal aorta (DA) and the posterior cardinal vein (PCV), are formed by a distinct morphogenetic mechanism called vasculogenesis in all vertebrates (Isogai et al., 2001). In zebrafish, angioblasts are specified well before the first blood vessels are formed. Expression of molecular markers such as *fli1a* shows that angioblasts are located in two lateral stripes at 12–14 hpf. By 28–30 hpf, the DA and the PVC can be discerned and are fully lumenized (Roman et al., 2002). In vivo imaging, using a *Tg(fli1a:EGFP)* reporter fish line, has shown that angioblasts migrate as individual cells towards the embryonic midline where they coalesce (Lawson and Weinstein, 2002b). During recent years, a considerable amount of research has focused on how this migration process is regulated, how these cells form the axial vessels and how DA and PCV are specified. As indicated in Fig. 2, the PCV forms subsequently to the DA (Eriksson and Löfberg, 2000; Herbert et al., 2009; Jin et al., 2005), and this relationship appears to be conserved among vertebrates (Coffin and Poole, 1988; Hirakow and Hiruma, 1981; Meier, 1980).

Formation of the DA in zebrafish has been studied by transmission electron microscopy (TEM) (Eriksson and Löfberg, 2000; Meier, 1980) and more recently by analysis of transgenic zebrafish embryos (Herbert et al., 2009; Jin et al., 2005; Lawson and Weinstein, 2002b). During vasculogenesis, angioblasts are attracted towards the midline by guidance cues thought to emanate from the endoderm
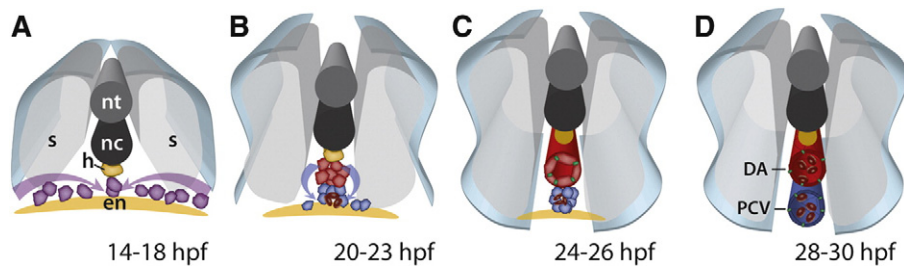
Fig. 2. Phases of vasculogenesis in the zebrafish embryo. Schematic cross sections of the trunk region at representative stages of development (according to Herbert et al., 2009 and Jin et al., 2005). (A) Medial migration. From 14 hpf onward, angioblasts (purple) that originate in the lateral plate mesoderm migrate over the endoderm towards the midline just below the hypochord, where they aggregate to form a vascular cord (B). (B) Arterio-venous segregation and ventral sprouting. At around 17 hpf, angioblasts start to express markers of arterio-venous differentiation, such as *ephrin-b2a* in arterial cells (marked in red). These cells are located in the dorsal portion of the vascular rod and will give rise to the DA, whereas *ephb4a* expressing cells are located more ventrally and will contribute to the PCV and CV. At 21 hpf, angioblasts located in the ventral part of the vascular cord start migrating ventrally and accumulate below the forming DA (B, C). (C) Lumen formation. The DA forms and lumenizes prior to the PCV and CV in the absence of blood cells (brown) by cord hollowing. Venous angioblasts aggregate and coalesce around the blood cells to ultimately form a tube. (D) Functional Vasculature. At 30 hpf, both vessels are fully formed and carry blood flow. Endothelial cell junctions are indicated in green.

(Jin et al., 2005; Fig. 2A). Once the angioblasts have reached the embryonic midline, they form aggregates and tube formation commences (Fig. 2B). TEM studies have shown that angioblasts initially form "aggregates of tightly packed cells" between hypochord and the underlying mesoderm (Eriksson and Löfberg, 2000). These aggregates are discontinuous along the anterior–posterior axis and the cells are spherical at the beginning of the process. At around the 17-somite stage (17.5 hpf), more flattened tube forming cells are found posterior to the 7th–9th somite in the fish embryo. From analysis of transgenic zebrafish, it has been suggested that endothelial cells migrate in two waves to the midline and it has been suggested that the first wave contributes to the DA while the cells of the second wave will form the primary vein (Jin et al., 2005). Alternatively, endothelial cells from both migratory waves may join in a single medial cord and segregate independently from this structure. The latter possibility has recently gained strong support from in vivo time-lapse analyses, which showed that the precursor cells of the caudal vein dissociate from the primordium of the DA by a process termed ventral sprouting (Herbert et al., 2009). Ventral sprouting is initiated around 20 h post-fertilization shortly before the emergence of dorsal sprouts, which will give rise to segmental arteries (SA) (see below) at a time when the DA is not yet lumenized. This finding together with the observation that the expression of the arterial marker *ephrinb2a* (*efnb2a*) is restricted to a subpopulation within the vascular cord suggested that the primary arteries and veins are derived from a common primordium that contains a mixed population of arterial as well as venous angioblasts (Herbert et al., 2009; Jin et al., 2005).

Specification of arterial versus venous fates has been shown to depend on the interaction of the VEGF and Notch signaling pathways (reviewed by Lawson and Weinstein, 2002a; Siekmann et al., 2008). Sonic hedgehog (SHH) signals from the notochord lead to an activation of *vegf-a* expression in ventral somites (Lawson et al., 2002). VEGF-A is sensed by the angioblasts via VEGF-receptor-2/ KDR/FLK1 (KDR-Like/KDRL in zebrafish), which leads to the activation of Notch signaling and the transcriptional activation of other factors which results in arterial differentiation in a subset of angioblasts (Cermenati et al., 2008; Lawson et al., 2003; Pendeville et al., 2008; Zhong et al., 2001). In contrast to arterial development, specification of venous fates is independent of VEGF-A signaling (Covassin et al., 2006; Lawson et al., 2003). In agreement with these concepts, modification of VEGF or Notch signaling levels influences the segregation and ventral sprouting behavior. Angioblasts showed excessive ventral migration, when VEGF-A and Notch signals were blocked, whereas downregulation of FLT4 led to a reduction in ventral sprouting (Herbert et al., 2009).

Arterial and venous specification of angioblasts is reflected by particular gene expressions (Lawson and Weinstein, 2002a). Notably,

two members of the Eph-ephrin subclass of the receptor tyrosine kinase family are differentially expressed in arteries (EphrinB2/*Efnb2*) and veins (EphB4) (Adams et al., 1999; Lawson et al., 2001). Genetic analyses in mouse have demonstrated an important role for bidirectional Ephb4-Efnb2 signaling for vascular morphogenesis (reviewed by Adams and Alitalo, 2007). In mouse and fish, EPHB4-Efnb2 signaling has been shown to be involved in sorting of neuronal cells, which leads to their segregation into adjacent hindbrain segments (Kemp et al., 2009; Mellitzer et al., 1999). To test whether these factors also play a role in the segregation of arterial and venous angioblasts in the primary vascular cord, Herbert and colleagues (2009) modified EPHB4a and EfnB2a levels and interfered with forward and reverse properties of EPHB4a-EfnB2a signaling. Either overexpression or knockdown of EPHB4a/Efnb2a function caused aberrant migration of transplanted angioblasts consistent with defects in arterio-venous segregation. Taken together, these findings show that repulsive EPH4a-EfnB2 signaling regulates arterio-venous segregation, thereby controlling the directionality of angioblast sprouting.

Anterior–posterior differences in artery formation

While the process of vasculogenesis has been best described in the dorsal aorta of the trunk, there is increasing evidence of regional differences in the way the primary vessels form and it has been proposed that distinct cues guide endothelial cells in different domains of the body (Coffin and Poole, 1991; Eriksson and Löfberg, 2000). In agreement with this view, several zebrafish mutants have been isolated that exhibit vascular defects in particular regions of the body (Jin et al., 2007).

Some experiments have shed light on the differences that regulate the formation of the DA of the trunk and the paired lateral dorsal aortae (LDA), which is located in anterior body regions. In an earlier study, the role of the endoderm for formation of the DA was examined in *casanova* (*sox32*) mutants that lack endoderm (Jin et al., 2005). In these embryos, medial migration of angioblasts was slowed but the DA formed normally, suggesting that endoderm is dispensable for DA formation. However, it has more recently been shown that the endoderm plays an essential role for LDA formation in the anterior region of the embryo (Siekmann et al., 2009). Strikingly, mutants for the chemokine receptor *cxcr4a*, which is expressed in the LDA, lack the LDA. CXCR4 is known to bind to CXCL12, which is specifically expressed in the anterior endoderm underlying the developing LDA. Furthermore, loss of CXCL12 function phenocopies the *cxcr4a* deficiency. These findings illustrate the molecular diversity in endothelial cells and the importance of local extrinsic cues for the formation and patterning of the primary aorta.

Transforming a cord into a tube: lumen formation in the primary blood vessels

The morphogenesis of biological tubes has been a longstanding interest in developmental biology and it has been shown that tubes can form in very different ways (Baer et al., 2009; Lubarsky and Krasnow, 2003). After angioblasts have aggregated into a cord-like structure, they ultimately have to assemble a tube. This could in principal occur by different morphogenetic processes, including (i) cell hollowing, where cells form vacuoles that fuse between cells to form a continuous intracellular lumen; (ii) wrapping, where cells migrate in a polarized state and surround the future lumen; (iii) cord hollowing, where cells within the cord attain apical–basal polarity and the lumen is formed by membrane separation and fluid influx; or by (iv) cavitation, where cells in the middle of the rod undergo apoptosis leaving a luminal space behind (Hogan and Kolodziej, 2002; Kucera et al., 2007; Lubarsky and Krasnow, 2003).

Tube formation of the DA has been studied at the cellular level by transgenic and immunofluorescent analyses in zebrafish embryos (Jin et al., 2005). Shortly after angioblasts have formed a cord, the DA begins to lumenize (21 hpf; Figs. 2B, C). Analysis of proteins involved in apical–basal polarization, such as fibronectin or β-catenin, has shown that this process is preceded by endothelial polarization and the formation of junctions between ECs, suggesting that a cord hollowing process forms the lumen of the DA. At the 20-somite stage (19 hpf), cell junctions, as visualized by ZO-1 and Claudin5, are discernable between the cells forming the dorsal aorta (Jin et al., 2005). The mechanisms of lumen formation in the zebrafish dorsal aorta and caudal vein have recently been examined by in vivo time-lapse analyses (Herbert et al., 2009). These studies confirmed a cord hollowing mechanism in the DA, whereas the lumen of the CV is formed by ventrally sprouting venous angioblasts that coalesce around resident blood cells. This mode of lumen formation has not been described before and it is likely to be different from cell wrapping as described above because the sprouting angioblast do not seem to migrate as an epithelial sheet of cells.

In a recent, comprehensive study, lumen formation of the paired dorsal aortae has been examined in the mouse embryo (Strilić et al., 2009). By anatomical and immunofluorescent analyses, Strilić and colleagues show that the lumen of the dorsal aortae forms in discrete steps similar to those observed in the zebrafish and, for the first time, they were able to decipher the molecular mechanisms involved in this process. Consistent with observations in zebrafish, the first steps of lumen formation are initiated upon formation of intercellular adherens junctions between angioblasts. Junctional remodeling then leads to an apical interface between adjacent ECs, followed by an accumulation of anti-adhesive CD34-sialomucins, such as CD34 and Podocalyxin (PODXL). Proper localization of these proteins to the apical surface depends on the presence of VE-cadherin. The subsequent formation of the aortic lumen is driven by a VEGF-A-dependent constriction of the apical surfaces as well as EC elongation induced by the F-actin cytoskeleton. These cell shape changes apparently rely on interactions between Moesin with CD34-sialomucins, which lead to an apical localization of F-actin. This view is supported by the analysis of Moesin and of *Podxl* mutants which both exhibit reduced levels of apical F-actin and a delay in aortic lumen formation. Furthermore, loss of *Podxl* leads to a reduction of Moesin at the sites of endothelial contacts, suggesting that PODXL connects with Moesin in order to recruit F-actin.

In summary, these studies indicate that the morphogenetic mechanisms that drive lumen formation in the dorsal aorta/aortae have been conserved between teleosts and mammals. In either case, coalescence of ECs and subsequent apical–basal polarization of a vascular cord appear to be the primary steps. The lumen is then formed between apical surfaces of apposing ECs by a cord hollowing process. Whether the molecular mechanisms that underlie lumen

formation are conserved between fish and mouse remains to be determined. Furthermore, it will be interesting to learn about the morphogenetic processes that may be required to further inflate the lumen.

Angiogenesis

While the primary axial vessels are formed by vasculogenesis, elaboration of the vasculature, i.e. the formation of secondary blood vessels, occurs via angiogenesis, a process by which new blood vessels are generated from a pre-existing one. However, with respect to morphogenetic cell behaviors, angiogenesis can occur in quite different ways. Originally, it has been described as a sprouting process, by which a new vessel is branching off a primary vessel (reviewed by Patan, 2000). In addition to sprouting, a considerably different mode of angiogenesis called intussusception has been described in mammals (reviewed by Makanya et al., 2009). During intussusceptive angiogenesis, a vessel splits along its longitudinal axis into two new branches, thus effectively enlarging the vascular surface area. This process plays an important role in vascular remodeling during plexus formation. In zebrafish, angiogenesis by intussusception has not yet been described and therefore we focus our discussion on sprouting angiogenesis.

Sprouting angiogenesis

Sprouting angiogenesis was described as a general mechanism of microvascular growth during the 1970s, and its relevance for tumor growth and metastasis was soon recognized (Folkman, 1982). Early on angiogenesis was studied in a variety of in vivo and tissue culture systems such as the chorion allantoic membrane of the chick or the corneal pocket (reviewed by Patan, 2000). As an outcome of these studies, sprouting angiogenesis was described as a sequence of events that include (i) migration of ECs toward the angiogenic stimulus, (ii) alignment of ECs in a bipolar mode, (iii) lumen formation and cell divisions distant to the tip of the sprout and (iv) connection of individual sprouts to initiate circulation (Ausprunk and Folkman, 1977; Patan, 2000).

In recent years, much progress has been made in establishing systems in which angiogenic processes can be followed in detail. These include the retinal vasculature of the mouse, which develops postnatally, and the zebrafish embryo, in which all aspects of angiogenesis can be followed in vivo. Embryonic vasculogenesis and angiogenesis in zebrafish occur in ways very similar to those in mammals. In contrast to the latter, zebrafish embryos do not require extra-embryonic vasculogenesis due to their extrauterine development. This greatly facilitates the analysis of embryonic blood vessel formation, as it is not influenced by prior extra-embryonic events. Although all major blood vessels are easily accessible in the zebrafish embryo, the intersegmental blood vessels (ISV) have been most thoroughly studied because of their metameric organization and relatively simple anatomy.

ISV formation in the zebrafish embryo

Formation of ISVs in the zebrafish embryos involves two waves of angiogenic sprouting (Isogai et al., 2003). ECs of the primary wave form the segmental arteries (SA). During the primary wave, ECs sprout from the DA at ~22 hpf. These sprouts grow dorsally and – once they have reached the level of the dorsal neural tube – connect with their neighbors from anterior and posterior segments to form the future dorsal longitudinal anastomotic vessel (DLAV). The second wave, which starts at 32 hpf, involves ECs from the PCV (Yaniv et al., 2006). These sprouts will either connect to an existing SA, thereby transforming it into a vein (SV), or, alternatively, they will grow up to the level of the horizontal myoseptum and form a population of cells

named parachordal lymphangioblasts (PLs) (Hogan et al., 2009; Isogai, 2003). The majority of these cells eventually migrates away from the horizontal myoseptum and contributes to the lymphatic vasculature (Hogan et al., 2009).

Formation of the SA has been described in detail by in vivo time-lapse and immunofluorescent analyses (Blum et al., 2008; Childs et al., 2002; Isogai et al., 2003; Lawson and Weinstein, 2002b). These studies have led to several models of SA morphogenesis. While earlier studies suggested that the SA is made up by 3 cells that are arranged serially in a head to tail fashion (Childs et al., 2002), mosaic analyses and the analysis of endothelial cell junctions showed that SAs are composed of 4–6 cells that extensively overlap along the proximodistal axis of the vessel (Blum et al., 2008). Taken together, these findings suggest a model of SA formation, as shown in Fig. 3. Initially, one or two cells migrate out of the epithelium of the DA forming the sprout (Fig. 3A). During dorsal outgrowth, this sprout consists usually of 3–4 cells, one tip cell and two or three stalk cells (Fig. 3B). When the tip cell has made contacts with its anterior and posterior neighbors, the basic scaffold of the SA is formed (Fig. 3C). Because of cell divisions that occur at varying time points, the stalk can consist of a variable number of cells generating a large degree of morphological heterogeneity, which is illustrated by the variation of junctional patterns (Blum et al., 2008). However, further cell divisions and cellular rearrangements during vessel assembly lead to a paired configuration of cells along the proximodistal extent of the SA, which then forms a lumen. In the following section, we discuss some of the morphogenetic and molecular mechanisms that govern the different aspects of SA formation. Since much progress has also been made in other angiogenesis models, we will discuss them in comparison with SA formation.

Sprouting of SA and SV appears to be triggered by different signals. For example, VEGF-A is critical for SA formation, while it appears dispensable for SV formation, since SV sprout normally in embryos that are mutant for phospholipase C-γ (plc-γ , which is a downstream mediator of VEGF-A/VEGFR-2 signaling; Bahary et al., 2007; Habeck et al., 2002; Lawson et al., 2003; Nasevicius et al., 2000; Covassin et al., 2009; Covassin et al., 2006). Here, we will focus on the morphogenesis of the SA. The regulation of angiogenesis by VEGFs and their receptors has been studied in many previous publications in great detail (reviewed by Cébe-Suarez et al., 2006; Matsumoto and Mugishima, 2006; Olsson et al., 2006; Shibuya and Claesson-Welsh, 2006; Yamazaki and Morita, 2006). While early studies focused on general pro-angiogenic functions of VEGF signaling, more specific roles for VEGF signaling in patterning of angiogenic sprouts have recently been revealed (Covassin et al., 2006; Gerhardt et al., 2003; Ruhrberg et al., 2002). Upon VEGF-A/VEGFR-2 signals, ECs initiate the angiogenic

program, which entails the loosening of junctional connections with neighboring cells, migratory behavior towards the angiogenic stimulus and cell division (reviewed by Lampugnani and Dejana, 2007). Cells within the nascent sprout respond in different ways to the VEGF-A. Whereas cells located at the base (termed stalk cells) show increased rates of proliferation, the leading cell (termed tip cell) sends long and dynamic filopodia into the surrounding environment to guide the growing sprout towards the stimulus (Gerhardt et al., 2003). Endothelial tip and stalk cells do not only have different functions and behaviors (discussed below), they also show differences in gene expression. For example, Platelet derived growth factor B (Pdgfb) and Flt4 are expressed at higher levels in the tip cell than in the stalk cell (Gerhardt et al., 2003; Siekmann and Lawson, 2007).

Patterning and angiogenic behavior of sprouts are regulated by the cooperation of the Notch and VEGFR-2 signaling pathways (Hellström et al., 2007; Siekmann et al., 2008; Siekmann and Lawson, 2007; Suchting et al., 2007; reviewed by Phng and Gerhardt, 2009; Siekmann et al., 2008). The tip cell, receiving the highest level of VEGFR-2 signal, responds with an upregulation of the Notch ligand Delta-like-4 (DLL4), which leads to increased intracellular Notch signaling in the neighboring stalk cells (Hellström et al., 2007). In zebrafish, loss of DLL4 function leads to prolonged angiogenic activity in the ISVs, whereas over-activation of Notch signaling leads to a quiescent phenotype (Leslie et al., 2007; Siekmann and Lawson, 2007). DLL4 also regulates angiogenesis by suppressing VEGF-C dependent FLT4 (VEGFR-3) signaling in endothelial cells in mouse and fish (Hogan et al., 2009; Tammela et al., 2008). In zebrafish, VEGF-C/FLT4 signaling is required for venous and lymphatic development (Covassin et al., 2006; Küchler et al., 2006). However, a "kinase-dead" allele of FLT4 is able to rescue the hyperbranching phenotype caused by the loss of DLL4 function (Hogan et al., 2009). Furthermore, in the absence of DLL4, arterial cells become more sensitive to varying levels of VEGF-C in the embryo (Hogan et al., 2009). These experiments point out a mechanism for how different endothelial lineages can respond specifically to sources of VEGF-C in the trunk. Venous and lymphatic cells, which do not express dll4, are able to respond to VEGF-C/FLT4, whereas in arterial cells this pathway is inhibited by DLL4 (Hogan et al., 2009).

Although the molecular mechanisms that control angiogenic behavior in the sprout may not be identical in fish and mouse, there is a common theme in that differences in intracellular Notch signaling confer different cell behaviors along the proximodistal axis of the sprout. Tip cells (low Notch) extend numerous filopodia, are highly migratory and thus display the strongest angiogenic behavior while the proximal stalk cells (high Notch) appear less migratory. It has
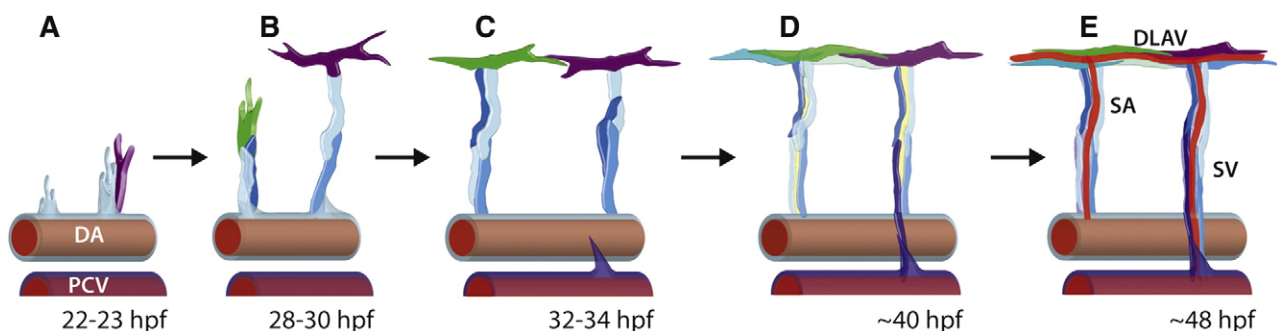
Fig. 3. A model for the morphogenetic events that lead to the formation of ISV and DLAV in the Trunk. Two neighboring sprouts are depicted as representative examples. The leading cells are indicated in green and purple, respectively. At 22 hpf ECs of the DA form sprouts (A) that grow along the somite boundaries up to the dorsal roof of the neural tube (B). During these stages, the sprout consists of 2 to 4 cells that are stabilized by interendothelial junctions (not indicated). At the dorsal side of the embryo, the tip cells send extensions toward their anterior and posterior neighbors to establish connections. During this phase, the ECs establish a scaffold consisting of a vascular cord that is not yet lumenized (B, C). Further cell rearrangements and cell divisions lead to formation of a continuous apical surface that may surround initial luminal spaces (yellow) (D). At around 32 hpf, a secondary wave of angiogenic sprouts emerges from the PCV. These sprouts either generate a group of lymphatic cells, called parachordal lymphangioblasts (not shown), or connect with the adjacent primary vessel (D, on the right), which will become a segmental vein. Blood flow in ISVs commences after SA, SV and DLAV have been established (E).

been proposed that the reduced migratory behavior of stalk cells is important to maintain sprout integrity and connection to the DA (Siekmann et al., 2008).

While the general aspects of angiogenesis in the ISVs of the fish and the postnatal vasculature of the mouse retina are very similar, there appear to be differences in gene expression and pattern of cell proliferation. While in the mouse retina cell proliferation is largely restricted to the stalk (Gerhardt et al., 2003), in fish similar rates can be observed in stalk and tip cells (Blum et al., 2008). Furthermore, based on gene expression—intersegmental sprouts in the fish appear not as polarized as those in the mouse retina. In contrast to the mouse retina, the tip cell markers *dll4* and *flt4* are quite uniformly expressed in tip and stalk cells of the sprouting SA (Hogan et al., 2009; Leslie et

al., 2007; Siekmann and Lawson, 2007). Similar to zebrafish, ISV sprouts in the mouse embryo show a relatively even distribution of DLL4 protein (Tammela et al., 2008). These differences between distinct types of blood vessels raise the possibility that, compared to the mouse retina, the state of the tip cell in ISV is less defined. It will be interesting to see whether these differences are due to different interpretations of VEGF/Notch signals or whether they are connected to different morphogenetic processes occurring in the two systems (see below).

How the angiogenic sprout lumenizes is still controversial. Different morphogenetic behaviors and cellular configurations in the sprout can have significant impact on how a vessel is formed. In principle, there are at least 3 different morphogenetic processes of tubulogenesis that may occur in an angiogenic sprout: budding, cord hollowing or cell hollowing (see Fig. 4A). When a novel tube is formed by budding, the ECs that follow the tip cells maintain their epithelial character with a defined apical–basal polarity. During budding, the luminal space of the sprout remains continuous with that of the parent vessel, extending up to the tip cell. Tube branching by budding has been described in many experimental systems including the tracheal system in *Drosophila* and several branched organs in mammals (Baer et al., 2009). Vessel branching by budding appears to occur in larger caliber capillaries that are constantly perfused. In the mouse retina, the lumen is located immediately adjacent to the tip cell (see Fig. 4B). In addition, in vivo time-lapse recording of blood vessels in the zebrafish brain appears consistent with such morphogenetic mode of tubular branching (Huisken and Stainier, 2009).

Formation of ISV does not occur by budding since the initial sprouts do not contain a lumen continuous with the DA (Fig. 4C). Rather, the lumen becomes patent at the time when SA, DLAV and SV have formed proper connections. After labeling circulating blood with fluorescent tracer dyes, it was observed that (from the perspective of the DA) the lumen opens up in a stepwise manner from proximal to
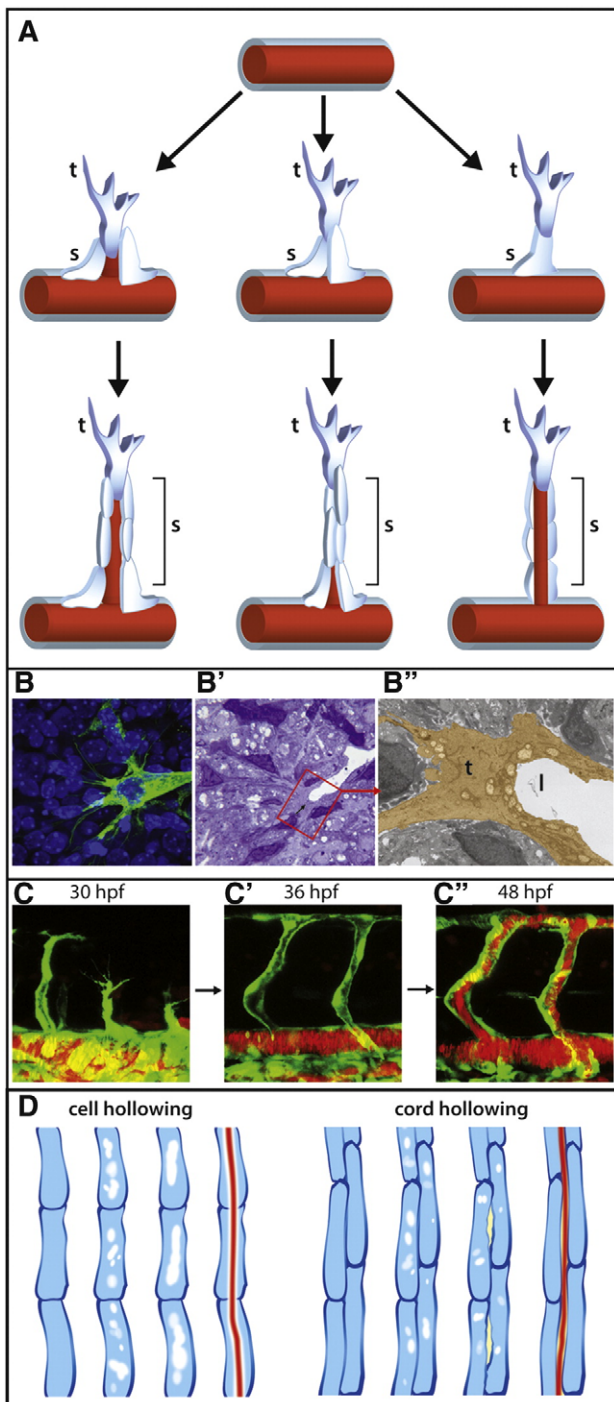

Fig. 4. Different morphogenetic mechanisms that underlie sprouting angiogenesis. (A) Three examples for the cellular organization of an angiogenic sprout. Depending on how the cells are arranged in the sprout, different types of vessels may form. Left: Branching morphogenesis by budding. ECs remain epithelial, while the sprout grows via cell division within the stalk. The lumen remains open and continuous at all times. Middle: Formation of a multicellular tube by cord hollowing. This shows an example, where cells grow in a paired configuration maintaining an apical surface in between. The lumen remains open at the base but is closed in distal region. Close to the tip, cells may be of a more mesenchymal character and undergo cell divisions. Cellular rearrangements will then lead to a continuous apical surface and open up the luminal space. Right: Formation of a unicellular tube with an intracellular lumen. At the tip of a capillary, the lumen may also form within a string of cells. The cells hollow out by vacuole formation followed by exocytosis. This mode of lumen formation will generate a so-called intracellular lumen. (B) Lumen formation behind the leading tip cell in the mouse retina. The lumen of the nascent sprout extends to the tip of the growing sprout. This situation is in agreement with the configuration shown in panel A. Isolectin B4 labeling (green) of an endothelial tip cell projecting long filopodia. Nuclei, Dapi, blue (B). Semithin (B′) and close up of ultrathin (B″) en face section of the sprouting front in the retina illustrating continuous lumen formation (l) just behind the tip cell (t). The endothelial tip cell in panel C is pseudocolored brown. Figure courtesy of Denise Stenzel and Holger Gerhardt, London Research Institute—Cancer Research UK. © Gerhardt et al., 2003. Originally published in J. Cell Biol. doi:10.1083/jcb.200302047. (C) Lumen formation in the ISV and DLAV of a zebrafish embryo. During scaffold formation, neither ISV nor DLAV are perfused, suggesting that the lumen is formed subsequently. Blood flow is initiated after subsequent remodeling and establishment of the intersegmental veins (compare to Fig. 3). Confocal still pictures from an in vivo time-lapse movie of a transgenic zebrafish embryo (*TG:fli1a:EGFP^y1;gata1:DsRed^sd2*). ECs are labeled in green; erythrocytes are labeled in red. (D) Alternate models of lumen formation in the zebrafish ISV. Depending on the cellular arrangement of cells in an angiogenic sprout, de novo lumen formation can occur in at least two different ways. If cells are arranged in a serial fashion, the lumen may be generated by cell hollowing (left, see also A). In this process, ECs pinocytose solutes from extracellular space and form vacuoles that coalesce and fuse to give rise to an intracellular lumen. Eventually intracellular vacuoles of neighboring cells will fuse by exocytosis and form a patent lumen (see Kamei et al., 2006). Alternatively, if cells are arranged in a paired fashion, they may form a lumen by cord hollowing (right, see also A). This process requires establishment of a continuous apical surface that is bounded by at least two ECs. Vacuoles can then be exocytosed into this intercellular space, which will eventually become the vascular lumen.

distal (Kamei et al., 2006). Because vacuole formation and fusion has long been considered an important component of lumen formation, the stepwise expansion of luminal space was interpreted as a succession of vacuolar fusion events that generate a unicellular tube containing an intracellular lumen (Kamei et al., 2006; Fig. 4D). Capillaries that contain intracellular lumens have indeed been described (Bar et al., 1984) and have been called "seamless tubes" because they are characterized by the absence of cell junctions along the longitudinal axis of the vessel. More recently, analyses of cell junctions within nascent sprouts and patent ISVs showed that the cells in the stalk overlap extensively along the proximodistal axis and that ISVs are multicellular tubes containing an extracellular lumen (Blum et al., 2008). This cellular configuration is more consistent with a lumen formation process by cord hollowing (Fig. 4D). In this model, cells in the stalk rearrange to form a continuous apical surface. The lumen is then formed by a process, in which small pre-luminal spaces (rather than vacuoles) are formed by exocytosis and/or paracellular influx of liquids. The stepwise opening of the lumen from the direction of the aorta would then be consistent with the completion of cell rearrangements in the stalk. The events described here would be quite comparable to those described above for the lumen formation in the dorsal aorta.

The three mechanisms discussed here are not necessarily mutually exclusive. For example, it is possible that sprouting angiogenesis contains aspects of both, budding and chord hollowing, depending on the extent to which apical–basal polarity is maintained in the stalk cells. Likewise, it is possible that a single blood vessel contains regions of intracellular as well as regions of extracellular lumen. Taken together, it is clear that different vessels can form by various morphogenetic mechanisms. It remains to be explored what the decisive factors are that determine which mechanism is used. It is likely that parameters such as vessel caliber, blood pressure of the parental vessel as well as cell number within the sprout play important roles.

Guidance cues along the way—endothelial pathfinding

To effectively oxygenate a given organ, blood vessels have to be evenly distributed within this tissue. This can be achieved in different ways, for example by controlling the number of angiogenic sprouts that are generated (e.g. ISV) or by the formation of a plexus (e.g. retinal vasculature in the mouse), which is then remodeled by a pruning process. In recent years, a number of ligands (and their respective receptors) that provide endothelial guidance cues have been described, including the Semaphorin, Netrin, Ephrin and Slit systems (reviewed by Larrivée et al., 2009). Interestingly, these signals were originally described as cues for axonal growth cones (reviewed by Eichmann et al., 2005). It has become clear since that many of the signaling pathways that act during axonal pathfinding are also employed for guidance of angiogenic sprouts.

In the zebrafish, the guidance of angiogenic sprouts is best studied during SA formation. Segmental arteries sprout from the DA at the intersomitic boundary; as they grow out, they follow the intersomitic fissure up to the horizontal myoseptum, from where they change their path to grow more or less straight to the dorsal roof of the neural tube. The exit point of intersegmental sprouts is regulated by molecular guidance cues. In *out of bounds* (*obd*) mutants, angiogenic sprouts form ectopically along the ventral somite border (Childs et al., 2002). Furthermore, these sprouts no longer avoid the ventral somite and the ISVs take on a plexus-like organization. Molecular analyses showed that *obd* encodes the receptor PlexinD1 that is expressed in ECs and interacts with the ligands SEMA3A1/2, which is expressed in ventral somites. Upon ligand binding, a repulsive signal is activated in the ECs prohibiting them from moving into the somite region (Torres-Vazquez, 2004). Recently, it has been shown that the interaction of different Plexins and Semaphorins is also important for the timing of SA sprout formation (Lamont et al., 2009).

Analyses in mouse have uncovered an additional and quite different molecular mechanism that limits the number of sprouts. Bautch and coworkers have shown that a soluble form of FLT-1 (VEGFR-1), sFLT-1, is secreted from ECs adjacent to the forming sprout (Chappell et al., 2009). This isoform is able to bind VEGF, thereby removing it from the environment surrounding the sprout. It is thought that sFLT-1 serves two purposes: it ensures the ordered formation of sprouts from an activated endothelium and it prevents the early sprout to connect back to its original vessel.

The sharing of attracting and repulsive signaling pathways by neurons and ECs appears to be a common theme. In fact, it has been shown that growing neurons and nascent capillaries can walk the same tracks (Mukouyama et al., 2002). It will be interesting to see whether in these instances neurons and ECs simply use the same cues provided by the stromal cells or whether they also navigate by direct cell–cell interactions. It is noteworthy that not only the tip cell but also stalk cells appear to express guidance receptors albeit at lower levels (Larrivée et al., 2009). In zebrafish, for example, the guidance receptor *PlexinD1* is expressed at comparable levels in the tip and the stalk of nascent SA (Torres-Vázquez et al., 2004). This raises the possibility that also stalk cells are involved in angiogenic pathfinding. Indeed, it appears that the tip cell fate is not fixed and that cells at the stalk can become tip cells and vice versa. In murine allantoic explant cultures, migratory ECs are passing each other at the tip (Perryn et al., 2008). In a similar fashion, ECs are changing lead during the outgrowth of vascular cords that sprout from differentiating murine embryonic stem cells (Holger Gerhardt, personal communication). It has been suggested that these tip cell turnovers are regulated by oscillations in Notch signaling along the vascular sprout (Phng and Gerhardt, 2009). It should be noted that these vascular cords are not perfused during early outgrowth and are, in that respect, similar to developing SAs rather than vessels in the postnatal mouse retina.

Cell–cell adhesion during sprouting angiogenesis

The above observations indicate that the angiogenic sprout is highly plastic with regard to signaling events and cell–cell interactions and that cellular rearrangements play an important role in blood vessel morphogenesis. It is generally believed that cellular rearrangements involve remodeling of intercellular junctions (Baer et al., 2009). In *Drosophila*, adherens junctions play an important role for cellular rearrangement during various processes, such as border cell migration or tracheal morphogenesis (Pacquelet and Rørth, 2005; Ribeiro et al., 2004). In the case of border cell migration very different cell behaviors, invasive cell migration and cell adhesion require DE-cadherin. These distinct cellular activities are mediated by homophilic interactions of DE-cadherin between different cell types: interactions among border cells maintain cohesion of the migratory cells while interactions between border cells and nurse cells allow invasive migration into the substratum (Niewiadomska et al., 1999). The role of VE-cadherin during vertebrate angiogenesis is less clear. Mice that are mutant for VE-cadherin die at mid-gestation exhibiting vascular defects that are consistent with a role for VE-cadherin in maintaining vascular integrity (Carmeliet et al., 1999; Crosby, 2005). Further in vitro analyses have also emphasized a role of VE-cadherin in endothelial cell survival and stabilizing the endothelium, in part by antagonizing VEGFR-2 signaling (reviewed by Lampugnani and Dejana, 2007; Vestweber et al., 2009). Recent organotypic cell culture and knockdown experiments in zebrafish point at a role of VE-cadherin in angiogenic sprouting (Abraham et al., 2009). In these studies, quiescent endothelial tubes did not respond to VEGF stimulation unless VE-cadherin function was reduced. They further showed that VE-cadherin suppresses sprouting by inhibiting VEGF-R2/RAC1 signaling. In the zebrafish ISV, knockdown of VE-cadherin led to the formation of ectopic "branch points" along the proximo-

distal axis of the ISV, which were interpreted as prolonged angiogenic behavior of the ECs within the ISV.

While the above results suggest an anti-angiogenic function, other studies indicate a more pro-angiogenic role for VE-cadherin. As discussed above, blood vessel formation is a very dynamic process involving cell rearrangements and cell migration. These dynamics have been studied using murine allantoic explant cultures, which allow to measure the migration of individual and groups of ECs in a process called vasculogenic sprouting, which involves the outgrowth of multicellular sprouts from a primary plexus (Perryn et al., 2008; Rupp et al., 2004). ECs actively migrate over the substrate, frequently passing each other during outgrowth of the vascular rod. These rearrangements are effectively inhibited by addition of a VE-cadherin blocking antibody (Perryn et al., 2008), indicating that VE-cadherin is required for cellular rearrangements as they occur during vasculogenic sprouting. In zebrafish, we have observed that VE-cadherin is also essential for cellular rearrangements during SA formation (H.-G. Belting and M. Affolter, unpublished observation). Therefore, it appears that in addition to functions in vascular integrity and cell survival, VE-cadherin is also involved in sprouting angiogenesis. One can easily imagine that, analogous to the role of DE-cadherin in border cell migration, VE-cadherin may fulfill dual functions at the same time: maintenance of cell–cell contacts and cellular rearrangements.

Conclusions and perspectives

Blood vessel formation includes a spectrum of different morphogenetic processes such as budding, cord hollowing, cell hollowing, cell wrapping and intussusception. The genetic and molecular bases, which initiate and control these different processes is not known. It is clear, however, that ECs of different vascular beds are different in their gene expression profile and that blood vessels are anatomically highly diverse (Rocha and Adams, 2009). Morphogenesis may also be influenced by extraneous factors such as diverse extracellular matrices and signals, shear stress due to blood pressure or differences in cell number (Aird, 2007; Nguyen et al., 2006; Sottile, 2004).

The morphogenetic events that underlie blood vessel formation are likely to determine the way a vessel ultimately lumenizes. During sprouting angiogenesis, larger vessels appear to extend their lumens in conjunction with the outgrowing sprout, while small capillaries may form their lumens de novo by cell hollowing or cord hollowing. The respective contribution to lumen formation in different vessels remains to be determined.

Elaboration of the vascular tree requires additional processes, such as vessel fusion and pruning. How these processes occur at the morphogenetic level has not yet been described in much detail. With regard to vessel fusion, one can envisage that cellular remodeling plays a major role. Furthermore, it is likely that the fusion process occurs differently depending on vessel type. In the zebrafish, the DLAVs form in a non-perfused state and blood circulation commences subsequently. Recently, VE-cadherin localization during DLAV formation revealed that cells from adjacent sprouts undergo extensive rearrangements (Blum et al., 2008). Initial contacts between neighboring sprouts require VE-cadherin, as knockdown of VE-cadherin function leads to slowed-down formation of cell–cell contacts (Montero-Balaguer et al., 2009). It will be interesting to examine the exact cellular mechanisms that drive vessel fusion during DLAV formation and compare them with those occurring in perfused vessels.

Acknowledgments

References

Abraham, S., Yeo, M., Montero-Balaguer, M., Paterson, H., Dejana, E., Marshall, C.J., Mavria, G., 2009. VE-cadherin-mediated cell–cell interaction suppresses sprouting via signaling to MLC2 phosphorylation. Curr. Biol. 19, 1–7.

Adams, R.H., Alitalo, K., 2007. Molecular regulation of angiogenesis and lymphangiogenesis. Nat. Rev., Mol. Cell Biol. 8, 464–478.

Adams, R.H., Wilkinson, G.A., Weiss, C., Diella, F., Gale, N.W., Deutsch, U., Risau, W., Klein, R., 1999. Roles of ephrinB ligands and EphB receptors in cardiovascular development: demarcation of arterial/venous domains, vascular morphogenesis, and sprouting angiogenesis. Genes Dev. 13, 295–306.

Aird, W.C., 2007. Phenotypic heterogeneity of the endothelium: II. Representative vascular beds. Circ. Res. 100, 174–190.

Andrew, D., Ewald, A., 2010. Morphogenesis of epithelial tubes: Insights into tube formation, elongation, and elaboration. Dev. Biol. 341, 66–96.

Armulik, A., Abramsson, A., Betsholtz, C., 2005. Endothelial/pericyte interactions. Circ. Res. 97, 512–523.

Ausprunk, D.H., Folkman, J., 1977. Migration and proliferation of endothelial cells in preformed and newly formed blood vessels during tumor angiogenesis. Microvasc. Res. 14, 53–65.

Baer, M.M., Chanut-Delalande, H., Affolter, M., 2009. Cellular and molecular mechanisms underlying the formation of biological tubes. Curr. Top. Dev. Biol. 89, 137–162.

Bahary, N., Goishi, K., Stuckenholz, C., Weber, G., Leblanc, J., Schafer, C.A., Berman, S.S., Klagsbrun, M., Zon, L.I., 2007. Duplicate VegfA genes and orthologues of the KDR receptor tyrosine kinase family mediate vascular development in the zebrafish. Blood 110, 3627–3636.

Bar, T., Guldner, F.H., Wolff, J.R., 1984. "Seamless" endothelial cells of blood capillaries. Cell Tissue Res. 235, 99–106.

Beis, D., Stainier, D.Y.R., 2006. In vivo cell biology: following the zebrafish trend. Trends Cell Biol. 16, 105–112.

Blum, Y., Belting, H.-G., Ellertsdottir, E., Herwig, L., Lüders, F., Affolter, M., 2008. Complex cell rearrangements during intersegmental vessel sprouting and vessel fusion in the zebrafish embryo. Dev. Biol. 316, 312–322.

Carmeliet, P., 2003. Angiogenesis in health and disease. Nat. Med. 9, 653–660.

Carmeliet, P., Lampugnani, M.G., Moons, L., Breviario, F., Compernolle, V., Bono, F., Balconi, G., Spagnuolo, R., Oosthuyse, B., Dewerchin, M., Zanetti, A., Angellilo, A., Mattot, V., Nuyens, D., Lutgens, E., Clotman, F., de Ruiter, M.C., Gittenberger-de Groot, A., Poelmann, R., Lupu, F., Herbert, J.M., Collen, D., Dejana, E., 1999. Targeted deficiency or cytosolic truncation of the VE-cadherin gene in mice impairs VEGF-mediated endothelial survival and angiogenesis. Cell 98, 147–157.

Cébe-Suarez, S., Zehnder-Fjällman, A., Ballmer-Hofer, K., 2006. The role of VEGF receptors in angiogenesis; complex partnerships. Cell. Mol. Life Sci. 63, 601–615.

Cermenati, S., Moleri, S., Cimbro, S., Corti, P., Del Giacco, L., Amodeo, R., Dejana, E., Koopman, P., Cotelli, F., Beltrame, M., 2008. Sox18 and Sox7 play redundant roles in vascular development. Blood 111, 2657–2666.

Chappell, J.C., Taylor, S.M., Ferrara, N., Bautch, V., 2009. Local guidance of emerging vessel sprouts requires soluble Flt-1 (VEGFR-1). Dev. Cell 1–40.

Childs, S., Chen, J.-N., Garrity, D.M., Fishman, M.C., 2002. Patterning of angiogenesis in the zebrafish embryo. Development 129, 973–982.

Coffin, J.D., Poole, T.J., 1988. Embryonic vascular development: immunohistochemical identification of the origin and subsequent morphogenesis of the major vessel primordia in quail embryos. Development 102, 735–748.

Coffin, J.D., Poole, T.J., 1991. Endothelial cell origin and migration in embryonic heart and cranial blood vessel development. Anat. Rec. 231, 383–395.

Covassin, L.D., Villefranc, J.A., Kacergis, M.C., Weinstein, B.M., Lawson, N.D., 2006. Distinct genetic interactions between multiple Vegf receptors are required for development of different blood vessel types in zebrafish. Proc. Natl. Acad. Sci. U. S. A. 103, 6554–6559.

Covassin, L.D., Siekmann, A.F., Kacergis, M.C., Laver, E., Moore, J.C., Villefranc, J.A., Weinstein, B.M., Lawson, N.D., 2009. A genetic screen for vascular mutants in zebrafish reveals dynamic roles for Vegf/Plcg1 signaling during artery development. Dev. Biol. 329, 212–226.

Crosby, C.V., 2005. VE-cadherin is not required for the formation of nascent blood vessels but acts to prevent their disassembly. Blood 105, 2771–2776.

De Val, S., Black, B.L., 2009. Transcriptional control of endothelial cell development. Dev. Cell 16, 180–195.

De Val, S., Chi, N.C., Meadows, S.M., Minovitsky, S., Anderson, J.P., Harris, I.S., Ehlers, M.L., Agarwal, P., Visel, A., Xu, S.-M., Pennacchio, L.A., Dubchak, I., Krieg, P.A., Stainier, D.Y.R., Black, B.L., 2008. Combinatorial regulation of endothelial gene expression by ETS and forkhead transcription factors. Cell 135, 1053–1064.

Detrich, H.W., Kieran, M.W., Chan, F.Y., Barone, L.M., Yee, K., Rundstadler, J.A., Pratt, S., Ransom, D., Zon, L.I., 1995. Intraembryonic hematopoietic cell migration during vertebrate development. Proc. Natl. Acad. Sci. U.S.A. 92, 10713–10717.

Dooley, K., Davidson, A., Zon, L., 2005. Zebrafish functions independently in hematopoietic and endothelial development. Dev. Biol. 277, 522–536.

Eichmann, A., Yuan, L., Moyon, D., Lenoble, F., Pardanaud, L., Breant, C., 2005. Vascular development: from precursor cells to branched arterial and venous networks. Int. J. Dev. Biol. 49, 259–267.

Eriksson, J., Löfberg, J., 2000. Development of the hypochord and dorsal aorta in the zebrafish embryo (Danio rerio). J. Morphol. 244, 167–176.

Folkman, J., 1982. Angiogenesis: initiation and control. Ann. N.Y. Acad. Sci. 401, 212–227.

Gerhardt, H., Golding, M., Fruttiger, M., Ruhrberg, C., Lundkvist, A., Abramsson, A., Jeltsch, M., Mitchell, C., Alitalo, K., Shima, D., Betsholtz, C., 2003. VEGF guides angiogenic sprouting utilizing endothelial tip cell filopodia. J. Cell Biol. 161, 1163–1177.

Gering, M., Rodaway, A.R., Göttgens, B., Patient, R.K., Green, A.R., 1998. The SCL gene specifies haemangioblast development from early mesoderm. EMBO J. 17, 4029–4045.

Habeck, H., Odenthal, J., Walderich, B., Maischein, H., Schulte-Merker, S., consortium, T.s., 2002. Analysis of a zebrafish VEGF receptor mutant reveals specific disruption of angiogenesis. Curr. Biol. 12, 1405–1412.

Hellström, M., Phng, L.-K., Hofmann, J.J., Wallgard, E., Coultas, L., Lindblom, P., Alva, J., Nilsson, A.-K., Karlsson, L., Gaiano, N., Yoon, K., Rossant, J., Iruela-Arispe, M.L., Kalén, M., Gerhardt, H., Betsholtz, C., 2007. Dll4 signalling through Notch1 regulates formation of tip cells during angiogenesis. Nature 445, 776–780.

Herbert, S.P., Huisken, J., Kim, T.N., Feldman, M.E., Houseman, B.T., Wang, R.A., Shokat, K.M., Stainier, D.Y.R., 2009. Arterial-venous segregation by selective cell sprouting: an alternative mode of blood vessel formation. Science 326, 294–298.

Hirakow, R., Hiruma, T., 1981. Scanning electron microscopic study on the development of primitive blood vessels in chick embryos at the early somite-stage. Anat. Embryol. (Berl.) 163, 299–306.

Hogan, B.L., Kolodziej, P.A., 2002. Organogenesis: molecular mechanisms of tubulogenesis. Nat. Rev., Genet. 3, 513–523.

Hogan, B.M., Bos, F.L., Bussmann, J., Witte, M., Chi, N.C., Duckers, H.J., Schulte-Merker, S., 2009. Ccbe1 is required for embryonic lymphangiogenesis and venous sprouting. Nat. Genet. 41, 396–398.

Hogan, B.M., Robert, H., Witte, M., Heloterä, H., Alitalo, K., Duckers, H.J., Schulte-Merker, S., 2009. Vegfc/Flt4 signalling is suppressed by Dll4 in developing zebrafish intersegmental arteries. Development 136, 4001–4009.

Huisken, J., Stainier, D.Y.R., 2009. Selective plane illumination microscopy techniques in developmental biology. Development 136, 1963–1975.

Isogai, S., 2003. Angiogenic network formation in the developing vertebrate trunk. Development 130, 5281–5290.

Isogai, S., Horiguchi, M., Weinstein, B.M., 2001. The vascular anatomy of the developing zebrafish: an atlas of embryonic and early larval development. Dev. Biol. 230, 278–301.

Isogai, S., Lawson, N.D., Torrealday, S., Horiguchi, M., Weinstein, B.M., 2003. Angiogenic network formation in the developing vertebrate trunk. Development 130, 5281–5290.

Jin, S., Herzog, W., Santoro, M., Mitchell, T., Frantsve, J., Jungblut, B., Beis, D., Scott, I., Damico, L., Ober, E., 2007. A transgene-assisted genetic screen identifies essential regulators of vascular development in vertebrate embryos. Dev. Biol. 307, 29–42.

Jin, S.-W., Beis, D., Mitchell, T., Chen, J.-N., Stainier, D.Y.R., 2005. Cellular and molecular analyses of vascular tube and lumen formation in zebrafish. Development 132, 5199–5209.

Kamei, M., Saunders, W.B., Bayless, K.J., Dye, L., Davis, G.E., Weinstein, B.M., 2006. Endothelial tubes assemble from intracellular vacuoles in vivo. Nature 442, 453–456.

Kemp, H.A., Cooke, J.E., Moens, C.B., 2009. EphA4 and EfnB2a maintain rhombomere coherence by independently regulating intercalation of progenitor cells in the zebrafish neural keel. Dev. Biol. 327, 313–326.

Kimmel, C.B., Ballard, W.W., Kimmel, S.R., Ullmann, B., Schilling, T.F., 1995. Stages of embryonic development of the zebrafish. Dev. Dyn. 203, 253–310.

Kucera, T., Eglinger, J., Strilic, B., Lammert, E., 2007. Vascular lumen formation from a cell biological perspective. Novartis Found. Symp. 283, 46–56 discussion 56-60, 238-241.

Küchler, A.M., Gjini, E., Peterson-Maduro, J., Cancilla, B., Wolburg, H., Schulte-Merker, S., 2006. Development of the zebrafish lymphatic system requires VEGFC signaling. Curr. Biol. 16, 1244–1248.

Lamont, R., Lamont, E., Childs, S., 2009. Antagonistic interactions among Plexins regulate the timing of intersegmental vessel formation. Dev. Biol. 331, 199–209.

Lampugnani, M.G., Dejana, E., 2007. Adherens junctions in endothelial cells regulate vessel maintenance and angiogenesis. Thromb. Res. 120 (Suppl 2), S1–S6.

Larrivée, B., Freitas, C., Suchting, S., Brunet, I., Eichmann, A., 2009. Guidance of vascular development: lessons from the nervous system. Circ. Res. 104, 428–441.

Lawson, N.D., Weinstein, B.M., 2002a. Arteries and veins: making a difference with zebrafish. Nat. Rev., Genet. 3, 674–682.

Lawson, N.D., Weinstein, B.M., 2002b. In vivo imaging of embryonic vascular development using transgenic zebrafish. Dev. Biol. 248, 307–318.

Lawson, N.D., Scheer, N., Pham, V.N., Kim, C.H., Chitnis, A.B., Campos-Ortega, J.A., Weinstein, B.M., 2001. Notch signaling is required for arterial-venous differentiation during embryonic vascular development. Development 128, 3675–3683.

Lawson, N.D., Vogel, A.M., Weinstein, B.M., 2002. Sonic hedgehog and vascular endothelial growth factor act upstream of the Notch pathway during arterial endothelial differentiation. Dev. Cell 3, 127–136.

Lawson, N.D., Mugford, J.W., Diamond, B.A., Weinstein, B.M., 2003. Phospholipase C gamma-1 is required downstream of vascular endothelial growth factor during arterial development. Genes Dev. 17, 1346–1351.

Leslie, J.D., Ariza-Mcnaughton, L., Bermange, A.L., Mcadow, R., Johnson, S.L., Lewis, J., 2007. Endothelial signalling by the Notch ligand Delta-like 4 restricts angiogenesis. Development 134, 839–844.

Liao, E.C., Paw, B.H., Oates, A.C., Pratt, S.J., Postlethwait, J.H., Zon, L.I., 1998. SCL/Tal-1 transcription factor acts downstream of cloche to specify hematopoietic and vascular progenitors in zebrafish. Genes Dev. 12, 621–626.

Liu, F., Patient, R., 2008. Genome-wide analysis of the zebrafish ETS family identifies three genes required for hemangioblast differentiation or angiogenesis. Circ. Res. 103, 1147–1154.

Lubarsky, B., Krasnow, M.A., 2003. Tube morphogenesis: making and shaping biological tubes. Cell 112, 19–28.

Makanya, A., Hlushchuk, R., Djonov, V., 2009. Intussusceptive angiogenesis and its role in vascular morphogenesis, patterning, and remodeling. Angiogenesis 12, 113–123.

Matsumoto, T., Mugishima, H., 2006. Signal transduction via vascular endothelial growth factor (VEGF) receptors and their roles in atherogenesis. J. Atheroscler. Thromb. 13, 130–135.

Meier, S., 1980. Development of the chick embryo mesoblast: pronephros, lateral plate, and early vasculature. J. Embryol. Exp. Morphol. 55, 291–306.

Mellitzer, G., Xu, Q., Wilkinson, D.G., 1999. Eph receptors and ephrins restrict cell intermingling and communication. Nature 400, 77–81.

Montero-Balaguer, M., Swirsding, K., Orsenigo, F., Cotelli, F., Mione, M., Dejana, E., 2009. Stable vascular connections and remodeling require full expression of VE-cadherin in zebrafish embryos. PLoS ONE 4, e5772.

Mukouyama, Y.-s., Shin, D., Britsch, S., Taniguchi, M., Anderson, D.J., 2002. Sensory nerves determine the pattern of arterial differentiation and blood vessel branching in the skin. Cell 109, 693–705.

Nasevicius, A., Larson, J., Ekker, S.C., 2000. Distinct requirements for zebrafish angiogenesis revealed by a VEGF-A morphant. Yeast 17, 294–301.

Nguyen, T.-H., Eichmann, A., Le Noble, F., Fleury, V., 2006. Dynamics of vascular branching morphogenesis: the effect of blood and tissue flow. Phys. Rev., E, Stat. Nonlinear Soft Matter Phys. 73, 061907.

Niewiadomska, P., Godt, D., Tepass, U., 1999. DE-cadherin is required for intercellular motility during Drosophila oogenesis. J. Cell Biol. 144, 533–547.

Nikolova, G., Lammert, E., 2003. Interdependent development of blood vessels and organs. Cell Tissue Res. 314, 33–42.

Olsson, A.-K., Dimberg, A., Kreuger, J., Claesson-Welsh, L., 2006. VEGF receptor signalling—in control of vascular function. Nat. Rev., Mol. Cell Biol. 7, 359–371.

Pacquelet, A., Rørth, P., 2005. Regulatory mechanisms required for DE-cadherin function in cell migration and other types of adhesion. J. Cell Biol. 170, 803–812.

Patan, S., 2000. Vasculogenesis and angiogenesis as mechanisms of vascular network formation, growth and remodeling. J. Neuro-oncol. 50, 1–15.

Patterson, L.J., Gering, M., Eckfeldt, C.E., Green, A.R., Verfaillie, C.M., Ekker, S.C., Patient, R., 2007. The transcription factors Scl and Lmo2 act together during development of the hemangioblast in zebrafish. Blood 109, 2389–2398.

Pendeville, H., Winandy, M., Manfroid, I., Nivelles, O., Motte, P., Pasque, V., Peers, B., Struman, I., Martial, J.A., Voz, M.L., 2008. Zebrafish Sox7 and Sox18 function together to control arterial-venous identity. Dev. Biol. 317, 405–416.

Perryn, E.D., Czirók, A., Little, C.D., 2008. Vascular sprout formation entails tissue deformations and VE-cadherin-dependent cell-autonomous motility. Dev. Biol. 313, 545–555.

Phng, L.-K., Gerhardt, H., 2009. Angiogenesis: a team effort coordinated by Notch. Dev. Cell 16, 196–208.

Poole, T.J., Coffin, J.D., 1989. Vasculogenesis and angiogenesis: two distinct morphogenetic mechanisms establish embryonic vascular pattern. J. Exp. Zool. 251, 224–231.

Red-Horse, K., Crawford, Y., Shojaei, F., Ferrara, N., 2007. Endothelium-microenvironment interactions in the developing embryo and in the adult. Dev. Cell 12, 181–194.

Ribeiro, C., Neumann, M., Affolter, M., 2004. Genetic control of cell intercalation during tracheal morphogenesis in Drosophila. Curr. Biol. 14, 2197–2207.

Risau, W., 1995. Differentiation of endothelium. FASEB J. 9, 926–933.

Risau, W., Sariola, H., Zerwes, H.G., Sasse, J., Ekblom, P., Kemler, R., Doetschman, T., 1988. Vasculogenesis and angiogenesis in embryonic-stem-cell-derived embryoid bodies. Development 102, 471–478.

Rocha, S., Adams, R., 2009. Molecular differentiation and specialization of vascular beds. Angiogenesis 12, 139–147.

Roman, B.L., Pham, V.N., Lawson, N.D., Kulik, M., Childs, S., Lekven, A.C., Garrity, D.M., Moon, R.T., Fishman, M.C., Lechleider, R.J., Weinstein, B.M., 2002. Disruption of acvrl1 increases endothelial cell number in zebrafish cranial vessels. Development 129, 3009–3019.

Ruhrberg, C., Gerhardt, H., Golding, M., Watson, R., Ioannidou, S., Fujisawa, H., Betsholtz, C., Shima, D.T., 2002. Spatially restricted patterning cues provided by heparin-binding VEGF-A control blood vessel branching morphogenesis. Genes Dev. 16, 2684–2698.

Rupp, P.A., Czirók, A., Little, C.D., 2004. alphavbeta3 integrin-dependent endothelial cell dynamics in vivo. Development 131, 2887–2897.

Sakaguchi, T.F., Sadler, K.C., Crosnier, C., Stainier, D.Y.R., 2008. Endothelial signals modulate hepatocyte apicobasal polarization in zebrafish. Curr. Biol. 18, 1565–1571.

Shibuya, M., Claesson-Welsh, L., 2006. Signal transduction by VEGF receptors in regulation of angiogenesis and lymphangiogenesis. Exp. Cell Res. 312, 549–560.

Siekmann, A.F., Lawson, N.D., 2007. Notch signalling limits angiogenic cell behaviour in developing zebrafish arteries. Nature 445, 781–784.

Siekmann, A.F., Covassin, L., Lawson, N.D., 2008. Modulation of VEGF signalling output by the Notch pathway. BioEssays 30, 303–313.

Siekmann, A.F., Standley, C., Fogarty, K.E., Wolfe, S.A., Lawson, N.D., 2009. Chemokine signaling guides regional patterning of the first embryonic artery. Genes Dev. 23, 2272–2277.

Sottile, J., 2004. Regulation of angiogenesis by extracellular matrix. Biochim. Biophys. Acta 1654, 13–22.

Stainier, D.Y., Weinstein, B.M., Detrich III, H.W., Zon, L.I., Fishman, M.C., 1995. Cloche, an early acting zebrafish gene, is required by both the endothelial and hematopoietic lineages. Development 121, 3141–3150.

Strilić, B., Kucera, T., Eglinger, J., Hughes, M.R., Mcnagny, K.M., Tsukita, S., Dejana, E., Ferrara, N., Lammert, E., 2009. The molecular basis of vascular lumen formation in the developing mouse aorta. Dev. Cell 17, 505–515.

Suchting, S., Freitas, C., Le Noble, F., Benedito, R., Bréant, C., Duarte, A., Eichmann, A., 2007. The Notch ligand Delta-like 4 negatively regulates endothelial tip cell formation and vessel branching. Proc. Natl. Acad. Sci. U.S.A. 104, 3225–3230.

Tammela, T., Zarkada, G., Wallgard, E., Murtomäki, A., Suchting, S., Wirzenius, M., Waltari, M., Hellström, M., Schomber, T., Peltonen, R., Freitas, C., Duarte, A., Isoniemi, H., Laakkonen, P., Christofori, G., Ylä-Herttuala, S., Shibuya, M., Pytowski, B., Eichmann, A., Betsholtz, C., Alitalo, K., 2008. Blocking VEGFR-3 suppresses angiogenic sprouting and vascular network formation. Nature 454, 656–660.

Thisse, C., 2002. Organogenesis—heart and blood formation from the zebrafish point of view. Science 295, 457–462.

Thompson, M.A., Ransom, D.G., Pratt, S.J., MacLennan, H., Kieran, M.W., Detrich, H.W., Vail, B., Huber, T.L., Paw, B., Brownlie, A.J., Oates, A.C., Fritz, A., Gates, M.A., Amores, A., Bahary, N., Talbot, W.S., Her, H., Beier, D.R., Postlethwait, J.H., Zon, L.I., 1998. The cloche and spadetail genes differentially affect hematopoiesis and vasculogenesis. Dev. Biol. 197, 248–269.

Torres-Vazquez, J., 2004. Semaphorin-plexin signaling guides patterning of the developing vasculature. Dev. Cell 7, 117–123.

Torres-Vázquez, J., Gitler, A.D., Fraser, S.D., Berk, J.D., Pham, V.N., Fishman, M.C., Childs, S., Epstein, J.A., Weinstein, B.M., 2004. Semaphorin-plexin signaling guides patterning of the developing vasculature. Dev. Cell 7, 117–123.

Vestweber, D., Winderlich, M., Cagna, G., Nottebaum, A.F., 2009. Cell adhesion dynamics at endothelial junctions: VE-cadherin as a major player. Trends Cell Biol. 19, 8–15.

Walls, J.R., Coultas, L., Rossant, J., Henkelman, R.M., 2008. Three-dimensional analysis of vascular development in the mouse embryo. PLoS ONE 3, e2853.

Yamazaki, Y., Morita, T., 2006. Molecular and functional diversity of vascular endothelial growth factors. Mol. Divers. 10, 515–527.

Yaniv, K., Isogai, S., Castranova, D., Dye, L., Hitomi, J., Weinstein, B.M., 2006. Live imaging of lymphatic development in the zebrafish. Nat. Med. 12, 711–716.

Zhong, T.P., Childs, S., Leu, J.P., Fishman, M.C., 2001. Gridlock signalling pathway fashions the first embryonic artery. Nature 414, 216–220.

Zon, L.I., Mather, C., Burgess, S., Bolce, M.E., Harland, R.M., Orkin, S.H., 1991. Expression of GATA-binding proteins during embryonic development in *Xenopus laevis*. Proc. Natl. Acad. Sci. U. S. A. 88, 10642–10646.

5.2 Effects of the protein kinase inhibitor PKC412 on gene expression and link to physiological effects in zebrafish *Danio rerio* eleuthero-embryos

Oggier DM, Lenard A, Küry M, Hoeger B, Affolter M, Fent K.

Contribution:

I performed the analyses of the protein kinase inhibitor PKC412 influence on the vascular anatomy of developing zebrafish embryo using transgenic fish expressing EGFP in endothelial cells (Figure 2). I prepared the text regarding these analyses.

Effects of the Protein Kinase Inhibitor PKC412 on Gene Expression and Link to Physiological Effects in Zebrafish *Danio rerio* Eleuthero-Embryos

Daniela M. Oggier,*,† Anna Lenard,‡ Michael Küry,* Birgit Hoeger,§ Markus Affolter,‡ and Karl Fent*,¶,1

*University of Applied Sciences Northwestern Switzerland, School of Life Sciences, CH-4132 Muttenz, Switzerland; †Division of Limnology,
University of Zürich, Institute of Plant Biology, CH-8802 Kilchberg, Switzerland; ‡Biozentrum der Universität Basel, CH-4056 Basel, Switzerland;
§Novartis Pharma AG, Schwarzwaldallee 215, CH-4058 Basel, Switzerland; and ¶Department of Environmental Sciences, Swiss Federal Institute of Technology
(ETHZ), CH-8092 Zürich, Switzerland

[1]To whom correspondence should be addressed at University of Applied Sciences Northwestern Switzerland, School of Life Sciences, Gründenstrasse 40,
CH-4132 Muttenz, Switzerland. Fax: +0041-61-467-44-60. E-mail: karl.fent@fhnw.ch or karl.fent@bluewin.ch.

To identify molecular effects of the antineoplastic agent protein kinase C inhibitor 412 (PKC412) (midostaurin), we applied gene expression profiling in zebrafish using whole-genome microarrays. Behavioral, developmental, and physiological effects were investigated in order to analyze for correlations between altered gene expression profiles with effects on development and physiology. Zebrafish blastula-stage embryos were exposed for 6 days postfertilization to nominal levels of 2 and 40 µg/l PKC412. Among the 259 and 511 altered transcripts at both concentrations, respectively, the expressions of genes involved in the circadian rhythm were further investigated. Alteration of swimming behavior was not observed. Pathways of interest affected by PKC412 were angiogenesis, apoptosis, DNA damage response, and response to oxidative stress. Angiogenesis was analyzed in double-transgenic zebrafish embryos Tg(fli1a:EGFP)y1;Tg(gata1:dsRed)sd2; no major defects were induced by PKC412 treatment at both concentrations. Apoptosis occurred in olfactory placodes of embryos exposed to 40 µg/l, and DNA damage was induced at both PKC412 concentrations. However, there were no significant effects on reactive oxygen species formation. This study leads to the conclusion that PKC412-induced alterations of gene transcripts are partly paralleled by physiological effects at high, but not at low PKC412 concentrations expected to be of environmental relevance.

Key Words: PKC412; *Danio rerio*; transgenic zebrafish; microarray; angiogenesis; apoptosis.

Antineoplastic agents have widespread use in cancer treatment. They include different classes, such as antibodies, protein kinase inhibitors (such as protein kinase C inhibitor 412 [PKC412]), topoisomerase I and II inhibitors, antimetabolites, alkylating agents, and others (Chabner *et al*., 2006). Antineoplastic agents are mainly found in the nanograms per liter to the lower micrograms per liter range in effluents (Fent *et al*., 2006; Monteiro and Boxall, 2010). For example, ifosfamide was found in Germany up to a concentration of 2.9 µg/l (Ternes, 1998).

As many pharmacological targets are evolutionary conserved, antineoplastic agents are supposed to have similar effects in aquatic organisms as in humans (Christen *et al*., 2010; Gunnarsson *et al*., 2008; Jones *et al*., 2007) Therefore, environmental exposure may pose a risk for negative effects on nontarget species because of the mutagenic and cancerogenic properties of such compounds.

A newly developed antineoplastic agent is midostaurin (PKC412, $\log K_{OW} = 4.26$; Novartis Pharma AG, Basel, Switzerland; internal data), which belongs to the family of indolocarbazoles and is a selective inhibitor of several isoforms of protein kinase C in humans (Karaman *et al*., 2008). It is a sugar ring variant of staurosporine, which was originally isolated from *Streptomyces staurosporeus* (Takahashi *et al*., 1989). PKC412 inhibits a large variety of tyrosine kinases including FMS-like tyrosine kinase (FLT3), platelet-derived growth factor (PDGF) receptors, and c-kit (stem cell factor) receptor (Fabbro *et al*., 2000). PKC412 has been developed as a therapeutic agent against acute myeloid leukemia because of its ability to inhibit growth, angiogenesis, and P-glycoprotein–mediated multidrug resistance in tumor cells (Fabbro *et al*., 2000). In addition, PKC412 affects other cellular processes such as immune responses or neuronal functions, as shown by effective inhibition of human T-cell activation, proliferation, and tumor necrosis factor alpha production (Si *et al*., 2005).

Only very few data are available on the toxicity of PKC412 to organisms that may be exposed via wastewater. Exposure of zebrafish blastula-stage embryos to 100nM (57 µg/l) PKC412 resulted in a curved body axis (Chan *et al*., 2002). Recent data indicate that the no observed effect concentration (NOEC) of PKC412 was 14 µg/l in a *Danio rerio* early life–stage test and the lowest observed effect concentration for mortality was 43 µg/l. The 96-h LC_{50} in adult *D. rerio* was 25 µg/l and the NOEC 19 µg/l (Novartis Pharma AG, internal data). The estimated predicted environmental concentration is 1.5 µg/l (Novartis Pharma AG, internal data).

Currently, there is a lack of chronic toxicity studies with focus on the modes of action on this pharmaceutical in vertebrates and invertebrates. Furthermore, ecological risk assessments of PKC412 within the framework of the European Medicines Agency (2006), in particular at environmentally realistic concentrations in aquatic organisms, are not publicly available. Ecotoxicological tests used for risk assessments are often not sensitive enough to identify subtle adverse effects of pharmaceuticals. They may be more accurately determined by focusing on the modes of action (Christen *et al.*, 2010; Fent *et al.*, 2006; Runnalls *et al.*, 2007). Therefore, potential environmental consequences of PKC412 are unknown. In detail, data on the gene expression profile and their correlation to environmentally relevant endpoints such as behavior and mortality are missing.

In our present study, we aim at determining the modes of action of this novel antineoplastic agent in zebrafish embryos to clarify its potential molecular effects by analyzing the global gene expression pattern. The toxicogenomics approach allows to identify several thousands of genes and the corresponding expression profiles upon exposure, which will assist in the elucidation of the molecular effects and the compound's modes of action (Robbens *et al.*, 2007). We analyze effects at low concentrations in zebrafish embryos and compare the effects on the transcriptional level with effects on mortality and physiological outcomes. We hypothesize that the response of zebrafish to PKC412 exposure is similar to the human response, as their targets, the protein kinases, are evolutionary conserved. Therefore, we searched for alterations in gene expression patterns associated with cellular signaling (e.g., angiogenesis and apoptosis) and oxidative stress. We also hypothesized that alterations in gene expression—because of multiple endpoints and mechanistic information—are more sensitive than physiological or morphological parameters (although they are perhaps less ecologically relevant) but that the observed molecular effects correlate with and propagate to higher levels of the biological organization. In addition, gene expression analysis may also reveal unknown regulatory mechanisms in fish not directly related to the modes of action of PKC412 in humans.

MATERIALS AND METHODS

Chemicals

PKC412 ($\geq$ 99%, molecular weight: 570.6, $\log K_{OW} = 4.26$) was kindly provided by Novartis Pharma AG. Acetonitrile was purchased from Brunschwig (Basel, Switzerland) and methanol was from Stehelin (Basel, Switzerland). Ammonium formiate, dimethyl sulfoxide (DMSO), formic acid, 4-(2-hydroxyethyl)-1-piperazineethanesulfonic acid (HEPES), $MgCl_2$, NaCl, sucrose, Triton X-100, H_2O_2, 4′,6-diamidino-2-phenylindole (DAPI), and dichlorofluorescein-diacetate (DCFH-DA) were obtained from Sigma-Aldrich (Buchs, Switzerland). 4-2-Aminoethyl-benzensulfonyl fluoride hydrochloride (AEBSF), EDTA, low melting agarose, and Tris-HCl were purchased from AppliChem.GmbH (Darmstadt, Germany). Roti-Histofix (10%) was purchased from Carl Roth GmbH & Co. KG (Karlsruhe, Germany). PBS was obtained from F. Hoffmann-La Roche Ltd (Basel, Switzerland).

Exposure Experiment

For the microarray, behavioral, and toxicity studies, freshly fertilized zebrafish embryos were obtained from Harlan Laboratories Ltd (Itingen, Switzerland). Embryos were transferred to the laboratory and examined under a stereomicroscope. All embryos used in the experiments were at blastula stage (Kimmel *et al.*, 1995). They were placed in 750-ml covered glass beakers of reconstituted water (total hardness of 125 mg/l as $CaCO_3$ and a conductivity of 270 μS/cm) and the appropriate concentration of PKC412 or DMSO (0.01%, solvent control). The water temperature was held constant at 27°C $\pm$ 1°C with the photoperiod set at 16:8 h light/dark.

The semistatic exposure setup consisted of six replicates of water control, solvent control (0.01% DMSO), and two PKC412 doses. A total of 100 fertilized eggs per replicate ($n = 6$) were exposed up to 6 days postfertilization (dpf) to nominal concentrations of 2 and 40 μg/l PKC412, respectively. This exposure duration seemed to be appropriate as lethal effects occurred already after 3 dpf in the early life stages test. Every 24 h, lethal and sublethal effects were evaluated, dead embryos or eleuthero-embryos were removed, and the water was changed. The quality of the exposure water was continuously monitored by oxygen concentration determination (> 70%), the pH value (6.7–7.2), and the temperature (27°C $\pm$ 1°C). At the end of exposure, eleuthero-embryos were anesthetized in a clove oil solution (Fluka AG, Buchs, Switzerland). A total of 80 eleuthero-embryos per replicate were pooled in RNAlater for microarray and quantitative real time polymerase chain reaction (qRT-PCR). Total RNA was extracted using the RNeasy Mini Kit (Qiagen, Basel, Switzerland).

Chemical Analysis

To determine actual exposure concentrations, 10-ml aliquots of exposure water were taken during the experiment for PKC412 analysis. Water samples of each treatment group were taken at the beginning (0 h) and prior to full water renewal (24 h). This was done three times on different days from different randomly selected replicate tanks. Acetonitrile (2 ml) was added to the water samples for liquid chromatography-mass spectrometry (LC-MS) analysis preparation and then stored at −20°C until analysis. The chemical analysis was performed separately for the microarray experiment, the behavioral experiment, and additional experiments (terminal deoxynucleotidyl transferase dUTP nick end labeling [TUNEL] assay, comet assay and reactive oxygen species [ROS] assay).

PKC412 concentrations were determined by LC-MS. The chromatographic separation was achieved by using an Inertsil ODS-3 column (2.1 × 50 mm; 3 μm particle size) from Ercatech AG (Bern, Switzerland) at a column temperature of 30°C. For the analysis, a binary gradient mixture containing eluent A (0.1% [vol/vol] in formic acid in water:acetonitrile [95:5]) and eluent B (0.1% [vol/vol] in formic acid in water:acetonitrile [5:95]) was used at a flow rate of 0.4 ml/min. The gradient started with a mixture of 60% eluent A and 40% eluent B and increased to 100% eluent B after 4 min. The conditions were held for 1 min, and then the system was set back to the initial conditions. The column was reequilibrated for 2 min before the next injection. Five microliters of the samples were injected. The retention time for PKC412 was 3.3 min. Data were then quantified using DataAnalysis for 6300 Series Ion Trap LC/MC version 3.4. Quantification of PKC412 was based on an external calibration curve.

RNA Isolation, Array Hybridization, and Sample Selection

Total RNA was extracted from zebrafish eleuthero-embryos using the RNeasy Mini Kit (Qiagen). Total RNA concentrations were measured spectrophotometrically using a NanoDrop ND-1000 UV-VIS Spectrophotometer at 260 nm. The integrity of each RNA sample was verified using an Agilent 2100 Bioanalyzer (Agilent Technologies, Basel, Switzerland). Only samples containing a 260/280 nm ratio between 1.8 and 2.1, a 28S/18S ratio between 1.5 and 2, and an RNA integrity number > 8 were processed further. A total of 16 arrays (Agilent 4 × 44 K Zebrafish Microarray) were used, including four for the water control group, four for the solvent control group, four for the 2 μg/l, and four for the 40-μg/l PKC412 dose group. Total RNA samples (600 ng) were reverse transcribed into double-strand complementary DNA

TABLE 1
Primer Sequences for Quantitative Real-Time PCR Analysis

Probe ID	Gene	Sequence accession #	Direction	Sequence	Amplicon size (bp)
—	RpL13α		fw	agc tca aga tgg caa cac	100
			rv	ag aag ttc ttc tcg tcc tcc	
A_15_P104624	abcc4	NM_001007038	fw	ctg gaa aca cga ctc agc aa	122
			rv	gct cac cag agc att gaa ca	
A_15_P103946	cry5	NM_131788.1	fw	cat gga gag aac gaa ctg gg	115
			rv	gtg cag aca gc agc cga ac	
A_15_P196411	ndrg1l	NM_200692.1	fw	agc gtc ttt gag ctg gac at	113
			rv	tgg aag tc agg atg gta gg	
A_15_P544897	opn1mw2	NM_182891.2	fw	cca tgg cag ttt aag gca ct	100
			rv	ttt tgt gct gag ctg tga cc	
A_15_P112731	pdpk1	NM_001077344.1	fw	cgt tta gag ctg gga acg ag	103
			rv	cgc tgg acc aga tct tta gc	
A_15_P236266	per1	NM_001030183.1	fw	atg cgt gca aga agt ggt g	131
			rv	acg tcc tca ttt agc gga ctc	
A_15_P197856	sos	XM_685079.2	fw	ctg ccc tca ctt ctc acc tc	109
			rv	cac tgg tcc aca cca aac ac	
A_15_P134231	xpc	NM_001045210.1	fw	aag aag tcg gca gtg agg aa	101
			rv	gca tat ttt cac ggc tcc at	

(cDNA) in the presence of RNA poly-A controls with the Agilent One-Color RNA Spike-In Kit. Cyanine 3 (Cy3) labeling and hybridization were performed according to the manufacturer's manual.

After reverse transcription of RNA into double-stranded cDNA, double-strand cDNA was *in vitro* transcribed into complementary RNA (cRNA) in the presence of Cy3-labeled nucleotides using a Low RNA Input Linear Amp Kit +Cy dye (Agilent Technologies), performed at the Functional Genomic Center (ETHZ and University of Zürich, Switzerland). The Cy3-labeled cRNA was purified using an RNeasy Mini Kit (Qiagen), and quality and quantity was determined using a NanoDrop ND-1000 UV-VIS Spectrophotometer and an Agilent 2100 Bioanalyzer, respectively. Only cRNA samples with a total cRNA yield higher than 2 µg and a dye incorporation rate between 9 and 20 pmol/µg were used for hybridization. Cy3-labeled cRNA samples (1.65 µg) were mixed with Agilent blocking solution, subsequently fragmented randomly to 100–200 bp at 65°C with fragmentation buffer, and resuspended in hybridization buffer as provided by the Gene Expression Hybridization Kit (Agilent Technologies). Target cRNA samples (100 µl) were hybridized to the Agilent Zebrafish 4 × 44 K Gene Expression Microarray for 17 h at 65°C. The hybridized arrays were then washed using Agilent GE wash buffers 1 and 2 according to the manufacturer's instructions and scanned by an Agilent Microarray Scanner (Agilent p/n G2565BA) at 5-µm resolution with the green photomultiplier tube set to 100% and a scan area of 61 × 21.6 mm. Image generation and feature extraction were performed using the Agilent Feature Extraction (FE) software version 9.5.3. Quality control was additionally considered before performing the statistical analysis. These included array hybridization pattern inspection: absence of scratches, bubbles, areas of nonhybridization, proper grid alignment, spike performance in controls with a linear dynamic range of five orders of magnitude, and the number of green-feature nonuniformity outliers, which should be below 100 for all samples.

qRT-PCR Analysis

One microgram of total RNA of the microarray experiment template was reverse transcribed using Moloney murine leukemia virus reverse transcriptase (Promega Biosciences Inc., Wallisellen, Switzerland) in the presence of random hexamers (Roche Diagnostics) and deoxynucleoside triphosphate (Sigma-Aldrich). The reaction mixture was incubated for 5 min at 70°C and then for 1 h at 37°C. The reaction was stopped by heating at 95°C for 5 min.

The cDNA was used to perform SYBR-PCR based on SYBR-Green Fluorescence (FastStart Universal SYBR Green Master, Roche Diagnostics). Eight differentially expressed genes of interest (ATP-binding cassette, subfamily C [abcc4], cryptochrome 5 [cry5], N-myc downstream–regulated gene 1, like [ndrg1l], opsin 1 [cone pigments], medium wave–sensitive, 2 [opn1mw2], 3-phosphoinositide-dependent protein kinase-1 [pdpk1], period homolog 1 [per1], similar to son of sevenless homolog 2 [sos], and xeroderma pigmentosum, complementation group C [xpc]) were selected for confirmation of microarray results using qRT-PCR. Gene-specific primers were designed based on published zebrafish sequences (Table 1).

The following PCR reaction profile was used: one cycle at 95°C for 10 min followed by 40 cycles at 95°C for 15 s and 59°C for 60 s followed by a melting curve analysis after run.

The delta threshold cycle (CT) value was derived by subtracting the CT value for the housekeeping gene ribosomal protein L13 α (RpL13α), which served as an internal control, from the CT value of the target gene, respectively. All reactions were run in duplicate using the Biorad CFX96 RealTime PCR Detection System (Biorad, Reinach, Switzerland). The messenger RNA expression level of the different genes was expressed as fold increase according to the formula:

$$2^{\Delta CT(\text{untreated sample}) - \Delta CT(\text{treated sample})}$$

Measurement of Locomotor Activity

Multispecies Freshwater Biomonitor. Effects of PKC412 on locomotor activity were measured in zebrafish eleuthero-embryos. Their locomotor activity was observed using a flow-through test chamber with quadrupole impedance conversion as measuring device, connected to a measuring unit and personal computer with data analysis software (Gerhardt *et al.*, 1994). Measurement chambers, made of an acryl glass cylinder sealable on both ends, with a size of 4 cm in length and a diameter of 2 cm allowed free movement of the eleuthero-embryos during measurement.

For locomotor activity measurements, embryos in the blastula stage were exposed to 2.1 and 31 µg/l PKC412, respectively, for 6 dpf as described above. Locomotor activities of hatched eleuthero-embryos were assessed 6 dpf for 20 animals per PKC412 dose and the appropriate controls, respectively, as described above. Following an acclimation phase of 10 min, measurements

were started and behavior was monitored with a recording duration lasting 4 min for a period of 2 h with intervals of 10 min each. For locomotor activity measurements, means of locomotor activities (percent time spent on locomotion) for each individual were calculated for 2-h time period.

Angiogenesis

Double-transgenic zebrafish embryos (Tg(fli1a:EGFP)y1;Tg(gata1:dsRed)sd2) (Lawson and Weinstein, 2002; Traver *et al.*, 2003) were exposed to 2 and 40 μg/l PKC412 and held in water and DMSO control water (50 embryos each) for 6dpf as described above. Embryos were monitored for morphological defects using a fluorescent binocular at 24 hours postfertilization (hpf), 48 hpf, and 6dpf. Formation of blood vessels was observed with transgenic expression of enhanced green fluorescent protein in endothelial cells and red fluorescent protein from *Discosoma* sp. expression in blood cells. Transgenic fish were kept heterozygotic; therefore, only half of the progeny is double transgenic and these were analyzed in detail. Representative embryos taken from treated and control groups were imaged using a Leica TCS SP5 Confocal Microscopy System.

Apoptosis Assay

Apoptotic cells of eleuthero-embryos were determined by the TUNEL assay. Eleuthero-embryos were exposed 6 dpf as described above. Embryos exposed to 1% H_2O_2 served as a positive control. After 6 dpf, the eleuthero-embryos were fixed in 4% Roti-Histofix at 4°C for 24 h. Thereafter, the embryos were rehydrated through a series of methanol (100, 90, 70, and 50%). The TUNEL assay (Roche "*In situ* Cell Death Detection Kit, TMR red") was performed as described in the manufacturer's manual. In brief, single eleuthero-embryos ($n = 3$ per replicate) were permeabilized in PBS containing 0.1% Triton X-100 for 8 min. Thereafter, they were washed twice with PBS and then labeled for 60 min at 37°C. The embryos were then embedded in agarose and analyzed under the fluorescent microscope at excitation and emission wavelength of 360–370 and 420 nm, respectively.

Alkaline Comet Assay

This assay allows detecting DNA breakages induced by genotoxic agents. The comet assay was performed as described (Duong *et al.*, 2010). Briefly, embryos were exposed to PKC412 as described above for 6 dpf. As a positive control, embryos were exposed to 1% H_2O_2 for 10 min prior to anestization. A pool of eight eleuthero-embryos per replicate ($n = 4$) was macerated in 1 ml PBS containing 20mM EDTA for 5 min. The supernatant was removed, and the embryos were shred in 500 μl PBS containing 20mM EDTA for 10 min. The remaining tissue was sedimented for 2 min, and the supernatant was embedded in agarose on a microscope slide. Cells were then lysed at 4°C for 1 h with lysis buffer (2.5M NaCl, 0.1M EDTA, 10mM Tris-HCl, pH 10, 1% Triton X-100) and electrophoresed for 5 min at 25 V. Damaged DNA fragments migrate faster in the electric field than intact DNA, which can be visualized after staining with DAPI. Cells (24 cells per replicate) were observed under the fluorescence microscope, and the length of comets, percent DNA in tail, tail moment, and olive tail moment were calculated using CometScore 1.5 (TriTek, Sumerduck, VA).

ROS Measurements

In this assay, the nonfluorescent probe DCFH-DA is oxidized into the highly fluorescent 2,7-dichlorofluorescein in the presence of ROS. ROS measurements were conducted according to Deng *et al.* (2009). In brief, eight pre-exposed eleuthero-embryos (pre-exposure for 6 dpf as described for the microarray experiment) were washed with cold PBS and then homogenized in cold lysis buffer containing 0.32mM sucrose, 20mM HEPES, 1mM $MgCl_2$, and 0.5mM AEBSF, pH 7.4. As a positive control, eight eleuthero-embryos were exposed for 10 min to water containing 1% H_2O_2. Thereafter, the homogenate was centrifuged at $15,000 \times$ g at 4°C for 20 min, and the supernatant was discharged. The pellet was then resuspended in PBS, and 20 μl were added to a 96-well plate and incubated for 5 min at room temperature. Thereafter, 100 μl of PBS and 8.3 μl of DCFH-DA (stock solution in DMSO, 10 mg/ml) were added to each well. The plate was incubated at 37°C for 30 min, and

fluorescence measurements were made with excitation at 485 nm and emission at 530 nm, respectively.

Data Analysis and Statistics

Raw microarray data were analyzed using the GeneSpring GX 10 software (Agilent Technologies). In a first step, the Agilent FE software output was filtered on the basis of feature saturation, nonuniformity, pixel population consistency, and signal strength relative to background level (Agilent FE Manual). Only positively marked entities were accepted for further evaluation. All data were quantile normalized. In a second step, several quality control steps (e.g., correlation plots and correlation coefficients, quality metric plots, and principal components analysis) using the quality control tool of GeneSpring were performed to ensure that the data were of good quality.

Differentially expressed genes from the microarray were determined using a Benjamini-Hochberg multiple correction ANOVA test ($p < 0.05$) followed by a Tukey honestly significant difference technique *post hoc* test. The genes were considered differentially expressed when $p < 0.05$ and the fold change (FC) ≥ 2. To determine gene ontology (GO) categories of differentially expressed genes, the GO analysis tool in GeneGo, San Diego, CA, was used. Only those categories where $p < 0.05$ were considered differentially altered. MetaCore (GeneGo) was used to identify and visualize the involvement of the differentially expressed genes in specific pathways (false discovery rate [FDR] < 0.05). The microarray data used in this analysis have been submitted to the National Center for Biotechnology Information Gene Expression Omnibus database under accession number GSE23156 (http://www.ncbi.nlm.nih.gov/geo/query/acc.cgi?token=fnotryskkqyaoba&acc=GSE23156).

Data from microarray analysis, qRT-PCR, locomotor activity, comet assay, and ROS assay were illustrated graphically with GraphPad Prism 5 (GraphPad Software, San Diego, CA). Data distribution for normality was assessed with the Kolmogorov-Smirnov test and the variance homogeneity with the Bartlett test. Differences between treatments were assessed by ANOVA followed by a Tukey test (Bartelett test $p < 0.05$) to compare treatment means with respective controls. If the data were not normally distributed, differences between treatments were assessed by the Kruskal-Wallis test followed by Dunn's multiple comparison test. Results are given as mean ± SEM. Differences were considered significant at $p \leq 0.05$.

RESULTS

PKC412 Concentrations and Embryo Survival

PKC412 concentrations in the exposure water were measured at 0 and 24 h in order to determine the actual exposure concentrations. The PKC412 concentrations measured independently in the different experiments are given in Table 2. In the microarray experiment, actual concentrations were lower than nominal, and they decreased during exposure. Geometric mean concentrations ($n = 3$) were 1.3 and 21 μg/l. Also in the behavioral experiment using the Multispecies Freshwater Biomonitor (MFB), the PKC412 concentration decreased during the 24-h exposure and the mean measured concentration was 2.1 and 31 μg/l. In the experiments where the comet assay, TUNEL assay, and ROS assay were performed, the initial concentrations were close to nominal and decreased again during the 24-h exposure. The mean measured concentrations were 1.6 and 31 μg/l. No significant mortality was observed in any of the different experiments and treatment groups.

Alteration of Gene Expression

Gene expression profiles derived from microarray results of control and PKC412-exposed embryos ($n = 4$) are based on 80

TABLE 2

Nominal and Measured Concentrations of PKC412 in Exposure Waters after 6 dpf of Exposure for the Microarray, Multispecies Freshwater Biomonitor Experiment and Comet Assay

	Exposure waters				
	Measured concentration (μg/l)				
Nominal concentration	0 h	% Nominal	24 h	% Nominal	Geometric mean
Microarray					
2 μg/l	1.50 ± 0.1	75.2	1.06 ± 0.2	52.9	1.3
40 μg/l	25.12 ± 1.6	62.8	17.20 ± 3.1	43.0	21
Multispecies Freshwater Biomonitor					
2 μg/l	2.36 ± 0.1	117.8	1.90 ± 0.2	95.1	2.1
40 μg/l	37.45 ± 1.7	93.6	25.10 ± 1.7	62.7	31
TUNEL assay, comet assay, and ROS assay					
2 μg/l	2.19 ± 0.2	109.5	1.23 ± 0.1	61.7	1.6
40 μg/l	38.60 ± 6.4	96.5	24.93 ± 5.2	62.3	31

TABLE 3

FCs of Selected Genes Differentially Regulated in Zebrafish Eleuthero-Embryos Determined by Microarray and qRT-PCR after Exposure to 1.3 and 21 μg/l PKC412. Values Are Expressed as Average FC. Asterisks Show Statistically Significant Difference to Control ($p < 0.05$)

	FC ($\log_2$)			
	1.3 μg/l PKC412		21 μg/l PKC412	
Gene name	Array	qPCR	Array	qPCR
abcc4	−2.00*	−1.21*	−2.98*	−1.03*
cry5	−2.68*	−2.35*	−2.86*	−2.12*
ndrg1l	4.00*	1.99*	4.10*	2.41*
opn1mw2	2.60*	0.45*	2.36*	1.00*
pdpk1	2.60*	0.88*	1.71*	1.05*
per1	−9.80*	−3.58*	−6.41*	−3.16*
sos	0.85*	−0.27	2.03*	0.62
xpc	−2.90*	−1.40*	−2.20*	−0.55

pooled individuals. As listed in Supplementary table S1, 259 and 511 genes were differentially expressed in zebrafish eleuthero-embryos ($\log_2 \geq 2$, $p < 0.05$) after exposure to 1.3 and 21 μg/l PKC412, respectively. At 1.3 μg/l PKC412, 112 (43%) genes were downregulated and 147 (57%) upregulated. Of the 511 genes differentially expressed at 21 μg/l PKC412, 130 (25%) genes were downregulated and 381 (75%) were upregulated. Only 101 of the significantly altered genes were regulated at both concentrations; however, all of them were regulated in the same direction. At both concentrations, most functional groups of genes (FC, $\log_2$ at least twofold, $p \leq 0.05$) were similar. GO analysis was performed to identify functional groups of genes. GO defines terms representing gene product properties and covers three domains, namely, cellular components, molecular functions, and biological processes. At both concentrations, functionally identified genes fell into more than 1500 different categories. In Supplementary table S2, the top 100 GO processes are listed. GO categories including all kind of different detections or responses to stimuli are of particular importance, e.g., detection of light stimulus, detection of abiotic stimulus, detection/response to external stimulus, visual perception, etc. (Supplementary table S2).

In addition to the GO analysis, we performed a pathway analysis with MetaCore. The different treatments had 28 maps (1.3 μg/l PKC412: 29 maps; 21 μg/l PKC412: 34 maps) with their corresponding pathways in common (Supplementary table S3). These maps include pathways for lipid biosynthesis and regulation, cholesterol and bile acid homeostasis, angiogenesis, vitamin and cofactor metabolism and its regulation, mitogenic signaling, and apoptosis. For validation of these results, additional experiments were performed focusing on five significantly

altered maps (Table 3). Effects on angiogenesis were analyzed by performing an additional experiment with transgenic zebrafish. In addition, effects on apoptosis were analyzed by performing a TUNEL assay, DNA damage was assessed by a comet assay, and oxidative stress response by a ROS assay.

In order to confirm the microarray results, qRT-PCR was performed for eight selected genes (Table 3, Fig. 1). These genes belong to different pathways and were selected on their importance in different pathways: abcc4, cry5, ndrg1l, opn1mw2, pdpk1 1, per1, sos, and xpc. A downregulation occurred for abcc4, cry5, per1, and xpc, whereas an upregulation was found for ndrg1l, opn1mw2, pdpk, and sos (Fig. 1, Table 3). In all cases, except sos, the same tendency for up- or downregulation occurred for the microarray and for qRT-PCR analysis.

Effects on the Circadian Rhythm and Locomotor Activity

As shown in Supplementary table S1, PKC412 altered the expression of genes regulating circadian rhythm, e.g., cry1-5 (1.3 μg/l PKC412: −2.08, 3.9, −4.4, 2.3, −2.7 FC $\log_2$, respectively; 21 μg/l PKC: −1.54, 2.7, −3, 1.8, −2.9 FC $\log_2$, respectively), per1,2,4 (1.3 μg/l PKC412: −9.8, −2.04, −4.5 FC $\log_2$, respectively; 21 μg/l PKC: −6.4, −3.08, −3.17 FC $\log_2$, respectively), arntl (1.3 μg/l PKC412: 2.5 FC $\log_2$; 21 μg/l PKC: 3.12 FC $\log_2$), clock (1.3 μg/l PKC412: 2.9 FC $\log_2$; 21 μg/l PKC: 2.7 FC $\log_2$), etc. In mammals, the circadian rhythm controls a diversity of behavioral and physiological rhythmic processes such as regulation of sleep wakefulness, secretion of hormones, and locomotor activity (Hastings, 1997). In zebrafish, diazepam alters the same set of genes and influences the swimming behavior (Oggier et al., 2010). Therefore, an additional set of experiments was performed to evaluate whether changes found in the gene expression pattern of circadian genes

TABLE 4
Four Maps and Pathways to Which Additional Experiments
Were Performed Represented in MetaCore (FDR < 0.05)

Map	Pathway	p Value
Vascular development (angiogenesis)	Transcription_Role of Akt in hypoxia-induced HIF1 activation	3.414×10^{-2}
	Transcription_Receptor-mediated HIF regulation	
	Development_FGFR signaling pathway	
Apoptosis	Transcription_P53 signaling pathway	5.423×10^{-2}
	Development_Flt3 signaling	
	Apoptosis and survival_Role of CDK5 in neuronal death and survival	
	Apoptosis and survival_BAD phosphorylation	
	Apoptosis and survival_Antiapoptotic action of gastrin	
	Apoptosis and survival_HTR1A signaling	
DNA damage response	Transcription_P53 signaling pathway	1.146×10^{-1}
	DNA damage_Role of Brca1 and Brca2 in DNA repair	
	DNA damage_Brca1 as a transcription regulator	
	DNA damage_Nucleotide excision repair	
	Apoptosis and survival_BAD phosphorylation	
Oxidative stress regulation	Development_Dopamine D2 receptor transactivation of EGFR	4.140×10^{-1}

Note. EGFR: epidermal growth factor receptor.

in eleuthero-embryos were paralleled by changes in the locomotor activity. The behavioral experiments revealed that exposure of the embryos to PKC412 did not significantly affect their locomotor activity (Supplementary fig. S1).

Effects on Angiogenesis

Angiogenesis is an important process during cancerogenesis, which is affected by PKC412 in humans (Fabbro *et al.*, 2000). We hypothesized that similar effects occur in zebrafish embryos during development. Important genes in angiogenesis are the vascular endothelial growth factor (*vegf*), which is downregulated by PKC412 in humans (Fabbro *et al.*, 2000), and angiopoietin (*ang*). In our study, we did not find a significant alteration in *vegf* transcript levels in zebrafish eleuthero-embryo (data not shown). However, there is a significant upregulation of *ang2* (3.6 FC $\log_2$) in the higher PKC412 concentration of 31 μg/l (Supplementary table S1). *Ang2* is an antagonist of *ang1* and disrupts blood vessel formation when overexpressed (Maisonpierre *et al.*, 1997). In addition to alterations in gene expression, we also found a significant alteration of pathways involved in vascular development (Table 4).

In order to link these findings with physiological changes in blood vessel development, we exposed (Tg(fli1a:EGF-P)y1;Tg(gata1:dsRed)sd2) double-transgenic zebrafish embryos to 2 and 40 μg/l PKC412. Although focusing mostly on the trunk vasculature, we did not observe any abnormalities in cardiovascular development compared with control embryos. At 24 hpf, the dorsal aorta and the posterior cardinal vein developed normally and normal sprouting of the intersegmental vessels was observed. At 6 dpf, all the main vessels looked virtually identical in treated and control embryos (Fig. 2). Dorsal aorta, posterior cardinal vein, and intersegmental vessels were normally developed, and normal heart beat and blood flow was observed.

Twenty-five double-transgenic embryos from each treatment were analyzed in detail. We also looked at general morphology of the embryos. Single embryos from treated and control groups showed mild developmental abnormalities, which can occasionally be observed in nontreated fish, especially in transgenic lines. Five of 25 embryos treated with 40 μg/l PKC412 had a slightly misshaped trunk with the tail bend dorsally. However, the vasculature of these embryos was normal (Fig. 2). More analyses on wild-type embryos would be needed to find out whether this misshaping is because of the drug treatment.

Therefore, PKC412 did not negatively interfere up to 6 days with the vascular development of zebrafish embryos at both concentrations. However, the vascular network at this stage is already very complicated and subtle differences might have been gone unnoticed.

Effects on Apoptosis in Olfactory Placodes

PKC inhibitors can induce apoptosis in humans (Tenzer *et al.*, 2001). Thereby, the phosphatidylinositol 3′-kinase (PI3K3)/Akt pathway is of high importance as the cytotoxic effect of PKC412 is mediated by this pathway. In the apoptosis pathway, the phosphoinositide-dependent kinase (PDK) 1 (also called PDPK1) leads to phosphorylation of v-akt murine thymoma viral oncogene homolog Akt and therefore to its activation. Constitutively active Akt results in an enhanced protection against apoptotic cellular insults. In contrast to findings in humans, we found an upregulation of *pdpk* (Supplementary table S1, 2.6 FC $\log_2$) in the lower PKC412 concentration.

In addition, we found a downregulation of transcripts of *xpc*, a gene that is important for DNA damage recognition. Additionally, apoptotic pathways are of significance (Table 4). Based on these findings, we conducted a TUNEL assay to search for regions and tissue in the eleuthero-embryo where apoptosis is induced by PKC412. Supplementary figure S2 illustrates that apoptosis mostly occurred in the head region. The olfactory placode, which is important for the perception of odorants, is mainly affected. This finding is in parallel to the observed upregulation of gene transcripts of some odorant receptors *or102-3* (2.8 FC $\log_2$) and *or11-10* (2.2 FC $\log_2$) found by microarray analysis for the highest PKC412 concentration (Supplementary table S1), suggesting a repair of these affected cells.

OGGIER ET AL.
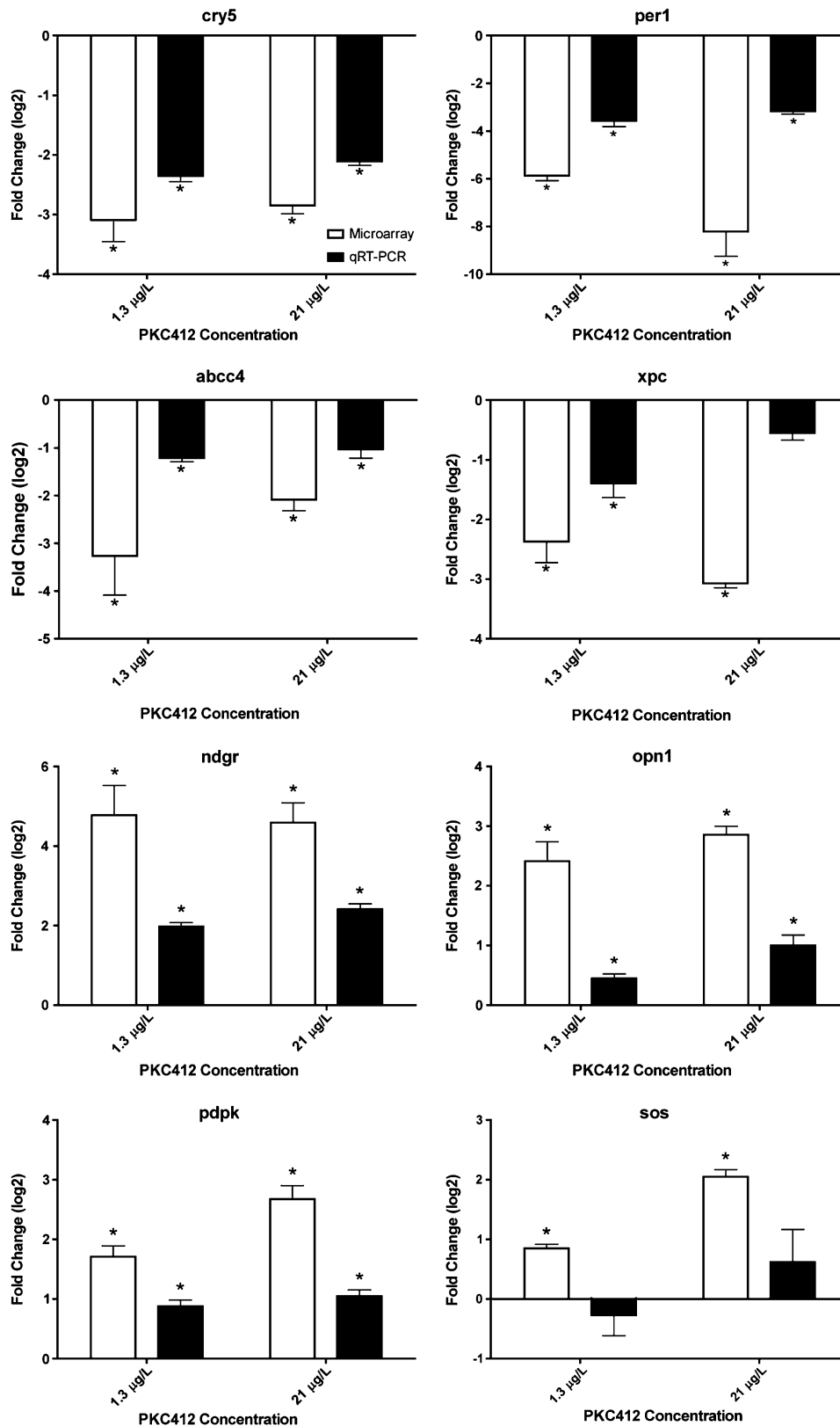
FIG. 1 Comparison of gene expression in zebrafish larvae determined by microarray ($n = 4$ replicates, 80 eleuthero-embryos pooled, white bars) and qRT-PCR ($n = 6$, 80 eleuthero-embryos, black bars) after exposure to 1.3 and 21 μg/l PKC412, respectively. Values are expressed as average FC ($\log_2$) with SE compared with control animals as indicated for selected genes. Asterisks (*) indicate statistically significant difference to control ($p < 0.05$).
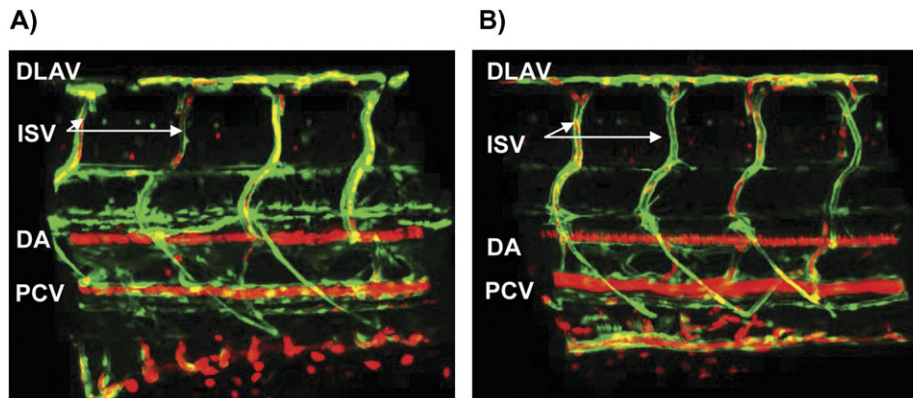
FIG. 2 Vascular development is not affected by PKC412 treatment. The vascular system was visualized in a double-transgenic zebrafish eleuthero-embryo (TG:fli1a:EGFPy1; gata1:DsRedsd2) on a Leica TCS SP5 Confocal Microscope. Endothelial cells are labeled in green and erythrocytes are labeled in red. (A) DMSO solvent control and (B) 40 µg/l PKC412. The pictures are maximal intensity projections of confocal z-stacks. DA, dorsal aorta; PCV, posterior cardinal vein; ISV, intersomitic vessel; DLAV, dorsal longitudinal anastomotic vessel. No major defects were detected in treated PKC412 embryos.

Effects on DNA Damage

PKC412 led to significant downregulation of *xpc*. At 1.6 and 31 µg/l PKC412, we found a 2.9 and 2.2 FC log$_2$, respectively, in *xpc* transcripts (Table 3, Fig. 1). Additionally, there was a downregulation of *apex* nuclease 1 (−2.7 FC log$_2$) at 31 µg/l PKC412. As *xpc* is important in DNA damage recognition and APEX1 for DNA repair, we conducted a comet assay to evaluate whether this alteration occurs not only on the transcription but also on the physiological level. Further support for potential DNA damage induced by PKC412 comes from the fact that pathways involved in DNA damage response were significantly affected (Table 4). The comet assay demonstrates a dose-dependent increase in DNA damage in eleuthero-embryos exposed to PKC412 (Fig. 3). Significant DNA damage occurred in the embryos at 31 µg/l PKC412. At the lower concentration of 1.6 µg/l PKC412, a significant increase in tail length, but not in percent DNA in tail, tail moment, and olive tail moment, occurred (Fig. 3).

Effects on Formation of ROS

MetaCore pathway analysis indicated that there is an alteration in oxidative stress regulation. To evaluate whether this is related to increased formation of ROS by PKC412, we performed an additional experiment to determine formation of ROS. The results show that the ROS levels remained unchanged at both PKC412 concentrations as compared with the control (Supplementary fig. S3), and thus PKC412 is not inducing ROS.

DISCUSSION

This is the first study investigating the effects of PKC412 on gene expression on nontarget organisms in aquatic systems. We show effects of PKC412 at low concentrations in zebrafish eleuthero-embryos. Thereby, we demonstrate that this human pharmaceutical exhibits its effects in aquatic organisms by similar molecular modes of action as in humans because of target conservation in vertebrates (Christen *et al.*, 2010 Gunnarsson *et al.*, 2008). We also tested the hypothesis that alteration in gene expression propagates into physiological effects.

PKC412 was designed as tyrosine kinase inhibitor with a broad inhibition spectrum of the human kinome. It was shown that at high-affinity interactions (Kd < 100nM), this compound was not highly selective for kinases (Karaman *et al.*, 2008). Consequently, it is not surprising that PKC412 alters more than 500 genes in zebrafish eleuthero-embryos at a concentration of 21 µg/l. Furthermore, the broad spectrum of kinases inhibited by the nonselective PKC412 makes the interpretation of the results challenging because of the involvement of many cellular pathways.

In humans, PKC412 inhibits FLT3, PDGF receptors, VEGF, and c-kit by preventing the tyrosine autophosphorylation (Fabbro *et al.*, 2000). In addition, this compound inhibits P-glycoprotein–mediated multidrug resistance in tumor cells. When comparing our results with human effects and gene expression changes obtained in MV4-11 cells (human lymphoblast cells) after treatment with 570 µg/l PKC412 (Stolzel *et al.*, 2010), some similarities show up. In zebrafish eleuthero-embryos, there were also alterations of solute carriers as in human cells (Stolzel *et al.*, 2010), albeit a solute carrier of family 2 was significantly downregulated in the lower concentration only. In addition, we similarly found a significant downregulation of the ABC transporter *abcc4*, which is important for the efflux of anticancer drugs. However, there was no alteration of *flt3*, *pdgfr*, *vegf*, and *c-kit* at the transcript level in zebrafish embryos. Binding of PKC412 leads to inhibition of these kinases; therefore, we hypothesize that PKC412 does not interfere with gene expression but protein function. One important identified GO category is visual
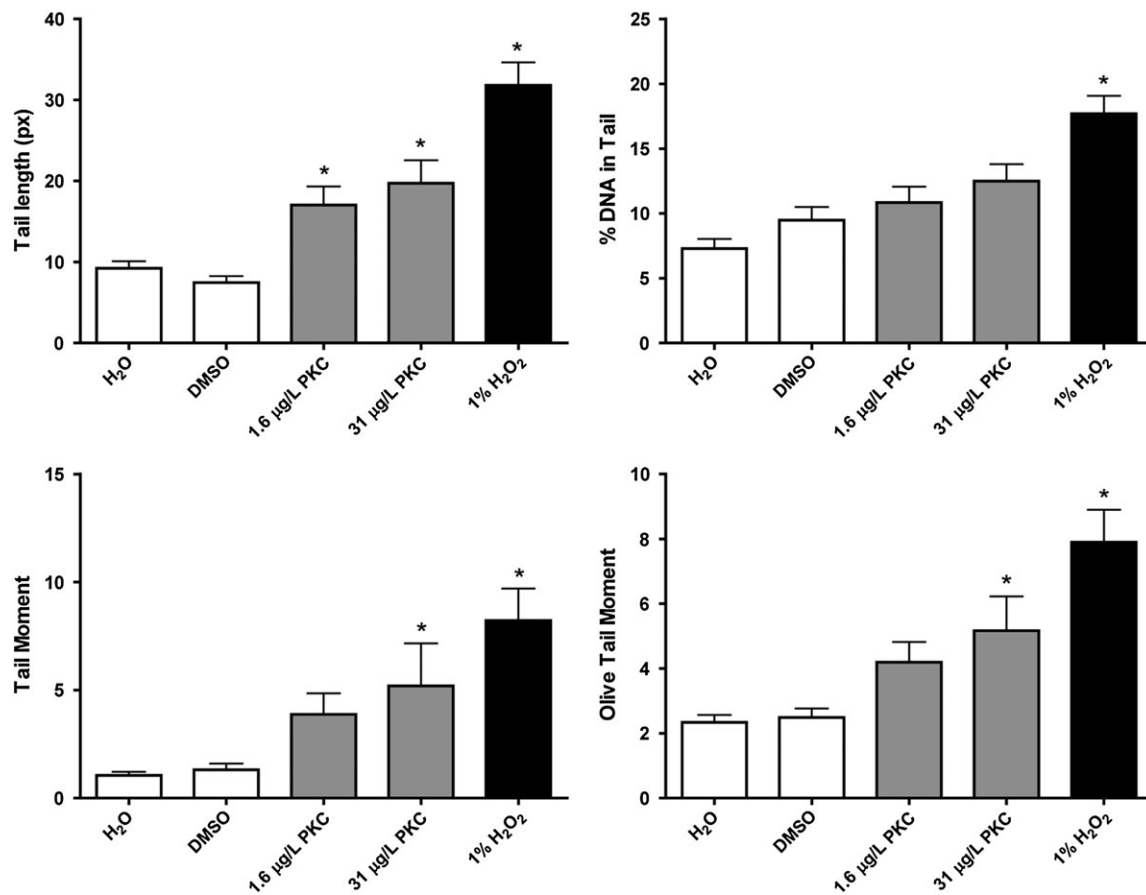
FIG. 3 Comet assay in zebrafish eleuthero-embryos exposed to 1.6 and 31 µg/l PKC412. (A) Tail length, (B) percent DNA in Tail, (C) Tail Moment, and (D) Olive Tail Moment were calculated using CometScore. Four slides per dosage were examined, and 24 cells per slide were scored. The values are presented as the mean ± SEM. Asterisks (*) indicate values that are significantly different from the control (Kruskall-Wallis test followed by *post hoc* Dunn's multiple comparison test; $p < 0.05$).

perception. Expression of genes encoding proteins involved in vision such as crystallins and opsins were significantly altered by PKC412. Crystallins are important for the protection against lens opacity (Clark, 2004), and opsins are important for dim-/daylight vision and color vision (Takechi and Kawamura, 2005). These findings in zebrafish are similar to results obtained in mice and humans after treatment with PKC412. There are several VEGF and PDGF receptors in the retina. The inhibition of these receptors can lead to decreased epiretinal membrane formation in mice (Saishin *et al.*, 2003) and reduction in macular edema in humans (Campochiaro, 2004). Therefore, upregulation of crystallins and opsins may be a response to the inhibition of VEGF and PDGF receptors.

In addition to visual perception, we also found that responses to light and external/internal stimuli are important targets of PKC412. As the circadian rhythm is dependent on stimuli, namely, Zeitgeber, there is a significant alteration of those genes at both PKC412 concentrations in zebrafish. It is known that in mice, several protein kinases C are expressed in the hypothalamic suprachiasmattic nuclei (SCN) (Van der Zee and

Bult, 1995), the region which is important for circadian processes. Therefore, protein kinases C play an important role in the mammalian circadian rhythm, and inhibition of PKC can lead to phase advances (Jakubcakova *et al.*, 2007; Schak and Harrington, 1999). As PKC is already expressed in the early zebrafish development (Patten *et al.*, 2007; Slatter *et al.*, 2005), it could be affected in the SCN. Additionally, it was shown in the marine dinoflagellate *Lingulodinium polyedrum* that staurosporine (precursor of PKC412) leads to phase shifting and it increases the free running period of the circadian rhythm (Comolli and Hastings, 1999). At the behavioral level, altered expression of clock genes is correlated with changes in the locomotor activity (Jakubcakova *et al.*, 2007). For this reason, we investigated the effects of PKC412 on the locomotor activity. However, PKC412 had no significant effect on the locomotor activity in our experimental setup. A reason could be that an observation over 2 h is too short to obtain significant effects. Also the time point when the measurements took place could have an influence. We performed our measurements at daylight, and effects would have probably been more pronounced at night.

In addition to exploring effects on different GO categories, we performed a pathway analysis in order to elucidate altered maps and pathways after PKC412 exposure. Out of the 28 maps, we chose four different maps with their corresponding pathways to perform additional experiments. It is known from humans that PKC412 can have effects on angiogenesis and apoptosis including DNA damage repair. However, there are no indications from mammalian studies that PKC412 exposure can lead to the formation of ROS.

The need for new blood vessels is important during embryogenesis, as well as in processes during cancerogenesis (Carmeliet and Jain, 2000). The formation of blood vessels and evaluation of blood flow can be observed in zebrafish eleuthero-embryos, rendering it an ideal model organism to study angiogenesis. As angiogenesis is affected by PKC412 in humans (Fabbro *et al.*, 2000), we hypothesize that similar effects occur in zebrafish eleuthero-embryos. Thereby, angiopoietins play an important role (Kubota *et al.*, 2005; Pham *et al.*, 2001). In fact, we found a significant upregulation of *ang2*. It was shown that overexpression of *ang2* can lead to blood vessel disruption in the mouse embryo (Maisonpierre *et al.*, 1997). There is also a simultaneous regulation of VEGF and angiopoietin. However, angiopoietins do not participate in the initial vascular phase of vascular development but rather play an important role in angiogenic outgrowth, vessel remodeling, and maturation (Dumont *et al.*, 1994; Suri *et al.*, 1996). Our results obtained after the exposure of double-transgenic zebrafish eleuthero-embryos support the findings that angiopoietins do not participate in the initial vascular phase. In addition, our findings are in agreement with those obtained after exposure of zebrafish eleuthero-embryos to 57 µg/l for 24 hpf (Chan *et al.*, 2002). PKC412 did not generate measurable antiangiogenic effects during the exposure time. It may be possible that there are strain differences between zebrafish that account for our failure to detect vascular defects in transgenic fish. However, our results are in line with the microarray data in the sense that we did not find any alteration in *vegf* transcript levels. In addition, the defects in the vasculature might be too subtle to detect upon PKC412 treatment, so that they went unnoticed in our assays.

PKC inhibitors can induce apoptosis in humans (Tenzer *et al.*, 2001). To protect mammals from apoptotic stress stimuli, the PI3K/Akt survival pathway is important. In this pathway, Akt needs to be phosphorylated by the PDK1, which was found to be downregulated in mice after treatment with staurosporine (Hill *et al.*, 2001). In mice, PKC412 can mediate its cytotoxic effects partly via downregulation of this pathway. Additionally, PKC412 decreased the site-specific phosphorylation of Akt required for its activity (Tenzer *et al.*, 2001). In contrast to these findings, we found an upregulation of the upstream *pdpk1* at the lower PKC412 concentration. This leads to the hypothesis that there is no downregulation of the Akt pathway but a protection against apoptosis. However, there is the indication that the failure in DNA damage recognition

(downregulation of *xpc*) is more important, and therefore, apoptosis is induced in limited regions of the eleutheroembryo. The TUNEL assay showed that apoptotic cells were located in the olfactory placodes (fig. S2). As there is also an upregulation of odorant receptors, which are mainly expressed in the olfactory placodes, we suggest that this is a reaction to the damage and associated to repairing the loss of cells. Yet, there is no evidence for this phenomenon in mammals.

DNA damage can be paralleled with apoptosis. To evaluate whether alterations in *xpc* and *apex* can be linked to DNA damage, we performed comet assays. There is a clear link between gene expression alteration and DNA damage at both PKC412 concentrations. Although there is not significantly more DNA in the tail, there is a significant increase in tail length indicating that DNA damage took place. Data from the comet assay demonstrate that gene expression changes in DNA damage recognition are paralleled with intracellular DNA damage. These data are in agreement with the results obtained in human lymphoblast cells after treatment with PKC412 (Seedhouse *et al.*, 2006).

We also showed that physiological outcomes of maps of low significance, as the regulation of oxidative stress, do not correlate with the obtained gene expression. Nevertheless, several markers such as metallothionein (*mt*, 2.3-fold downregulated at 21 µg/l) and glutathione *S*-transferase M (*gstm*, 1.1- and 1.2-fold downregulated at 1.3 and 21 µg/l, respectively) were significantly altered. It is known that *mt* is upregulated by free radicals in rainbow trout cells (Kling and Olsson, 2000). Our findings on the alteration of *gst* are in contrast with those obtained in goldfish after treatment with gemfibrozil, which is supposed to downregulate the antioxidant defense system (Mimeault *et al.*, 2006). However, the gene expression of other markers such as the superoxide dismutase (*sod*) or the catalase (*cat*) was not altered.

In our study, we demonstrate that the response of zebrafish eleuthero-embryo to different PKC412 concentrations is partly similar to the response in humans. Significant changes in gene expression occurred at low concentrations of 1.3 µg/l PKC412. This demonstrates that alterations in gene expression are more sensitive than mortality and physiological effects. Additionally, the gene expression profile points to the modes of action of PKC412 in zebrafish. Because of the very broad kinase inhibition spectrum of PKC412, a correlation to physiological alterations is difficult. In some cases, gene expression changes were not paralleled by physiological changes at low concentrations and sometimes even at high concentrations. This raises the question whether and when gene expression changes propagate to toxicological relevant measures such as reduction of the ability to find food, to reproduce, or to escape from predators.

In conclusion, the present study confirms that the toxicogenomic approach provides important data to identify and characterize molecular effects and to investigate potential modes of action of an antineoplastic agent. This allows for establishing

new biomarkers, not regularly assessed in routine ecotoxicological studies. PKC412-induced alterations of gene transcripts were partly paralleled by physiological effects at high, but not at low, PKC412 concentrations that may be of environmental relevance. Our study also shows that molecular studies should be paralleled with ecotoxicological investigations of known ecological relevance to interrelate sensitive changes in gene expression to physiological effects.

SUPPLEMENTARY DATA

Supplementary data are available online at http://toxsci.oxfordjournals.org/.

REFERENCES

Campochiaro, P. A. (2004). Reduction of diabetic macular edema by oral administration of the kinase inhibitor PKC412. *Invest. Ophthalmol. Vis. Sci.* **45,** 922–931.

Carmeliet, P., and Jain, R. K. (2000). Angiogenesis in cancer and other diseases. *Nature* **407,** 249–257.

Chabner, B. A., Ryan, D. P., Paz-Ares, L., Garcia-Carbonero, R., and Calabresi, P. (2006). Antineoplastic agents. In *Goodman and Gilman's—The Pharmalogical Basis of Therapeutics* (Hardman, J. G. and Limbird, L. E., Eds.), pp. 1396–1397. McGraw-Hill, New York.

Chan, J., Bayliss, P. E., Wood, J. M., and Roberts, T. M. (2002). Dissection of angiogenic signaling in zebrafish using a chemical genetic approach. *Cancer Cell* **1,** 257–267.

Christen, V., Hickmann, S., Rechenberg, B., and Fent, K. (2010). Highly active human pharmaceuticals in aquatic systems: A concept for their identification based on their mode of action. *Aquat. Toxicol.* **96,** 167–181.

Clark, J. I. (2004). Order and disorder in the transparent media of the eye. *Exp. Eye Res.* **78,** 427–432.

Comolli, J. C., and Hastings, J. W. (1999). Novel effects on the Gonyaulax circadian system produced by the protein kinase inhibitor staurosporine. *J. Biol. Rhythms* **14,** 11–19.

Deng, J., Yu, L., Liu, C., Yu, K., Shi, X., Yeung, L. W., Lam, P. K., Wu, R. S., and Zhou, B. (2009). Hexabromocyclododecane-induced developmental toxicity and apoptosis in zebrafish embryos. *Aquat. Toxicol.* **93,** 29–36.

Dumont, D. J., Gradwohl, G., Fong, G. H., Puri, M. C., Gertsenstein, M., Auerbach, A., and Breitman, M. L. (1994). Dominant-negative and targeted null mutations in the endothelial receptor tyrosine kinase, tek, reveal a critical role in vasculogenesis of the embryo. *Genes Dev.* **8,** 1897–1909.

Duong, F. H., Christen, V., Lin, S., and Heim, M. H. (2010). Hepatitis C virus-induced up-regulation of protein phosphatase 2A inhibits histone modification and DNA damage repair. *Hepatology* **51,** 741–751.

European Medicines Agency (EMEA). (2006). *Guideline on the Environmental Risk Assessment of Medicinal Products for Human Use.* EMEA, London.

Fabbro, D., Ruetz, S., Bodis, S., Pruschy, M., Csermak, K., Man, A., Campochiaro, P., Wood, J., O'Reilly, T., and Meyer, T. (2000). PKC412—a protein kinase inhibitor with a broad therapeutic potential. *Anticancer Drug Des.* **15,** 17–28.

Fent, K., Weston, A. A., and Caminada, D. (2006). Ecotoxicology of human pharmaceuticals. *Aquat. Toxicol.* **76,** 122–159.

Gerhardt, A., Clostermann, M., Fridlund, B., and Svensson, E. (1994). Monitoring of behavioral patterns of aquatic organisms with an impedance conversion technique. *Environ. Int.* **20,** 209–219.

Gunnarsson, L., Jauhiainen, A., Kristiansson, E., Nerman, O., and Larsson, D. G. (2008). Evolutionary conservation of human drug targets in organisms used for environmental risk assessments. *Environ. Sci. Technol.* **42,** 5807–5813.

Hastings, M. H. (1997). Central clocking. *Trends Neurosci.* **20,** 459–464.

Hill, M. M., Andjelkovic, M., Brazil, D. P., Ferrari, S., Fabbro, D., and Hemmings, B. A. (2001). Insulin-stimulated protein kinase B phosphorylation on Ser-473 is independent of its activity and occurs through a staurosporine-insensitive kinase. *J. Biol. Chem.* **276,** 25643–25646.

Jakubcakova, V., Oster, H., Tamanini, F., Cadenas, C., Leitges, M., van der Horst, G. T., and Eichele, G. (2007). Light entrainment of the mammalian circadian clock by a PRKCA-dependent posttranslational mechanism. *Neuron* **54,** 831–843.

Jones, O. A., Voulvoulis, N., and Lester, J. N. (2007). Ecotoxicity of pharmaceuticals. In *Analysis, Fate and Removal of Pharmaceuticals in the Water Cycle* (Petrovic, M., and Barcelo, D., Eds.), pp. 387–424. Oxford, Elsevier.

Karaman, M. W., Herrgard, S., Treiber, D. K., Gallant, P., Atteridge, C. E., Campbell, B. T., Chan, K. W., Ciceri, P., Davis, M. I., Edeen, P. T., *et al.* (2008). A quantitative analysis of kinase inhibitor selectivity. *Nat. Biotechnol.* **26,** 127–132.

Kimmel, C. B., Ballard, W. W., Kimmel, S. R., Ullmann, B., and Schilling, T. F. (1995). Stages of embryonic development of the zebrafish. *Dev. Dyn.* **203,** 253–310.

Kling, P. G., and Olsson, P.-E. (2000). Involvement of differential metallothionein expression in free radical sensitivity of RTG-2 and CHSE-214 cells. *Free Radic. Biol. Med.* **28,** 1628–1637.

Kubota, Y., Oike, Y., Satoh, S., Tabata, Y., Niikura, Y., Morisada, T., Akao, M., Urano, T., Ito, Y., Miyamoto, T., *et al.* (2005). Cooperative interaction of Angiopoietin-like proteins 1 and 2 in zebrafish vascular development. *Proc. Natl. Acad. Sci. U.S.A.* **102,** 13502–13507.

Lawson, N. D., and Weinstein, B. M. (2002). In vivo imaging of embryonic vascular development using transgenic zebrafish. *Dev. Biol.* **248,** 307–318.

Maisonpierre, P. C., Suri, C., Jones, P. F., Bartunkova, S., Wiegand, S. J., Radziejewski, C., Compton, D., McClain, J., Aldrich, T. H., Papadopoulos, N., *et al.* (1997). Angiopoietin-2, a natural antagonist for Tie2 that disrupts *in vivo* angiogenesis. *Science* **277,** 55–60.

Mimeault, C., Trudeau, V. L., and Moon, T. W. (2006). Waterborne gemfibrozil challenges the hepatic antioxidant defense system and down-regulates peroxisome proliferator-activated receptor beta (PPARβ) mRNA levels in male goldfish (*Carassius auratus*). *Toxicology* **228,** 140–150.

Monteiro, S. C., and Boxall, A. B. (2010). Occurrence and fate of human pharmaceuticals in the environment. *Rev. Environ. Contam. Toxicol.* **202,** 53–154.

Oggier, D. M., Weisbrod, C., Stoller, A., Zenker, A., and Fent, K. (2010). Effects of diazepam on gene expression and link to physiological effects in different life stages in zebrafish. *Danio rerio. Environ. Sci. Technol.* **44,** 7685–7691.

Patten, S. A., Sihra, R. K., Dhami, K. S., Coutts, C. A., and Ali, D. W. (2007). Differential expression of PKC isoforms in developing zebrafish. *Int. J. Dev. Neurosci.* **25,** 155–164.

Pham, V. N., Roman, B. L., and Weinstein, B. M. (2001). Isolation and expression analysis of three zebrafish angiopoietin genes. *Dev. Dyn.* **221,** 470–474.

Robbens, J., van der Ven, K., Maras, M., Blust, R., and De Coen, W. (2007). Ecotoxicological risk assessment using DNA chips and cellular reporters. *Trends Biotechnol.* **25,** 460–466.

Runnalls, T. J., Hala, D. N., and Sumpter, J. P. (2007). Preliminary studies into the effects of the human pharmaceutical clofibric acid on sperm parameters in adult fathead minnow. *Aquat. Toxicol.* **84,** 111–118.

Saishin, Y., Takahashi, K., Seo, M. S., Melia, M., and Campochiaro, P. A. (2003). The kinase inhibitor PKC412 suppresses epiretinal membrane formation and retinal detachment in mice with proliferative retinopathies. *Invest. Ophthalmol. Vis. Sci.* **44,** 3656–3662.

Schak, K. M., and Harrington, M. E. (1999). Protein kinase C inhibition and activation phase advances the hamster circadian clock. *Brain Res.* **840,** 158–161.

Seedhouse, C. H., Hunter, H. M., Lloyd-Lewis, B., Massip, A. M., Pallis, M., Carter, G. I., Grundy, M., Shang, S., and Russell, N. H. (2006). DNA repair contributes to the drug-resistant phenotype of primary acute myeloid leukaemia cells with FLT3 internal tandem duplications and is reversed by the FLT3 inhibitor PKC412. *Leukemia* **20,** 2130–2136.

Si, M. S., Reitz, B. A., and Borie, D. C. (2005). Effects of the kinase inhibitor CGP41251 (PKC 412) on lymphocyte activation and TNF-alpha production. *Int. Immunopharmacol.* **5,** 1141–1149.

Slatter, C. A. B., Kanji, H., Coutts, C. A., and Ali, D. W. (2005). Expression of PKC in the developing zebrafish, *Danio rerio. J. Neurobiol.* **62,** 425–438.

Stolzel, F., Steudel, C., Oelschlagel, U., Mohr, B., Koch, S., Ehninger, G., and Thiede, C. (2010). Mechanisms of resistance against PKC412 in resistant FLT3-ITD positive human acute myeloid leukemia cells. *Ann. Hematol.* **89,** 653–662.

Suri, C., Jones, P. F., Patan, S., Bartunkova, S., Maisonpierre, P. C., Davis, S., Sato, T. N., and Yancopoulos, G. D. (1996). Requisite role of angiopoietin-1, a ligand for the TIE2 receptor, during embryonic angiogenesis. *Cell* **87,** 1171–1180.

Takahashi, I., Saitoh, Y., Yoshida, M., Sano, H., Nakano, H., Morimoto, M., and Tamaoki, T. (1989). UCN-01 and UCN-02, new selective inhibitors of protein kinase C. II. Purification, physico-chemical properties, structural determination and biological activities. *J. Antibiot. (Tokyo)* **42,** 571–576.

Takechi, M., and Kawamura, S. (2005). Temporal and spatial changes in the expression pattern of multiple red and green subtype opsin genes during zebrafish development. *J. Exp. Biol.* **208,** 1337–1345.

Tenzer, A., Zingg, D., Rocha, S., Hemmings, B., Fabbro, D., Glanzmann, C., Schubiger, P. A., Bodis, S., and Pruschy, M. (2001). The phosphatidylinositide 3'-kinase/Akt survival pathway is a target for the anticancer and radiosensitizing agent PKC412, an inhibitor of protein kinase C. *Cancer Res.* **61,** 8203–8210.

Ternes, T. A. (1998). Occurrence of drugs in German sewage treatment plants and rivers. *Water Res.* **32,** 3245–3260.

Traver, D., Paw, B. H., Poss, K. D., Penberthy, W. T., Lin, S., and Zon, L. I. (2003). Transplantation and *in vivo* imaging of multilineage engraftment in zebrafish bloodless mutants. *Nat. Immunol.* **4,** 1238–1246.

Van der Zee, E. A., and Bult, A. (1995). Distribution of AVP and Ca2+-dependent PKC-isozymes in the suprachiasmatic nucleus of the mouse and rabbit. *Brain Res.* **701,** 99–107.

5.3 Distinct cellular mechanisms contribute to vessel anastomosis and lumen formation in the zebrafish DLAVs

Lukas Herwig[1], Yannick Blum[1], Alice Krudewig, Elin Ellertsdottir, Anna Lenard, Heinz-Georg Belting and Markus Affolter

Contribution:

I performed experiments for visualization of apical membrane during anastomosis in wild type and *silent heart* embryos using anti-Podocalyxin 2 and anti-ZO-1 antibodies (Figure 4). I made the schematic cellular model of blood vessel fusion (Figure 5). I contributed to the figure preparation and discussions during writing of the manuscript.

Report

Distinct Cellular Mechanisms of Blood Vessel Fusion in the Zebrafish Embryo

Lukas Herwig,[1,2] Yannick Blum,[1,2] Alice Krudewig,[1]
Elin Ellertsdottir,[1] Anna Lenard,[1] Heinz-Georg Belting,[1,*]
and Markus Affolter[1,*]
[1]Biozentrum der Universität Basel, Klingelbergstrasse 70,
CH-4056 Basel, Switzerland

Summary

Although many of the cellular and molecular mechanisms of angiogenesis have been intensely studied [1], little is known about the processes that underlie vascular anastomosis. We have generated transgenic fish lines expressing an EGFP-tagged version of the junctional protein zona occludens 1 (ZO1) to visualize individual cell behaviors that occur during vessel fusion and lumen formation in vivo. These life observations show that endothelial cells (ECs) use two distinct morphogenetic mechanisms, cell membrane invagination and cord hollowing to generate different types of vascular tubes. During initial steps of anastomosis, cell junctions that have formed at the initial site of cell contacts expand into rings, generating a cellular interface of apical membrane compartments, as defined by the localization of the apical marker podocalyxin-2 (Pdxl2). During the cord hollowing process, these apical membrane compartments are brought together via cell rearrangements and extensive junctional remodeling, resulting in lumen coalescence and formation of a multicellular tube. Vessel fusion by membrane invagination occurs adjacent to a preexisting lumen in a proximal to distal direction and is blood-flow dependent. Here, the invaginating inner cell membrane undergoes concomitant apicobasal polarization and the vascular lumen is formed by the extension of a transcellular lumen through the EC, which forms a unicellular or seamless tube.

Results and Discussion

Generation and expansion of vascular beds by vascular remodeling involves a variety of morphogenetic mechanisms such as angiogenic sprout and lumen formation, as well as blood vessel fusion (anastomosis) and vessel pruning. Anastomosis is the essential process that converts dead-end sprouts into a functional vascular network. Angiogenic sprouts are guided by so-called tip cells, which are more motile and send out more filopodia than the trailing stalk cells [2]. During the first step of anastomosis, tip cells from neighboring sprouts establish contact with each other [3, 4]. Subsequently, endothelial cells (ECs) from neighboring sprouts form a continuous endothelium and their lumens are connected. How these events are achieved and coordinated at the cellular level is not known. We have used the zebrafish dorsal longitudinal anastomotic vessels (DLAV) as a model to analyze the cellular mechanisms that underlie vascular anastomosis in vivo. To this end,

we generated transgenic reporter lines that label endothelial cell junctions [Tg(*fli1ep:GAL4FF*[ubs2-4]) and Tg(*UAS:EGFP-ZO1*[ubs5-6]), see Figure S1 available online]. These lines allowed us to follow individual cell junctions and, consequently, relative cell movements and cell shape changes, as they occur during vascular remodeling.

The DLAV is formed in a seemingly stereotypic pattern by the anastomosis of neighboring segmental arteries (SA) [5]. Tip cells of individual SAs that have reached the roof of the neural tube extend processes laterally both in rostral and caudal directions. Some of these filopodia emanating from neighboring tip cells eventually contact each other, stabilize, and integrate into the DLAV. During further development, a lumen extends through the SA and the DLAV (see Figure 1A and Figure S1A). We first examined the cellular architecture of the DLAV to determine whether this vessel is made of unicellular or multicellular tubes. By photoconversion of the fluorophore KAEDE in Tg(*fli1ep:GAL4FF*[ubs3]; *UAS:KAEDE*[rk8]) embryos, we labeled single cells within the DLAV and determined whether these spanned the circumference of the DLAV either entirely or partially (Figures 1B and 1C). In 16 out of 24 cases, we found cells enclosing the entire lumen representing a unicellular tube, whereas in 8 out of 24 cases, labeled cells covered the vessel only partially, which is indicative for multicellular tubes. To test whether the different cellular arrangements correspond to the patterns of EC junctions, we performed photoconversion experiments and subsequently visualized adherens junctions by immunofluorescence using an antibody against zebrafish-VE-cadherin (zf-VE-cad) [6]. Consistently, we found that unicellular regions did not contain junctions (Figures 1D and 1D′), whereas photoconverted cells, which are nested within a multicellular region, were demarcated by longitudinal lines of VE-cad (Figures 1E and 1E′).

To visualize endothelial cell contacts in vivo, we generated transgenic reporter lines Tg(*UAS:EGFP-ZO1*[ubs5-6]) (Figure S1B). In double transgenic embryos (Tg*fli1ep:GAL4FF*[ubs3]; *UAS:EGFP-ZO1*[ubs5]), we compared the localization of the EGFP-zona occludens 1 (ZO1) fusion protein with the distribution of VE-cad and found that it specifically labels cell junctions, albeit in a mosaic fashion (Figure S1C). Furthermore, we confirmed the heterogeneity in vascular architecture described above by the junctional patterns observed in vivo in these embryos. We found regions that had predominantly ring-shaped cell contacts (Figure 1F) as well as regions that contained more complex junctional patterns (Figure 1G). Thus, DLAVs are heterogeneous in their architecture and can consist of different types of tubes: unicellular tubes, multicellular tubes, and tubes of mixed cellular arrangements.

To analyze the cellular dynamics of DLAV formation, we first focused on the initial events of contact formation between neighboring tip cells. From studies using immunofluorescent detection of ZO-1, we previously proposed a model in which interactions between tip cells lead to the generation of junctional spots at the contact sites [6]. These spots elaborate into rings as the cells increase their mutual surface area. Analysis of VE-cad protein revealed identical patterns (Figures 1H–1J). Because this sequence of events was inferred from observations in fixed tissues, we wanted to test this model in

[2]These authors contributed equally to this work
*Correspondence: heinz-georg.belting@unibas.ch (H.-G.B.), markus.affolter@unibas.ch (M.A.)
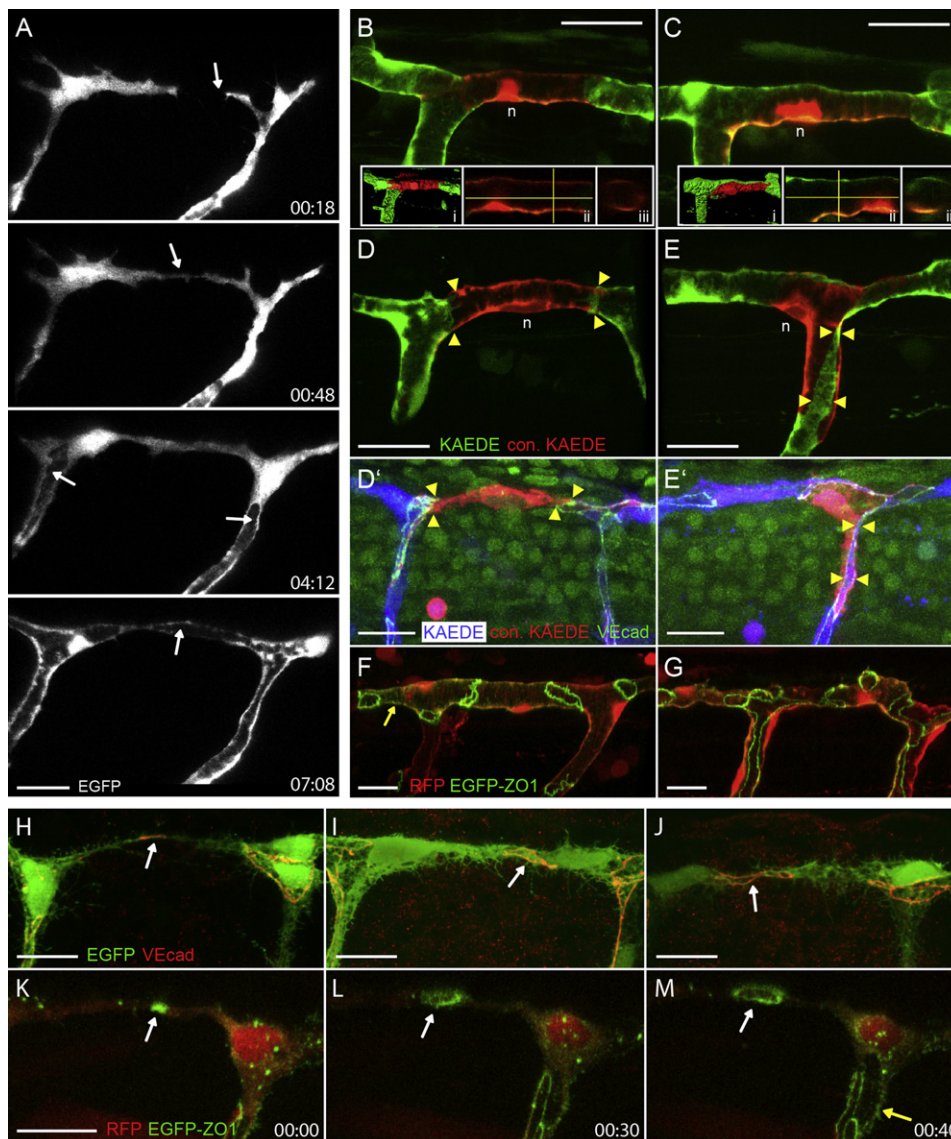
Figure 1. Anastomosis and Heterogeneity of Endothelial Tubes

(A) Still pictures of a time-lapse movie (data not shown) showing steps during dorsal longitudinal anastomotic vessel (DLAV) formation. Tip cells reach the dorsal side of the embryo and send filopodia in anterior and posterior directions (arrow in 00:18 [hr:min]). The tip cells contact each other and form the future DLAV (arrow in 00:48). Later the lumen opens from the stalk and proceeds into the DLAV (arrows in 4:12 and 7:08).

(B–G) Different vessel architectures are found in the intersegmental vessel (ISV)/DLAV. Single, photoconverted cells (red) show a unicellular (B) or a multicellular arrangement (C). Inserts (i–iii) in (B) and (C) show a surface calculation (i), a sagittal section (ii), and a cross-section (iii) at the sites indicated by crosshairs (n = nucleus).

(D–E′) Single photoconverted cells (red) and corresponding VE-cadherin (VE-cad) immunostainings. Arrowheads indicate regions of unicellular (D and D′) and multicellular (E and E′) tubes. A unicellular tube outlined by EGFP-zona occludens 1 (ZO1) fusion protein is shown in (F), and multicellular/unicellular and mixed arrangements represented by EGFP-ZO1 protein are shown in (G). The yellow arrow in (F) points at delocalized EGFP-ZO1 protein in the cell membrane, most likely due to elevated levels of protein.

(H–J) VE-cad immunostainings of 30 hrs postfertilization (hpf) old *fli:EGFP* embryos. Spots and small and larger rings are shown in (H), (I), and (J), respectively (see arrows).

(K–M) Still pictures of Movie S1 showing a time-lapse of a *fli:GAL4FF; UAS:RFP; UAS:EGFP-ZO1* embryo. An initial contact spot of EGFP-ZO1 (arrow in K) is elaborated into a small (arrow in L) and subsequently into a larger loop (arrow in M; Movie S1). The yellow arrow in (M) points to delocalized EGFP-ZO1 in the cell membrane (compare F and Figure S1). Scale bar in all pictures represents 20 μm.

an in vivo situation by performing confocal time-lapse analyses on our EGFP-ZO1 reporter lines. In essence, the pattern of EGFP-ZO1 was congruent with our previous observations, thus confirming the above model (Figures 1K–1M; Movie S1). Moreover, junctional remodeling is extremely dynamic—the transformation from spots to rings occurs within less than 40 min.

Whereas initiation of anastomosis appeared to be consistently associated with formation of ring-shaped junctions, the subsequent establishment of the DLAV showed considerably greater complexity and variety—in respect to (1) junctional remodeling, which corresponds to extensive cell rearrangements, (2) the generation of a continuous endothelium with apical-basal polarity, and (3) lumen formation. After
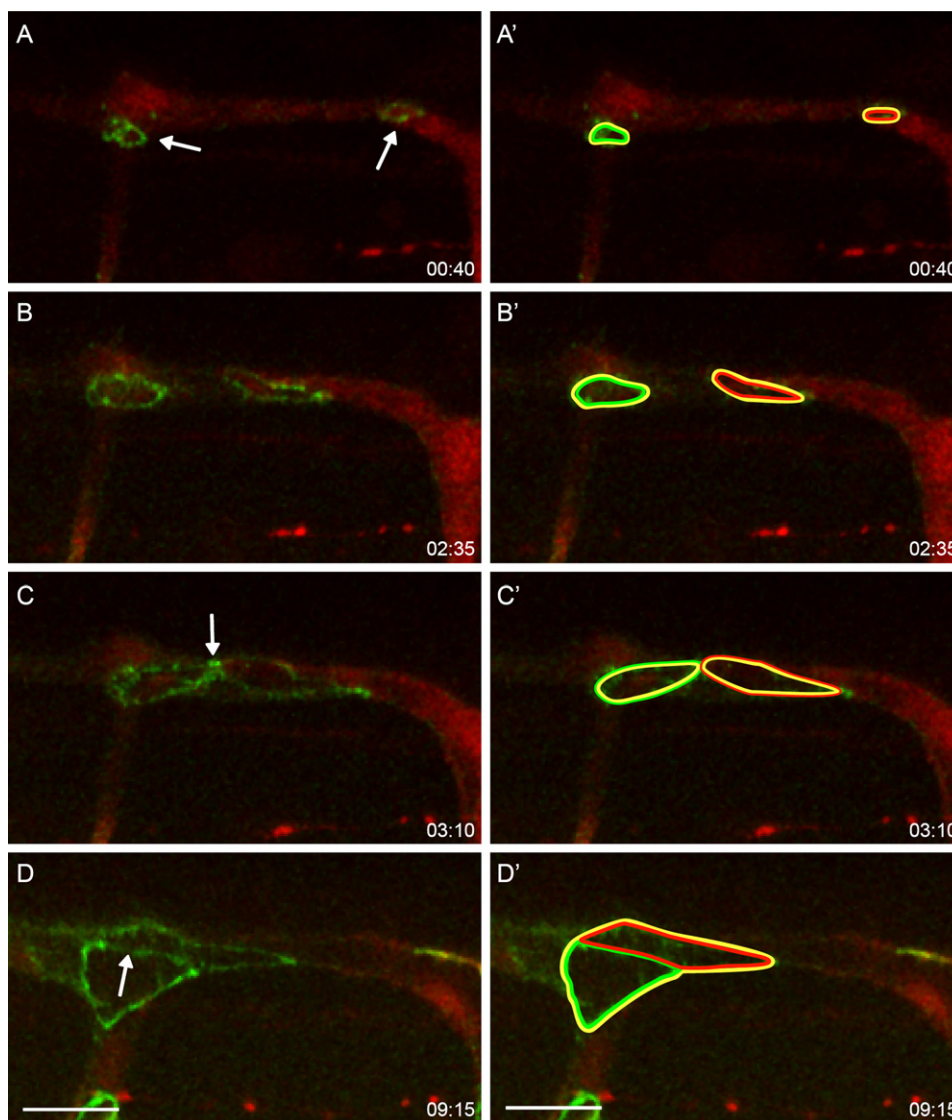
Figure 2. Anastomosis by Cord Hollowing

Still pictures from Movie S2 showing a time-lapse of a *fli:GAL4FF; UAS:RFP; UAS:EGFP-ZO1* embryo (total length: 9:20).

(A–C) A tip cell has established contact with an adjacent tip cell (right arrow) and has contact with a stalk cell (left arrow), which results in two loops of EGFP-ZO1 (A). These loops extend and eventually meet (B and C).

(A′–D′) shows the junctional outline of participating cells (yellow: "central" cell, green: stalk cell, red: DLAV cell moving in from posterior [right]). The two initial cell contacts are shown in yellow/green and yellow/red, respectively. When the stalk cell and the adjacent DLAV cell meet, they establish a new contact with "green and red" junctions (arrow in D, green and red line in D′). Scale bar in all pictures represents 20 μm.

analysis of 15 time-lapse movies representing 19 fusion events, we were able to discern two distinct behaviors with regard to junctional remodeling, which show two alternative cellular mechanisms that underlie DLAV formation (Figure 2; Figure 3).

In many instances (7 out of 19 events), we observed a mechanism that is primarily driven by cell rearrangements (Figure 2; Movie S2). Here, cell contacts between at least three adjacent cells generate two junctional rings, which converge toward each other as the outer cells migrate over a central cell. This convergence ultimately leads to novel contacts between the outer cells, the establishment of a new junction, and the detachment of the medial cell at this site of contact (summarized in Figure S2). Thus, the outcome of this process is the merging of local lumens, which are contained within the

junctional rings, to form a continuous luminal space. In principle, this mechanism of luminal coalescence can act locally or, if occurring iteratively, can be used to lumenize longer stretches to generate a patent tube.

In the majority of time-lapse movies (12 out of 19 events), we observed an alternate mechanism of vessel fusion that is intrinsically connected to a different mechanism of lumen formation. In these instances, junctional rings did not move or extend toward each other, the cells exhibited much less migratory behavior, and we did not find continuous adherens junctions along the vascular axis (Figure 3; Movie S3). Instead, the ECs maintained their junctions in a ring shape throughout the process of lumenization. Imaging the dynamics of lumen formation in vivo, either by intravascular quantum dot injection or by lack of cytoplasmic RFP, revealed that the lumen
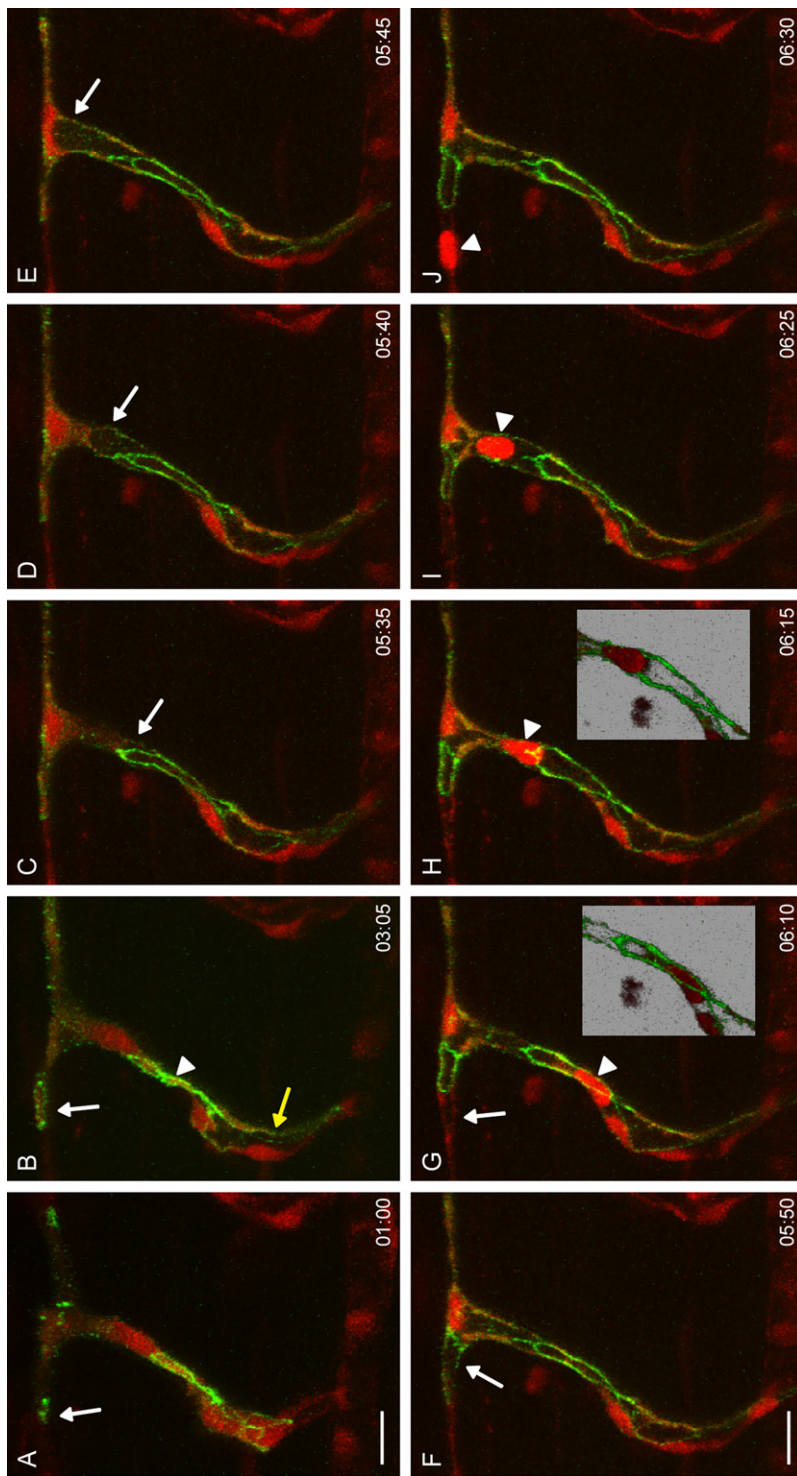
Figure 3. Anastomosis by Membrane Invagination

Still pictures from Movie S3 showing a time-lapse of a Tg(*fli:GAL4FF*^{ubs3}; *UAS:mRFP*^{rk8}; *UAS:EGFP-ZO1*^{ubs5}) embryo (total length: 10:25).

(A and B) A tip cell has formed initial contacts and subsequently forms loops of EGFP-ZO1 with its adjacent partner (white arrows). The stalk shows a multicellular organization (two lines of EGFP-ZO1, arrowhead in B) and an opening lumen (yellow arrow in B).

(C) The lumen projects into the fusion cell (follow arrow from C to E) and finally reaches the left ring of EGFP-ZO1, which is subsequently inflated (arrow in F). The lumen then continues to extend into the unlabeled fusion cell on the left (arrow in G). A blood cell then passes through the newly formed lumen (follow arrowhead from G–J). Insets show the blood cell passing behind the junction (G) and in front of the junction (H). More examples of membrane invagination are shown in Movie S4, Movie S6, and Figures S3B and S3C. Scale bar in all pictures represents 20 μm.

the CD35 family of sialomucins have been shown to localize to the luminal (apical) membrane compartments of ECs in the mammalian vascular system [8]. To examine apical polarization during DLAV formation, we generated antibodies against zebrafish podocalyxin-2 (Pdxl2) and found that it specifically localized to the luminal membranes throughout the zebrafish vasculature (Figure 4A; Figure S1D; data not shown). Importantly, we observed Pdxl2 in membrane compartments within junctional rings shortly after contact formation (Figure 4B), indicating that the future luminal membrane becomes apically polarized during early steps of anastomosis prior to the morphogenetic movements that lead to lumen coalescence during cord hollowing. In agreement with our live observation, we also found Pdxl2 in junction-free segments of DLAVs and intersegmental vessels (ISVs) (Figure S1D). Examination of younger embryos (36 hrs postfertilization [hpf]) revealed patterns of Pdxl2 protein extending from a multicellular base of SAs into the tip cell (Figure 4C). This continuous Pdxl2 domain is consistent with an expansion of the vascular lumen from a multicellular into a unicellular surrounding and indicates that the tip cell becomes polarized as its cell membrane invaginates.

Because cell membrane invagination occurs directionally and can form a patent lumen within a few hours, we tested whether blood flow is required for lumen formation during anastomosis by the injection of antisense morpholinos against cardiac troponin (silent heart, *sih*, *tnnt2a*) [9] into Tg(*fli:gal4FF;UAS:GFP-ZO1*) embryos. We recorded a total of six time-lapse movies and observed that the initial steps of anastomosis, i.e., the formation and elaboration of the initial junctional rings, were relatively normal and that cell movements appeared unaffected (Figure S3A; Movie S5; data not shown). However, the vascular lumen of *sih* morphants does not inflate, and lumen formation proved difficult to monitor in vivo. Therefore, we used the Pdxl2 antibodies

extended through a single cell between two separate sites of contact (Figure S3B; Movie S3; Movie S4, summarized in Figure S2). This mechanism thus leads to a transformation of the tip cell into a "fusion cell," which forms a unicellular tube. This was demonstrated by a blood cell serendipitously passing through the two junctional rings of a hollowed-out EC (insets in Figure 3 and Movie S3).

De novo formation of an epithelial lumen is initiated by the apical-basal polarization of cell membranes [7]. Members of
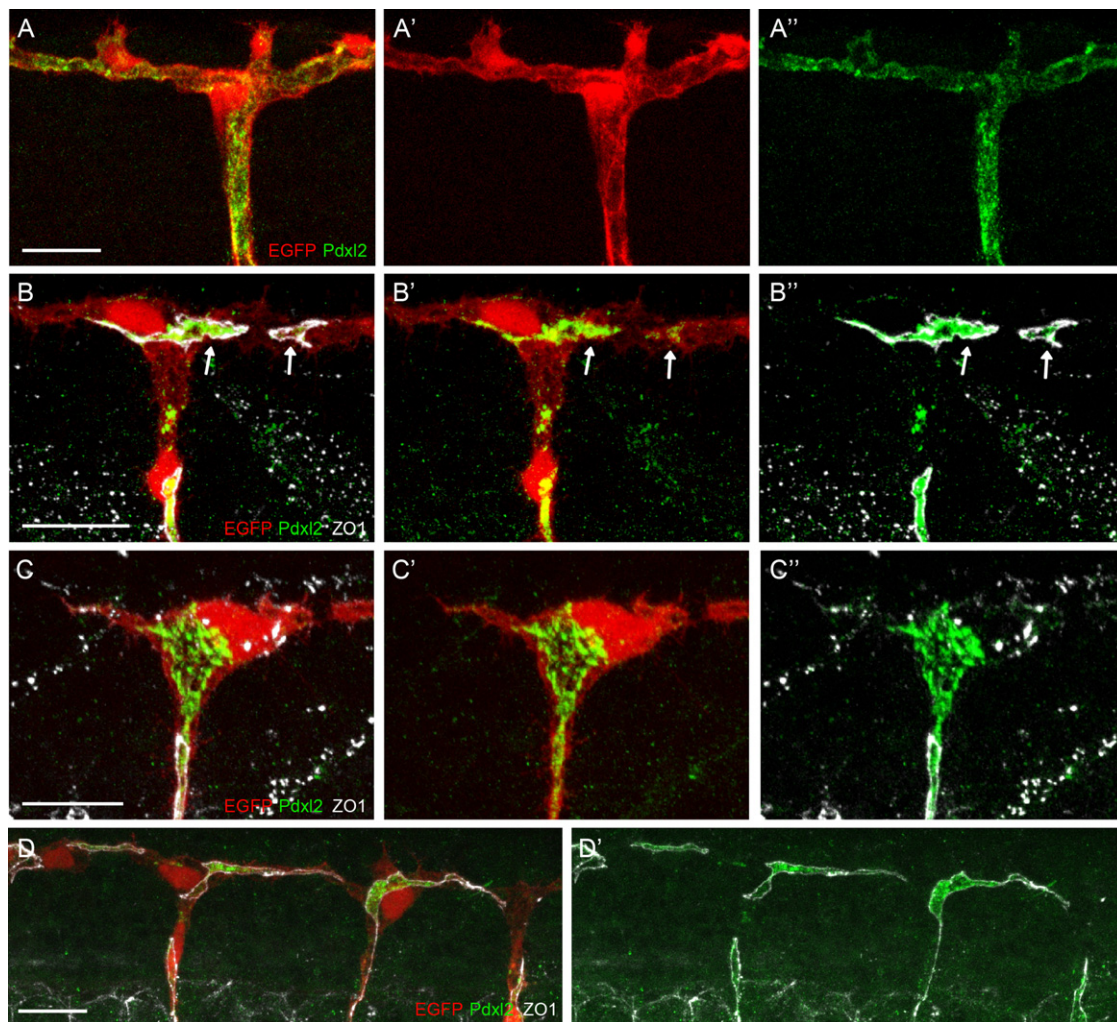
Figure 4. Visualization of Apical Membrane during Anastomosis

(A–A″) Pdxl2 antibodies label apical cell membranes in ISVs and DLAV at 48 hpf.

(B–B″) Pdxl2 is localized within a junctional ring (arrow) at the contact site of two tip cells at the onset of anastomosis (36 hpf).

(C–C″) Apical membrane invaginating into a tip cell at 36 hpf is shown by Pdxl2 immunostaining.

(D–D′) In *sih* morphants at the same stage, the Pdxl2 staining is only seen within the junctional rings, indicating that apical membrane invagination does not take place in the absence of blood flow.

Also compare Movie S3 and Figure S3A. α-ZO1 is shown in white, α-Pdxl2 in green, and *kdrl:EGFP* in red. Scale bar in all pictures represents 20 μm.

to examine the formation of apical cell membranes in *sih* morphant embryos and found that Pdxl2 was largely restricted to multicellular domains except for spurious signals in unicellular regions (Figure 4D). During examination of 60 tip cells at 36 and 48 hpf, respectively, we did not find any occurrence of membrane invagination (see Table S1). These findings indicate that blood flow is dispensable for cell rearrangements during DLAV formation and for EC polarization per se. It is, however, required for membrane invagination, which leads to the formation of unicellular tubes, indicating that blood pressure may be the driving force of this morphogenetic process.

Taken together, we have shown that vascular anastomosis during DLAV formation can occur by very different morphogenetic mechanisms, either by a cord hollowing process generating a multicellular tube or by cell membrane invagination resulting in a unicellular tube, as summarized in Figure 5. In both cases, anastomosis is intrinsically connected with de novo lumen formation at the site of vessel fusion, and the future luminal membrane compartments show apical polarization before the blood vessel becomes patent. At the cellular level, these mechanisms are drastically different because they are driven by cell rearrangements and cell shape changes, respectively. Cord hollowing mechanisms have been described in different vertebrate tissues including the mouse dorsal aorta [8] and the zebrafish neural tube [10, 11] and intestine [12]. However, the cord hollowing mechanism we describe appears unique, because it is driven by cell rearrangements rather than lumen expansion. In contrast, a mechanism of remarkable similarity has been described for hollowing the notochord in the ascidian *Ciona intestinalis* [13]. In both systems, the zebrafish DLAV and *Ciona* notochord, lumenization commences with the de novo establishment of apical domains between neighboring cells and is followed by cell movements and cell shape changes, which result in the fusion of luminal spaces and the formation of a continuous endothelium.
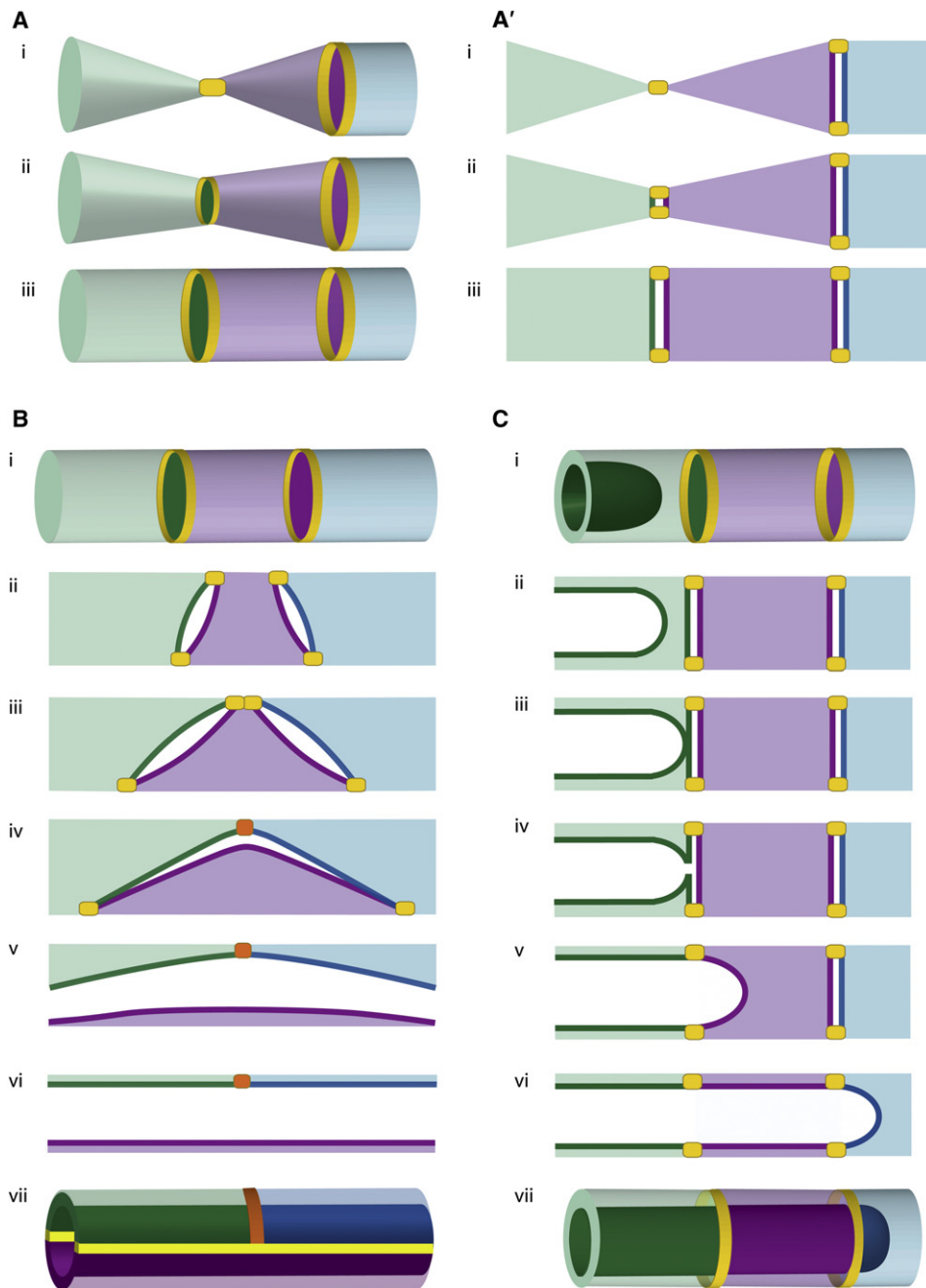
Figure 5. A Model of Cellular Mechanisms during Anastomosis

(A and A′) Contact formation during vessel fusion is shown in (A) and corresponding sagittal sections in (A′). At the contact site of two neighboring tip cells (green and purple), junctional proteins are deposited (yellow spot in i). As the cells increase their mutual surface, this spot transforms into a ring (ii and iii), and the enclosed membrane compartment becomes apically polarized (dark green and dark purple areas). Subsequently, two different cellular mechanisms are used to complete the fusion process (see B and C).

(B) A cord hollowing mechanism results in a multicellular tube. Cell rearrangements bring together two junctional rings, i.e., two apical membrane compartments that then merge into one membrane compartment. This is achieved by the formation of a new junction (orange) between the green and blue cell, which leads to the detachment of the middle cell (purple) at the site of the new contact.

(C) Cell membrane invagination leads to the formation of a unicellular, seamless tube. Here, apical membrane of the green cell invaginates into the green cell. It then fuses with its own apical membrane at the previously formed contact side between the green and purple cells (see A). From here the lumen, i.e., the apical membrane of the neighboring cell (dark purple), begins to invaginate.

Endothelial cells are shown in green, purple, and blue; apical membranes are shown in dark green, dark purple, and dark blue; endothelial cell junctions are shown in yellow; and new endothelial cell junctions are shown in orange.

During the formation of unicellular tubes, the fusion cell undergoes drastic cell shape changes, as the proximal apical cell membrane compartment, which faces the preexisting lumen, invaginates into the cell along the future vascular axis (Figure 5). It thereby generates an extracellular space, which extends through the cell and can be classified as

a "transcellular lumen." According to our model, the invaginating membrane fuses with the distal membrane compartment to convert the fusion cell into a patent tube. Although we are not able to directly visualize membrane fusion in vivo, intracellular cell membrane fusion has been described during the development of the tracheal system of *Drosophila* [14–16]. The fusion cell of the DLAV may be considered analogous to the so-called doughnut cell, which is important for tubular fusion within the *Drosophila* tracheal system and eventually forms a seamless tube. In the case of the tracheal doughnut, it has been shown that this unicellular tube is generated by cell shape changes, which eventually lead to an intracellular membrane fusion [17]. The cell shape changes, which occur during vascular fusion, are far more dramatic than those in the tracheal system. We observed asymmetric cell shape changes, because the tip cell became hollowed in a proximodistal direction. Furthermore, the direction of invagination was independent of the anatomical orientation and occurred either in a ventral to dorsal or dorsal to ventral direction (Figures S3B and S3C; Movie S4; Movie S6). In all cases, the lumen was formed in a continuous fashion, and we did not detect isolated luminal spaces within the cell.

Here, we have studied the anastomosis of ISVs, which results in the formation of a new vessel, the DLAV. We describe two morphogenetic mechanisms that govern vascular tube formation. These mechanisms, although used by the same type of blood vessel, employ very different cellular activities, cell rearrangements and cell invagination, respectively, to form and connect novel lumens and therefore lead to vessels of distinct cellular architectures. Both mechanisms are used at a comparable rate of instances, suggesting a stochastic selection of the process. Future experiments will explore the parameters, such as blood pressure, vessel size, and cell motility and number, which may influence the choice of mechanism, as well as the molecular mechanisms that underlie blood vessel fusion.

Supplemental Information

Supplemental Information includes three figures, one table, Supplemental Experimental Procedures, and six movies and can be found with this article online at doi:10.1016/j.cub.2011.10.016.

References

1. Herbert, S.P., and Stainier, D.Y.R. (2011). Molecular control of endothelial cell behaviour during blood vessel morphogenesis. Nat. Rev. Mol. Cell Biol. *12*, 551–564.
2. Gerhardt, H., Golding, M., Fruttiger, M., Ruhrberg, C., Lundkvist, A., Abramsson, A., Jeltsch, M., Mitchell, C., Alitalo, K., Shima, D., and Betsholtz, C. (2003). VEGF guides angiogenic sprouting utilizing endothelial tip cell filopodia. J. Cell Biol. *161*, 1163–1177.
3. Lawson, N.D., and Weinstein, B.M. (2002). In vivo imaging of embryonic vascular development using transgenic zebrafish. Dev. Biol. *248*, 307–318.
4. Ellertsdóttir, E., Lenard, A., Blum, Y., Krudewig, A., Herwig, L., Affolter, M., and Belting, H.-G. (2010). Vascular morphogenesis in the zebrafish embryo. Dev. Biol. *341*, 56–65.
5. Isogai, S., Lawson, N.D., Torrealday, S., Horiguchi, M., and Weinstein, B.M. (2003). Angiogenic network formation in the developing vertebrate trunk. Development *130*, 5281–5290.
6. Blum, Y., Belting, H.-G., Ellertsdottir, E., Herwig, L., Lüders, F., and Affolter, M. (2008). Complex cell rearrangements during intersegmental vessel sprouting and vessel fusion in the zebrafish embryo. Dev. Biol. *316*, 312–322.
7. Martin-Belmonte, F., and Mostov, K. (2008). Regulation of cell polarity during epithelial morphogenesis. Curr. Opin. Cell Biol. *20*, 227–234.
8. Strilić, B., Kucera, T., Eglinger, J., Hughes, M.R., McNagny, K.M., Tsukita, S., Dejana, E., Ferrara, N., and Lammert, E. (2009). The molecular basis of vascular lumen formation in the developing mouse aorta. Dev. Cell *17*, 505–515.
9. Sehnert, A.J., Huq, A., Weinstein, B.M., Walker, C., Fishman, M., and Stainier, D.Y.R. (2002). Cardiac troponin T is essential in sarcomere assembly and cardiac contractility. Nat. Genet. *31*, 106–110.
10. Tawk, M., Araya, C., Lyons, D.A., Reugels, A.M., Girdler, G.C., Bayley, P.R., Hyde, D.R., Tada, M., and Clarke, J.D.W. (2007). A mirror-symmetric cell division that orchestrates neuroepithelial morphogenesis. Nature *446*, 797–800.
11. Munson, C., Huisken, J., Bit-Avragim, N., Kuo, T., Dong, P.D., Ober, E.A., Verkade, H., Abdelilah-Seyfried, S., and Stainier, D.Y.R. (2008). Regulation of neurocoel morphogenesis by Pard6 gamma b. Dev. Biol. *324*, 41–54.
12. Bagnat, M., Cheung, I.D., Mostov, K.E., and Stainier, D.Y.R. (2007). Genetic control of single lumen formation in the zebrafish gut. Nat. Cell Biol. *9*, 954–960.
13. Dong, B., Horie, T., Denker, E., Kusakabe, T., Tsuda, M., Smith, W.C., and Jiang, D. (2009). Tube formation by complex cellular processes in Ciona intestinalis notochord. Dev. Biol. *330*, 237–249.
14. Tanaka-Matakatsu, M., Uemura, T., Oda, H., Takeichi, M., and Hayashi, S. (1996). Cadherin-mediated cell adhesion and cell motility in Drosophila trachea regulated by the transcription factor Escargot. Development *122*, 3697–3705.
15. Steneberg, P., Hemphälä, J., and Samakovlis, C. (1999). Dpp and Notch specify the fusion cell fate in the dorsal branches of the Drosophila trachea. Mech. Dev. *87*, 153–163.
16. Lee, S., and Kolodziej, P.A. (2002). The plakin Short Stop and the RhoA GTPase are required for E-cadherin-dependent apical surface remodeling during tracheal tube fusion. Development *129*, 1509–1520.
17. Kakihara, K., Shinmyozu, K., Kato, K., Wada, H., and Hayashi, S. (2008). Conversion of plasma membrane topology during epithelial tube connection requires Arf-like 3 small GTPase in Drosophila. Mech. Dev. *125*, 325–336.

5.4 Hemodynamic regulation of Notch signaling controls developmental blood vessel pruning in zebrafish embryos

Eva Kochhan, Anna Lenard, Elin Ellertsdottir, Lukas Herwig, Heinz-Georg Belting, Markus Affolter and Arndt F. Siekmann

Contribution:

I performed the time lapse analyses of blood vessel pruning in the eye of the zebrafish embryo, using live junctional marker VE-cadherin-EGFP. I described the stepwise cellular mechanism of this process (as described in more detail in the result section 5.7).

Abstract:

The embryonic vasculature meets the challenge to function while it is still developing. This leads to the later refinement of an initially primitive vasculature via remodeling and pruning. While we have a detailed knowledge on the molecules required for the early growth of the vasculature, the mechanisms controlling vascular pruning remain largely undefined. Here, we report on the cellular events that occur during pruning of a defined blood vessel in the eye of zebrafish embryos. We show that initially angiogenesis leads to the formation of a Y-shaped branch point structure, in which one of the two arms will regress. Prior to blood vessel pruning, endothelial cells rearrange from a multicellular into a unicellular tube, thereby sealing this vessel off from the active

circulation. We furthermore provide evidence that the Notch ligand dll4 is differentially expressed within endothelial cells constituting the branch point structure, leading to the distinct activation of Notch signaling in a subset of endothelial cells. Via performing gain and loss of Notch function experiments, we demonstrate that this differential activation of Notch signaling is important for the initiation of the pruning process. Finally, we show that changes in blood flow influence dll4 expression and thereby regulate the robustness of endothelial pruning. Together, our findings suggest that haemodynamics control blood vessel pruning via establishing the differential expression of the Notch ligand dll4 in distinct vessel branch points.

5.5 Mechanisms of blood vessel remodeling

Claudio A. Franco, Anna Lenard, Martin Jones, Jieqing Fan, Dominique Sauvaget, Eleonora Lapi, Heinz-Georg Belting, Richard Lang, Markus Affolter, Holger Gerhardt

In preparation, to be submitted by the end of 2012

Contribution:

I performed the time lapse analyses of blood vessel regression during ISV formation in the zebrafish embryo, using a live junctional marker EGFP-ZO-1. I described the stepwise cellular mechanism of this process (as described in more detail in the result section 5.7).

Abstract:

Sprouting and anastomosis constitute the first steps in angiogenesis, creating a dense but immature vascular plexus. Such vascular networks must subsequently remodel in order to efficiently deliver oxygen and nutrients to vascularized tissues. One of the key mechanisms promoting vascular remodeling is vessel regression. Current literature suggests that vessel regression involves endothelial cell death, creating empty basement-membrane sleeves. However, details of the cellular and molecular mechanisms of vessel regression remain poorly understood. Here, we present a systematic analysis of the cellular principles and molecular mechanisms regulating vessel regression, in the retina and zebrafish. We observed that blood vessel lumen

constriction is an initiating step in vessel regression followed by extensive endothelial cell migration and rearrangements with endothelial cells incorporating in neighboring branches, without signs of endothelial cell death. Single cell analysis showed that regressing endothelial cells are highly active, extending filopodia away from the regressing branch. Studying lumen, junctional profiles, endothelial cell shape and endothelial cell polarity, we propose that regression involves at least four discrete steps: 1) selection of the regressing branch; 2) physical lumen constriction; 3) junction remodeling during endothelial cell retraction; and 4) resolution of the vessel segment regression, which leaves behind a pericyte covered basement membrane sleeve.

Previous work suggested that loss of Wnt-signaling promotes regression. Interestingly, genetic manipulation impairing endothelial Wnt ligand-secretion leads to excessive vessel regression, indicating that endothelial cells themselves secrete Wnt ligands relevant for stabilizing the immature vessel branch.

We propose that Wnt is involved in the initial selection step of the remodeling branch and affects coordinated and polarized endothelial cell migration. Our mechanistic conceptualization of vessel regression uncovers an extraordinary level of endothelial cell plasticity during vascular remodeling and opens new therapeutic perspectives on retinal vascular diseases and remodeling after stroke.

5.6 Dynamic cell rearrangements shape the cranial vascular network of developing zebrafish embryos

Anna Lenard, Ellin Ellertsdottir, Lukas Herwig, Alice Krudewig, Heinz-Georg Belting and Markus Affolter

Ready to be submitted by the end of 2012

Contribution:

I performed all experiments in this project. The manuscript is presented in the following chapters (5.6.1-8) of the thesis.

5.6.1 Abstract

While much is known about how vessels develop via sprouting angiogenesis, little is known about how such new vessels connect and integrate with other sprouts or with pre-existing vessels. Studying developing vessels in the zebrafish head, we describe a multistep process underlying vessel fusion. The early steps of fusion process involve *de novo* polarization of endothelial cells, apical membrane invagination and apical membrane fusion. In the later steps, the initial unicellular tubes transform into multicellular tubes via cell rearrangements and cell splitting. Sprouts also fuse to existing patent vessel via the same multistep process. VE-cadherin plays an important role in the early steps of vessel anastomosis. Although endothelial tip cells still interact and connect to each other, they fail to generate a single apical membrane patch between tip cells, leading to multiple lumens and a failure to undergo the subsequent steps in a coordinated fashion.

5.6.2 Introduction

The vasculature of vertebrate species is necessary for the distribution of oxygen, nutrients, metabolites and blood cells to and from all organs of the body. The interconnected network of vascular tubes develops to a large extent during embryogenesis and serves from early stages onwards to maintain vital functions (Risau and Flamme, 1995).

To form an interconnected network of endothelial tubes, blood vessels develop via a number of distinct cellular mechanisms. During vasculogenesis, endothelial cells come together, establish contacts and eventually form the first endothelial tubes, i.e. the dorsal aorta and the posterior cardinal vein. During sprouting angiogenesis, new vessels grow out from pre-existing ones leading to the formation of a highly ramified vascular network (Adams and Alitalo, 2007; Carmeliet, 2003; Risau and Flamme, 1995). To generate a circulatory system, a number of vessels of the developing vasculature have to connect to each other and anastomose. While much is known about vessel sprouting (Adams and Alitalo, 2007; Gerhardt et al., 2003; Siekmann and Lawson, 2007), little is known about vessel anastomosis or vessel fusion, both at the morphological and at the molecular level. On the one hand, this is due to the fact that vascular fusion has not been studied extensively in tissue culture, due to the lack of blood pressure and blood flow in the *in vitro* systems. On the other hand, *in vivo* studies have been hold back by the difficulty to image developing blood vessels in mice. Recent studies in zebrafish embryos have used fluorescent proteins labelling different cellular structures, most importantly cell-cell junctions, to describe the cellular events during fusion of individual angiogenic sprouts in the formation of the dorsal longitudinal anastomotic vessel (DLAV), which is among the first vessels formed through angiogenesis in the zebrafish embryo (Herwig et al., 2011; Isogai et al., 2003; Lawson and Weinstein, 2002).

While these studies provided the first description of cellular events occurring during vessel anastomosis, it is not clear to what extent the fusion events in the DLAV reveal the cellular activities underlying this process during later stages, when blood pressure on the embryo is fully established. In addition, vessel sprouts often fuse to existent opened vessels, a process that involves a single sprout and thus, most likely, only a single tip cell. Whether this altered cellular architecture uses similar mechanisms

to establish functional connections is not known. Furthermore, molecular players important for distinct events during the fusion process have not been identified thus far. Here, we describe different anastomosis events in the zebrafish head and brain at high cellular resolution in live embryos with the help of a number of novel transgenic reported lines and mutants. We define a multi-step model, which describes the fusion process and the transformation of blind-ended vascular sprouts into fully functional vascular branches. Furthermore, we find that VE-cadherin plays an important role in coordinating the early steps of the anastomosis process but is not required for the initial tip cell polarization upon contact. Our studies provide a cellular and molecular framework for future studies on vessel fusion.

5.6.3 **Experimental Procedures**

Generation of Transgenic Zebrafish Lines

(*kdrl*:mKate-nls)[ubs13]

pmKate2-N (Evrogen) was used to amplify the mKate2 sequence that was ligated with the 3NLS synthesized sequence and inserted into the pBSII vector using PstI/BamHI/XbaI restriction sites. The mKate-3NLS sequence was subsequently inserted intohte pG1flk1_tol2 vector. 7.5 ng/µl of the vector together with 6 ng/µl Tol2 transopsase was injected into 1-cell-stage zebrafish embryos that were screened for transient expression at 24-48 hpf. Positive embryos were grown separately and screened for germ line transmission.

TgBAC(*kdrl*:mKate2-CAAX)[ubs16]

The BAC construct was generated using BAC recombineering method described before (Warming 2005). Clone CH211-276G21 containing the full *kdrl* gene sequence was purchased from BACPAC Resources. pmKate2-N (Evrogen) was used to amplify mKate red fluorescent protein coding sequence, which was inserted into pBS with a CAAX tag added at the C terminus. mKate2-CAAX was inserted into pG1 using BamHI/XhoI. This construct was used as a template to generate the PCR product used for recombineering. Primers used for this step contained 50 bp overhangs (homologous to the 50 bp upstream and downstream of the ATG of *kdrl* gene, respectively). Recombineering was performed using SW102 bacteria strain, following the protocol (Warming et al., 2005). The BAC DNA was isolated using the NucleoBond BAC isolation kit and injected into 1-cell-stage zebrafish embryos that were screened for transient expression at 24-48 hpf. Positive embryos were grown separately and screened for germ line transmission.

Tg(*kdrl*:tdEos2)[ubs15]

Eos2 fluorescent photoconvertible protein sequence (McKinney et al., 2009) was inserted in 2 copies (tandem Eos2, tdEos2) into pBS_II vector. The pBS_II_tdEos2 was used to amplify the tdEos2 and inserted with EcoRI/NotI into pG1flk1MCS_tol2 expression vector.

Immunofluorescence and Imaging

Antibody staining was performed as described previously (Blum et al., 2008; Herwig et al., 2011). The following antibodies were used: rabbit anti-zf-pdxl2 1:200 (Herwig et al., 2011), rabbit anti-zf-CDH5 (Blum et al., 2008), 1:200; mouse anti-hZO-1 (Zymed), rabbit anti-ESAMa (this study) Alexa-568 goat anti-rabbit IgG, 1:1000; Alexa-568 goat anti-mouse IgG, 1:1000; Alexa-633 goat anti-mouse IgG, 1:1000 (all secondary antibodies were purchased from Invitrogen.). Images were taken with Leica SP5 confocal microscope using a 63x glycerol immersion objective or a 40x water immersion objective. Images were analyzed using Imaris (Bitplane) and Image J software (http://imagej.nih.gov/ij/).

In Vivo Time-Lapse Analysis

Transgenic embryos were selected using a Leica MZ FLIII fluorescent stereomicroscope for presence of red and green fluorescence. Selected embryos were anaesthetized using tricaine and mounted in a 35 mm glass bottom petri dish (0.17 mm, MatTek), using 0.7% low melting agarose (Sigma) containing 0.01% tricaine and 0,003% PTU. The movies have the frame size of 512x512 or 1024x512 pixels. A standard z-stack consisted of 50-90 slices with a step size of 0.7-1 µm. Stacks were taken every 5-12 minutes. All images are maximal z-stack projections. Leica TCS SP5 confocal microscope was used. Images were taken with objectives: 20x air, 40x water and 63x glycerol immersion.

Dextran injections

Fluorescein labeled 500 kDa Dextran (Molecular Probes) was injected into the sinus venosus of mounted embryos using glass needles (Biomedical Instruments, Jena, Germany) with tip opening of 10 µm and beveled tip.

Morpholino injections

1-2 cell-stage embryos were injected with 4ng of antisense morpholino oligonucleotide targeting the start codon region of the cardiac Troponin T2a (*5'-CATGTTTGCTCTGATCTGACACGCA-3'*). The morpholino causes complete loss of heart beat (Sehnert et al., 2002). The analyzed embryos were selected based on this criterion.

Fish Maintenance and Stocks

Zebrafish were maintained at standard conditions (Westerfield, 2000). Embryos were staged by hours post-fertilization (hpf) at 28.5 °C (Kimmel et al., 1995). The following zebrafish lines were used in this study: wild-type fish (AB/EK and EK/TL), Tg(*kdrl*:EGFP)[S843] (Jin et al., 2005) Tg*(UAS:EGFP-ZO1-cmlc:EGFP)*[UBS5-7] (Herwig et al., 2011), Tg(UAS:RFP) and Tg*(fli1ep:GAL4FF)*[UBS2-4] (Totong et al., 2011; Zygmunt et al., 2011), Tg(BAC:*kdrl*:mKate2-CAAX)[ubs16] this study, Tg(*kdrl*:tdEos2)[ubs15] this study, Tg(*kdrl*:mKate2-3NLS)[ubs13] this study.

5.6.4 Results

Formation of the palatocerebral artery (PLA) in the zebrafish cranial vasculature

The palatocerebral artery (PLA) is one of the first cranial vessels that form via angiogenesis in the head of a developing zebrafish embryo (fig.1A). It is a unique vessel that extends rostrally along the base of the forebrain (Isogai et al., 2001) and connects the two cranial division of the internal carotid artery (CrDI) vessels that encircle the optic capsules on both sides of the embryo head. At ~36 hpf, sprouts of the PLA vessel (PLA and PLA', fig. 1B) start to grow ventrally from the CrDIs both on the left and the right side of the embryo head. The sprouts meet centrally and establish a connection. The vessel is perfused at ~40 hpf and blood flow is present in one direction (fig.1B'). Subsequently, the communicating vessels CMV and CMV' sprout ventrally from the prosencephalic arteries (PrA and PrA') and connect to the center of the PLA, making up the PLA junction (PLAJ) (fig.1B''). After this connection is made, blood flow is redirected and blood cells start to move from both parts of the PLA towards the centrally situated PLAJ and upwards to the CMVs.

To gain first insights into cellular aspects of PLA formation, we performed high resolution 4D confocal imaging using transgenic zebrafish lines with endothelial specific cytoplasmic EGFP and nuclear mKate2 expression (Tg(*kdrl*:EGFP)[s843];(*kdrl*:mKate-nls)[ubs13]). We found that each of the PLA sprouts consisted of 2-3 endothelial cells (fig. 1 C). The sprouts moved towards each other and finally connected in a process called vessel fusion or anastomosis (fig.1C-C'', Movie 1). The newly formed vessel was subsequently lumenized and soon after blood flow started (fig.1C''', red bars show lumenized regions). Since cytoplasmic EGFP expression is uniform in all endothelial cells, in this experiment it was not possible to resolve individual cell shapes and cell behavior within the developing blood vessel.

De novo cell polarization initiates the formation of the PLA

In order to follow individual cells of the developing PLA during contact formation and anastomosis, we generated a transgenic fish line which expresses Eos2 photoconvertible protein in endothelial cells: (Tg(*kdrl*:tdEos2)[ubs15]).

In these experiments we used spatially restricted UV illumination to convert Eos2 in the leading cell of one of the PLA sprouts (the tip cell), thus changing its fluorescence from green to red, while the contra-lateral tip cell remained green (fig.1D, Movie 2). In time lapse analyses after photoconversion we observed that, upon first contact, the tip cells kept moving over each other and expanded the contact surface extensively as the fusion process continued (fig.1D-D''' white bar). The tip cell occupied the leading end of the sprout and later took part in the initial lumen formation process (fig.1D-D''', red arrows point at the end of lumen).

To describe the process in greater detail, we decided to visualize cell-cell junctions during the fusion process, as we have previously done to study the anastomosis process in the DLAV (Herwig et al., 2011). In this study we used the Gal4-UAS expression system to express fusion proteins of junction localized ZO-1 (Zona occludens 1) tagged with EGFP. The Tg(*fliep*:GFF)[ubs3];(UAS:mRFP);(UAS:EGFP-ZO-1)[ubs5] lines showed extremely mosaic expression with very few cells expressing the EGFP-ZO-1 transgene in the head vasculature, which made the analyses rather difficult. We therefore decided to generate additional lines expressing different fluorescently tagged proteins at cell junctions. The most useful transgenic reporter we generated expressed a truncated version of the zebrafish VE-cadherin protein, which is an adhesion molecule localized to cell-cell junctions in endothelial cells and therefore marks the borders of each cell where it connects to its neighboring cells. In this transgene the cytoplasmic domain of VE-cadherin was replaced by EGFP (Tg(UAS:VE-cadherinΔC-EGFP)[ubs12]). We performed time lapse experiments using the VE-cadherin-EGFP in the presence of cytoplasmic mRFP transgene, to visualize both cell bodies (red) and cell-cell junctions (green). In over 20 time lapse experiments we observed the dynamic cell behavior and junctional rearrangements that enabled us to define a general and recurrent multistep model of PLA fusion, described in detail in following chapters.

We observed that in each sprout a single tip cell was leading the front of the sprout and was connected to the following stalk cells by a ring-shaped junction (fig.2A, arrow heads). Upon contact of two tip cells from opposing sprouts, a spot of VE-cadherin-EGFP appeared at the contact site, demonstrating the *de novo* deposition of junctional material (fig.2A', white arrow). This spot was subsequently transformed into a

ring as the cells moved over each other and their contact surface expanded (fig.2 A'-A''', white arrow, Movie 3). The occurrence of spots and rings of junctional VE-cadherin during the early anastomosis process was confirmed using antibody staining (fig.2B-B''', white arrows). During the fusion process, cell membranes within the ring of VE-cadherin-EGFP underwent *de novo* apical polarization, as shown by presence of Podocalyxin-like 2 (Pdxl2), a marker for apical membrane, in immunostaining experiments (fig.S1 B). Interestingly, the tip cells at this stage were bipolar and had two apical membrane compartments: one at the new contact site and one facing the lumen, where the cell was connected to the following stalk cells (fig.S1 B, arrows). This biapical polarization was transient and resolved during further steps of vessel formation leading to connection of all apical membranes into a continuous one.

Contact and lumen formation in the PLA

The formation of a new contact and apical polarization was followed by lumen perfusion. The PLA forms at ~36 hpf when the developing embryo has already established heart beat and blood flow. We observed that the process of lumen formation seemed to be highly dependent on the presence of blood plasma pressure. The outgrowing sprouts were already lumenized, in many cases almost to the very tip, thus including part of the tip cells. The lumen extended from the CrDI vessel, between the stalk cells of the sprout into the tip cell causing its luminal/apical membrane invagination towards the end of the sprout (Fig.2A-A'', red arrows), making a blunt ended tube. The inflated luminal space extended beyond the ring-like junctional connection into the tip cell, as visible by the lack of red fluorescence in the middle part of the vessel and confirmed by immunostaining for the apical Pdxl2 marker (Fig. S1 A, red arrow). After the tip cell contact formation, the lumen extended towards the new contact site and eventually pushed through the newly formed junctional ring, suggesting that the perfusion of a new vessel involved further tip cell membrane invagination and finally apical membrane fusion leading to formation of a unicellular tube with continuous transcellular lumen (Fig.2A''', fig.2 F-G, red arrows).

We confirmed the presence of transcellular lumen in the newly anastomosed PLA vessel with antibody staining showing a continuous apical membrane within single tip

cells (Fig.S1 C). Furthermore, we saw in several cases in live embryos that blood cells traveled through single, lumenized endothelial cells (data not shown).

To confirm the initial events in PLA fusion, we also performed single cell live imaging analyses using the junctional marker EGFP-ZO-1, which is expressed in a mosaic fashion (Fig.2 E, Movie 5). In the particular experiment shown, only a single tip cell was labeled with the fluorescent junctional marker. We were able to follow the formation of a new junction spot that later transformed into a ring-like structure, as well as the formation of the transcellular lumen, demonstrating that during the fusion process, a single labeled tip cell formed a unicellular tube connected on both sides to neighboring cells with junctional rings (Fig.2E-E''', arrows).

Since membrane invagination appears to be an important cellular aspect of vessel fusion, we wanted to visualize the membrane in more detail and therefore generated a transgenic line expressing a membrane tagged version of mKate2 red fluorescent protein in endothelial cells using BAC recombineering (TgBAC(*kdrl*:mKate2-CAAX)[ubs16]). In these embryos the fluorescent protein marks membranes, the apical and the basal, of each endothelial cell and therefore allows observing the membrane invagination process in much more detail. The leading basal membrane of the tip cell extended numerous filopodia that contacted the opposite sprout (fig.2C and D, arrowheads, Movie 4). The apical membrane was visible within the sprout as it invaginated towards the tip (fig.2C and D, red arrows). When the contact was established, the apical membrane of each tip cell kept on invaginating to finally reach the other, newly formed, apical membrane of the same cell (fig.2 C'-C'', D'-D'', G-model). Since the invagination happened in both sprouts simultaneously, albeit not at the same ratio, the apical membranes could meet at the contact site to another cell, if the pressure was stronger on one side (fig2D - model), or within the cell body, if the pressure from both sides pushed on both apical membranes with similar strength. This process lead to connection of all luminal/apical compartments of each tip cell into a continuous one resulting in lumen perfusion in both tip cells (fig.2C''' and D''', red arrows, fig.2F and 2G, models).

To find out whether the expanding luminal space was constantly connected to the vascular network, we performed angiography experiments by injecting fluorescein labeled 500 kDa Dextran (FITC-Dextran, Molecular Probes) into the vascular system of

zebrafish embryos. In these experiments all open vessels which are connected to the flow were filled with the fluorescent dye (fig.2C, green). We observed that the sprouting PLA filled up with dextran as far as the membrane invagination proceeded (Fig. 2 C –C'', red arrows), demonstrating that the lumen in each sprout was continuous and connected to the vascular network, forming as an extension of the lumen in the CrDIs, from which the PLA sprouts grew out. As the vessel perfused, the lumens from both sprouts connected and the vessel opened up, allowing the dextran to flow through (fig.2 C'-C''' and D'-D''', red arrows).

Transformation of the PLA into a multicellular tube

The above experiments demonstrate that the initial lumen which forms during PLA fusion involves cell membrane invagination and results in a transcellular lumen within the two participating tip cells, which form unicellular tubes. However, using antibody staining for junctional proteins and live imaging experiments with photoconversion and junctional markers, we observed that the PLA had a clearly multicellular structure at later stages (~48 hpf) (fig.S1 F). This suggests that the initial unicellular conformation, present right after the fusion process, is transient and that endothelial cells engage in a series of dynamic cell rearrangements within the existing vessel to finally form a multicellular tube.

Unexpected cell splitting during tube maturation

In order to understand the cellular events during the transition of a unicellular tube to a multicellular tube, we followed tube maturation using both fluorescent proteins marking the cell-cell junctions, EGFP-ZO-1 and VE-cadherin-EGFP. The initial new PLA vessel consisted of two cells with transcellular lumen connected to each other by a junctional ring (fig.2A''' arrow, fig2.F''') and connected to the following cells by rings and/or lines of junctions (fig.2A''' arrowheads). During subsequent development, the junctional rings dynamically moved towards each other reflecting the rearrangement of cells within the existing vessel (fig.3 A and B, Movie 5 and 6). In time lapse experiments we observed that the rings connecting the unicellular tube to its neighbors moved closer and closer

together on one side of the vessel (fig.3 A-A', B-B', white arrows), meaning that the neighboring cells approached each other (fig.3C-C', red and yellow cell). Finally, the junctional rings touched and extended the contact area forming a new line of junctions (fig.3A", white arrow). This means that a new connection has been made between cells within the vessel, which were beforehand separated by a single cell making the initial unicellular tube (Fig.3C, red and yellow cell). At the same time, the unicellular tube cell had to split on one side of the tube to make space for the other cells to meet (Fig.3C, green cell). This process was seen very clearly in the single cell labeling experiments, in which only the "splitting cell" was labeled with the EGFP-ZO-1 marker (fig.3 B-B", Movie 5). The borders of the cell moved closer together, thereby narrowing the cell body on one side of the tube and eventually forming a very thin cytoplasmic bridge (fig.3B-B', red arrow). This bridge was subsequently broken and the cell membranes reconnected in a different confirmation, perpendicular to the previous one (fig.3B"). At that point the cell no longer had a transcellular lumen but took shape of a half-pipe with a single, large ring of junctions (fig. 3B", white arrow) and became a part of the multicellular tube with now an extracellular lumen (fig.3C"). As mentioned before, both tip cells can form unicellular tubes after the fusion is completed. Also both of them undergo the "cell splitting", usually one by one. As they are right next to each other, they directly participate in the splitting of one another, temporarily taking the role of a "neighboring cell". For simplicity this was not shown in the model, but can be observed in time lapse analyses with the junctional markers.

Using live imaging and novel transgenic lines we thus defined a multistep process underlying the formation of the PLA. Tip cell contacts through filopodia establish the first connection, leading to the accumulation of adherens junction material and to the formation of novel apical membrane patches at the contact site. Subsequently, membrane invagination within the tip cell connects the existing luminal space to the new apical patches, resulting in lumen coalescence and formation of unicellular tubes. Unexpectedly, after lumenization, the PLA transforms into a multicellular tube, which happens through a novel process that we name "cell splitting". The two initial tip cells which first form a transcellular lumen (and display a doughnut-like shape with toroid membrane), undergo cell splitting to change their shape into a regular, flat endothelial

cell embedded in a multicellular tube (with spherical membrane and a half-pipe-like shape) (see model in Fig. 8).

Fusion of angiogenic sprouts occurs through the same multistep process in various vascular beds in the zebrafish embryo

Since the described multistep process involved some unexpected cell behavior, we were interested in finding out whether other fusion events in the developing zebrafish also include all these steps. Using the same transgenic tools as in above experiments, we analyzed a number of other vessel fusion events in the developing cranial vasculature and we showed that all of the described steps take place during fusion of vessels of different shapes and sizes and at various embryonic stages, as shown in the examples below. This suggests that the multistep process is conserved and can be considered a general model for blood vessel anastomosis.

The PCeV forms through similar cell rearrangement and cell splitting events

To verify whether the described cellular processes also underlie fusion of larger vessel sprouts at later embryonic stages, we looked at the posterior (caudal) cerebral vein (PCeV) that forms in the dorso-lateral region of the embryo head and connects dorsal longitudinal vein (DLV) to the primary head sinus (PHS) on both sides of the brain (fig.4 A-D, dorsal view, anterior up). The vessel fuses between 2.5-3 dpf and is relatively large. The sprouts coming from the DLV and the PHS were wide and multicellular, but, like in the case of the PLA, were led by single tip cells (Fig.4A-A', arrows, Movie 7). The tip cells extended long filopodia and were partially lumenized through membrane invagination (fig.4A'', white bar). A new spot of junctional proteins accumulated upon contact of the filopodia and subsequently elaborated into a ring-like structure (fig.4A''-B'', arrows). The initial transcellular lumen was formed in both tip cells (fig.4B'-C'', bars) and further cellular rearrangements, virtually identical to those observed in the PLA, transformed the open vessel into a multicellular tube (fig.4D'-D'', arrows). Thus, the multistep process we describe during PLA formation, including transcellular lumen formation and cell splitting, appears to be a common feature of vessel anastomosis.

Fusion of CMV to PLA reveals common features of vascular anastomosis events

Many vessels in a developing embryo are formed through fusion of two sprouts outgrowing from existing vessels, similar to the PLA or the PCeV. However, novel connections also form through fusion of a sprout to an existing, lumenized vessel, making a vascular junction with three or more branches. Such a situation exists in the formation of the PLAJ, which connects the two CMVs to the PLA (see fig.1B"). The CMV sprouted ventrally towards the PLA (fig.5A, arrow, Movie 8), which was at that time already a lumenized, multicellular vessel. The leading tip cell of the CMV connected to the PLA via filopodia, leading to the formation of a junctional spot (fig.5B, arrow). This first contact was either made to the cell body or to a junctional connection of two cells within the PLA. When the contact was made with a cell body, we observed that the junctional spot rapidly elaborated into a ring, which eventually moved and contacted existing junctions within the PLA (fig.5C, arrow). The newly formed apical membrane of the tip cell of the CMV sprout invaginated into the sprout leading to transcellular lumen formation in the tip cell, from the PLA up towards the stalk of the sprout (fig.5C-F, white bar, 5G, red bar). The initial unicellular tube was later transformed into a multicellular tube through dynamic cell rearrangements similar to the ones observed in PLA and PCeV (data not shown, model in fig.5I, blue bars). In some cases, the lumen inflation occurred in the opposite direction, from the CMV towards PLA (fig.5 H, red bar), but resulting in a similar cellular arrangement. Even though the shape of the CMV-PLA connection is more complex than the previously described vessels, we still observe the same cellular mechanisms, following the multistep fusion model adapted to this different arrangement. Thus, the same cellular events connect either two sprouts or a single sprout with an existing patent vessel.

The initial transcellular lumen formation step is highly influenced by blood flow

All of the analyzed cranial vessels form in the presence of blood flow in the neighboring and parental branches. As described before, the presence of blood plasma pressure in the sprouts appears to be important for the initial lumen formation by providing force for membrane invagination. Therefore we asked whether the presence of

this force is necessary and if so, which steps of the fusion process are most dependent on the presence of blood pressure. To characterize embryos that do not have any blood flow, we performed knock-down experiments using a morpholino that targets cardiac *troponin T2a* (*tnnt2a*) and causes the *silent heart* phenotype. We analyzed transgenic embryos expressing VE-cadherin-GFP in endothelial cells, which now lacked blood flow. The initial steps of PLA fusion occurred normally. The sprouts grew out and upon contact, a junctional spot containing VE-cadherin and ZO-1 was present and subsequently transformed into a ring (Fig.6A-C, white arrow points at the new connection, green arrows at the tip cell-stalk cell contacts, Movie 9). The membrane within the junctional ring was apically polarized, as shown by Pdxl2 staining (fig. S1 H). However, due to the lack of plasma pressure, no transcellular lumen was formed and no apical staining was present outside of membrane compartments defined by junctional rings and lines, confirming that membrane invagination did not take place (Fig. S1 G-I, white bars). However, despite the lack of transcellular lumen, the cells within the vessel still rearranged (Fig.6 D-F, arrows, Movie 9). Initially, the new connection was made by single tip cells connected via a ring of junctions (Fig.6C), but the neighboring cells from both sides kept moving towards each other and established new connections, transforming the vessel into a multicellular cord with continuous lines of junctions (Fig.6D-F, arrows). Also continuous apical staining was present along the multicellular vessel, showing that cell polarization is independent of blood flow presence (Fig. S1 I). Due to the lack of pressure and thus, unicellular tubes, the cell rearrangements did not result in cell splitting. Therefore we conclude that blood pressure is crucial for transcellular lumen formation through cell membrane invagination but is not necessary for cellular rearrangements within an existing vessel. Cell splitting needs to be preceded by formation of a unicellular tube stabilized in this shape by the plasma pressure within the forming vessel.

VE-Cadherin is necessary for single contact formation during vessel fusion

The proper formation of a junctional connection is essential for the new vessel formation and is one of the first steps of the vessel fusion model we have proposed. It was previously reported that the zebrafish VE-cadherin gene plays an important role in

122

stabilizing novel vascular sprouts; reduction of VE-cadherin expression results in a lack of correct connections (Montero-Balaguer et al., 2009; Wang et al., 2010). Since these studies were performed using a morpholino knock-down strategy, and the phenotypes of such experiments can be quite variable and dose-dependent, we decided to isolate null mutants in the single zebrafish *ve-cadherin* gene. We analysed its function by studying homozygous mutant embryos, using the different live cell markers and antibodies with the goal to identify more clearly the role of VE-cadherin in the proposed multi-step fusion process we described above.

We used zinc finger nucleases to generate deletions in the *ve-cadherin* gene and isolated a mutation (*ubs8*) which leads to a premature stop codon and a truncated, non-functional protein (Krudewig et al., to be published elsewhere). This mutation allowed us to investigate the role of VE-cadherin in a genetically well-defined background. We analysed PLA anastomosis using single cell photoconversion experiments in wild type and *ve-cadherin*[ubs8/ubs8] embryos. We additionally used *silent heart* embryos (Figure S2, Movie 11 and 14) as a control, because the VE-cadherin mutants do not develop proper blood flow due to severe heart defects. In both wild type and *ve-cadherin*[ubs8/ubs8] embryos, tip cells displayed numerous filopodia and migrated towards each other in a similar fashion (fig. 7 A-B, white arrows, fig. S2 C, Movies 10-12). However, when wild type tip cells upon first contact withdrew filopodia and rapidly extended their contact surface (fig.7A to A''', fig. S2 C-C'''-*sih,* blue bars), the *ve-cadherin* mutant tip cells did not (fig. 7 B-B''', blue bar). In contrast, they continued sprouting activity long after the opposing cells had met and kept on extending new filopodia (fig. 7 B'-B''', white arrows), which resulted in formation of several short connections (fig. 7 B''-B''', yellow arrows) instead of expanding the existing ones.

Surprisingly, antibody staining analyses showed that ZO-1 and ESAM-a (Endothelial cell-selective adhesion molecule a) were localized to the contact points between the two connecting sprouts, demonstrating that tip cell interaction/recognition occurred (fig 7 E-E'''). In many cases, apical membrane also started to accumulate between contact areas, as evidenced by the presence of Podocalyxin 2 (data not shown). Consistent with the live imaging data, in most cases more than a single contact spot was formed between the two tip cells and these spots did not refine into proper

ring-like structures at later stages (Fig. 7 E'-E''', yellow arrows). These findings suggest that the VE-cadherin protein is necessary for a single polarisation event between interacting tip cells.

In order to analyse the initial fusion events in more detail, both in wild type and in *ve-cadherin*[ubs8/ubs8] embryos, we imaged the process using the much higher time resolution of a spinning disc microscope (recording every 15 seconds), which allowed observation of the dynamic filopodial activity.

We analysed tip cell behavior using the membrane marker described before (TgBAC(*kdrl*:mKate2-CAAX)[ubs16]). We found indeed that filopodial activity was high before tip cell contact, both in wild type and in *ve-cadherin*[ubs8/ubs8] embryos (Fig. 7C-D, Fig. S2 D, Movies 13-15). While wild type tip cells established contact quickly, mutant tip cells took much longer and established several connections over a large area, resulting in independent contact sites and holes within the contact surface (Fig.7 C-D, red arrows). In addition, filopodial activity continued for much longer in *ve-cadherin*[ubs8/ubs8] mutants than in wild type embryos (Fig. 7 D, black arrows, Movies 13-15).

To observe the dynamics of the junctional contact formation in the mutant, we analysed *ve-cadherin*[ubs8/ubs8] embryos expressing EGFP-ZO-1 transgene (Fig. 7 F-G, Movie 16). Similarly to the wild type analyses (fig. 2E and 3B, Movie 5) we observed a single labelled tip cell during the PLA formation. The sprouting tip cell expressed EGFP-ZO-1 uniformly at the membrane and upon contact with the other tip cell deposited the junctional protein at the contact site (Fig. 7 F-F'). However, subsequently it failed to properly form a junctional ring. The connection was changing shape and the ring seemed to collapse, break and split over time (Fig. 7F'-F''', Movie 16). In the meantime the tip cell continued sprouting activity and established a new connection a bit further up the other sprout, resulting in a new junctional spot. This repeated and in total 3 contact sites were observed (Fig. 7 F''-F''', yellow arrows, Movie 16). These eventually merged into one as the cells kept on moving over each other. This observation of the dynamic junctional rearrangements corresponds to the other live imaging data and explains the disturbed junctional patterns observed in the antibody staining experiments.

These results clearly demonstrate that VE-cadherin plays a central role in coordinating the anastomosis process at the early steps, but appears to be dispensable

for its initiation. In vessels lacking VE-cadherin, cells do not seem to recognize the contact formation and continue to search for the other tip cell instead of proceeding to the next steps of the process. This results in multiple contact sites over small areas of the cells that do adhere and polarize, but fail to form a continuous contact surface (Fig. 7 H, model).

5.6.5 Discussion

Comparison of fusion events in the early zebrafish embryo

To describe the dynamic behavior of endothelial cells during the formation of a complex vascular network and obtain insight into the cellular events underlying vascular anastomosis, we previously generated transgenic fish lines expressing EGFP-fused versions of the junctional protein ZO-1, which marks the presence and the *de novo* formation of AJ/TJ and the outline of endothelial cell contacts (ECs). We described the fusion of intersegmental vessels (ISVs) in the tail of the fish embryo (Herwig et al., 2011); since the ISVs form very early, they develop in the absence of stable heart beat and are not subjected to blood/plasma pressure during the initial fusion steps. Because we aim to understand how hemodynamic forces influence vascular network development and study the role of blood pressure in anastomosis, we analysed different vessel fusion events in the head region of older zebrafish embryos, in which stable plasma pressure is present. For this purpose, we generated a number of new transgenic fish lines and mutant fish lines, which allowed us to follow cell polarization and cell rearrangements as well as membrane dynamics using high resolution live imaging approaches and study its molecular control.

A multistep model for vascular anastomosis

We found that different vessels in the head (PLA, PCeV and CMV) fuse via a conserved multistep process (see Fig. 8 for a detailed description). This also includes vessel sprouts which fuse to a pre-existing, perfused vessel and thus involve single tip cells. The fusion process involves different cellular activities in distinct steps, which we will describe and discuss in the following sections.

Initial steps of fusion initiate cell polarization

We have observed that the initial steps of the vessel fusion process are similar to the ones characterized for the ISVs (Blum et al., 2008). They include deposition of new junctional material at the contact site of two tip sprouts in the form of an overlapping spot of VE-cadherin and ZO-1 proteins. This spot (which we call an "apical membrane insertion site" (in short "AMIS", according to (Bryant et al., 2010) is subsequently elaborated into a ring, accompanied by *de novo* apical membrane deposition, as shown by the localization of the apical marker Pdxl2 within the VE-cadherin and ZO-1 ring. This process is rather similar to *de novo* lumen formation in vasculogenesis as described by Strilic et al (Strilic et al., 2009) for the dorsal aorta. VE-cadherin deposition is followed by the accumulation of Podocalyxin, which might add de-adhesive forces to generate a narrow luminal space between the two tip cells (Strilic et al., 2010). In this particular state, the tip cells are bi-polar; they have an apical membrane domain towards the stalk and a new apical patch at the contact site.

After the establishment of this new connection and the apical membrane compartment, the process of lumen formation is highly influenced by the presence of plasma pressure and therefore differs to some extent from the ISVs. The vessel sprouts in the head are already lumenized as they establish the new contact. The apical membrane of the tip cell invaginates towards the sprouting tip, as shown by antibody staining and confocal time lapse imaging using membrane markers as well as angiography experiments. Perfusion of the new vessel involves further tip cell membrane invagination and finally apical membrane fusion at the contact site with the novel apical membrane, to form a unicellular tube with a continuous transcellular lumen.

During the initial fusion process, the novel apical patch grows in size, visually delimited by the junctional complexes, which form a growing ring-like structure. It will be interesting to find out how apical vesicles are transported to this single novel site and how this is molecularly regulated. Recent data obtained in the MDCK system demonstrate that a transcriptionally regulated complex is responsible for this (Bryant et al., 2010). Interestingly, the apical membrane of a tip cell grows much faster when it is in contact with a perfused vessel and rapidly generates a transcellular lumen. This suggested that pressure exerted onto the apical membrane increases its growth rate;

indeed, we showed that the apical membrane does not invaginate into tip cells in *silent heart* morphants that lack heartbeat. It would be most interesting to find molecular players involved in this pressure-dependent membrane growth regulation.

Lumen formation connects the two apical surfaces of tip cells

It has been put forward numerous times that one of the characteristics of tip cells is their lack of a lumen. However, we find that tip cells are already lumenized to a large extent; in many cases, the lumen extends up to the tip of the cell body of tip cells but does not break through until tip cells have established a contact with each other and an apical membrane patch has formed at the contact site. The lumen formation process is thus limited to two short distances (from the point of contact between two tip cells to the tip cell lumen in either cell).

Complex, unexpected cell shape changes transform unicellular into multicellular tubes

Unexpectedly, we consistently observed that the initial unicellular conformation, with the two former tip cells having trans-cellular lumens, is transient and that endothelial cells engage in a series of dynamic cell movements within the existing perfused vessel to finally form a multicellular tube. We characterized the cellular rearrangements involved in this process in great detail and observed that cells that initially had a transcellular lumen later split on one side of the tube to allow the neighbouring cells to establish a new contact. We have observed this process in several head vessels of 2.5-4-day-old fish embryos and we showed that cell splitting and new contact formation within the existing tube are essential cell behaviours involved in the transformation of unicellular to multicellular vessels. The sequence of events we observed is recurrent and appears to represent the major mechanism for vessel fusion in the zebrafish head. It will be interesting to find out whether particular proteins are necessary to split the cells. In the case of cell divisions, where the cell also splits, cell fission is regulated by distinct molecular machines (Gromley et al., 2005). In the case of developing blood vessel, it is possible that the process is "self-controlled", meaning that it might rely on a membrane

healing process (often referred to as membrane "resealing") cells are generally endowed with (Roostalu and Strahle, 2012).

During the formation of ISVs, we have also observed cell rearrangements similar to those described here. In this particular case, however, these rearrangements occurred in the absence of membrane invagination, and the small lumens generated in-between cells coalesced during DLAV formation without the necessity of cell splitting.

Molecular control of vessel anastomosis

Based on the existing literature and on our description of the cellular steps involved in vascular anastomosis, a number of predictions can be made. Studies on cell polarization and lumen formation in MDCK and in endothelial cells have shown important roles for many intracellular proteins, for example the Par3, Par6, aPKC complex, Rasip1 (Xu et al., 2011), CCM1 (Lampugnani et al., 2010) and the Exocyst (Bryant et al., 2010) in initial polarisation and subsequent apical membrane formation and lumen generation. It is very likely that the same molecules act in endothelial cells in the early fusion steps (step II to IV). However, due to the important role of these proteins in many cells in the developing embryo, it will not be easy to test their functional involvement connecting tip cells without using conditional mutagenesis methods or novel methods.

The driving forces underlying the cell rearrangements seen upon initial lumen perfusion remain unknown. Do cells actively migrate during this process, eventually using the neighbors as substrates? Or do these cell rearrangements rely on intracellular forces active at the adherens junctions? It is possible that bi-polar cells with two AJ rings are in a certain dis-equilibrium against which they fight until they have merged the two junctional compartments and united the two apical membrane patches. Cell rearrangements similar to those described here also occur during lumen formation in the *Ciona* notochord (Denker and Jiang, 2012; Dong et al., 2009). In this particular case, it is thought that the cells rearrange by active movement over each other (Dong et al., 2011).

Role of VE-cad in vascular anastomosis

The fusion of vascular sprouts bears some similarity to the fusion of adjacent tracheal metamers in the *Drosophila* embryo (Lee et al., 2003; Lee and Kolodziej, 2002). The first events, including filopodial contacts between tip cells and the formation of AJ spots, which were further elaborated into rings, is conserved. In the fly embryo, E-cadherin plays a pivotal role in fusion; in the absence of the *e-cadherin* gene (in *shotgun* mutants), filopodial contact does not lead to the accumulation of junctional proteins and the neighbouring tracheal metamers remain completely disconnected (Samakovlis et al., 1996b; Tanaka-Matakatsu et al., 1996). Dejana and colleagues have previously reported that zebrafish VE-cadherin plays an important role in stabilizing novel vascular sprouts; MO-induced reduction of *ve-cadherin* expression results in a lack of correct connections (Montero-Balaguer et al., 2009). In addition, it has been shown that VE-cadherin is strictly required for the polarisation of endothelial cells *in vitro* and *in vivo* (Lampugnani et al., 2010; Strilic et al., 2009).

To describe the role of VE-cadherin in more detail, we isolated null mutants in the single zebrafish *ve-cadherin* gene and analyse its function by studying homozygous mutant embryos (*ve-cadherin*[ubs8/ubs8]) and using the different live cell markers and antibodies with the aim to define at which step of the multi-step fusion process VE-cadherin might act. Surprisingly, we find that tip cell *de novo* polarisation still occurs in the absence of VE-cadherin, demonstrating that tip cells still recognize each other upon filopodial contact and that these contacts lead to *de novo* polarisation. However, the process does not lead to the emergence of a single luminal compartment between the tip cells; rather, several disorganised patches are formed and tip cells continue to extend filopodia and eventually generate more contacts. It has been shown before that following initial endothelial cell-cell assembly, VE-cadherin signalling to actomyosin contractibility is necessary for the uniform distribution of VE-cadherin at cell junctions in the established quiescent state (Abraham et al., 2009). It is possible that the lack of this particular function of VE-cadherin during vessel fusion generates part of the phenotype we observe. In addition, it has been shown that VE-cadherin affects the function of VEGF receptors, and in this way likely regulates filopodia dynamics (Abraham et al., 2009).

It has been described that the aortic lumen in mice develops extracellularly at the cell-cell contact between adjacent endothelial cells (Strilic et al., 2009). Apical proteins, such as CD34-sialomucins, insert at such endothelial contacts in a VE-cadherin dependent fashion. During anastomosis in zebrafish, we also find that the lumen forms at contact site. However, in this particular case, the contact formation lead to bi-polar endothelial cells and apical protein localisation does not require VE-cadherin. These findings are in line with those reported by Wang et al. (Wang et al., 2010), these authors also found ZO-1 accumulation in embryos where *ve-cadherin* was knocked down using MO injection. Since VE-cadherin is dispensable for the accumulation of ZO-1 and apical membrane components at tip cell contacts in zebrafish embryos, it remains open how tip cells recognize and interact with each other. This interaction is most likely mediated by the recognition of endothelial-specific cell surface molecules; but what are these molecules? Candidates include the Netrins and the JAMs (i.e. ESAM). We have also generated null mutation in the endothelial-specific *claudin5b* gene in zebrafish, but we do not see any fusion phenotype (data not shown). It will be very important to identify the molecules which mediate tip cell recognition and allow vascular sprouts to specifically connect to other sprouts and not to any other cell types.

The most striking defect we observed in VE-cadherin mutant embryos was the generation of several independent apical membrane patches at contact sites, rather than a single one. Recent studies in the MDCK system have shown that Synaptotagmin-like proteins control the formation of a single membrane domain in epithelial cells via the spatiotemporal organization of vectorial apical transport (Galvez-Santisteban et al., 2012). It will be interesting to investigate the role of these proteins during *de novo* polarisation of endothelial cells during vascular fusion events.

Our study provides a cellular framework to study vascular anastomosis. Future studies will allow dissecting the molecular pathways involved in exerting or regulating the different steps of the fusion process. Ultimately such studies might allow manipulating the process, rendering it more or less efficient. Since the vasculature is a therapeutic target in many human pathologies (reviewed e.g. in Carmeliet, 2003), such insight might ultimately contribute to better treatment strategies.

5.6.6 Figure legends

Fig.1 Palatocerebral artery (PLA) forms through fusion of two lumenized angiogenic sprouts.

A. Front view of a zebrafish Tg(*kdrl*:EGFP)[s843] embryo head at ~36 hpf. Blood vessels (green) together with bright field image show the location of PLA within the head tissue. The PLA extends rostrally along the base of the forebrain (arrow) and connects the two CrDI (Cranial division of the internal carotid artery) vessels (arrows) that encircle the optic capsules on both sides of the embryo head.

B-B''. Schematic representation of PLA development (green) in the head vasculature from 32 hpf to 48 hpf. PLA - palatocerebral artery, PLAJ - junction of the palatocerebral arteries, CrDI - cranial division of the internal carotid artery, DCV - dorsal ciliary vein, PrA - prosencephalic artery, PMBC - primordial midbrain channel, ACeV - anterior (rostral) cerebral vein, CMV - communicating vessel, NCA - nasal ciliary artery.

C. Still pictures of a time-lapse movie showing formation of the PLA in a transgenic embryo Tg(*kdrl*:EGFP)[s843];(*kdrl*:mKate-nls)[ubs13]. Endothelial cell cytoplasm is marked in green and the nuclei in red. The PLA sprouts (C, arrows) extend from the CrDI and grow towards each-other. Red bars mark the lumen length. The sprouts contact each other and anastomose (white arrow) to form a lumenized vessel (red bars mark lumen) that consists of 5-6 cells, visible by the yellow nuclei (C'-C''').

D. Still pictures of a time lapse movie showing the development of the PLA in a transgenic embryo Tg(*kdrl*:tdEos2)[ubs15]. Photoconversion was used to change the fluorescence in one of the sprouts (red) to distinguish it from the contra-lateral sprout (green). White bars (D'-D''') show the overlap of the sprouts (cell connection length). Red arrow (D-D'') marks the margin of the lumen in the red fluorescent sprout.

Scale bars: 20 µm.

Fig.2 Contact and lumen formation in the PLA

A. Still pictures of a time lapse movie showing the formation of the PLA in a transgenic embryo, Tg(*fliep*:GFF)[ubs3],(UAS:mRFP),(UAS:VE-cadherinΔC-EGFP)[ubs12]. Cell-cell junctions are shown in green and cell cytoplasm in red. PLA sprouts (A, white arrows) are led by single tip cells connected to the stalk by a ring-shaped junction (A-A''', white arrowheads). Red arrows show the lumen margin in each sprout.

Upon contact of the sprouts, a spot of VE-cad-GFP appears (A', white arrow). The spot elongates into a ring-shaped junction (A'', A''', white arrow) and lumen is pushed through the junction for vessel perfusion (A''-A'''). Lack of red fluorescence within the vessel marks the lumen.

B-B'''. Antibody staining of time points corresponding to images in A. Tg(*kdrl:*EGFP)[s843] embryos (red) and anti-VE-cadherin antibodies (white) were used. White arrows mark the sprouts (B), junctional spot (B') and junctional rings (B''').

C-D. Still pictures of a time lapse movie showing lumen formation in the PLA in a transgenic embryo TgBAC(*kdrl*:mKate-CAAX)[ubs16] injected with FITC-dextran. Endothelial cell membranes are visible in white in C and black in D, lumen filled with dextran is green (C only).

As the contact is established (C, D, arrowheads), the luminal membrane invaginates towards the contact site (C, D, red arrow). Dextran (green) reaches the end of the luminal membrane, showing that the lumen is connected to the blood circulation. As fusion proceeds, the invagination is advancing from both sides (C'-C'', D'-D'', red arrows) until the two lumens are only separated by a small part of the cell body (C'',D'' arrowheads). Perfusion of the lumen involves membrane fusion and connects the two lumens allowing the dextran to flow through (C''', D''', red arrow). The "n" marks a nucleus visible as a space not filled with dextran in C''' and D'''.

E. Still pictures of a time lapse movie showing contact and lumen formation in a transgenic embryo Tg(*fliep*:GFF)[ubs3],(UAS:mRFP),(UAS:EGFP-ZO-1)[ubs5]. Due to mosaic expression only one of the tip cells is labeled with EGFP-ZO-1 (green). The cytoplasm of endothelial cells is marked in red. Insets show the EGFP-ZO-1 alone (black). White arrows show the sprouts (E), the connection site with a spot of EGFP-ZO-1 (E') that transforms into a ring (E''). Finally the tip cell becomes a unicellular tube with transcellular lumen connected to the neighboring cells by junctional rings (E''', arrows).

F. A cellular model of PLA fusion. Time points correspond to the images shown above. Red and green cells are tip cells, grey and yellow are stalk cells. Black arrows show the sprouts (F) and the contact formation (F'-F'''). Red arrows show the luminal cell membrane.

G. A 3D model of a tip cell undergoing transcellular lumen formation through cell membrane invagination. The basal membrane is light grey; the apical/luminal membrane is dark grey. Red arrows point out the lumen end and the lumen length (in the cross section models). Black arrows show the new contact formation site, with junctions marked in black and new apical membrane in dark grey within.

Scale bars: 20 μm.

Fig.3 Formation of a multicellular tube through cell rearrangements

A. Still pictures of a time lapse movie showing proceeding development of the PLA in a transgenic embryo Tg(*fliep*:GFF)[ubs3],(UAS:mRFP),(UAS:VE-cadherinΔC-EGFP)[ubs12]. Cell-cell junctions are marked in green and cell cytoplasm in red. One of the cells is a unicellular tube (A, red arrow) connected to the neighboring cells by ring shaped junctions (A, white arrows). A blood cell is visible within the lumen. With time the junctional rings move closer together meaning the neighboring cells migrate towards each other (A', white arrows) and the middle cell (red arrow) narrows on one side of the tube. Finally the rings meet making a new connection visible as a line of junctions (A'', white arrow) meaning the middle cell (red arrow) split on one side and become a part of the multicellular tube. At this time point several blood cells go through the vessel.

B. Still pictures of a time lapse movie showing contact and lumen formation in a transgenic embryo Tg(*fliep*:GFF) [ubs3],(UAS:mRFP),(UAS:EGFP-ZO-1)[ubs5]. The images show time points corresponding to A, with only a single cell marked with EGFP-ZO-1 (green) and the endothelial cell cytoplasm in red. The cell (B, red arrow) is connected to the neighboring cells by ring shaped junctions (white arrows). The cell body narrows on one side of the tube (B', red arrow) as the junctional rings move closer together (white arrows). Finally the cell splits on one side (B'', red arrow) becoming a part of the multicellular tube with one continuous junctional ring (white arrow).

C. A cellular model of unicellular to multicellular tube transformation. The middle cell (green) is initially a unicellular tube (C). The neighboring cells (red, yellow) move closer together making the green cell narrow on one side of the tube (C', black arrows). Finally the green cell splits on one side of the tube (C'') and takes shape of a half pipe to allow the red and yellow cells to meet and establish a new connection (E'', arrow).

Scale bars: 20 μm.

Fig.4. PCeV forms through cell rearrangement and cell splitting events

Still pictures of a time lapse movie showing anastomosis of the PCeV (posterior (caudal) cerebral vein). Images A-D show a dorsal view (anterior up) of the head vasculature (green) at 60-72 hpf of a zebrafish embryo Tg(*kdrl*:EGFP)[s843]. The fusing PCeV and DLV (dorsal longitudinal vein) are marked with white arrows.

A'-D'' show close up of the PCeV at time points corresponding to A-D of a transgenic embryo Tg(*fliep*:GFF)[ubs3],(UAS:mRFP),(UAS:VE-cadherinΔC-EGFP)[ubs12].

Two lumenized sprouts approach each other led by single tip cells (A', white arrows). A spot of Ve-cad-EGFP is visible upon contact (A'', white arrow). The spot becomes a ring as the cell contact surface expands (B', arrow). The length of the unicellular tube part is marked with a white bar. The newly formed ring becomes bigger (B'', C', arrow) and the lumen starts to push through into the other tip cell (B'', C', blue bar). When the lumen is perfused (C'', blue bar) the junctional rings start to move towards each other to finally touch (D', D'' arrows) and transform all unicellular tubes into multicellular ones.

Scale bars: 20 µm.

Fig.5. Fusion of a sprout to an existing vessel on the example of CMV and PLA

A-F. Still pictures of a time lapse movie showing fusion of CMV to PLA in a transgenic embryo Tg(*fliep*:GFF)[ubs3],(UAS:mRFP),(UAS:VE-cadherinΔC-EGFP)[ubs12]. CMV (communicating vein) sprouts ventrally towards the PLA (A, arrow). The leading tip connects to the PLA on the cell body of one of the cells making a spot of junctions (B, arrow). The newly formed ring connects to an existing junctional line on the PLA (C, arrow) and transcellular lumen starts to form in the CMV tip cell from the PLA upwards (C, white bar). The lumen extends through the whole sprout (E, F, white bar).

G. A cellular model of the CMV fusion. The CMV tip cell is green, followed by yellow stalk. The PLA is bright grey with dark grey junctions. CMV makes a new junctional connection to the PLA (black ring, arrow). Lumen (bright green, red bar) is pushed through the tip cell and goes up the sprout.

H. A model of an alternative lumen formation process, where the CMV sprout is lumenized as it touches the PLA (red bar). In this case the lumen is pushed down the CMV (follow the red bars) towards the new connection with the PLA (black arrow).

I. Blue bars mark the cellular/junctional rearrangements leading to transformation of the CMV into a multicellular tube.

Scale bars: 20 µm.

Fig.6. The initial transcellular lumen formation is highly influenced by blood flow

Still pictures of a time lapse movie showing development of the PLA in a transgenic embryo Tg(*fliep*:GFF)[ubs3],(UAS:mRFP),(UAS:VE-cadherinΔC-EGFP)[ubs12] injected with *tnnt2* morpholino (*sih*) blocking the heart beat and hence, blood flow. The formation of PLA sprouts in the *sih* embryos is normal. As in the wild type they are led by single tip cells (A, white arrows) attached to the stalk by ring shaped junctions (A, green arrows). All the steps of new contact formation

are conserved, including new spot formation (B, white arrow), ring formation (C, white arrow) and cellular rearrangements (D-F, white and green arrows point at borders of junctional rings and new contact formation spots).

Scale bars: 20 µm.

Fig.7. VE-cadherin^{ubs8/ubs8} embryos show defects in the initial steps of the fusion process

A-B. Still pictures of a time lapse movie showing development of the PLA in a transgenic line *ve-cad*^{ubs8/ubs8};Tg(*kdrl*:tdEos2)^{ubs15}; of a wild type embryo (A) and a *ve-cadherin*^{ubs8/ubs8} embryo (B). White arrows point at lamellipodia, single on each sprout in the wild type (WT) embryo (A) and multiple in *ve-cadherin*^{ubs8/ubs8} mutant (B). Upon contact formation, the WT sprouts have one connection spot (A', yellow arrows) and do not show additional lamellipodia formation until the end of the process, as the contact surface elaborates (A''-A''', red arrows point at the sprout end, blue arrows show the length of the contact surface). The *ve-cadherin*^{ubs8/ubs8} sprouts show multiple lamellipodia throughout contact formation (B'-B''', white arrows) and multiple connection points between the sprouts (yellow arrows). The continuous contact surface of the sprouts is much smaller (blue arrows).

C-D. Still pictures of a spinning disc time lapse movie showing development of the PLA in transgenic line TgBAC(*kdrl*:mKate2-CAAX)^{ubs16} of wild type (C) and VE-cadherin mutant (*ve-cad*^{ubs8/ubs8}) (D) embryos. Black arrows point at sprouting cell extensions, single or double in WT (C-C') and multiple in *ve-cadherin*^{ubs8/ubs8} vessels (D-D'). Red arrows point at contact sites, which resolve into a continuous contact surface in wild type (C''-C''''), whereas in the mutant they persist over time resulting in non-continuous contact surface (D''-D''').

E. Antibody staining of time points corresponding to images in A. *Ve-cad*^{ubs8/ubs8};Tg(*kdrl*:EGFP)^{s843} embryos (red) and anti-ZO-1 (blue) and anti-ESAM (green) antibodies were used. Junctions within vessels are visible as overlap of these (white). White arrows mark the sprouts (E). Yellow arrows mark the contact points where junctional proteins are deposited (E'-E''').

F-G. Still pictures of a time lapse movie showing contact formation in a transgenic embryo Tg(*fliep*:GFF)^{ubs3};(UAS:mRFP);(UAS:EGFP-ZO-1)^{ubs12} in the *ve-cadherin*^{ubs8/ubs8} background. EGFP-ZO-1 (green in F, black in G) is expressed in only one tip cell. Cell bodies are red (F). Upon contact of the tip cells a junctional ring forms (F', G', yellow arrows), but the cells keep on extending filopodia (white arrows). New contacts are formed as the additional filopodia connect to the other sprout (F''-F''', G''-G''', yellow arrows)

H-I. Cellular models of initial steps of the fusion process in wild type (H) and *ve-cadherin*[ubs8/ubs8] vessels. Initially, both sprouts form multiple extensions, which in the wild type are limited to 1-2 per tip cell (H-H') and in the mutant often reach 3-5 (I-I'). Multiple cells can be present at the leading tip of the mutant sprout (I, red and blue cell) increasing the number of the observed lamellipodia. When the filopodia touch, a contact is established with deposition of new junctional material in the wild type (H', black dots) as well as the mutant sprouts (I', black dots). Due to increased number of filopodia, more contact spots are present in the mutant. As the contact formation proceeds, the wild type sprouts merge all the contact sites into one to form a continuous contact surface framed by a junctional ring with new apical membrane patch inside (H''-H'''). In opposite, the mutant sprouts fail to merge all the contact sites resulting in multiple and disturbed junctional connections still forming rings and lines. *De novo* apical polarization within the new rings is maintained.

Scale bars: 20 µm.

Fig.8 A multi-step process underlies vessel anastomosis

In a first step, tip cells contact each other via filopodial extensions (A). After a certain time, such contacts result in the formation of stable cell connections, manifested by the co-localization of VE-cadherin and ZO-1 at specific sites (B). At these sites of contacts, apical membrane is inserted, manifested by the localisation of Podocalyxin (C). Concomitantly, filopodial activity of tip cells is dramatically reduced. While the luminal pocket generated by tip cell polarisation and apical membrane insertion are slowly enlarged, the apical membrane which connects the tip cells to their corresponding stalk cells are invaginating rapidly due to blood plasma pressure, and eventually connect to the de novo generated luminal pockets (D). These initial steps in the anastomosis process thus lead to a vessel in which the two tip cells have a trans-cellular lumen. In a subsequent step, tip cells rearrange (E) such that they eventually connect up to adjacent stalk cells (F) and form novel cell interactions (G). During these steps, the initial tip cells spit apart through a cell fission event. As a result of this multi-step process, a perfused multicellular vessel is generated. This novel vessel carries no obvious sign showing that it has been generated by a fusion process (rather than by a simple sprouting (budding) process).

Supplementary figure legends

Figure S1. Podocalyxin-like 2 (Pdxl2) staining labels apical/luminal membrane during PLA fusion

A-I'''. Antibody staining labelling Pdxl2 (green) on the invaginating apical membrane, extending beyond junctional staining for ZO-1 (white), in the PLA sprouts of Tg(*kdrl:*EGFP)[s843] embryos (red) (A). Red arrow marks the end of lumen; white arrow marks the end of a junctional ring. During fusion apical membrane is present within the new junctional ring (B, arrow). After transcellular lumen formation, continuous apical surface in the PLA marks perfused lumen, including unicellular parts (green bar) where the staining is seen within single cells, beyond junctional rings (white arrows). Continuous apical surface is present during subsequent cell rearrangements leading to formation of a multicellular tube (D-F green bars mark the unicellular part, white mark the multicellular).

G-I. The steps of PLA fusion in *silent heart* embryos. White bars mark the surface of cell-cell junctional contacts (ZO-1 staining in white). Pdxl2 apical staining (green) is only visible within the junctional rings and lines, since no membrane invagination takes place.

Scale bars: 20 μm.

Figure S2. Junctional staining and live imaging of PLA fusion in *silent heart* and wild type embryos

A-B. Antibody staining for ZO-1 (blue) and ESAM (green) in transgenic Tg(*kdrl*:EGFP)[s843] (red) embryos at stages corresponding to the time lapses in figure 7. The junctions within the vessels visible in white (ZO-1 and ESAM overlap) show the cellular architecture of the fusing sprouts in WT (A) and *silent heart* (B) embryos. White arrows point at lamellipodia, yellow arrows at contact points. Single cells are present at the leading edge of the sprouts embryos (A, B) as well as single connection points are visible at later stages (A'-A''', B'-B''').

C. Still pictures of a time lapse movie showing development of the PLA in a transgenic Tg(*kdrl*:tdEos2)[ubs15] silent heart embryo. One of the tip cells was converted to red, the other one is green (C, white arrows). Yellow arrows show the contact point of the sprouts (C'-C'''). Blue arrow shows the length of the connection.

D. Still pictures of a spinning disc time lapse movie showing development of the PLA in the transgenic line TgBAC(*kdrl*:mKate2-CAAX)[ubs16] in a *silent heart* embryo, at time points corresponding to Fig. 7 C-D. Black arrows point at filopodia, red arrows show the contact formation.

Scale bars: 20 μm.

5.6.7 Supplementary movies

Movie S1. Related to Figure 1 C. Development of the PLA in a Tg(*kdrl*:EGFP)[s843];(*kdrl*:mKate-nls)[ubs13] embryo.

The movie shows an overview of the PLA development in the head vasculature. Endothelial cell cytoplasm is marked in green and the nuclei in red. Images are maximal projections of 105 sections with 1.2 µm spacing. Images were acquired between 32-48 hpf with ~1 h between timepoints. The two PLA sprouts grow out of CrDI vessels encircling the eyes. The sprouts connect and lumen opens in the newly formed PLA.

Movie S2. Related to figure 1 D. Development of the PLA in a Tg(*kdrl*:tdEos2)[ubs15] embryo.

Photoconversion was used to change the fluorescence in one of the sprouts (red) to distinguish it from the contra-lateral sprout (green). The sprouts migrate and meet to establish a connection. After contact the tip cells move over each other to expand the contact surface. In the meantime the lumen opens in the newly formed PLA.

Images are maximal projections of 65 sections with 0.75 µm spacing. Images were acquired between 34- 40 hpf with 8 min between time points.

Movie S3. Related to Figure 2 A. Contact and lumen formation in the PLA in a Tg(*fliep*:GFF)[ubs3];(UAS:mRFP);(UAS:VE-cadherinΔC-EGFP)[ubs12] embryo.

Cell-cell junctions are marked in green and cell cytoplasm in red. The migrating sprouts are led by single tip cells connected to the following cells by ring-shaped junctions. Upon contact a new spot of junctional material is deposited and later transforms into a ring-like junction. The transcellular lumen opens in both tip cells making unicellular tubes connected with a ring of junctions.

Images are maximal projections of 62 sections 0.8 µm spacing. Images were acquired between 34-39.5 hpf with 10 min between time points.

Movie S4. Related to Figure 2 C-D. Transcellular lumen formation through membrane invagination in the PLA in a TgBAC(*kdrl*:mKate-CAAX)[ubs16] embryo injected with 500 kDa FITC-Dextran.

Time lapse movie showing lumen formation in the PLA in a transgenic embryo TgBAC(*kdrl*:mKate2-CAAX)[ubs16] injected with fluorescent 500 kDa FITC-dextran. Upper panel shows endothelial cell membranes in white and FITC-Dextran in green. Lower panel shows the membrane only in black. Red arrows follow the invaginating luminal membrane in both sprouts. At the end the luminal spaces connect right under a nucleus (non-filled space) and the lumen is perfused.

Images are maximal projections of 56 sections 0.7 µm spacing. Images were acquired between 36-40 hpf with 7 min between time points. The stack was cropped to better visualize the lumen formation.

Movie S5. Related to Figure 2 E and 3B. Contact and lumen formation followed by cell rearrangements in the PLA in a Tg(*fliep*:GFF)^{ubs3};(UAS:mRFP);(UAS:EGFP-ZO-1)^{ubs5} embryo.

A time lapse movie showing contact and lumen formation in a transgenic embryo Tg(*fliep*:GFF)^{ubs3};(UAS:mRFP);(UAS:EGFP-ZO-1)^{ubs5}. Due to mosaic expression only one of the tip cells is labeled with EGFP-ZO-1 (green). The cytoplasm of endothelial cells is marked in red. The lower panel shows the EGFP-ZO-1 alone (black). Junctional spot and ring formation is visible upon contact. Subsequently the single labeled cell becomes a unicellular tube as the lumen opens. Further rearrangements lead to cell shape changes. The borders of the cell come closer together on one side of the tube and finally connect when the cell splits on one side and changes shape from the unicellular tube into a flat, half-pipe cell.

Images are maximal projections of 65 sections with 0.75 µm spacing. Images were acquired between 36-40.5 hpf with 5 min between time points.

Movie S6. Formation of a multicellular tube through cell rearrangements in the PLA in a Tg(*fliep*:GFF)^{ubs3};(UAS:mRFP);(UAS:VE-cadherinΔC-EGFP)^{ubs12};embryo.

A time lapse movie showing development of the PLA in a transgenic embryo Tg(*fliep*:GFF)^{ubs3};(UAS:mRFP);(UAS:VE-cadherinΔC-EGFP)^{ubs12} Cell-cell junctions are marked in green and cell cytoplasm in red. The movie starts with an established PLA connection. Transcellular lumen forms in both tip cells connected by a junctional ring. Cell rearrangements are reflected in the junctional rings' movement towards each other (green arrows). The rings meet and form a new line of junctions meaning a new connection is made between the two cells first separated by a third one, that undergoes cell splitting.

Images are maximal projections of 48 sections with 0.5 µm spacing. Images were acquired between 36-40 hpf with 4 min between time points.

Movie S7. Related to Figure 4. Formation of the PCeV in a transgenic embryo Tg(*fliep*:GFF)^{ubs3};(UAS:mRFP);(UAS:VE-cadherinΔC-EGFP)^{ubs12}.

A time lapse movie showing development of the PCeV in a transgenic embryo Tg(*fliep*:GFF)^{ubs3};(UAS:mRFP);(UAS:VE-cadherinΔC-EGFP)^{ubs12}. See also Fig. 4 A'-D''. The

PCeV sprouts are led by single cells. A junctional spot forms upon tip cell contact (arrow). The spot elaborates into a ring and transcellular lumen extends in the tip cell (red arrow). Subsequent cell rearrangements on both sides transform the vessel into a multicellular tube (follow green arrows).

Images are maximal projections of 47 sections with 0.7 µm spacing. Images were acquired between 60-70 hpf with 8 min between time points.

Movie S8. Related to Figure 5. Fusion of a sprout to an existing vessel on (CMV to PLA) in a transgenic embryo Tg(*fliep*:GFF)[ubs3];(UAS:mRFP);(UAS:VE-cadherinΔC-EGFP)[ubs12]

A time lapse movie showing fusion of CMV to PLA in a transgenic embryo Tg(*fliep*:GFF)[ubs3];(UAS:mRFP);(UAS:VE-cadherinΔC-EGFP)[ubs12] See also fig.5. The CMV sprout connection to the PLA forming a spot of junctions on the cell body. The spot becomes a ring that connects to existing junctions within the PLA. Transcellular lumen forms in the sprout from the PLA upwards.

Images are maximal projections of 49 sections with 0.8 µm spacing. Images were acquired between 40-46.5 hpf with 10 min between time points.

Movie S9. Related to Figure 6. Formation of the PLA in the absence of blood flow (*silent heart*)

A time lapse movie showing development of the PLA in a transgenic embryo Tg(*fliep*:GFF)[ubs3];(UAS:mRFP);(UAS:VE-cadherinΔC-EGFP)[ubs12] injected with tnnt2 morpholino (*sih*) and lacking heart beat and hence, blood flow.

Sprouts led by single tip cells connect forming a spot and subsequently a ring of junctions. Further cell rearrangements lead to formation of a multicellular cord with continuous junctions. No transcellular lumen formation and thus, no cell splitting is present.

Images are maximal projections of 76 sections with 0.75 µm spacing. Images were acquired between 36-41 hpf with 10 min between time points.

Movie S10. Related to Figure 7 A. PLA formation in a wild type Tg(*kdrl*:tdEos2)[ubs15] embryo

A time lapse movie showing development of the PLA in transgenic line Tg(*kdrl*:tdEos2)[ubs15] of a wild type embryo. Upon contact of the sprouts the contact surface of the tip cells expands and the filopodial activity is reduced. Upon contact of the sprouts the contact surface of the tip cells expands and the filopodial activity is reduced.

Images are maximal projections of ~50 sections with 1 µm spacing. Images were acquired between 36-39.5 hpf with 7 min between time points.

Movie S11. Related to Figure S2 C. PLA formation in a *silent heart* Tg(*kdrl*:tdEos2)^{ubs15} embryo

A time lapse movie showing development of the PLA in transgenic line Tg(*kdrl*:tdEos2)^{ubs15} of an embryo injected with tnnt2 morpholino (*sih*)
Images are maximal projections of ~50 sections with 1 µm spacing. Images were acquired between 36-39.5 hpf with 7 min between time points.

Movie S12. Related to Figure 7 B. PLA formation in a *ve-cad*^{ubs8/ubs8};Tg(*kdrl*:tdEos2)^{ubs15} embryo

A time lapse movie showing development of the PLA in transgenic line *ve-cad*^{ubs8/ubs8};Tg(*kdrl*:tdEos2)^{ubs15} of a embryo. The sprouts extend numerous filopodia which do not regress after the contact formation. Instead additional connections are made by the additional filopodia.

Images are maximal projections of ~50 sections with 1 µm spacing. Images were acquired between 36-39.5 hpf with 7 min between time points.

Movie S13. Related to Figure 7 C High time resolution imaging of PLA formation in a wild type embryo TgBAC(*kdrl*:mKate2-CAAX)^{ubs16}

A spinning disc time lapse movie showing development of the PLA in transgenic line TgBAC(*kdrl*:mKate2-CAAX)^{ubs16} of a wild type embryo. Filopodia activity leads to contact formation. After the first connection the contact is rapidly sealed and the lumen formation through membrane invagination can be observed.

Images are maximal projections of 30 sections with 0.5 µm spacing. Images were acquired between 36-38 hpf with 15 sec between time points.

Movie S14. Related to FigureS2 D. High time resolution imaging of PLA formation in a *silent heart* embryo TgBAC(*kdrl*:mKate2-CAAX)^{ubs16}

A spinning disc time lapse movie showing development of the PLA in transgenic line TgBAC(*kdrl*:mKate2-CAAX)^{ubs16} of an embryo injected with tnnt2 morpholino (*sih*). Filopodia activity leads to contact formation. After the first connection the contact is rapidly sealed as the cells move over each other and extend the contact surface.

Images are maximal projections of 30 sections with 0.5 µm spacing. Images were acquired between 36-38 hpf with 15 sec between time points.

Movie S15. Related to Figure 7 D. High time resolution imaging of PLA formation in a *ve-cad*[ubs8/ubs8];TgBAC(*kdrl*:mKate2-CAAX)[ubs16] embryo.

A spinning disc time lapse movie showing development of the PLA in a transgenic *ve-cad*[ubs8/]ubs8;TgBAC(*kdrl*:mKate2-CAAX)[ubs16] embryo. Extensive filopodial activity leads to formation of multiple contacts between the tip cells. These contacts are maintained forming a non-continuous contact surface with small overlap surfaces and multiple holes.
Images are maximal projections of 30 sections with 0.5 µm spacing. Images were acquired between 36-38 hpf with 15 sec between time points.

Movie S16. Related to Figure 7 E. PLA formation in a Tg(*fliep*:GFF)[ubs3];(UAS:mRFP);(UAS:EGFP-ZO-1)[ubs5] embryo.

A time lapse movie showing contact and lumen formation in a transgenic embryo Tg(*fliep*:GFF)[ubs3];(UAS:mRFP);(UAS:EGFP-ZO-1)[ubs5]. Due to mosaic expression only one of the tip cells is labeled with EGFP-ZO-1 (green). The cytoplasm of endothelial cells is marked in red. The lower panel shows the EGFP-ZO-1 alone (black). Upon contact EGFP-ZO-1 accumulates at the contact site and eventually forms a ring. The tip cell continues the sprouting activity and forms additional connections with the other sprouts. The existing contact seems unstable and undergoes extensive shape changes. Eventually it merges into one continuous junctional connection as the cells keep moving over each other.
Images are maximal projections of 63 sections with 0.8 µm spacing. Images were acquired between 32-38 hpf with 4 min between time points.

The movie files can be found on the attached CD.
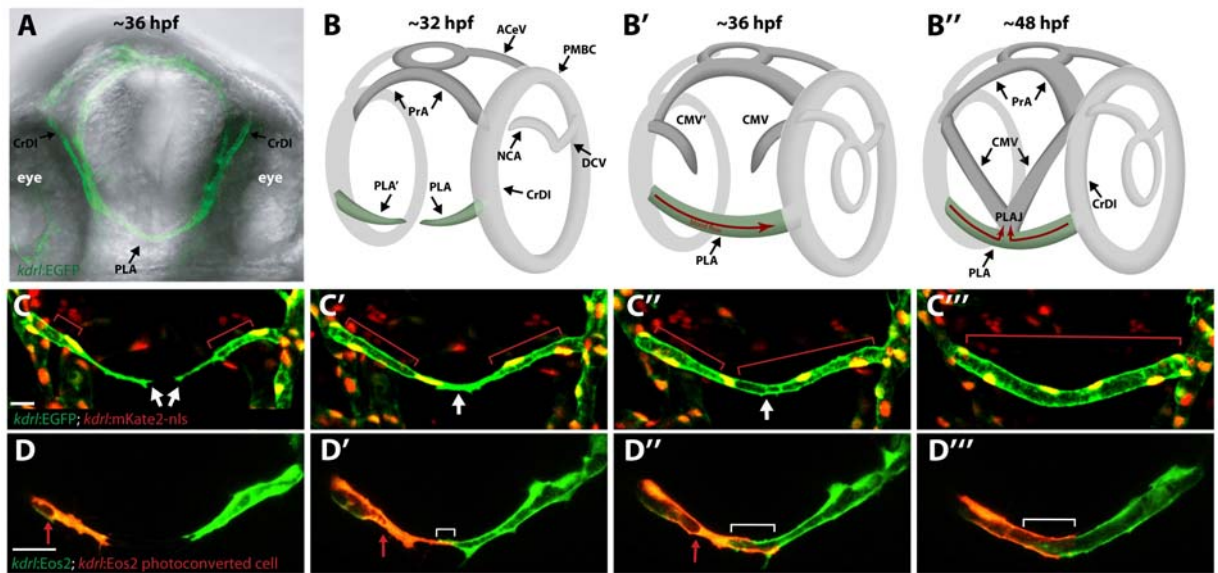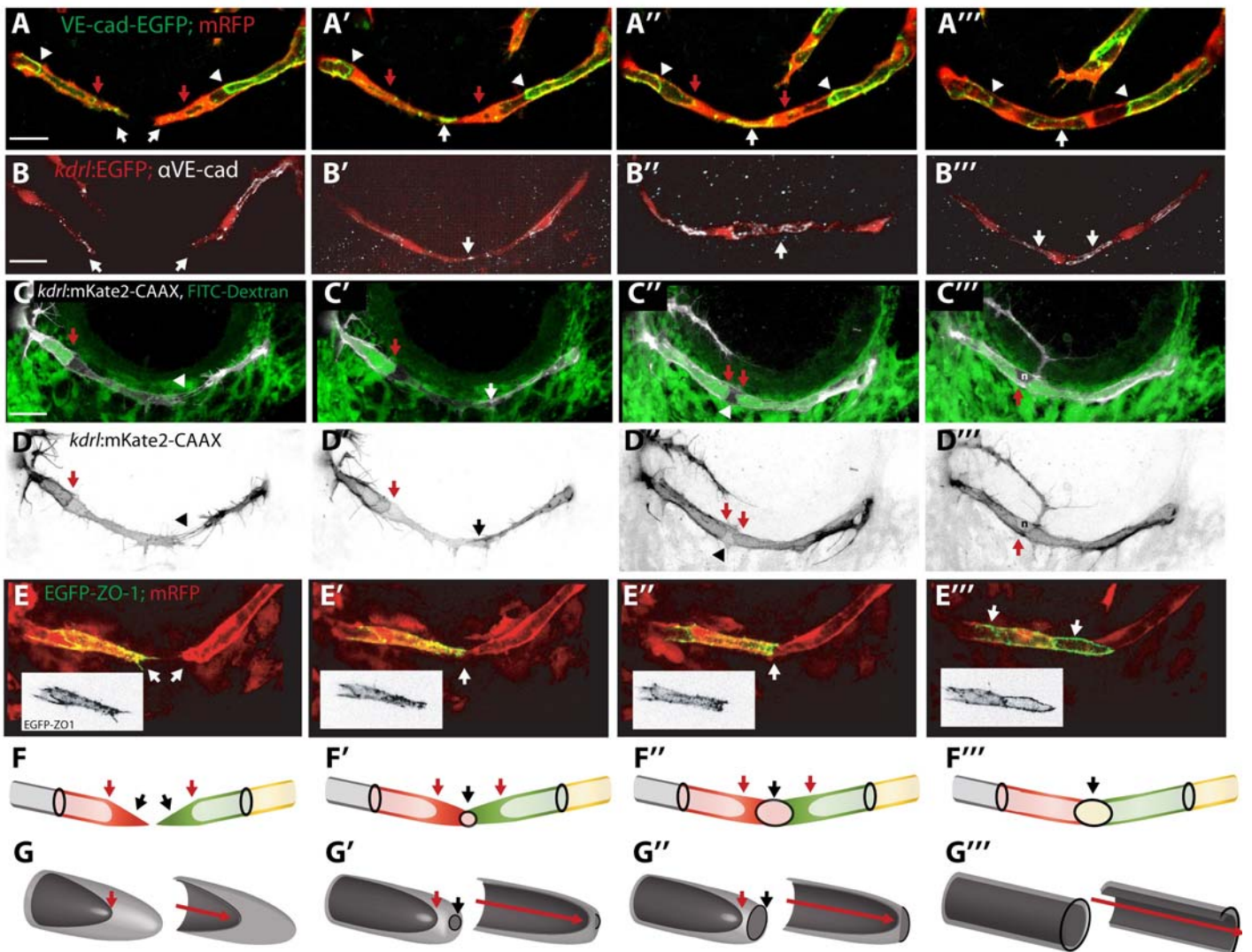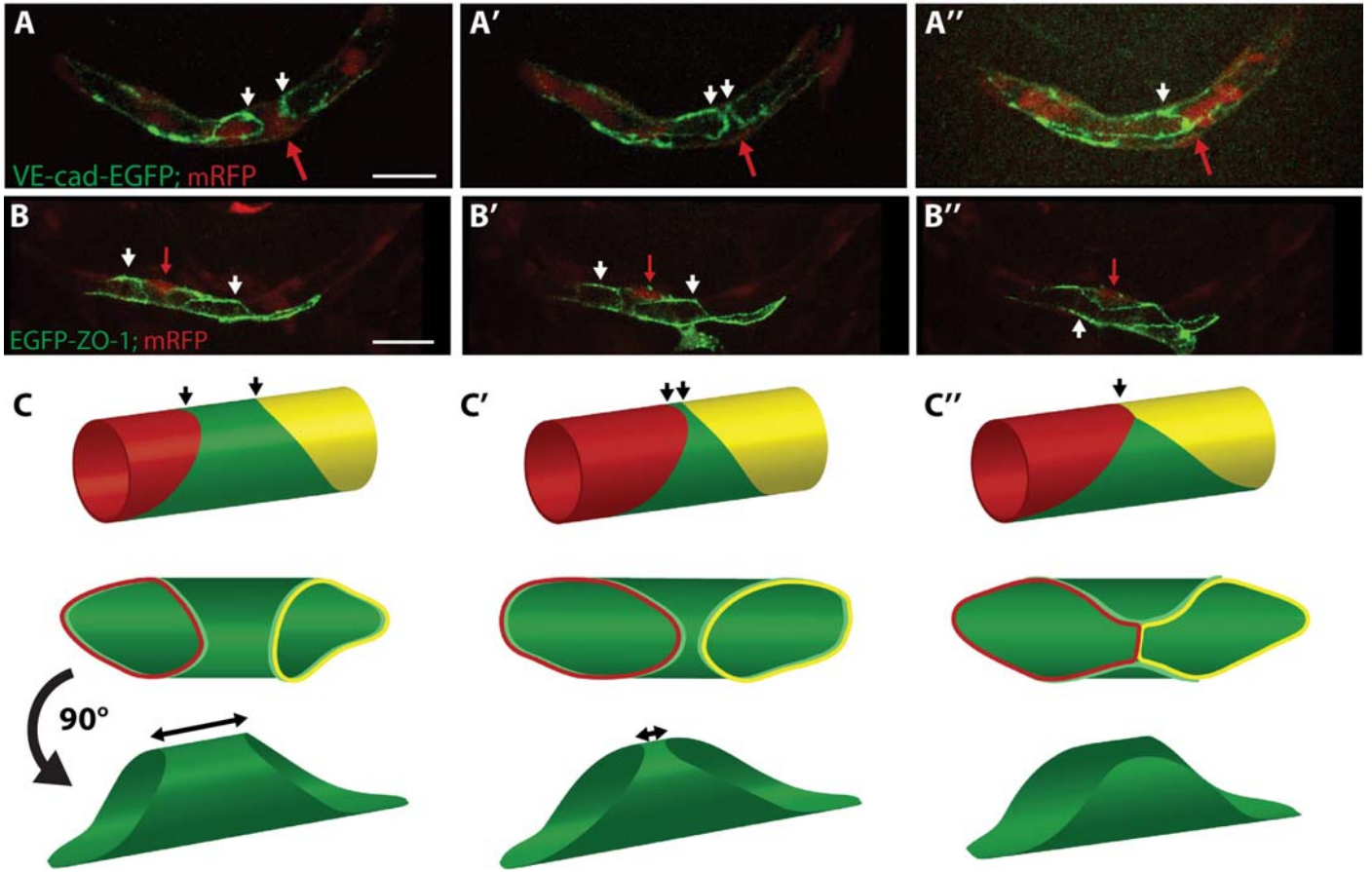
5.6.8 Figures

Figure 1

Figure 2

Figure3

Figure 4
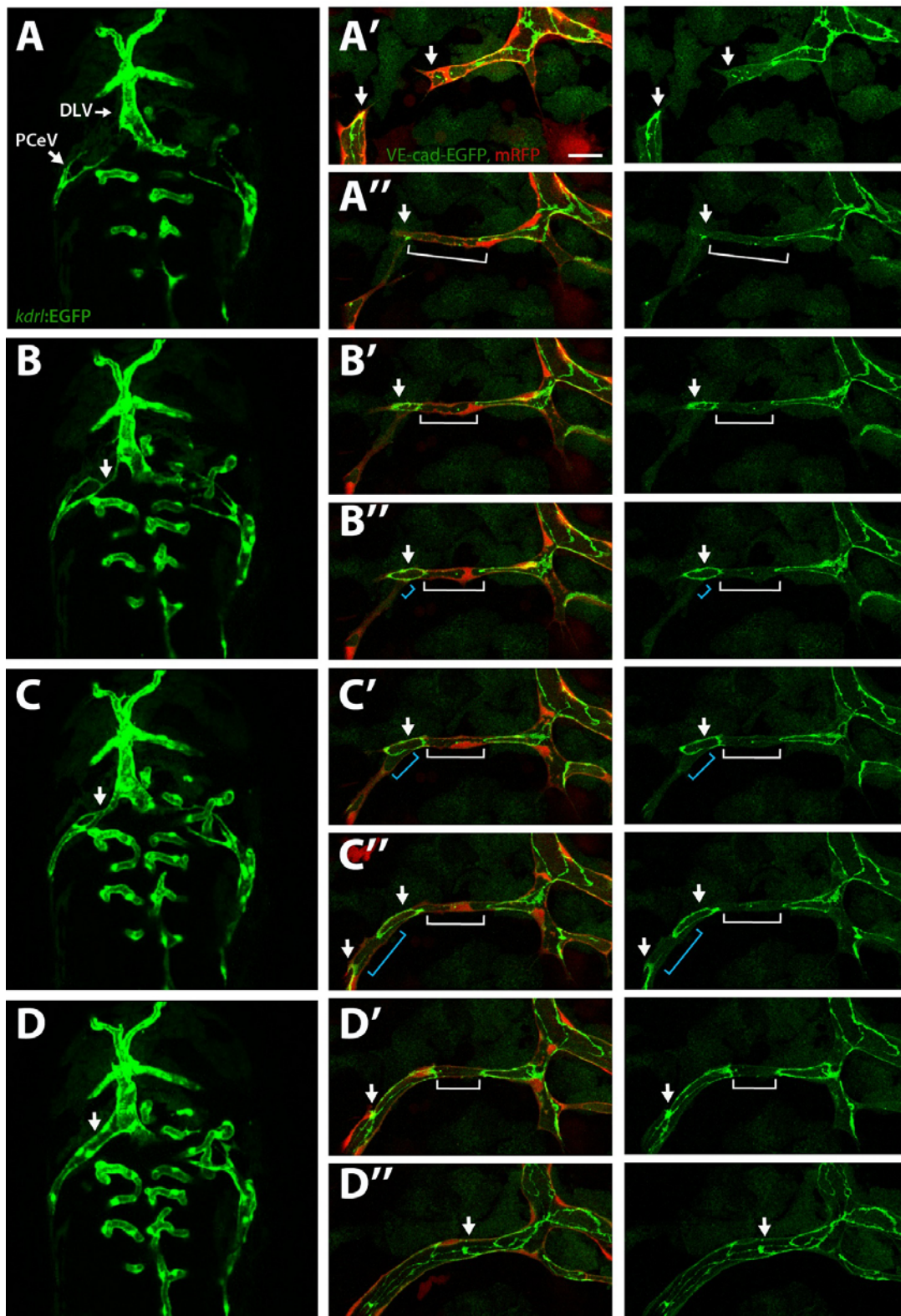
Figure 5
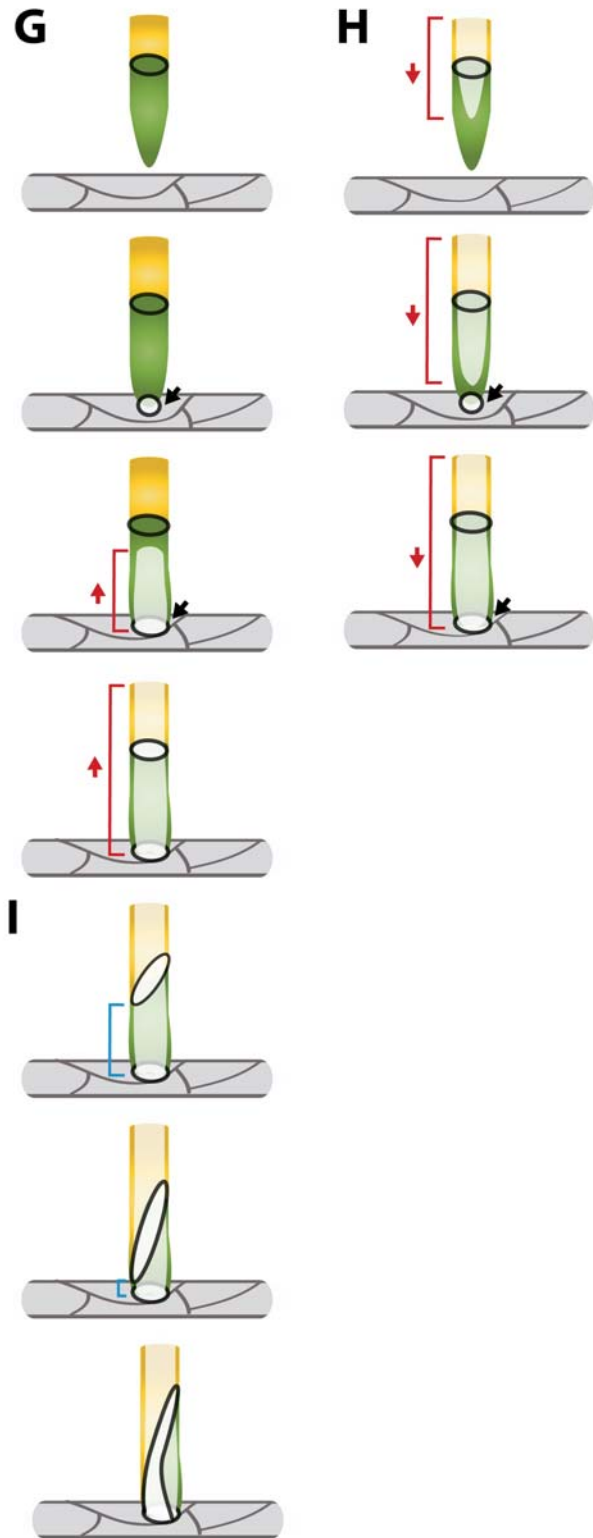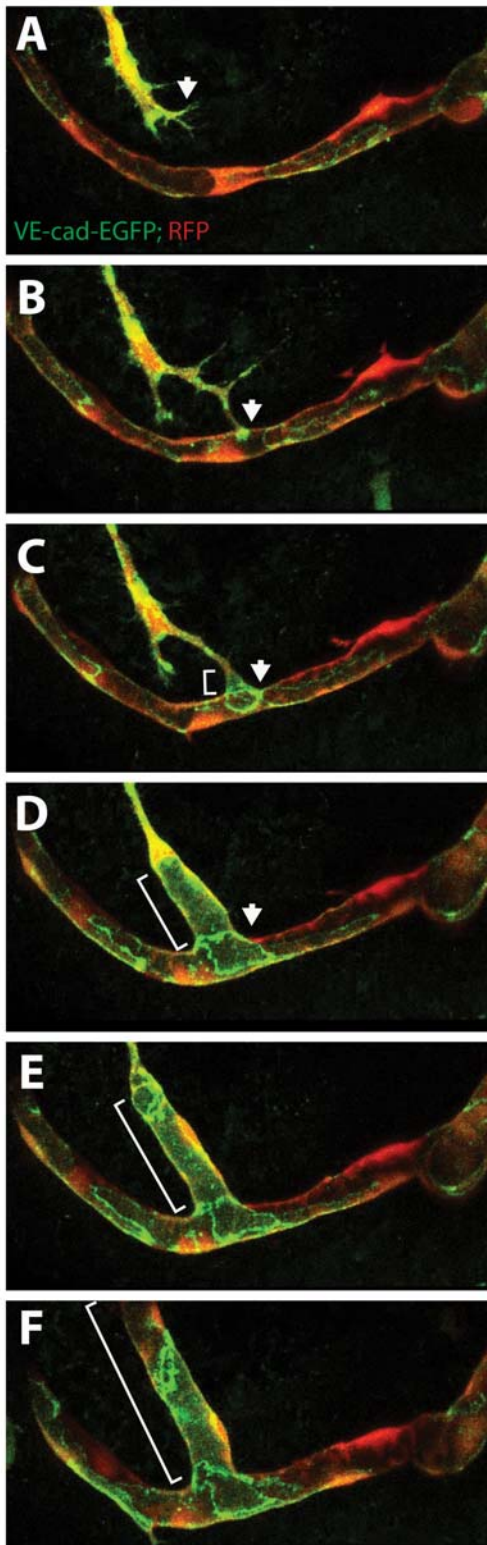
Figure 6
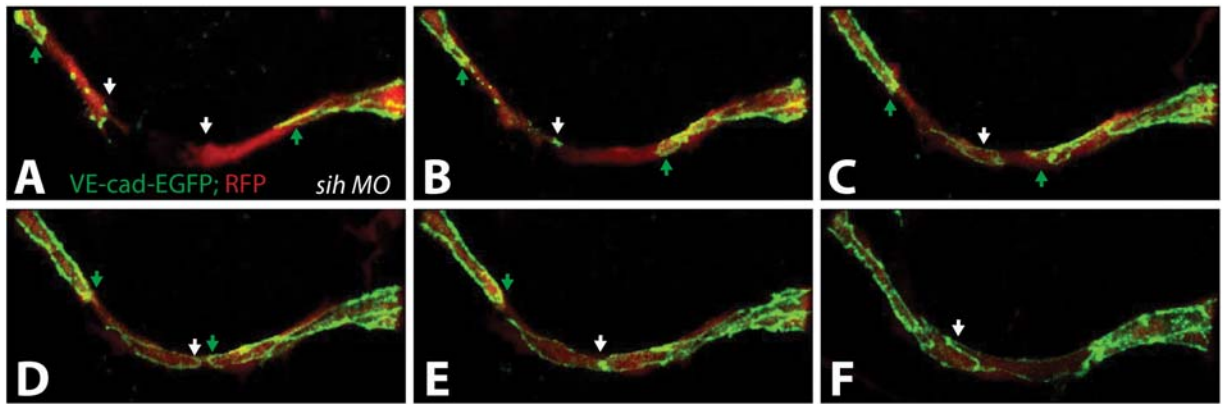
Figure 7
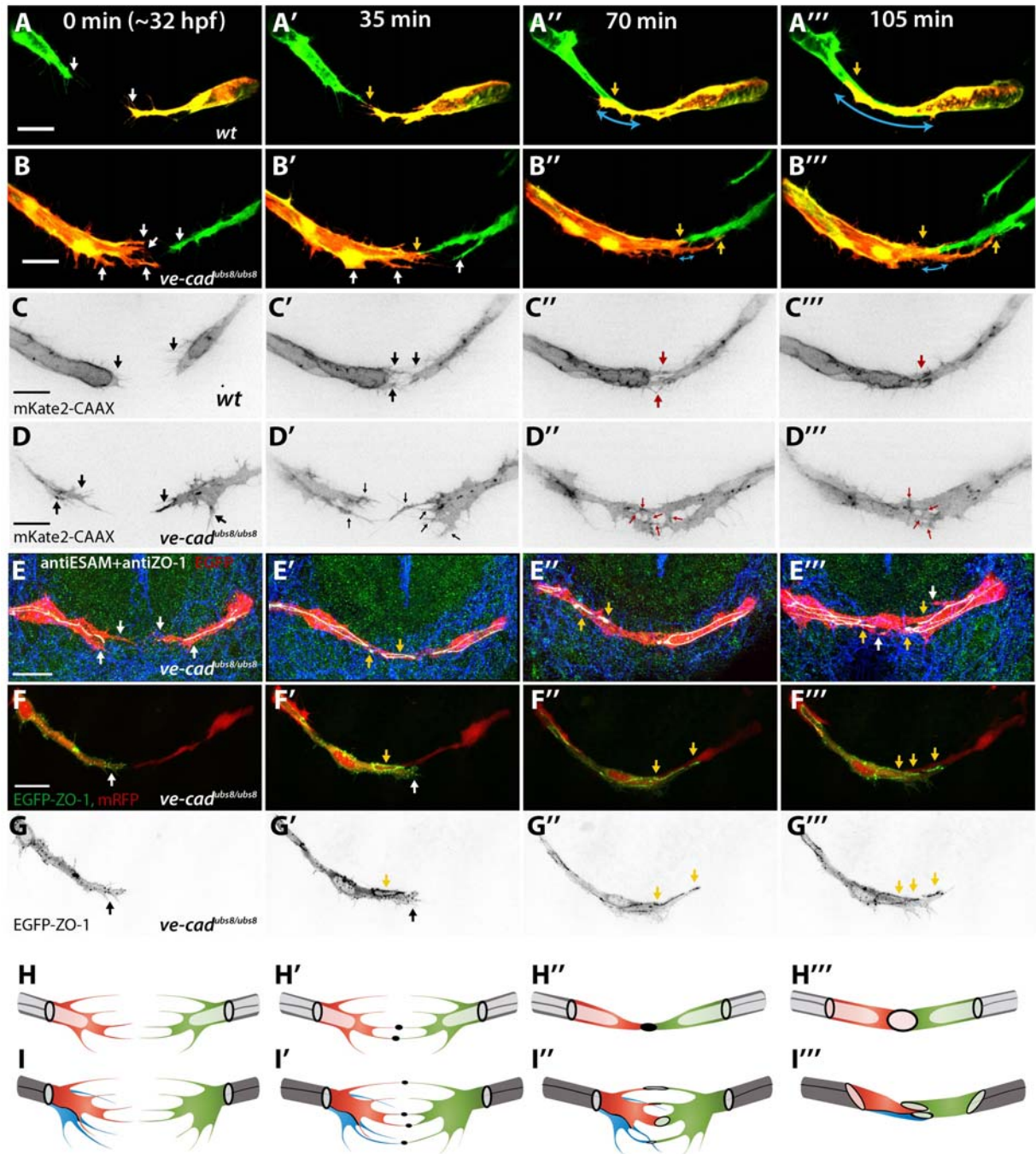
Figure 8
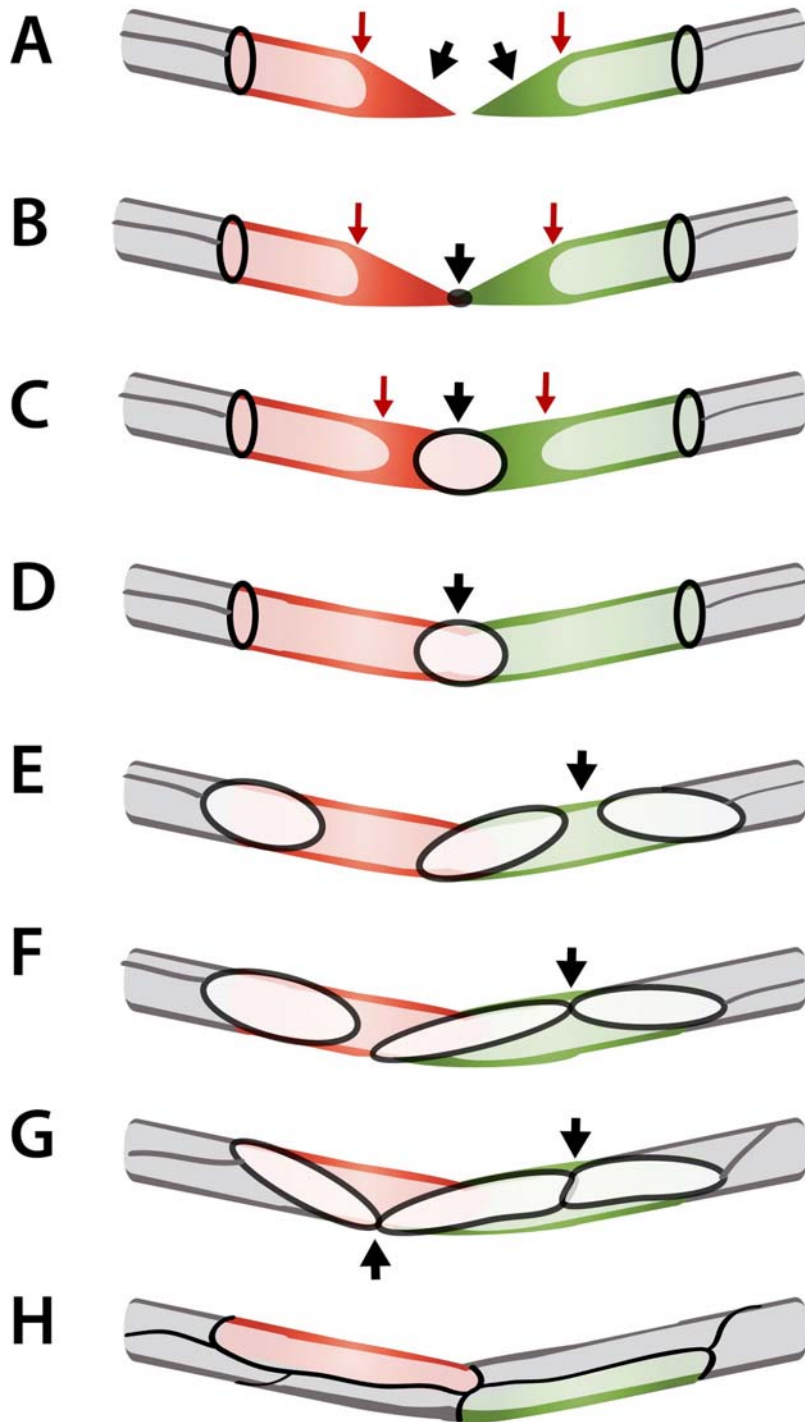
Supplementary figure 1
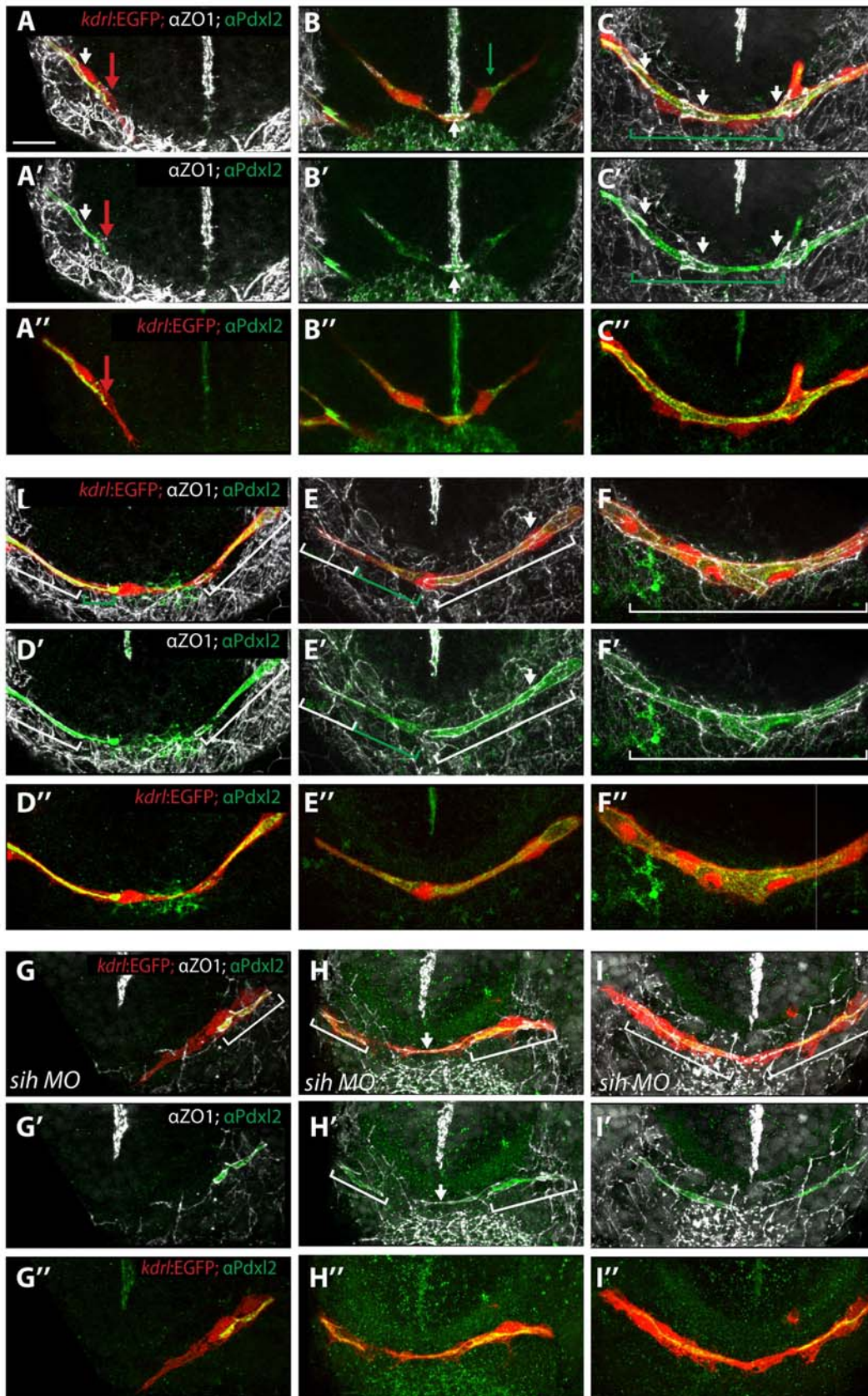
Supplementary figure 2
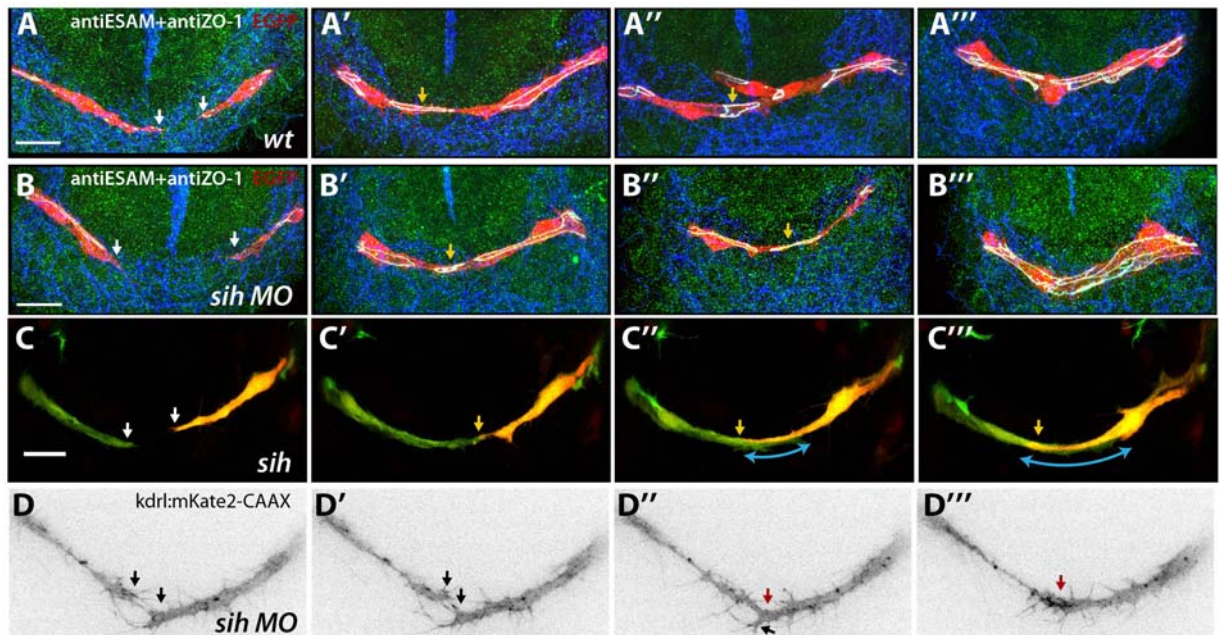
5.7 Cellular rearrangements lead to vessel pruning in developing zebrafish embryos

This chapter describes my contributions to two manuscripts that we prepared in collaboration with the group of Arndt Siekmann (see chapter 5.4) and the group of Holger Gerhardt (see chapter 5.5). I performed all the analyses of cell behavior during vessel regression in the tail and the eye of the zebrafish embryo, respectively.

5.7.1 Pruning leads to remodeling of existing vascular networks

The developing vasculature, initially formed through vasculogenesis and angiogenesis, undergoes further remodeling that transforms the network to its final shape. One process tightly linked to remodeling is vascular pruning, the regression of unnecessary vessels to regulate the density of vascular plexuses. Extensive remodeling of newly formed vascular networks has been observed in the developing mouse retina and in the zebrafish embryo vasculature (see introduction chapter 3.4.2 for more details). However, it is not clear how the pruning of unnecessary vessels is achieved and how it is regulated.

I analyzed vessel regression in developing zebrafish embryos and showed that it involves dynamic cell rearrangements. I described a stepwise process leading to detachment of vessel fragments and remodeling of the network. I showed that the cells involved in pruning do not undergo apoptosis but change positions as the detached vessel segment incorporates into the remaining part of the network.

5.7.2 Pruning in the intersegmental vessels

In the trunk vascular network of the zebrafish, remodeling occurs during intersegmental vessel (ISV) formation. Although all of the ISV sprouts grow out of the dorsal aorta (DA), 50 % of them are subsequently transformed into segmental veins (SV) connected to the posterior cardinal vein (PCV) (see Figure III of the Introduction and chapter 3.2.5). During that process, a new sprout grows out of the PCV and migrates over the dorsal aorta to connect to the closest intersegmental vessel. This new

contact is made to direct the blood flow in this ISV to the vein. Therefore the connection of the ISV to the aorta is no longer needed and has to be removed. I showed that this happens through dynamic cell rearrangements; endothelial cells in this vessel segment detach from the aorta and migrate upwards to incorporate into the ISV they are embedded in. To observe this process I used confocal time lapse imaging of transgenic zebrafish embryos expressing photoconvertible protein in endothelial cells (Tg(*fliep*:GFF)[ubs4]; Tg(UAS:Kaede)[rk8]). By targeted UV illumination I changed the fluorescence of the Kaede protein only in the cells incorporated in the PCV (Fig. 9 A, red arteries, green veins, Movie 17). I observed a venous sprout (A, green arrow) migrating dorsally towards the segmental vessel (red, white arrow) and making a new connection, followed by lumen opening (A'-A''', follow green arrows). Simultaneously, the aortic connection got narrower and its lumen partially collapsed. Finally, the ISV completely detached from the DA and the detaching cells incorporated into the dorsal segment of the newly formed segmental vein (Fig. 9 A-A''', follow the white arrow, Fig. 9 C, model, Movie 17). To further investigate single cell behavior during this process, I used the transgenic line labeling junctional complexes with EGFP (Tg(*fliep*:GFF)[ubs4]; Tg(UAS:mRFP);Tg(UAS:EGFP-ZO-1)[ubs5]). In one particular case, I observed a single cell in an ISV expressing the fusion protein EGFP-ZO-1 and followed its remodeling over time. Initially, the cell was connected to the DA with ring shaped junctions (Fig. 9 B, white arrow, Movie 18). As the venous sprout connected (Fig. 9 B, green arrow), the junctional ring got smaller as the cell started to move up the intersegmental vessel (Fig. 9 B', white arrow). Later, only a small spot of junctions connected the cell to the aorta. Finally, the cell detached completely and migrated up the intersegmental vessel to contribute to its dorsal segment (Fig. 9 B-B''', follow the white arrow, Movie 18).

In 20 time lapse experiments using photoconversion and 5 using the junctional markers, I analyzed cell behavior in 45 segmental veins. I observed that the architecture of the regressing arterial connection can differ depending on the initial cellular arrangement. However, the described steps of regression occur in every case and adapt to the cellular arrangement in particular vessels. In certain cases, the detachment happened not on the surface of the DA, but further up from it making one of the cells stay within the DA as the others migrated up. In this case, I observed more clearly the
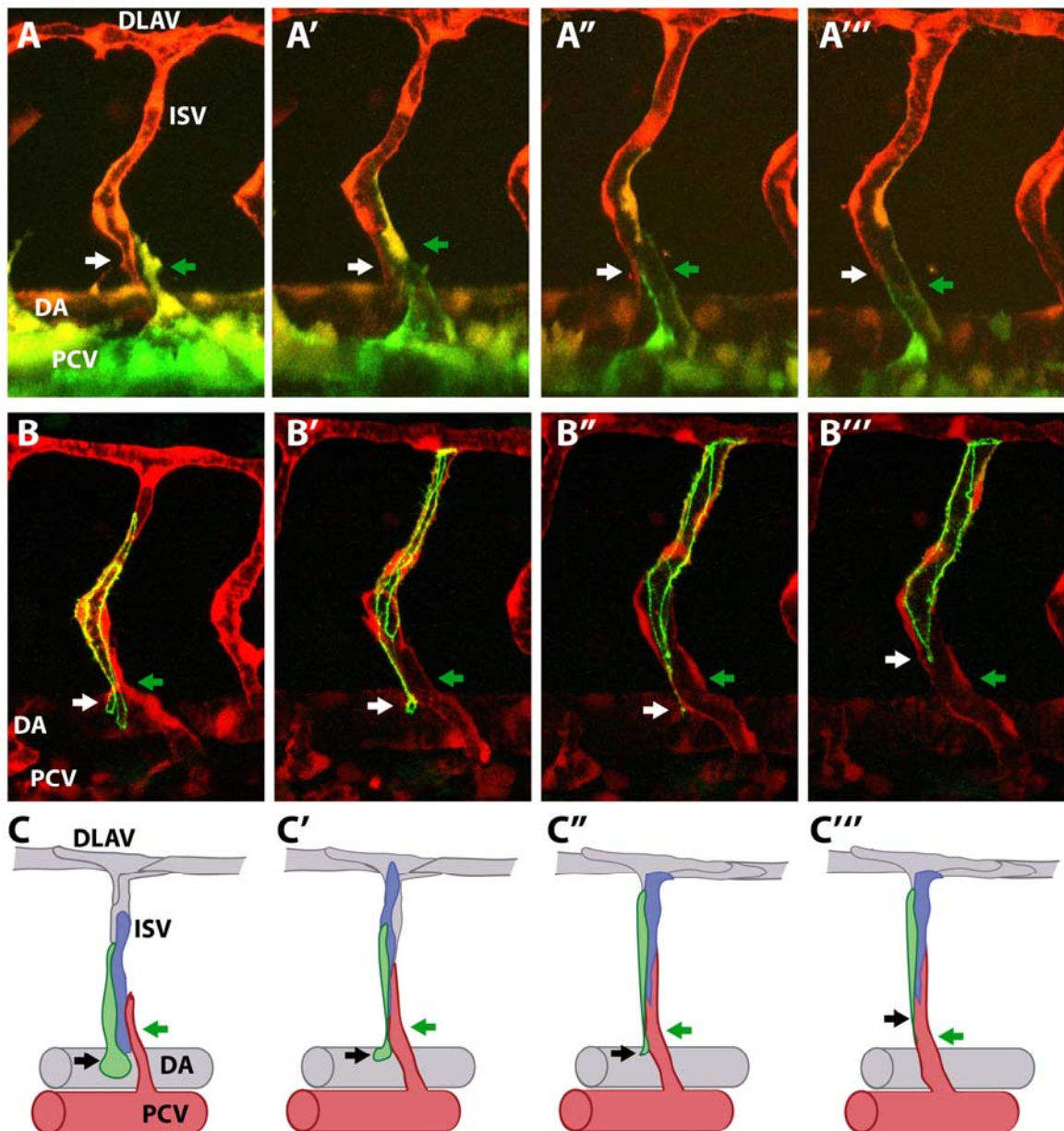
Figure 9. Dynamic cell rearrangements lead to vessel pruning during formation of segmental veins in the zebrafish trunk

A) Still images of the segmental vein formation in a transgenic embryo Tg(*fliep*:GFF)[ubs4]; Tg(UAS:Kaede)[rk8]. Arterial cells are marked in red, venous cells are green. A new venous sprout (A, arrow) grows up toward the segmental vessel (A, white arrow). As the venous sprout establishes a contact with the ISV, the aortic connection is narrowed and eventually detached as the cells move up the ISV to contribute to its dorsal part (A'-A''', white arrows). As a result, a segmental vein is formed half by venous and half by artery derived cells. No connection to the aorta is present at this time (A'''). **B)** Still images of the segmental vein formation in a transgenic embryo Tg(*fliep*:GFF)[ubs4]; Tg(UAS:mRFP);Tg(UAS:EGFP-ZO-1)[ubs5]. A single cell is expressing the EGFP-ZO-1 (green). The cell belongs to the ISV and is anchored in the DA. The connection is visible as a ring-shaped junction (B, white arrow). As the cells move up the ISV, the ring becomes smaller to finally become a spot and detach from the DA (B'-B''', white arrows). **C)** A cellular model of pruning during the segmental vein formation. Arteries are grey, venous cells are red. Green and blue cells are initially connected to the DA. As the venous sprout attaches to the ISV, the arterial cells detach from the DA and move up to contribute to the dorsal part of the ISV.

detachment, which allowed me to generate a cellular model of this process. Initially, the segmental vessel was a multicellular structure with junctional lines all along, marking the cell-cell contacts (Fig. 10 A, arrow, B, model, Movie 19). Two cells were observed in the most ventral part of the ISV (Fig. 10 A, blue and green brackets; B, green and red cell). Upon the venous sprout connection to the ISV, these cells started migrating, one upwards and one downwards, reducing their mutual contact surface. As a result, the
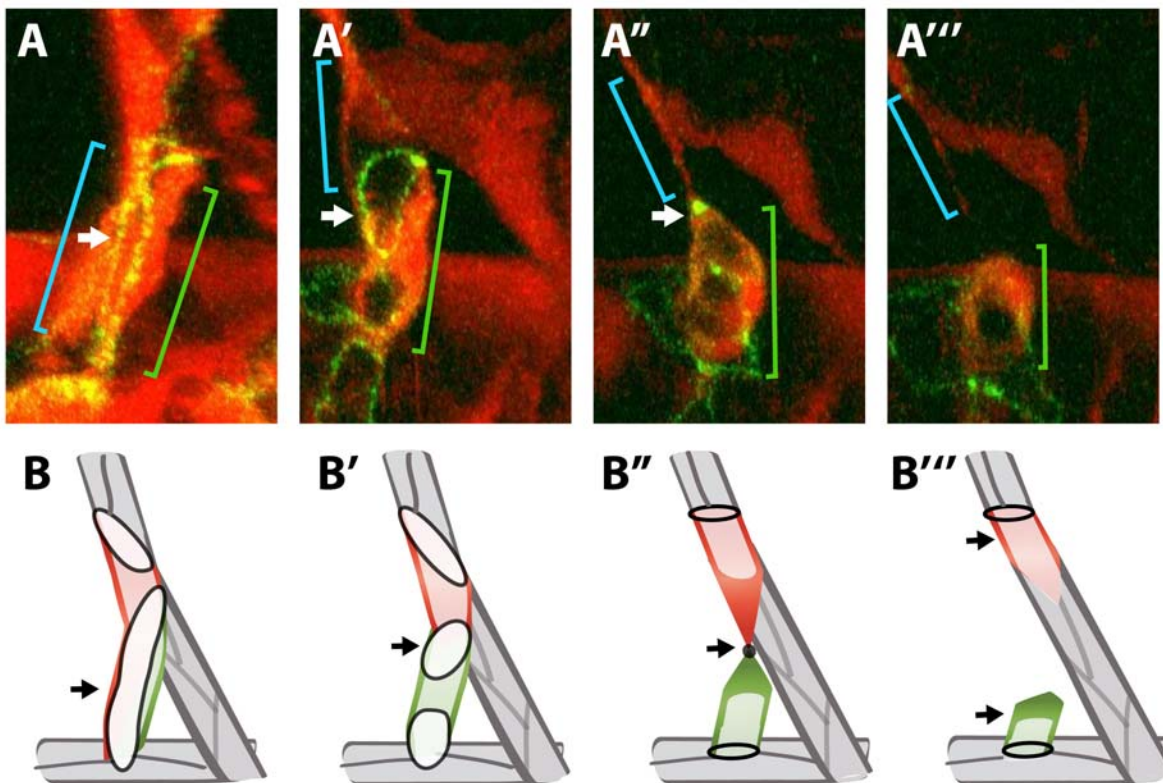
Figure 10. Pruning is a multistep process involving junctional rearrangements similar to reversed fusion

A) Still images of the segmental vein formation in a transgenic embryo Tg(*fliep*:GFF)[ubs4]; Tg(UAS:mRFP);Tg(UAS:EGFP-ZO-1)[ubs5]. Two cells expressing the EGFP-ZO-1 (green) are connected to the aorta in the visible part of the ISV (A, blue and green brackets indicate the cells) and to each other by long lines of juncitons (A, arrow). As the pruning proceeds, the cells move over each other and reduce the contact surface to a small circle, visualized by a junctional ring (A', arrow). The connection diminishes and eventually only narrow cytoplasmic extensions of the cells are connected to each other by a spot of junctions (A'', arrow). Finally the connection is resolved and one cell incorporates in the ISV as the other goes back to the DA (A''', brackets). **B)** A cellular model of vessel pruning steps corresponding to the stills in A. Green and red cell take part in the process, the other cells are grey. Black lines correspond to junctions of the two cells. First the cells are connected by long junctions and make a part of a multicellular tube (B, arrow). During pruning the cells reduce the contact surface and are only connected by a ring shaped junction (B', arrow) that keeps on narrowing to finally become only a spot (B'', arrow). At the end the cells lose connection with each other and incorporate into the ISV and the DA, respectively (B''', arrows).

vessel architecture changed and the two cells were on top of each other, connected by a junctional ring (Fig. 10 A' arrow, B' model). As the cells kept on moving away from each other, the ring narrowed and finally became a junctional spot (Fig. 10 A'' and B'', arrows). Eventually the cells detached and incorporated into the ISV and the DA, respectively (Fig. 10 A''', B''').

5.7.3 Pruning in the head vasculature

The cranial vascular network of zebrafish embryos undergoes extensive remodeling and a number of pruning vessels are observed during the head development. I focused on one of the eye vessels – CrDI (cranial division of the internal carotic artery), which is one of the first vessels to prune in the head. This vessel encircles the optic capsule and ~36 hpf, another vessel – NCA (nasal ciliary artery) – connects to the CrDI forming a Y-shaped vessel junction (see figure VIII of the Introduction). Subsequently, the dorsal part of the CrDI, above the new connection, detaches, leaving the CrDI-NCA vessel in place. I have observed the pruning process at cellular resolution using the live junctional marker VE-cadherin-EGFP in the transgenic line Tg(*fliep*:GFF)[UBS4];Tg(UAS:mRFP);Tg(UAS:VE.cadherinΔC-EGFP)[UBS12] (described before, see Results chapter 5.6). I showed that prior to NCA fusion, the CrDI was a multicellular tube with extracellular lumen and multiple continuous lines of junctions were visible along the vessel length (Fig. 11 A-B, Movie 20). After the NCA fusion, the dorsal part of the CrDI narrowed and the lumen collapsed near the contact point with the NCA (Fig.11 C). Subsequently, the cells making up the dorsal part of the vessel migrated away from the NCA connection and eventually a single cell was left connecting the two vessel parts to each other (Fig.11 D, bracket). The connection kept on narrowing on the NCA side and eventually the cell detached and migrated away to incorporate into the dorsal CrDI, which belonged to a different part of the vascular network at that time. These cellular events were similar to the ones described in the ISVs and I observed the same junctional rearrangements (see model in fig. 11).
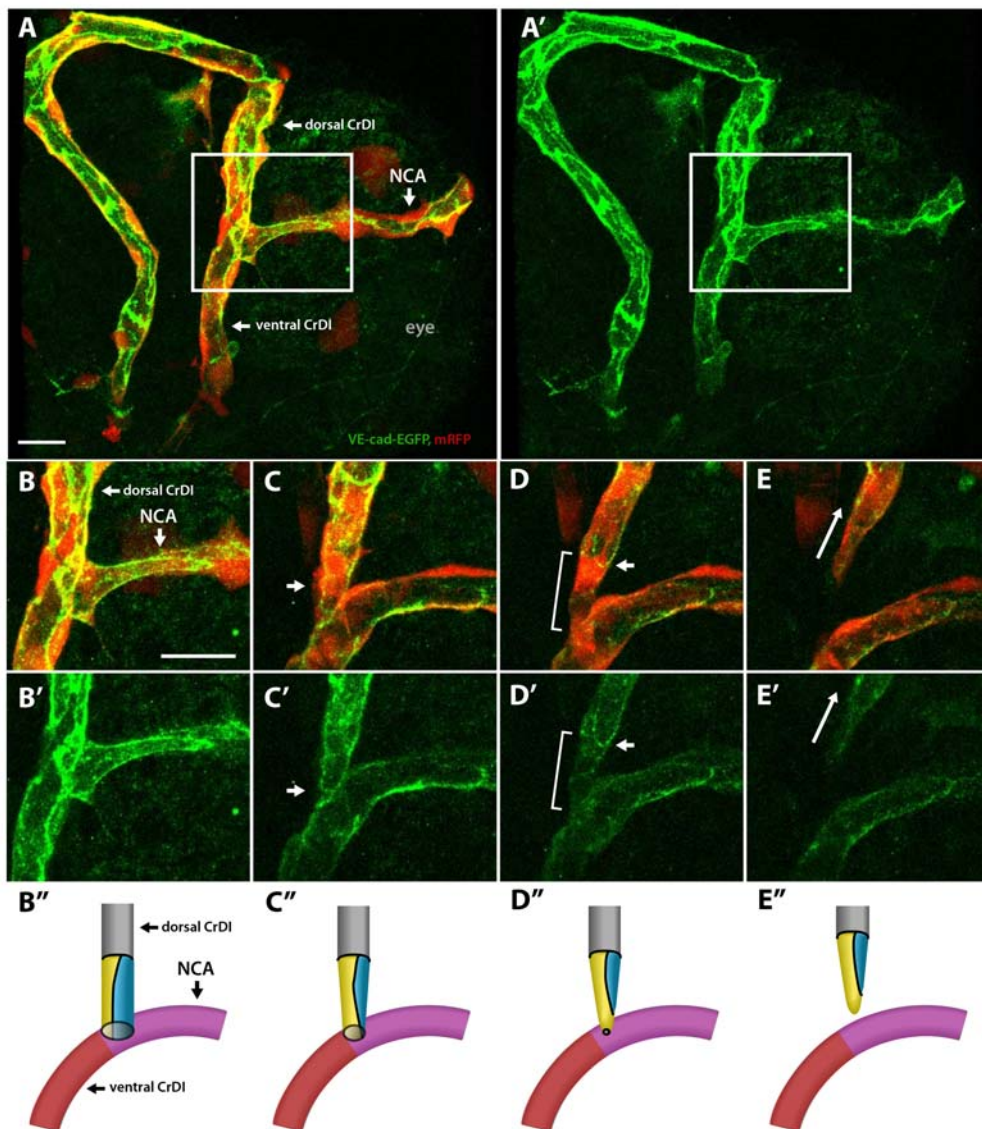
Figure 11. Pruning of the CrDI in the eye involves dynamic cell rearrangements.
A-A') A front view of the head vasculature in the eye region of a transgenic embryo Tg(*fliep*:GFF)^{UBS4};Tg(UAS:mRFP);Tg(UAS:VE.cadherinΔC-EGFP)^{UBS12} at ~36 hpf. Cell cytoplasm is marked in red and junctions in green. The NCA and dorsal and ventral CrDI parts are marked with arrows. **B-E'**) Still images from a time lapse showing the pruning of CrDI from ~36 till ~48 hpf. **B-B'**) The NCA has connected to the CrDI. The connection is a multicellular, lumenized, Y-shaped vessel. Continuous lines of junctions are present along this structure. **C-C'**) The dorsal CrDI narrows and the blood flow stops in this vessel part (arrow). The lumen collapses near the contact point with the NCA. **D-D'**) The cells in the dorsal CrDI migrate upwards and gradually detach. As a result only one cell is still connecting the dorsal CrDI to the ventral vessel (bracket). A junctional ring is visible connecting the cell to the dorsal CrDI (arrow). The connection to the ventral CrDI is not visible as it forms behind the vessel. **E-E'**) The dorsal CrDI detaches and migrates upwards (arrow) leaving the other part of the vessel below. **B''-E''**) A cellular model of CrDI pruning. The NCA is marked in purple, the ventral CrDI in red. In the dorsal CrDI single cells involved in the connection are highlighted (yellow and blue cells). The relevant junctional contacts are black. Initially, two cells of the dorsal CrDI are connected to the NCA (B''). As the pruning proceeds, the cells gradually migrate upwards (C''). The blue cell moves first and the connection at this point is maintained by a single (yellow) cell. This cell is connected to the dorsal and ventral CrDI by junctional rings (D''). This connection is subsequently resolved on the NCA side and the yellow cell detaches and migrates up to incorporate in the dorsal vessel (E'').

168

5.7.4 Pruning involves dynamic cell rearrangements leading to vessel regression

My findings show that pruning, during the formation of segmental veins and the cranial vessels in the zebrafish, is a multistep process involving dynamic cell rearrangements. I described the process at single cell resolution and described the junctional remodeling underlying vessel detachment. From a junctional perspective, the process resembles "reversed" fusion described by us previously (see Results Fig. 8). Instead of making a new connection, the cells resolve the contact in a stepwise fashion, involving formation of a junctional ring and later a junctional spot. It was previously proposed (Cheng et al., 2012) that pruning involves apoptosis of the unnecessary vessel fragments. We did not observed cell death, except of single cases (~5 % of time lapses) where a cell did not manage to incorporate in any of the existing vessels and died. Similar observations were made in the midbrain vasculature of the zebrafish where remodeling of the vascular network involved cell migration and detachment of vessel segments (Chen et al., 2012).

Currently a number of studies focus on the molecular mechanisms controlling blood vessel pruning. My findings are embedded in two collaboration projects that deal with this question. These papers are in preparation (collaboration with Holger Gerhardt) or submitted for publication (collaboration with Arndt Siekmann) and abstracts are presented in the "Contribution to Publications" section of this thesis (chapters 5.4 and 5.5).

6 Discussion

6.1 Blood vessel fusion is a multistep process crucial for angiogenic network formation

The development of tubular organs through branching morphogenesis involves sprouts that grow out of existing branches and connect in order to form a functional network with a continuous lumen. In vascular development, this last process, also called vessel fusion or anastomosis, is crucial for establishing the initial capillary network that transports blood cells in the growing embryos. Vascular sprouts have special characteristics; each sprout makes a multicellular structure led by a single tip cell, which is morphologically and genetically different from the following cells in the sprout, called the stalk cells (Gerhardt et al., 2003). The tip cells at the angiogenic sprouts interact with each other in the fusion process and mediate new contact formation, eventually leading to the opening of a new vessel. The process of vessel fusion involves a number of steps and specific cellular mechanisms. These mechanisms have not been previously described; the Affolter lab has therefore initiated a live imaging approach based on similar analyses performed in *Drosophila* during tracheal development.

In this study I performed detailed analyses of the fusion steps in cranial vessels of the developing zebrafish embryo. Using novel transgenic tools and high resolution live imaging, I proposed a multistep model of vessel fusion and showed that these steps are conserved in various vascular beds. I showed that in several studied cranial vessels, the initial fusion steps are the same and involve *de novo* deposition of junctional proteins, ZO-1 and VE-cadherin, in the form of a junctional spot that elaborates into a ring, accompanied by *de novo* apical membrane insertion. Subsequent lumen formation in the newly formed vessel takes place through luminal cell membrane invagination and fusion of apical membranes leading to lumen opening. In this process, the tip cells become unicellular/seamless tubes with a transcellular lumen. Furthermore I showed that vessels initially lumenized by this process subsequently undergo dynamic cellular rearrangements that lead to the transformation of the unicellular tubes into multicellular ones. This involves cell splitting which is a novel cellular mechanism that, to our knowledge, has not been described before. Additionally, I analyzed the fusion process in

VE-cadherin deficient embryos and showed that this adhesion molecule is necessary for formation of a single contact surface between the fusing vessel sprouts.

6.2 Studying head vessels brings new insights into the mechanisms of vascular fusion

6.2.1 The pattern and cellular architecture of cranial vessels differs from the ISVs

Due to its accessibility for live imaging, zebrafish has emerged as an excellent model to study the dynamics of vascular development. The first analyses of angiogenic sprouting in zebrafish showed that different regions in the embryo can be used to study this process, such as the head and in the tail/trunk of the embryo (Lawson and Weinstein, 2002). The intersegmental vessels (ISVs) in the fish form a very organized and repetitive pattern allowing simultaneous observation of multiple vessels and are easily accessible for confocal imaging. Many angiogenic events were observed in the head of the fish (Isogai et al., 2001; Lawson and Weinstein, 2002), but this vascular network is much more complex and the vessels are more unique in their shape and position. Due to tissue thickness, many analyses, including *in situ* hybridization and *in vivo* imaging, are much more challenging in the head than in the tail. Therefore, the majority of zebrafish vascular studies have been performed in the tail/trunk region of the embryo, until recently neglecting the cranial vascular network (Isogai et al., 2003; Jin et al., 2005; Kamei et al., 2006; Siekmann and Lawson, 2007).

In the Affolter lab, we also began to investigate the fusion process of angiogenic sprouts in the ISVs (Blum et al., 2008; Herwig et al., 2011). Our analyses of ISVs revealed the initial steps of this process and two possible mechanisms of lumen formation, i.e. cell rearrangements and transcellular lumen formation, described in the introduction (chapter 3.3.5) and discussed later on.

However, we have realized that the ISVs are in a way unique in their structure and in the environment that influences their formation. Even though individual ISVs are almost identical to each other, they are not very similar to other vessels in the embryo. Therefore it became necessary to study other types of vascular connections to verify whether the mechanisms described for ISVs can be applied to other types of vessels. In

general, the architecture of cranial vessels appears much more complex than in the body and the tail. However, I showed that single angiogenic sprouts in the head have a simpler cellular architecture. The shape of the ISV sprouts resembles a T connection, meaning that each sprout tip has to eventually connect to two neighboring T-shaped sprouts (see fig III of Introduction). This configuration is unique to the ISVs and is not observed in other vessels in the embryo. On contrary, most of the cranial vessels arising through angiogenesis form I-shaped sprouts, with a single migrating extension at the tip, that connect to other I-shaped sprouts making a new vessel in the shape of a straight or slightly bent tube (see model in Fig. 8 of Results), or connect to an existing tubular vessel making a vascular junction resembling a Y-shaped structure.

Therefore when it comes to single fusion events, it is much easier to use the cranial sprouts to analyze and interpret cellular behaviors, since only one fusion event takes place at the time and less cells are involved in this activity.

6.2.2 Cranial vessels, but not ISVs, form in the presence of stable blood pressure, which can influence vessel development

The ISVs form very early in the embryo development, with the first sprouts arising at ~18 hpf and the last ones finishing fusion at ~28 hpf. The onset of heart beat and circulation is observed at ~24-26 hpf and is initially quite weak, with low plasma pressure and only individual circulating blood cells (Isogai et al., 2001; Stainier et al., 1996). This means that the fusion process in the ISVs happens with no or very little influence from the intravascular pressure (Herwig et al., 2011), whereas most of the cranial vessels that arise at later stages fuse when the blood flow and blood pressure are fully established.

It has been shown that the shear stress produced by the plasma flow influences endothelial gene expression (Bussmann et al., 2011; Nicoli et al., 2010) and significant differences have been shown in angiogenic network formation in flow-subjected vessels. Bussmann et al have shown that chemokine signaling, dependent on flow, influences formation of central arteries (CtAs) in the hindbrain (formed between 30 and 60 hpf) but does not affect the earlier formed ISVs (see Introduction chapter 3.5.1 for more details).

Certain vessels in the embryo only form in the presence of flow, e.g. the aortic arches (AA5 and AA6) in the fish gills. Nicoli and colleagues (Nicoli et al., 2010) showed

that mechano-sensitive zinc finger transcription factor Kruppel-like factor 2a (Klf2a) (Parmar et al., 2006) is necessary for flow dependent activation of VEGF signaling that induces angiogenic sprouting of the AAs. The signal transduction is mediated by a microRNA mir126.

Accordingly, the blood flow activated *alk1* (*activin A receptor type II-like 1*) participates in the regulation of artery diameter. Its function is to narrow the arteries in response to high hemodynamic forces. Zebrafish embryos mutant for this gene show dilated arteries leading to formation of abnormal arterio-venous shunts – malformations linked with a number of human diseases (Corti et al., 2011).

All previously mentioned examples show the importance of flow in vascular development. Therefore we asked whether blood pressure plays a role also in the early steps of vascular network formation, i.e. during blood vessel fusion and first lumen formation.

Parallel analyses of the ISVs and the cranial vessels have provided a great system to compare between fusion in the presence or absence of flow and enabled me to show at which step of the fusion process flow is important.

6.2.3 Numerous fusion events in the cranial vasculature can be used to study the cellular mechanism of anastomosis

The first studies on ISVs fusion were published by our lab (Blum et al., 2008; Herwig et al., 2011) and are summarized in the introduction chapter 3.3.5. They led to a description of the mechanism of new contact formation between the fusing vascular sprouts and two possible mechanisms of subsequent lumen formation that will be discussed in detail below.

To see whether the fusion process takes place in a similar way in other vessel types, I looked in more detail at the head vasculature, where a very complex network of tubes forms within the first days of embryonic development. When I started the project, very little information was available regarding the formation of head vessels in the fish. Isogai and colleagues (Isogai et al., 2001) presented an extremely detailed map of the vascular network based on angiography experiments at different stages. However, only perfused vessels can be analyzed using this method, meaning that fusion and lumen

formation have already occurred. Therefore this atlas was not enough to provide information on the timing and dynamics of vessel sprouting and new contact formation. To be able to target single fusion events in the head I needed to first get an overview of the vascular development using transgenic markers labeling endothelial cells. Multiple live imaging experiments of different stages and angles enabled me to identify a number of fusion events within the first 3 days of the embryo development. After identifying the precise time and location of the fusion between vessels, I was able to target specific fusion events in a reproducible fashion. This was a crucial step for using the highest possible resolution of confocal imaging, with regards to both time and image quality. Due to tissue thickness and curvature of the head these experiments required very precise embryo micromanipulation and high-tech microscope equipment.

I have identified numerous vessel fusion events and selected 3 of them for detailed analyses. The criteria I used were: 1) accessibility, 2) embryo age at the fusion time and 3) the shape of the vessel. I chose the palatocerebral artery (PLA) as the main focus of my experiments, because it was one of the first vessels to fuse after the establishment of strong blood flow in the embryo; therefore I was certain that this vessel always forms under the influence of plasma pressure in the neighboring branches. Second, the vessel arises early enough that its formation is finished by 2 day-stage. This is important because many zebrafish mutants show progress of the phenotype severity with age, meaning that more defects, not necessarily specific ones, are seen in older embryos. This is especially true for mutations affecting the vasculature that often result in heart malformations and reduced or no blood flow. A number of angiogenic sprouts simply do not form in the absence of flow, so it becomes impossible to use them to look at fusion defects (Bussmann et al., 2011; Nicoli et al., 2010). The PLA still forms in the absence of blood flow, which will be discussed later. Additionally, the PLA is made by two single sprouts connecting and fusing with each other, containing only 3-4 cells each, which facilitates the detailed cell rearrangement analyses.

As a second fusion event, I chose the posterior cerebral vein (PCeV), allowing me to look at an older stage embryo (2.5-3.5 dpf) and a larger diameter vessel. It was very useful for analyses of wild type fusion in a different place and time then the PLA, which was necessary to generalize the obtained cellular fusion model. Unfortunately, this

vessel does not form correctly in the absence of flow; therefore it was not used for mutant analyses.

I chose the communicating vein (CMV) to look at fusion of a new sprout to an existing vessel to observe whether the model I described for the fusion of two equal sprouts can be adapted to this different topological arrangement. In this case, the morphology of the vessel is more flexible. At 48 hpf there are two CMV vessels present, connecting left and right CrDIs (cranial division of the internal carotid arteries) to the PLA, forming the PLA junction (PLAJ, see figure 1 of Results). The sprouting time is quite variable and it does not necessarily occur at the same time on both sides. Therefore in many cases only one of the CMV vessels can be seen in the time lapse analyses. The developmental flexibility of certain branches have been observed before (Bussmann et al., 2011) and seems to be a common feature of the brain vessels at later stages of development, when the network becomes very complex. Even though the main patterns are conserved, the architecture of single capillaries is not identical from embryo to embryo.

6.3 The initial steps of vessel fusion in the head are the same as in the ISVs and resemble these seen in the fly trachea

We have shown that in the cranial vessels and the ISVs the initial steps of the fusion process are conserved. The process starts with sprouting of endothelial cells from an existing vessel, driven by directional migration of selected tip cells. High filopodia activity of the tip cells mediates recognition of the fusing sprouts and first contact formation, which involves *de novo* deposition of junctional material at the new contact site and subsequent deposition of apical membrane components within the newly forming junctional ring that encircles the contact surface between the tip cells. This process resembles fusion of tracheal branches in *Drosophila melanogaster*, which will be discussed in detail in the following chapter.

6.3.1 Initiation of the fusion process

The fusion of two tubular branches has been studied in great detail in the *Drosophila* tracheal system, where epithelial cells form tubes that deliver air to places throughout the fly embryo and larvae. In the fusion process of dorsal branches (DB), two tubular branches sprout towards each other and connect to make a continuous, lumenized tube. Specialized cells, called fusion cells, lead the sprouting branches and play a key role in the fusion process (Samakovlis et al., 1996a), similarly to the vascular tip cells. Fusion cells express a number of specific markers, e.g. *escargot*; its expression is necessary for new contacts to form, as it induces some of the other fusion proteins and inhibits other cell type markers. Overexpression of *escargot* results in ectopic fusion points (Samakovlis et al., 1996b).

Fusion genes have not been described in the vasculature so far, although a homologue of *escargot* is known in mammals (*Snail*, Nieto et al., 1992). Tip cell specific genes in the angiogenic sprouts have not been shown so far to directly mediate the fusion process, but were shown to be crucial for sprouting behavior (Gerhardt et al., 2003; Siekmann and Lawson, 2007), see introduction chapter 3.3.5.2 for details.

6.3.2 Cadherins localize to the new contact site in the first step of fusion process

It was shown in *Drosophila* that the adherens protein E-cadherin is essential for epithelial cell rearrangements and proper formation of epithelial tubes (Uemura et al., 1996). In the trachea, E-cadherin accumulates at the new contact site as two fusion cells contact each other, forming a spot and later a ring-shaped junction. Inside the cell, E-cadherin is connected to cytoplasmic F-actin, which, through the plakin Shot, connects it to microtubules. This leads to the formation of a track within the cell, which is necessary for the fusion to proceed and for subsequent lumen formation (Lee et al., 2003; Lee and Kolodziej, 2002). Escargot was shown to act upstream of E-cadherin (Tanaka-Matakatsu et al., 1996). In these experiments *escargot* mutant tip cells failed to adhere to each other and instead continued filopodial activity, meaning that E-cadherin signaling is crucial for cell-cell recognition.

Knowing the importance of junctional proteins during fusion in the *Drosophila* tracheal system, we have decided to follow these proteins during the fusion process in

the vasculature of zebrafish. Using antibody staining, our group has previously shown that junctional proteins, VE-cadherin (a member of adherens junctions) and ZO-1 (a protein associated with tight and adherens junctions), are present at the new contact site of two angiogenic sprouts (Blum et al., 2008). Similarly to E-cadherin in epithelial tracheal cells of *Drosophila*, endothelial cells deposited new junctional material at the contact site, first visible as a small spot that later elaborated into a ring-shaped junction as the cell contact surface expanded. We wanted to observe the fusion dynamically, therefore we generated an *in vivo* junctional marker - EGFP-ZO-1 fusion protein- that enabled time lapse imaging of the junctional contact formation, confirming the stepwise character of this process and showing its dynamics (Herwig et al., 2011). Additionally, using antibodies against Podocalyxin-like-2 (Pdxl2), which is a member of CD34-sialomucins known to localize to the apical membrane in polarized endothelial cells, we showed *de novo* polarization of the membrane within the junctional ring at the new contact site. This again resembles the tracheal fusion, where apical determinants, such as Disc Lost (Dlt), Crumbs, a-PKC and Bazooka (Par3) are inserted at the new contact site of two fusion cells (Gervais et al., 2012; Lee and Kolodziej, 2002).

My results showed that the initial steps of fusion process just described for the ISVs also occur in the cranial vessels of the zebrafish embryo. Regardless of the vessel shape, position and the developmental stage of the embryo I observed that the initial contact forms between the leading tip cells of the sprouts and involves *de novo* junctional and apical protein deposition. This confirms the general character of the mechanism proposed in our previous studies. Additionally, I used a new live junctional marker – VE-cadherin-EGFP - to confirm the results obtained with the EGFP-ZO-1 transgene. This construct was made using a truncated version of zebrafish VE-cadherin, where the cytoplasmic domain was replaced with EGFP. This allowed to preserve the adhesion properties of this molecule and to prevent engagement in intracellular signaling which could cause an overexpression phenotype. All the results I obtained with the live markers were confirmed by antibody staining of the corresponding developmental stages to eliminate the risk of transgene specific phenotypes.

6.4 Lumen formation in the cranial vasculature

After contact formation between two angiogenic sprouts, the lumen has to open to allow blood flow through the new vessel. My work in the cranial vasculature, together with previous work in the lab on the ISVs, has revealed a general mechanism of lumen formation in the developing zebrafish vasculature. We have previously described two possible mechanisms of lumen formation in the developing ISVs: 1) transcellular lumen formation resulting in unicellular tubes, and 2) extracellular lumen formation through cell rearrangements, resulting in multicellular tubes. In the ISVs, these mechanisms occurred with approximately 50 % frequency (see introduction chapter 3.3.5.9 for details). To be able to generalize the model of blood vessel fusion I analyzed multiple head vessels to see whether both of these mechanisms are present there and what the frequency of their occurrence is.

My characterization of the cranial vessels showed that they predominantly follow the first mechanism – transcellular lumen formation – and I proved that this occurs through luminal cell membrane invagination. I described this process in great detail (discussed in chapter 6.4.2-3). Additionally, I showed that this initial conformation is transient and the cells within the lumenized vessel subsequently engage in dynamic rearrangements, transforming the tube into a multicellular vessel. This involves a novel mechanism of cell splitting (discussed in chapter 6.5).

6.4.1 Angiogenic sprouts in the cranial vasculature are lumenized

I analyzed a number of cranial vessels of different shapes and position within the network and could see that all the angiogenic sprouts in the head are lumenized almost to the very tip of the sprout. In the cranial vessels, branching usually starts with a single cell that has been embedded in an existing vessel, extending filopodia and moving out of the multicellular tube. This new tip cell is followed by other cells that eventually form a multicellular (usually 3-6 cells) lumenized branch. The lumen extends from the "mother" vessel, between the cells of the new branch and into the tip cell, almost to the very end of the cell, but does not perfuse. This means that an angiogenic sprout is a multicellular, lumenized, but blunt-ended tube. I have observed this cellular

conformation in all analyzed sprouts using junctional proteins as markers for the cell borders and single cell labeling.

6.4.2 In the cranial vasculature lumen in newly connected tip cells forms predominantly through membrane invagination resulting in unicellular tubes; a process highly dependent on the blood plasma pressure

In general, sprouts in the cranial vasculature are lumenized because the blood plasma pressure in the neighboring vessels is strong enough to push into the growing branch. This is different from the situation in ISVs where sprouts are always non-lumenized. We have observed that the mechanism of lumen formation is highly influenced by the presence of blood plasma in the sprouts and the surrounding vessels.

My analyses of multiple movies of the fusion process in the PLA, PCeV and the CMV revealed that the lumen formation in the cranial vasculature occurs predominantly through transcellular lumen formation via membrane invagination, in a very reproducible manner. This could be due to the fact that the blood pressure is much stronger in older embryos and could be additionally aided by the head proximity to the heart. This means that the fusing vessels are exposed to strong plasma pressure throughout contact formation and points to a direct role of pressure in the process of lumen formation. To verify whether a transcellular lumen could form in the absence of blood flow, I analyzed embryos with knocked-down cardiac troponin T2 (*tnnt2*), which resulted in non-functional heart smooth muscles and thus, in the lack of blood flow. In these embryos, no transcellular lumen formed at the fusion site. No membrane invagination was observed in the PLA vessel, neither with live imaging nor with antibody staining of Podocalyxin 2. The results obtained in this experiment correspond to our previous observations of the ISVs (Herwig et al., 2011).

In previous studies we showed that blood pressure is necessary for transcellular lumen formation through membrane invagination. I also showed that lumen in the newly fused head vessels forms almost only through this process. The high influence of plasma pressure can therefore explain the mixed character of lumen formation in the ISVs. As mentioned before, the ISVs form as a part of the axial vasculature and arise very early in development. This means that during lumen formation they are subjected to

mixed strength of blood pressure due to lower heart beat rates at this stage and the rather long distance to the heart. Therefore, we propose that the ISVs undergo cell rearrangements in the absence of plasma flow in the direct proximity of the fusing tip cells, whereas they form transcellular lumens if the plasma pressure is more prominent in the region of new contact formation. Analogously, the cranial vessels that fuse in the presence of constant and stable blood pressure only follow the second mechanism. In only single cases I observed that one of the sprouts underwent cell rearrangements right before or almost simultaneously with the lumen formation (see chapter 6.7 for details).

6.4.3 Membrane invagination during lumen formation is a dynamic process involving growth of the apical membrane compartment and changes in cell membrane conformation.

We have previously proposed that the transcellular lumen in the ISVs could form through cell membrane invagination (Herwig et al., 2011). However, at the time it was not possible to directly visualize this process due to the lack of transgenic tools.

In the ISVs only 50 % of the observed vessels formed transcellular lumens, making them an inconvenient system to study this mechanism due to lower probability of filming the right event. Therefore, the cranial vessels, which undergo transcellular lumen formation, enabled me to visualize the process in greater detail and provided *in vivo* proof for the previously published model.

In most of the previously described experiments we used cytoplasmic expression of fluorescent proteins to mark the bodies of endothelial cells. This proved to be very useful for analyses of cell and vessel shapes and, together with the junctional live markers, enabled us to describe the cellular behaviors and architecture of fusing vessels. In these transgenic embryos the lumen of vessels is visible as dark space encircled by the fluorescent cell bodies. This is due to the fact that the endothelial cells that contribute to the lumenized vessels are very thin (Wang et al., 2010) and therefore the fluorescent signal becomes too weak to be seen in the middle part of a lumenized vessel. In this way we can visualize where the lumen is open, but it is difficult to see how it actually forms.

Discussion

Since we expected that membrane movements must be involved in the formation of transcellular lumen, I have generated new transgenic tools to specifically visualize the cell membrane. I used BAC recombineering, which is a novel method of generating constructs containing large fragments of genomic DNA (Warming et al., 2005). I have inserted membrane-tagged mKate2 red fluorescent protein in a BAC containing the *kdrl* gene (*vegfr2, flk1*) to obtain endothelial cell specific expression (see Materials and Methods 4.3.1 for details). The new line enabled me to visualize the cell membrane of endothelial cells taking part in the fusion process and lumen formation. It has been proposed before that transcellular lumen forms in the ISVs of developing zebrafish embryos through coalescence of large vacuoles that form within the cell and eventually connect with the outer membrane to open the lumen to the flow (Kamei et al., 2006). This hypothesis has been challenged by our discovery of long multicellular segments in these vessels, suggesting extracellular lumen formation (Blum et al., 2008) and analyses with microangiography that suggested rather small vacuoles contribution to lumen formation (Wang et al., 2010). Finally we showed 2 distinct mechanisms of lumen formation, but did not address the vacuole contribution to this process (Herwig et al., 2011).

High resolution imaging of the membrane marker allowed me to differentiate between the leading basal membrane of the tip cell in the proximal part of the sprout, and the apical/luminal membrane in the distal part, within the sprout. Upon blood plasma entering in the new branch, the lumen was inflated and the fluorescence was enriched at the luminal membrane, visible as an oval shaped engulfment within the sprout. The luminal membrane was easily distinguishable from the basal membrane at the leading end of the cell, which produced multiple filopodia extensions (see Fig. 2 C-D of Results). To be sure that what I saw was the membrane invagination due to lumen opening and not a large vacuole, I performed microangiography with 500 kDa FITC-dextran. The dye injected into the heart of the embryo fills all the open vessels. I observed that the membrane invagination was filled with the dextran to the very tip and adjacent to the membrane staining, showing that no large vacuoles were present at this stage. As the fusion process proceeded, I observed a dynamic progress in the membrane invagination towards the new contact site, immediately followed by dextran filling of the new luminal

compartments. It is important to notice, that apical membrane invagination happened simultaneously with new contact formation between the tip cells, which involved new apical membrane deposition. This means that at this stage the tip cells were bi-polar and had two apical membrane compartments, which was a transient state resolved in the next steps of lumen formation.

The membrane invagination was present in both PLA sprouts and proceeded until the two leading luminal membranes were found in close proximity, opposite to each other, which could happen at the contact site of two cells or within one of the cells. This shows the plasticity and variability of the system that can adapt to various cellular shapes and continue the process in many different arrangements. When the two apical membranes of one cell were found in close proximity, they merged and fused together to finally open in a different arrangement, perpendicular to the previous one (Figure IX).
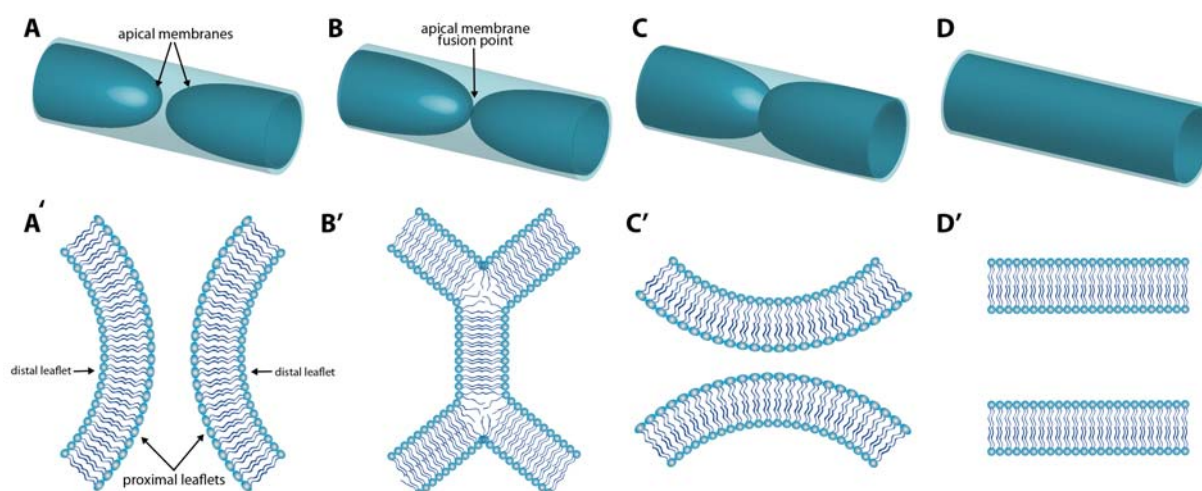
Figure IX Apical membrane fusion during transcellular lumen formation through membrane invagination
A-D) A model of a cell undergoing transcellular lumen formation through membrane invagination. Basal membrane is light blue, apical membranes are dark blue. A) The cell in a biapical state. Both apical membranes invaginate towards the middle of the cell, until they are found in a close proximity. B) The apical membranes contact, possibly undergoing membrane fusion, and later detach from each other in a perpendicular conformation (C) to allow opening of the transcellular lumen (D).
A'-D') A hypothetical model of cell membrane behavior during apical membrane fusion (Based on Chernomordik et al. 2008). Two parallel cell membranes (A') come close together and fuse forming an intermediate "hemifusion stalk", where the proximal membrane leaflets are fused and the distal are not (B'). The membranes detach in a conformation perpendicular to the initial one (C') and move away from each other as the lumen opens (D').

Discussion

This process was very fast and smooth, as observed in high time resolution live imaging using a spinning disc microscope (Movie 13), and eventually resulted in lumen perfusion, as visualized by dextran filling (Movie 4). Fusion of two separate membranes is a well-known process described in most details for vesicle formation. It is a part of the process leading to detachment of newly formed vesicles and connecting the vesicles to other membrane compartments, in order to release their content. In this case, membrane rearrangements are mediated by specific proteins that can influence membrane shape. It was also shown that the bend membrane shape that promotes membrane fusion can be achieved through changes of lipid composition within the membrane, as certain lipid types naturally arrange in a bend shape (reviewed in Chernomordik and Kozlov, 2008). It would be interesting to see whether any of the known membrane associated proteins are enriched in the endothelial cells or whether the lipid composition is altered during the cellular rearrangements.

The molecular mechanisms of transcellular lumen formation through membrane invagination in the vasculature are not known so far. It was initially proposed that intracellular vacuoles are involved and molecular factors such as cdc42 and moesin 1 were suggested to take part in vacuole formation and delivery to the apical membrane (Kamei et al., 2006; Wang et al., 2010). EM images of developing mouse aorta lumen showed that rounded structures of the cell membrane can be seen within endothelial cells (Strilic et al., 2009). These were, however, not vacuoles but membrane folds that in single sections looked like intracellular compartments. Therefore it is important to take into consideration the three dimensional character of blood vessels.

Using the cell membrane marker, I did not observe large vacuoles taking part in the process of lumen formation, but I did see small, vesicle-like structures, highlighted by the membrane marker, travelling along the cell body in the proximity of luminal cell membrane expansion. It is known from experiments in the *Drosophila* tracheal system that specific vesicle structures are involved in membrane fusion during transcellular lumen formation in the fusion cell. When two dorsal branches (DB) of the tracheal system fuse, single fusion cells are present at the leading edge of the sprouts and transform from sphere-shaped into toroid (doughnut)-shaped when the lumens open (Figure X). During this process, the fusion cells also exist in a transient, bi-apical state

184

and through the invagination of the "old" apical membrane towards the "new" one, they eventually lumenize (see Fig. VII of Introduction). This process involves membrane fusion mediated by exocytosis with a cytoplasmic microtubule tract that guides vesicles within the cells (Samakovlis et al., 1996b). Kakihara and colleagues (Kakihara et al., 2008) showed that a small GTP-ase (Arf-like 3) associated with Sec5 positive vesicles and microtubules was involved in the formation of an exocyst complex that mediated membrane fusion. This complex is also known to be involved in membrane fusion in other processes, such as cell abscission during cytokinesis (Gromley et al., 2005) or during growth of developing neurons (Murthy et al., 2003).
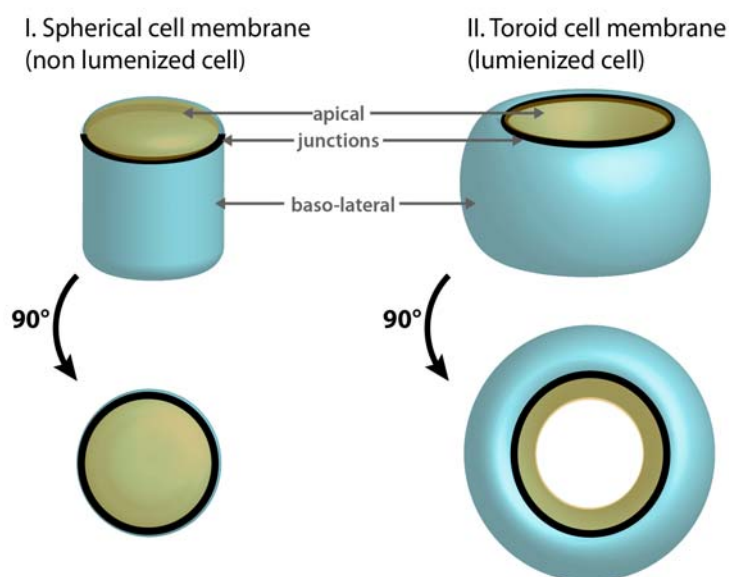
Figure. X. Different cell membrane shapes in lumenized and non lumenized cells
A) The fusion cell of the epithelial *Drosophila* tracheal system. I. Initially the cell has a spherical shape with a large baso-lateral membrane compartment (bright blue). A ring of junctions (black) encircles the apical membrane compartment (yellow) on top of the cell. II. After the transcellular lumen formation the cell changes shape and becomes toroid (doughnut-shaped). The apical membrane is now on the luminal side, the junctions are lateral, on the edge of the apical membrane. **B)** Endothelial cells can also have a spherical (I) or toroid (II) shape. I. Spherical ECs are present in multicellular vascular tubes. The apical membrane (yellow) is facing the lumen; the basal (dark blue) membrane faces the ECM. The lateral surface is very narrow and fully occupied by junctional complexes (black). II. An endothelial cell with transcellular lumen has a toroid shape, but differs from the tracheal fusion cell, because the lateral side (black) is very thin and the cell is elongated. For simplicity of the model, the nuclei are not marked.
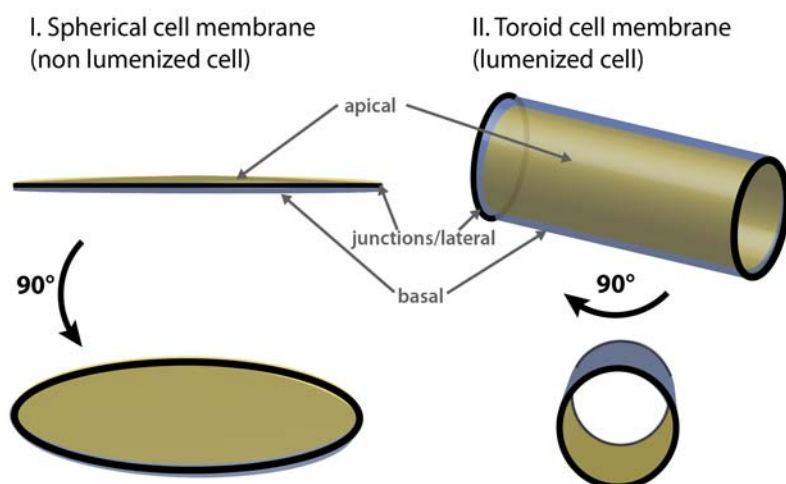
In the flies mutant for *arf-like 3*, the membranes of fusion cells failed to fuse and the lumen was not perfused. Additionally, Arf-like 3 positive vesicles containing Rab11 (a component of recycling endosomes), and Sec5 (a component of the exocyst) were shown to accumulate at the fusion site (Jiang et al., 2007).

Recent studies in the dorsal branch fusion cells of the *Drosophila* suggest that the cytoplasmic extension of a neighboring stalk cell can enter the fusion cell and participate in the transcellular lumen formation (Gervais et al., 2012). This model, described as "finger poking into a balloon", has been proposed before based on electron microscopy analyses (Uv et al., 2003). Its contribution to the transcellular lumen formation in the vasculature is not very likely but remains to be investigated.

Lumen formation through membrane invagination also occurs in the terminal cells of tracheal dorsal branches. These cells form long extensions with continuous lumen throughout the cell length. However, the lumen is not open at the end of the cell, meaning it forms a blunt-ended tube. This lumen forms by apical membrane invagination from the contact site to the other cells in the branch and proceeds along the cellular extensions towards the end of the terminal cell. This process involves delivery of the apical membrane components, including Bazooka (Par3), along the lumen length with participation of small vesicles and recycling endosomes (Gervais and Casanova, 2010).

Molecular components involved in the delivery of new apical membrane have been best described in *in vitro* experiments on MDCK cells that aggregate into cysts-like structures of polarized cells with lumen inside. Bryant and colleagues described in detail the molecular machinery that controls the formation of new apical membranes in these epithelial cells (Bryant et al., 2010). In this process, Podocalyxin is internalized from the cyst periphery into Rab8 and Rab11 positive vesicles that transport it to the apical surface. The exocyst, with cooperation of the Par3-aPKC complex, docks the vesicles to the apical surface, initiating the formation of the apical membrane initiation site (AMIS), which subsequently transforms into a pre-apical patch (PAP) as the junctional and apical components segregate. A number of other molecules are known to be involved in this process (see Fig.XI for details).

It will be interesting to see which factors identified in cell culture or in *Drosophila* are involved in the lumen formation process in the zebrafish vasculature endothelium.

We have now generated a number of GFP-fusion proteins from the Rab family to see whether we observe accumulation of any of them near the expanding, invaginating membrane. Also a number of chemicals blocking specific steps of vesicular transport are known and could be tested in zebrafish embryos.
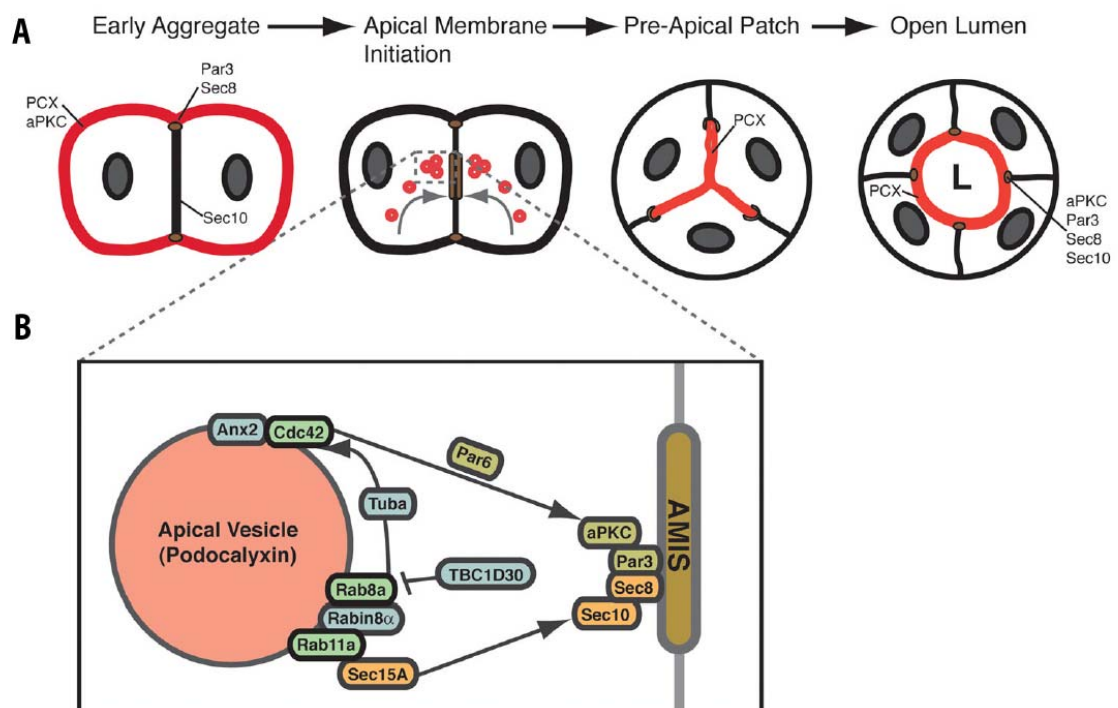
Figure XI.II A molecular network of *de novo* lumen generation in MDCK cell culture
A) A stepwise schematic of lumen formation in MDCK cysts. Podocalyxin (red) initially localized to the peripheries, is internalized by Rab8a and Rab11a positive vesicles and delivered to the AMIS (apical membrane initiation site). Pre-apical patch (PAP) forms when the junctional complexes (grey) and Podocalyxin in the AMIS segregate; this is followed by lumen opening. **B)** A schematic representation of the molecular network involved in the apical membrane initiation through apical vesicles delivery to the AMIS. (Adapted from (Bryant et al., 2010))

6.5 Cell splitting is a novel cellular mechanism necessary for rearrangements leading to transformation of unicellular tubes into multicellular ones

I have shown that in the cranial vessels the new lumen at the fusion site of two angiogenic sprouts is transcellular and forms through membrane invagination. After lumen opening, the vessels are immediately perfused, as shown by microangiography experiments, and carry blood flow. However, I observed that this unicellular conformation of the tubes is transient and cells within the existing tube engage in dynamic rearrangements to transform the vessel into a multicellular tube. I observed that the cells with transcellular lumen change their shape quite dramatically and split on one side of the tube to regain a spherical membrane conformation (see membrane shapes in Fig. X). This happens in a smooth, stepwise process and I have not observed any cell damage or tube breakage. After the transcellular lumen opening in the newly fused tip cells, the neighboring cells on the left and right side start to move towards each other. At the same time, the unicellular tube narrows on one side bringing its two edges, marked by the cell-cell junctions, closer together (see Fig. 3 in Results). Eventually the two edges of the cell merge together and most likely undergo membrane fission and fusion in a perpendicular conformation (as proposed in Fig. IX A'-D'). This leads to cell splitting and the transformation of a unicellular tube with toroid membrane into a "flat", half-pipe-shaped cell that becomes part of a multicellular vessel. As the cell splits, the neighboring cells contact each other, establishing a new connection marked by a new junctional line. The cell splitting mechanism was quite unexpected and, to our knowledge, has not been described before in any other model system. Similarly to the transcellular lumen perfusion, it involves membrane rearrangements. Since the same cells (previous tip cells) take part in both processes, it could be that they have some special features making them more flexible and susceptible to more prominent shape changes. It has been shown before that tip cells exhibit special features and gene expression (Gerhardt et al., 2003) so it would not be surprising if these are, among others, responsible for such behavior.

6.5.1 Why are multicellular tubes favored?

We have observed that all mature vessels are multicellular tubes and the unicellular state is transient and usually resolved within a couple of hours. What is the advantage of multicellular versus unicellular tubes?

In the zebrafish vasculature, the newly formed vessels often take part in further remodeling. First, they grow in diameter, which is much easier with a multicellular arrangement, because additional cells, migrating in from other branches, can easily incorporate into an existing vessel. Also cell division can happen without the need to collapse the tube, which would be necessary in case of a unicellular tube division.

Furthermore, the new vessels often take part in further branching by producing new sprouts or becoming a fusion target for another sprout. For a new sprout to form, a number of cells have to leave the vessel without disturbing its shape and function. This is only possible if the mother vessel is a multicellular tube, in which other cells can compensate for the migrating ones.

As mentioned before, in the vessels I studied, a seamless tube formation is forced by the presence of plasma pressure. With absent or low pressure, the cells preferentially undergo cell rearrangements to instantly form a multicellular tube. This suggests that the toroid membrane shape and the presence of two lateral sides and two separate junctional connections are not advantageous and cells can maintain it only for a limited time. A similar situation was observed in experiments in *Ciona intestinalis* notochord (Dong et al., 2009), where cells of biapical nature and two lateral sides eventually rearrange to regain the spherical membrane shape and single apical and lateral surface (see Fig. VII of Introduction). In contrast, in the *Drosophila* trachea, the fusion cells maintain the toroid shape throughout the tracheal development. In this system, however, the epithelial cells have strictly defined roles and position. In dorsal branches, the stalk of each branch is made of unicellular tubes with autocellular junctions and extracellular lumen. Only the single fusion cells form seamless tubes, which contribute to only a small part of the branch lumen. The cells within the branch do not divide and no additional branches are formed later on, meaning the system does not require much plasticity (Gervais et al., 2012; Samakovlis et al., 1996a).

6.5.2 Diverse cellular behaviors could drive the cell splitting

The driving force for cell splitting is not known. It could be that the unicellular tubes are not stable and having two lateral membranes with two junctional rings on the opposite sides of the cell disturbs the cell polarity and represents an unstable state. This would suggest that the splitting is driven by pulling forces within the cell that brings the opposite edges of the cell closer together and the neighboring cells follow, due to pulling of the junctional connections. However, splitting could also be forced by active migration of the neighboring cells leading to the invasion of the newly formed vessel part. Migrating cells would push the unicellular tube from two sides forcing the cell body to narrow and split. My analyses of *silent heart* embryos showed that unicellular tubes with transcellular lumen do not form in the absence of blood flow (as described before); therefore cell splitting does not take place. However, cell rearrangements still occur and the vessel eventually forms a multicellular cord. Cell rearrangements precede lumen formation in ~50 % of ISVs and happen in all cranial and trunk vessels when blood flow is removed (see Fig. XII). These experiments show that the rearrangement of cells is independent of blood flow and unicellular tube formation. However, the initial connection is always formed by single tip cells that become biapical and have two junctional rings after contact formation. Therefore it is still not clear whether the cellular rearrangements are driven by intracellular forces of these cells or by migration of the neighboring cells.

It has been shown in cell culture experiments that endothelial cells in confluent state are highly motile. Analyses with junctional live markers showed dynamic rearrangements of cell-cell junctions as the cells migrated within the endothelial sheet (Guo et al., 2007). These findings support the hypothesis of constant movement of cells within an existing vascular tube, which is in line with our observations of cellular rearrangements.

Cellular rearrangements within an existing tube have been observed in the *Drosophila* tracheal system (Caussinus et al., 2008; Ribeiro et al., 2004). In this case, the dorsal branch sprouts as a multicellular tube and two cells surround the lumen in every part of the branch at the time (except of the single fusion cell, described before). As the branch grows out, the cells undergo rearrangements leading to its transformation into a long and narrow tube made of single cells with autocellular junctions. This

happens through a dynamic process of cell wrapping around the lumen and zipping the autocellular junction. At the same time the neighboring cells move out of the way and wrap around the next lumen part (Ribeiro et al., 2004). This process, named cell intercalation, is driven by the pulling force of the sprouting fusion/tip cell that induces the shape change in following cells (Caussinus et al., 2008).

Cell splitting in the vasculature could resemble reversed cell intercalation. In this case a single cell starts "wrapped" around the lumen (though it has no autocellular junction) and other cells invade from the sides to finally "open" the unicellular-tube-cell and form a multicellular tube (see the model in Fig. 3 of results). In the dorsal branch, the cell rearrangements serve to make the tube longer and narrower without changing the cell number. I did not observe big changes in the vessel size and length in the time frame I looked at, but as the embryo grows rapidly over the next days, it is highly possible that by incorporating more cells the vessel is preparing for future growth.

6.6 Fusion of a new sprout to and existing vessel occurs through conserved mechanisms

To look at cellular rearrangements during new contact formation between a single angiogenic sprout and an existing tube, I analyzed the fusion process of the communicating vein (CMV) to the PLA (see the model in Fig. 1). I expected that the new contact in this case would occur preferentially at an existing junctional line in the multicellular part of the PLA and that new lumen would open between these cells. To my surprise, I observed that contact formation could happen at an existing contact site but the sprout could also connect the cell body of one of the ECs, making a new spot and a ring of junctions there (see the model in Fig. 5 of Results). This ring subsequently moved and connected to an existing junction resembling the previously described cell rearrangements. The lumen in the tip cell of the CMV sprout formed as transcellular, either from the PLA upwards or from the sprout towards the PLA. This could happen at any time point after contact establishment, regardless of the junctional conformation. This again points at the plasticity of the system and shows that the more complex shapes the vascular connection has, the more possible cell arrangements are observed.

Still, the main mechanisms remain the same and by dissecting the process into single steps we can observe the lumen formation and cell rearrangements described before.

6.7 The plasticity of the multistep mechanism leads to variability in observed cellular events

As mentioned before, nearly all observed tip cells in the cranial vessels form unicellular tubes right after fusion and cell rearrangements follow to form a multicellular tube. However, it is important to say that in multiple live imaging experiments I have never observed two absolutely identical situations. That is due to the cell plasticity, dynamic movements and shape changes. Lumen formation and cell rearrangements happen very fast and the process, starting from vessel sprouting up to multicellular tube formation, takes only 2-4 hours. Since the process is very dynamic and cell movements very plastic, in single cases I have observed cell rearrangements preceding lumen formation on one side of the vessel or happening almost at the same time. This is clearly due to the flexibility of the process necessary to buffer potential variations in cell shapes and blood pressure levels. In the first hours the pressure in the forming vessel is not always stable and it can easily collapse and inflate again. With respect to these observations, we propose that transcellular lumen formation followed by cell rearrangements and transformation into a multicellular tube is a predominant mechanism in cranial vessels but certain variability is present due to dynamic nature of the endothelial cells, lumen formation and the sprouting process itself.
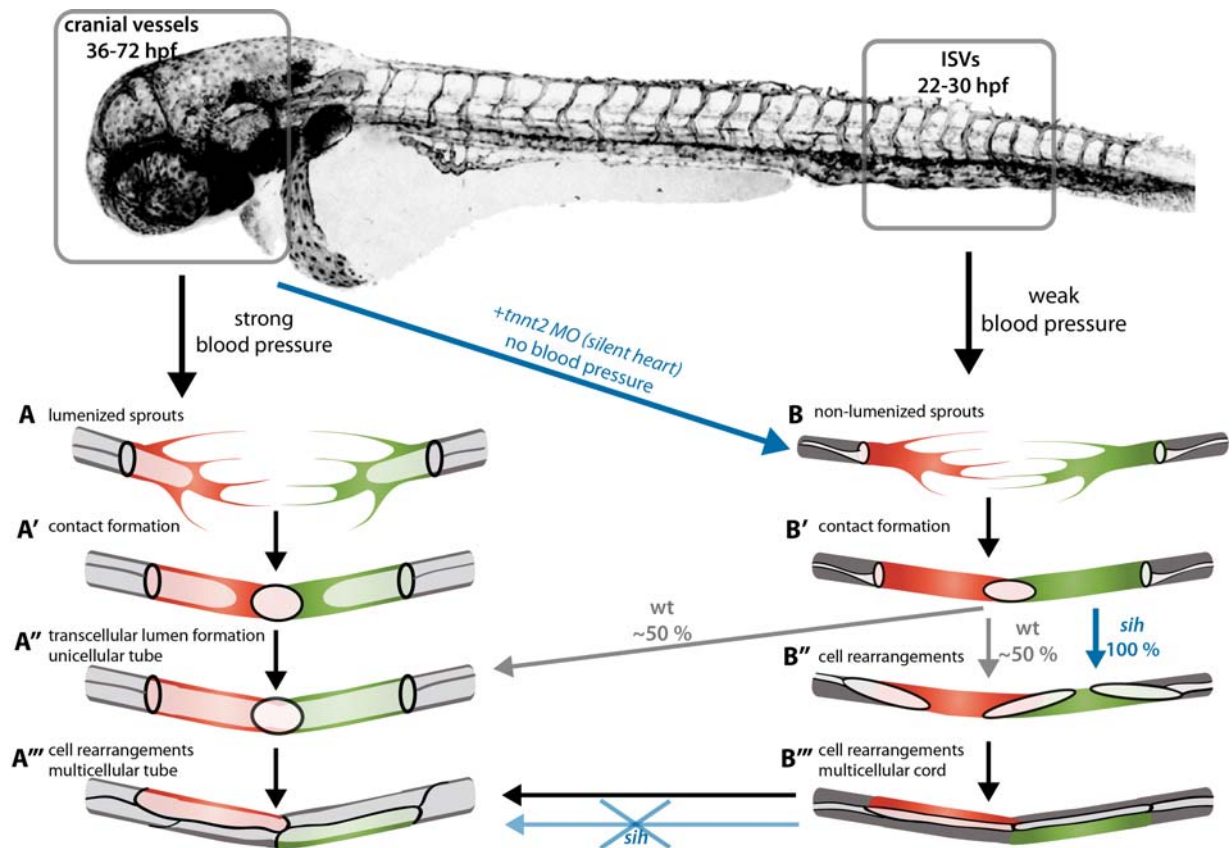
Figure XII. Influence of blood pressure on blood vessel fusion in the zebrafish
The steps of the fusion process differ depending on the presence of blood pressure in the neighboring branches and hence, in the fusing sprouts. **A)** In the cranial vasculature the pressure is strong and therefore the sprouts are lumenized till the very tip. After the contact formation (A'), a transcellular lumen forms making unicellular tubes (A''). Subsequent cell rearrangements transform the tube into a multicellular one (A'''). **B)** In the ISVs the blood pressure is weak, since they fuse at an early stage. Therefore the sprouts are not lumenized (B) as they establish the connection (B'). Subsequent lumen formation can follow one of two mechanisms; in ~50 % of the ISVs the cells rearrange to form a multicellular cord (B''-B''') and then the extracellular lumen is inflated (B'''-A''', arrow). The other 50 % of ISVs form transcellular lumen, following the mechanism described for cranial vessels (A''-A'''). In embryos injected with *tnnt2* morpholino (*silent heart, sih*) that do not have heartbeat, all the vessels (cranial and ISVs) follow only the second mechanism (B-B''') and neither transcellular lumen nor multicellular cord inflation is present (follow blue arrows).

6.8 The multistep model of blood vessel fusion represents a general mechanism

To summarize, I have analyzed in great detail blood vessel fusion in the developing zebrafish embryo. I have generated a multistep cellular model describing the process including membrane and junction remodeling (see Fig. 8 of Results). This multistep model is recurrent in all studied vessels and is adjustable to different vessel shapes and sizes. Blood flow is necessary for transcellular lumen formation but is dispensable for cell rearrangements (see Fig. XII for summary). I described in detail the membrane rearrangements during transcellular lumen formation, but the molecular mechanisms guiding membrane invagination and fusion remain unknown.

Cell splitting does not occur in the absence of blood flow since unicellular tube formation and plasma pressure within the tube are necessary steps preceding the splitting. Analyses of embryos without blood flow suggest that the splitting can be mediated by adjacent cells invading the unicellular tube or by pulling forces within the transiently bipolar cell. The driving force for the observed cell rearrangements and cell splitting remains to be discovered.

6.9 VE-cadherin mutant analyses

Having defined a multistep model of blood vessel fusion, we have started to uncover the molecular players involved in each of the described steps. We chose a candidate gene approach and the first target we wanted to analyze was VE-cadherin.

VE-cadherin (Vascular endothelial cadherin) is an endothelial cell specific adhesion molecule. It is crucial for proper vessel integrity as it mediates cell-cell adhesion creating zipper-like structures at cell borders through homophilic interactions. Through interactions with intracellular components, it coordinates actin-myosin cytoskeleton and cell response to signals, providing control for cell shape, behavior and proliferation. Mice mutant for this gene die at early embryonic stage due to vascular defects (Carmeliet et al., 1999; Corada et al., 1999). The role of VE-cadherin during angiogenesis is poorly understood and has been mostly studied in cell culture. In zebrafish its role has recently been analyzed using morpholino knock-down experiments (Abraham et al., 2009; Montero-Balaguer et al., 2009), which, although very informative, are not fully reliable and should always be confirmed by analyses in full knock-out animals.

In the lab we have generated a zebrafish mutant of *ve-cadherin* using the zinc finger nuclease technique (Krudewig et al., unpublished). The mutation results in a truncated nonfunctional version of the protein and is homozygous lethal. Heterozygous embryos do not show a phenotype, survive to adulthood and are fertile.

I have performed analyses on the mutant embryos with the transgenic markers used before for wild type experiments. I have not observed major malformations in the vascular network until 48 hpf. However, the embryos show defects of the heart, which is not properly connected to the large arteries. This results in very weak plasma pressure in the developing vessels, which is not strong enough to trigger blood cell circulation. This defect has been shown before in morpholino knock-down experiments (Montero-Balaguer et al., 2009). Therefore in all experiments I additionally compared the *ve-cadherin* mutant embryos to embryos injected with *tnnt2* morpholino and lacking heartbeat, to exclude the possibility that the observed defects are secondary to the impaired circulation.

6.9.1 Mutant vessels show increased sprouting activity

My detailed analyses of cranial vessels in the mutant embryos showed that in general, fusion events do occur. However, the dynamics of the process seemed to be disturbed. I have again focused on the PLA vessel, where I have described in most detail the fusion steps. The PLA formed in the normal position and became multicellular at 48 hpf in mutant embryos. However, the stepwise process did not occur normally and a number of defects were observed during certain steps of the fusion. I have focused on the dynamics of cell behavior and showed that cells lacking VE-cadherin have impaired ability to form proper new connections at the fusion site (see fig. 7 of Results, chapter 5.6).

In live imaging experiments with single cell labeling I observed that tip cell behavior was altered. Tip cells produced multiple protrusions spread in all directions and occupied much wider surface, comparing to the wild type and *silent heart* fish. In 50 % (5 of 10) of the movies multiple cells in the sprout showed tip cell characteristic behavior and migrated to the front of the sprout, thereby contributing to the exceeding number of protrusions.

It has been shown before that VE-cadherin, through interaction with VEGFR-2, can limit the activity of VEGFR-2 and therewith the EC response to proangiogenic cues. This activity of VE-cadherin leads to vessel stabilization and also contributes to the control of cell proliferation (Lampugnani et al., 2006). VE-cadherin deficient cells show enhanced angiogenic behavior in cell culture, similar to my observations in zebrafish. The tip cell selection process is also highly dependent on VEGFR-2 signaling, meaning that additional tip cells may also arise due to lack of VE-cadherin mediated VEGFR-2 inhibition (Gerhardt et al., 2003; Jakobsson et al., 2010).

Wild type sprouts can in some cases form more extensions. These are resolved as soon as a first contact with another sprout is established. The mutant cells, however, did not stop the protrusion activity after contacting another cell. On contrary, they kept on producing new filopodia and established multiple contacts with numerous extensions from the other sprout.

6.9.2 Other junctional molecules localize to contact sites during the fusion process in *ve-cadherin* mutant vessels

To confirm whether the cell-cell contacts that I see in the movies exhibit the previously described characteristics of a new connection, I analyzed the presence of other junctional markers and observed that both ZO-1 (Zona occludens 1) and ESAM-a (Endothelial cell-selective adhesion molecule a) proteins are present at cell-cell contacts at the fusion site and within the sprouts. This shows that cells are able to adhere to each other, which means that other junctional components could partially compensate for the lack of VE-cadherin and explain the mild vascular phenotype of the mutant fish at early embryonic stages. It was shown, that VE-cadherin can alter other junctional molecules. For example another adhesion molecule, N-cadherin, is up-regulated and localizes to the junctions in the ECs with reduced VE-cadherin (Giampietro et al., 2012). Additionally, VE-cadherin was shown to compete with N-cadherin at the junctional site of wild type EC and push it out to the membrane (Navarro et al., 1998). VE-cadherin but not N-cadherin can interact with VEGFR-2 to inhibit angiogenic cell behavior (mentioned before), which means that N-cadherin overexpression could compensate for cell adhesiveness but not for intracellular signaling (Giampietro et al., 2012). Due to lack of a zebrafish specific N-cadherin antibody I was not able to confirm this in zebrafish, but since I do observe localization of other junctional molecules (ESAM, ZO-1) at contact sites, it is likely that one of the other junctional components (e.g. N-cadherin) partially rescues the lack of VE-cadherin.

Additionally, VE-cadherin was shown to induce the assembly of certain proteins into tight junctions (TJs), such as Claudin-5, which is necessary for cell-cell contact stabilization (Taddei et al., 2008). This could explain the multiple connections and presence of multiple tip cells, which are not stabilized in the sprout.

For proper functioning, the C-terminus of VE-cadherin needs to be anchored to cytoplasmic cell components. Through this connection, which involves α- and β-catenin, VE-cadherin signals to the cell actin cytoskeleton and can trigger cell shape changes (reviewed in Dejana and Giampietro, 2012; Vestweber, 2008). Lack of this signaling can be the reason for observed tip cell malformations and excessive sprouting as well as

defects in contact formation. To asses changes in the cytoskeleton we are generating live markers for intracellular components, such as F-actin.

6.9.3 Multiple connections are present at the contact site in VE-cadherin deficient embryos

The observed multiple cell-cell connections at the fusion site showed deposition of both ZO-1 and ESAM proteins in the form of small rings and lines of junctions. These multiple connections eventually formed continuous lines of junctions, characteristic for multicellular vessels at 48 hpf, but they maintained the abnormal junction shapes for many hours after the first connection was made. In wild type embryos, even if a double connection occurred at the fusion point, it immediately merged to form one junctional ring or one of the contacts was detached.

Based on my antibody stainings and *in vivo* imaging I conclude that contact formation in the *ve-cadherin* mutant vessels is impaired and delayed. I propose that multiple tip cell protrusions result in numerous contacts forming at the fusion site. These contacts fail to resolve and are maintained until the cells eventually overlap completely due to continued cell migration. The fact that the cells make multiple contacts instead of a single continuous one slows down the process and results in aberrant junctional patterns. Additional analyses with the live junctional marker, EGFP-ZO-1, confirmed these findings. I observed that upon contact of two sprouts in *ve-cadherin* mutant embryos, the EGFP-ZO-1 did not immediately form a proper junctional ring, like it did in wild type embryos. The ring eventually formed, but in the meantime the front of the tip cell kept on migrating and made new connections further on. These multiple junctional spots eventually merged into one as cells kept on moving and overlapped over a large area (see Fig. 7 of Results, Movie 16). This shows that the cells fail to recognize the contact formation as a signal to stop sprouting, a mechanism known as contact inhibition. It has been shown that in cell culture experiments VE-cadherin mediates contact inhibition of EC sprouting behavior through Myosin light chain 2 (MLC-2) phosphorylation (Abraham et al., 2009). My findings are in line with these observations.

6.9.4 Lumen formation and polarity in *ve-cadherin* mutant zebrafish embryos

Cell polarity is necessary for proper lumen formation. Unfortunately we cannot observe lumen formation in the *ve-cadherin* mutant embryos, due to circulation defects present as a result of heart malformation. Single cell analyses using transplantation of *ve-cadherin* morphant cells suggested a cell autonomous lumen formation defect (Montero-Balaguer et al., 2009). I would like to repeat these experiments with our transgenic tools to look in more detail at lumen formation mechanisms.

Interestingly, I observed Podocalyxin-2 staining marking the apical membrane compartments, within the junctional lines and rings just like in the wild type embryos, meaning that cell polarization did occur at every place where a junctional contact was made. This was not expected since it has been shown before that Podocalyxin distribution is dependent on VE-cadherin and that it fails to properly localize in VE-cadherin deficient cells during aorta lumen formation in the mouse (Strilic et al., 2009). This could mean that cell polarization may be controlled differently in the angiogenic vessels, in comparison to vasculogenic ones (like the aorta). From my antibody staining experiments it is also not clear whether the polarization occurs at the right time. The dynamics of this process could be altered, as they are for the initial contact formation. To address this question we are currently generating live, fluorescently labeled apical markers. It will be also interesting to see what happens to other polarity components, such as the Par3 complex, since Podocalyxin is only one of many proteins involved in EC polarity.

6.9.5 The summary of *ve-cadherin* mutant analyses

In summary, I have shown that VE-cadherin is important for the establishment of a proper new connection although it is not crucial for cell-cell adhesion. This is in sharp contrast with findings in *Drosophila,* where E-cadherin is crucial for new contact formation and fusion does not happen in its absence. It is possible that in blood vessels multiple proteins are involved in this process and can compensate for each other's functions. Analyses of double mutant animals and mosaic analyses will be of great importance to reveal the key players in the process of blood vessel fusion.

6.10 Concluding remarks

The vascular system is one of the largest and most complex organs in the vertebrate body. Its proper functioning is crucial for survival of all the other organs, as it transports nutrients, metabolites and other molecules, as well as mediates the gas exchange in all tissues. The formation of new vessels is of great importance not only during vertebrate development, but also for tissue regeneration after injury. The vasculature is also an important factor in many diseases, where vessel degeneration or uncontrolled growth are related to the disease progression. Blood vessel anastomosis is a key step during the formation of new vessels as it leads to the transformation of blunt-ended vascular sprouts into functional tubes connected to the blood flow. In this PhD thesis, I have analyzed in great detail the process of blood vessel anastomosis in zebrafish embryos and defined a general, multistep vessel fusion process recurrent in all analyzed vessels. I showed that blood pressure plays an important role during blood vessel fusion and I described in detail novel cellular mechanisms involved in this process, namely transcellular lumen formation through membrane invagination and cell splitting. I showed that VE-cadherin is involved in the initial steps of fusion and is necessary for proper establishment of a new connection. Additionally, I described cellular behaviors involved in vessel pruning and defined a multistep model for this process.

The detailed description of vessel fusion provides the basis for further research aimed at the identification of molecular factors involved in this process. Mechanisms involved in vessel formation and regression in embryonic development are often similar to processes described in human pathologies. Therefore, these findings can serve to better understand the disease mechanisms and can help to find targets and methods for disease prevention and therapy development.

7 Acknowledgements

I would like to thank Professor Markus Affolter for giving me the opportunity to work in his group and enjoy this fascinating and inspiring scientific environment. I would like to thank Markus for letting me follow my fascination with live imaging and pursue the head vasculature analyses, which from a side project became my main interest and resulted in the manuscript presented in this thesis. The Affolter lab has been a fantastic working place and I enjoyed a lot coming there every day, whether there was a seminar, an apero or just a regular working time.

From all my heart I thank my parents, Piotr and Elzbieta, and my brother Krzysztof, for being there for me even though we have been so far apart. My family has been my strength in difficult moments and my happiness in the good ones, for which I am immensely grateful.

I would like to thank Dr Elin Ellertsdottir for supervising my work from my first day in the lab till the very last corrections in this thesis. She has been a great teacher, a dear friend and a strong supporter in both scientific and extra-scientific challenges I faced within the last four years.

I also thank all the "fish people" in the lab, especially Alice, Henry and Lukas & Yannick (a.k.a. the Swiss Boys) for inspiring scientific discussions, help in everyday experiments and all the fun we had during the trips to conferences and countless social activities.

I also would like to acknowledge all the current and previous members of the Affolter group who have created a great, family atmosphere and have become great friends of mine. Special thanks go to the Girls: Amanda, Magda, Fisun and Alice. You are fabulous!

I thank Helen for guidance through the maze of Swiss administration.

I also thank Kumu for great care of the zebrafish.

I would like to acknowledge the Imaging Core Facility of the Biozentrum for taking great care of the microscopes and making my work so much easier.

Last but not least I thank all my friends from the Biozentrum for making the institute and Basel a great place to live and work.

Thank you all!
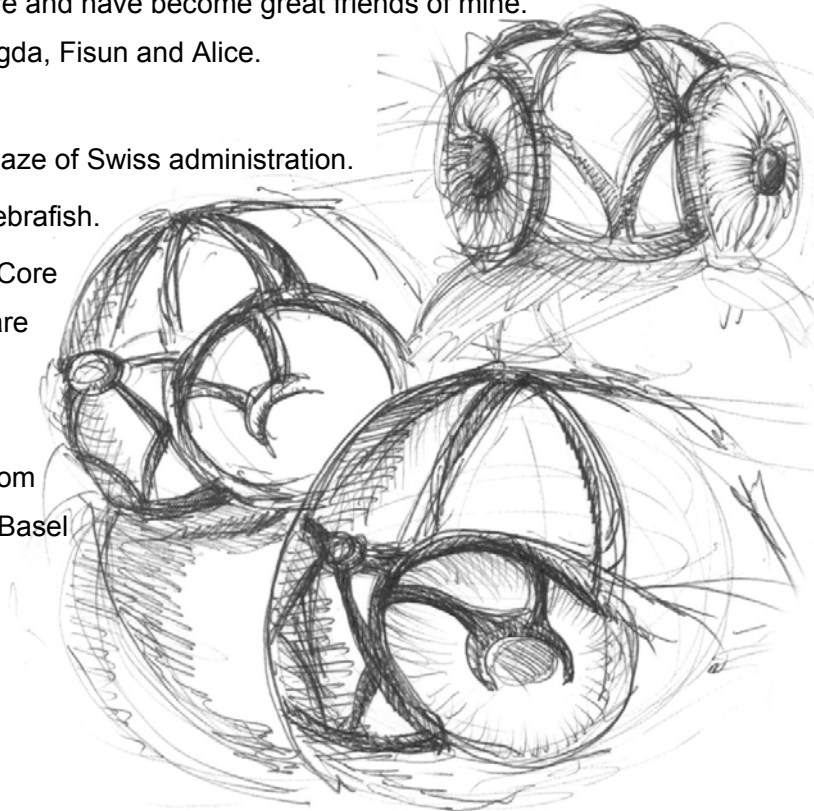
8 References

Abraham, S., Yeo, M., Montero-Balaguer, M., Paterson, H., Dejana, E., Marshall, C.J., and Mavria, G. (2009). VE-Cadherin-mediated cell-cell interaction suppresses sprouting via signaling to MLC2 phosphorylation. Curr Biol *19*, 668-674.

Adams, R.H., and Alitalo, K. (2007). Molecular regulation of angiogenesis and lymphangiogenesis. Nature reviews Molecular cell biology *8*, 464-478.

Affolter, M., Zeller, R., and Caussinus, E. (2009). Tissue remodelling through branching morphogenesis. Nature reviews Molecular cell biology *10*, 831-842.

Alon, T., Hemo, I., Itin, A., Pe'er, J., Stone, J., and Keshet, E. (1995). Vascular endothelial growth factor acts as a survival factor for newly formed retinal vessels and has implications for retinopathy of prematurity. Nature medicine *1*, 1024-1028.

Ashton, N. (1966). Oxygen and the growth and development of retinal vessels. In vivo and in vitro studies. The XX Francis I. Proctor Lecture. Am J Ophthalmol *62*, 412-435.

Ausprunk, D.H., Knighton, D.R., and Folkman, J. (1974). Differentiation of vascular endothelium in the chick chorioallantois: a structural and autoradiographic study. Dev Biol *38*, 237-248.

Baer, M.M., Chanut-Delalande, H., and Affolter, M. (2009). Cellular and molecular mechanisms underlying the formation of biological tubes. Curr Top Dev Biol *89*, 137-162.

Bayless, K.J., and Davis, G.E. (2002). The Cdc42 and Rac1 GTPases are required for capillary lumen formation in three-dimensional extracellular matrices. Journal of cell science *115*, 1123-1136.

Blum, Y., Belting, H.G., Ellertsdottir, E., Herwig, L., Luders, F., and Affolter, M. (2008). Complex cell rearrangements during intersegmental vessel sprouting and vessel fusion in the zebrafish embryo. Dev Biol *316*, 312-322.

Bryant, D.M., Datta, A., Rodriguez-Fraticelli, A.E., Peranen, J., Martin-Belmonte, F., and Mostov, K.E. (2010). A molecular network for de novo generation of the apical surface and lumen. Nature cell biology *12*, 1035-1045.

Burri, P.H., and Tarek, M.R. (1990). A novel mechanism of capillary growth in the rat pulmonary microcirculation. Anat Rec *228*, 35-45.

Bussmann, J., Wolfe, S.A., and Siekmann, A.F. (2011). Arterial-venous network formation during brain vascularization involves hemodynamic regulation of chemokine signaling. Development *138*, 1717-1726.

Caduff, J.H., Fischer, L.C., and Burri, P.H. (1986). Scanning electron microscope study of the developing microvasculature in the postnatal rat lung. Anat Rec *216*, 154-164.

Carmeliet, P. (2003). Angiogenesis in health and disease. Nature medicine *9*, 653-660.

Carmeliet, P., Ferreira, V., Breier, G., Pollefeyt, S., Kieckens, L., Gertsenstein, M., Fahrig, M., Vandenhoeck, A., Harpal, K., Eberhardt, C.*, et al.* (1996). Abnormal blood vessel development and lethality in embryos lacking a single VEGF allele. Nature *380*, 435-439.

Carmeliet, P., and Jain, R.K. (2011). Molecular mechanisms and clinical applications of angiogenesis. Nature *473*, 298-307.

Carmeliet, P., Lampugnani, M.G., Moons, L., Breviario, F., Compernolle, V., Bono, F., Balconi, G., Spagnuolo, R., Oosthuyse, B., Dewerchin, M.*, et al.* (1999). Targeted deficiency or cytosolic truncation of the VE-cadherin gene in mice impairs VEGF-mediated endothelial survival and angiogenesis. Cell *98*, 147-157.

Cattelino, A., Liebner, S., Gallini, R., Zanetti, A., Balconi, G., Corsi, A., Bianco, P., Wolburg, H., Moore, R., Oreda, B.*, et al.* (2003). The conditional inactivation of the beta-catenin gene in endothelial cells causes a defective vascular pattern and increased vascular fragility. The Journal of cell biology *162*, 1111-1122.

Caussinus, E., Colombelli, J., and Affolter, M. (2008). Tip-cell migration controls stalk-cell intercalation during Drosophila tracheal tube elongation. Curr Biol *18*, 1727-1734.

Chen, Q., Jiang, L., Li, C., Hu, D., Bu, J.W., Cai, D., and Du, J.L. (2012). Haemodynamics-driven developmental pruning of brain vasculature in zebrafish. PLoS Biol *10*, e1001374.

Cheng, C., Haasdijk, R., Tempel, D., van de Kamp, E.H., Herpers, R., Bos, F., Den Dekker, W.K., Blonden, L.A., de Jong, R., Burgisser, P.E.*, et al.* (2012). Endothelial cell-specific FGD5 involvement in vascular pruning defines neovessel fate in mice. Circulation *125*, 3142-3158.

Chernomordik, L.V., and Kozlov, M.M. (2008). Mechanics of membrane fusion. Nat Struct Mol Biol *15*, 675-683.

Chico, T.J., Ingham, P.W., and Crossman, D.C. (2008). Modeling cardiovascular disease in the zebrafish. Trends Cardiovasc Med *18*, 150-155.

Childs, S., Chen, J.N., Garrity, D.M., and Fishman, M.C. (2002). Patterning of angiogenesis in the zebrafish embryo. Development *129*, 973-982.

Corada, M., Mariotti, M., Thurston, G., Smith, K., Kunkel, R., Brockhaus, M., Lampugnani, M.G., Martin-Padura, I., Stoppacciaro, A., Ruco, L.*, et al.* (1999). Vascular endothelial-cadherin is an important determinant of microvascular integrity in vivo. Proceedings of the National Academy of Sciences of the United States of America *96*, 9815-9820.

Corti, P., Young, S., Chen, C.Y., Patrick, M.J., Rochon, E.R., Pekkan, K., and Roman, B.L. (2011). Interaction between alk1 and blood flow in the development of arteriovenous malformations. Development *138*, 1573-1582.

Covassin, L.D., Villefranc, J.A., Kacergis, M.C., Weinstein, B.M., and Lawson, N.D. (2006). Distinct genetic interactions between multiple Vegf receptors are required for development of different blood vessel types in zebrafish. Proceedings of the National Academy of Sciences of the United States of America *103*, 6554-6559.

Davis, G.E., Bayless, K.J., and Mavila, A. (2002). Molecular basis of endothelial cell morphogenesis in three-dimensional extracellular matrices. Anat Rec *268*, 252-275.

Davis, G.E., and Camarillo, C.W. (1996). An alpha 2 beta 1 integrin-dependent pinocytic mechanism involving intracellular vacuole formation and coalescence regulates capillary lumen and tube formation in three-dimensional collagen matrix. Experimental cell research *224*, 39-51.

Dejana, E., and Giampietro, C. (2012). Vascular endothelial-cadherin and vascular stability. Curr Opin Hematol *19*, 218-223.

Denker, E., and Jiang, D. (2012). Ciona intestinalis notochord as a new model to investigate the cellular and molecular mechanisms of tubulogenesis. Seminars in cell & developmental biology *23*, 308-319.

Detrich, H.W., 3rd, Kieran, M.W., Chan, F.Y., Barone, L.M., Yee, K., Rundstadler, J.A., Pratt, S., Ransom, D., and Zon, L.I. (1995). Intraembryonic hematopoietic cell migration during vertebrate development. Proc Natl Acad Sci U S A *92*, 10713-10717.

Djonov, V., Baum, O., and Burri, P.H. (2003). Vascular remodeling by intussusceptive angiogenesis. Cell and tissue research *314*, 107-117.

Djonov, V., Schmid, M., Tschanz, S.A., and Burri, P.H. (2000). Intussusceptive angiogenesis: its role in embryonic vascular network formation. Circulation research *86*, 286-292.

References

Djonov, V.G., Kurz, H., and Burri, P.H. (2002). Optimality in the developing vascular system: branching remodeling by means of intussusception as an efficient adaptation mechanism. Developmental dynamics : an official publication of the American Association of Anatomists *224*, 391-402.

Dong, B., Deng, W., and Jiang, D. (2011). Distinct cytoskeleton populations and extensive crosstalk control Ciona notochord tubulogenesis. Development *138*, 1631-1641.

Dong, B., Horie, T., Denker, E., Kusakabe, T., Tsuda, M., Smith, W.C., and Jiang, D. (2009). Tube formation by complex cellular processes in Ciona intestinalis notochord. Dev Biol *330*, 237-249.

Drake, C.J., Davis, L.A., and Little, C.D. (1992). Antibodies to beta 1-integrins cause alterations of aortic vasculogenesis, in vivo. Developmental dynamics : an official publication of the American Association of Anatomists *193*, 83-91.

Dumont, D.J., Jussila, L., Taipale, J., Lymboussaki, A., Mustonen, T., Pajusola, K., Breitman, M., and Alitalo, K. (1998). Cardiovascular failure in mouse embryos deficient in VEGF receptor-3. Science *282*, 946-949.

Ellertsdottir, E., Lenard, A., Blum, Y., Krudewig, A., Herwig, L., Affolter, M., and Belting, H.G. (2010). Vascular morphogenesis in the zebrafish embryo. Dev Biol *341*, 56-65.

Ferrara, N., and Davis-Smyth, T. (1997). The biology of vascular endothelial growth factor. Endocr Rev *18*, 4-25.

Flamme, I., Frolich, T., and Risau, W. (1997). Molecular mechanisms of vasculogenesis and embryonic angiogenesis. J Cell Physiol *173*, 206-210.

Fong, G.H., Rossant, J., Gertsenstein, M., and Breitman, M.L. (1995). Role of the Flt-1 receptor tyrosine kinase in regulating the assembly of vascular endothelium. Nature *376*, 66-70.

Fouquet, B., Weinstein, B.M., Serluca, F.C., and Fishman, M.C. (1997). Vessel patterning in the embryo of the zebrafish: guidance by notochord. Dev Biol *183*, 37-48.

Fujita, M., Cha, Y.R., Pham, V.N., Sakurai, A., Roman, B.L., Gutkind, J.S., and Weinstein, B.M. (2011). Assembly and patterning of the vascular network of the vertebrate hindbrain. Development *138*, 1705-1715.

Galvez-Santisteban, M., Rodriguez-Fraticelli, A.E., Bryant, D.M., Vergarajauregui, S., Yasuda, T., Banon-Rodriguez, I., Bernascone, I., Datta, A., Spivak, N., Young, K.*, et al.* (2012). Synaptotagmin-like proteins control the formation of a single apical membrane domain in epithelial cells. Nature cell biology *14*, 838-849.

Gerhardt, H., Golding, M., Fruttiger, M., Ruhrberg, C., Lundkvist, A., Abramsson, A., Jeltsch, M., Mitchell, C., Alitalo, K., Shima, D.*, et al.* (2003). VEGF guides angiogenic sprouting utilizing endothelial tip cell filopodia. J Cell Biol *161*, 1163-1177.

Gervais, L., and Casanova, J. (2010). In vivo coupling of cell elongation and lumen formation in a single cell. Curr Biol *20*, 359-366.

Gervais, L., Lebreton, G., and Casanova, J. (2012). The making of a fusion branch in the Drosophila trachea. Dev Biol *362*, 187-193.

Ghabrial, A.S., and Krasnow, M.A. (2006). Social interactions among epithelial cells during tracheal branching morphogenesis. Nature *441*, 746-749.

Giampietro, C., Taddei, A., Corada, M., Sarra-Ferraris, G.M., Alcalay, M., Cavallaro, U., Orsenigo, F., Lampugnani, M.G., and Dejana, E. (2012). Overlapping and divergent signaling pathways of N-cadherin and VE-cadherin in endothelial cells. Blood *119*, 2159-2170.

Gory-Faure, S., Prandini, M.H., Pointu, H., Roullot, V., Pignot-Paintrand, I., Vernet, M., and Huber, P. (1999). Role of vascular endothelial-cadherin in vascular morphogenesis. Development *126*, 2093-2102.

Gromley, A., Yeaman, C., Rosa, J., Redick, S., Chen, C.T., Mirabelle, S., Guha, M., Sillibourne, J., and Doxsey, S.J. (2005). Centriolin anchoring of exocyst and SNARE complexes at the midbody is required for secretory-vesicle-mediated abscission. Cell *123*, 75-87.

Guo, R., Sakamoto, H., Sugiura, S., and Ogawa, M. (2007). Endothelial cell motility is compatible with junctional integrity. J Cell Physiol *211*, 327-335.

Habeck, H., Odenthal, J., Walderich, B., Maischein, H., and Schulte-Merker, S. (2002). Analysis of a zebrafish VEGF receptor mutant reveals specific disruption of angiogenesis. Curr Biol *12*, 1405-1412.

Hamilton-Buchanan, F. (1822). An Account of the Fishes of River Ganges and its Branches. George Ramsay and Co *vii+405pp, 39 pls*.

Hatta, K., Tsujii, H., and Omura, T. (2006). Cell tracking using a photoconvertible fluorescent protein. Nat Protoc *1*, 960-967.

Hellstrom, M., Phng, L.K., Hofmann, J.J., Wallgard, E., Coultas, L., Lindblom, P., Alva, J., Nilsson, A.K., Karlsson, L., Gaiano, N.*, et al.* (2007). Dll4 signalling through Notch1 regulates formation of tip cells during angiogenesis. Nature *445*, 776-780.

Herbert, S.P., Huisken, J., Kim, T.N., Feldman, M.E., Houseman, B.T., Wang, R.A., Shokat, K.M., and Stainier, D.Y. (2009). Arterial-venous segregation by selective cell sprouting: an alternative mode of blood vessel formation. Science *326*, 294-298.

Herwig, L., Blum, Y., Krudewig, A., Ellertsdottir, E., Lenard, A., Belting, H.G., and Affolter, M. (2011). Distinct cellular mechanisms of blood vessel fusion in the zebrafish embryo. Curr Biol *21*, 1942-1948.

Hlushchuk, R., Ehrbar, M., Reichmuth, P., Heinimann, N., Styp-Rekowska, B., Escher, R., Baum, O., Lienemann, P., Makanya, A., Keshet, E.*, et al.* (2011). Decrease in VEGF expression induces intussusceptive vascular pruning. Arterioscler Thromb Vasc Biol *31*, 2836-2844.

Isogai, S., Horiguchi, M., and Weinstein, B.M. (2001). The vascular anatomy of the developing zebrafish: an atlas of embryonic and early larval development. Dev Biol *230*, 278-301.

Isogai, S., Lawson, N.D., Torrealday, S., Horiguchi, M., and Weinstein, B.M. (2003). Angiogenic network formation in the developing vertebrate trunk. Development *130*, 5281-5290.

Jakobsson, L., Franco, C.A., Bentley, K., Collins, R.T., Ponsioen, B., Aspalter, I.M., Rosewell, I., Busse, M., Thurston, G., Medvinsky, A.*, et al.* (2010). Endothelial cells dynamically compete for the tip cell position during angiogenic sprouting. Nat Cell Biol *12*, 943-953.

Jiang, L., Rogers, S.L., and Crews, S.T. (2007). The Drosophila Dead end Arf-like3 GTPase controls vesicle trafficking during tracheal fusion cell morphogenesis. Dev Biol *311*, 487-499.

Jin, S.W., Beis, D., Mitchell, T., Chen, J.N., and Stainier, D.Y. (2005). Cellular and molecular analyses of vascular tube and lumen formation in zebrafish. Development *132*, 5199-5209.

Kakihara, K., Shinmyozu, K., Kato, K., Wada, H., and Hayashi, S. (2008). Conversion of plasma membrane topology during epithelial tube connection requires Arf-like 3 small GTPase in Drosophila. Mechanisms of development *125*, 325-336.

Kamei, M., Saunders, W.B., Bayless, K.J., Dye, L., Davis, G.E., and Weinstein, B.M. (2006). Endothelial tubes assemble from intracellular vacuoles in vivo. Nature *442*, 453-456.

Kimmel, C.B., Ballard, W.W., Kimmel, S.R., Ullmann, B., and Schilling, T.F. (1995). Stages of embryonic development of the zebrafish. Developmental dynamics : an official publication of the American Association of Anatomists *203*, 253-310.

Kimmel, C.B., Warga, R.M., and Schilling, T.F. (1990). Origin and organization of the zebrafish fate map. Development *108*, 581-594.

Koh, W., Sachidanandam, K., Stratman, A.N., Sacharidou, A., Mayo, A.M., Murphy, E.A., Cheresh, D.A., and Davis, G.E. (2009). Formation of endothelial lumens requires a coordinated PKCepsilon-, Src-, Pak-

References

and Raf-kinase-dependent signaling cascade downstream of Cdc42 activation. Journal of cell science *122*, 1812-1822.

Lampugnani, M.G., Orsenigo, F., Gagliani, M.C., Tacchetti, C., and Dejana, E. (2006). Vascular endothelial cadherin controls VEGFR-2 internalization and signaling from intracellular compartments. J Cell Biol *174*, 593-604.

Lampugnani, M.G., Orsenigo, F., Rudini, N., Maddaluno, L., Boulday, G., Chapon, F., and Dejana, E. (2010). CCM1 regulates vascular-lumen organization by inducing endothelial polarity. Journal of cell science *123*, 1073-1080.

Lawson, N.D., Scheer, N., Pham, V.N., Kim, C.H., Chitnis, A.B., Campos-Ortega, J.A., and Weinstein, B.M. (2001). Notch signaling is required for arterial-venous differentiation during embryonic vascular development. Development *128*, 3675-3683.

Lawson, N.D., and Weinstein, B.M. (2002). In vivo imaging of embryonic vascular development using transgenic zebrafish. Dev Biol *248*, 307-318.

Lee, M., Lee, S., Zadeh, A.D., and Kolodziej, P.A. (2003). Distinct sites in E-cadherin regulate different steps in Drosophila tracheal tube fusion. Development *130*, 5989-5999.

Lee, S., and Kolodziej, P.A. (2002). The plakin Short Stop and the RhoA GTPase are required for E-cadherin-dependent apical surface remodeling during tracheal tube fusion. Development *129*, 1509-1520.

Lelievre, E., Lionneton, F., and Soncin, F. (2001). [Role of the ETS transcription factors in the control of endothelial-specific gene expression and in angiogenesis]. Bull Cancer *88*, 137-142.

Lieschke, G.J., Oates, A.C., Paw, B.H., Thompson, M.A., Hall, N.E., Ward, A.C., Ho, R.K., Zon, L.I., and Layton, J.E. (2002). Zebrafish SPI-1 (PU.1) marks a site of myeloid development independent of primitive erythropoiesis: implications for axial patterning. Dev Biol *246*, 274-295.

Lobov, I.B., Renard, R.A., Papadopoulos, N., Gale, N.W., Thurston, G., Yancopoulos, G.D., and Wiegand, S.J. (2007). Delta-like ligand 4 (Dll4) is induced by VEGF as a negative regulator of angiogenic sprouting. Proc Natl Acad Sci U S A *104*, 3219-3224.

Lubarsky, B., and Krasnow, M.A. (2003). Tube morphogenesis: making and shaping biological tubes. Cell *112*, 19-28.

Luo, Y., and Radice, G.L. (2005). N-cadherin acts upstream of VE-cadherin in controlling vascular morphogenesis. The Journal of cell biology *169*, 29-34.

McKinney, S.A., Murphy, C.S., Hazelwood, K.L., Davidson, M.W., and Looger, L.L. (2009). A bright and photostable photoconvertible fluorescent protein. Nature methods *6*, 131-133.

Montero-Balaguer, M., Swirsding, K., Orsenigo, F., Cotelli, F., Mione, M., and Dejana, E. (2009). Stable vascular connections and remodeling require full expression of VE-cadherin in zebrafish embryos. PLoS One *4*, e5772.

Murthy, M., Garza, D., Scheller, R.H., and Schwarz, T.L. (2003). Mutations in the exocyst component Sec5 disrupt neuronal membrane traffic, but neurotransmitter release persists. Neuron *37*, 433-447.

Navarro, P., Ruco, L., and Dejana, E. (1998). Differential localization of VE- and N-cadherins in human endothelial cells: VE-cadherin competes with N-cadherin for junctional localization. The Journal of cell biology *140*, 1475-1484.

Nicoli, S., Standley, C., Walker, P., Hurlstone, A., Fogarty, K.E., and Lawson, N.D. (2010). MicroRNA-mediated integration of haemodynamics and Vegf signalling during angiogenesis. Nature *464*, 1196-1200.

Nieto, M.A., Bennett, M.F., Sargent, M.G., and Wilkinson, D.G. (1992). Cloning and developmental expression of Sna, a murine homologue of the Drosophila snail gene. Development *116*, 227-237.

Ochoa-Espinosa, A., and Affolter, M. (2012). Branching morphogenesis: from cells to organs and back. Cold Spring Harbor perspectives in biology *4*.

Parmar, K.M., Larman, H.B., Dai, G., Zhang, Y., Wang, E.T., Moorthy, S.N., Kratz, J.R., Lin, Z., Jain, M.K., Gimbrone, M.A., Jr*., et al.* (2006). Integration of flow-dependent endothelial phenotypes by Kruppel-like factor 2. The Journal of clinical investigation *116*, 49-58.

Patan, S., Haenni, B., and Burri, P.H. (1993). Evidence for intussusceptive capillary growth in the chicken chorio-allantoic membrane (CAM). Anat Embryol (Berl) *187*, 121-130.

Proulx, K., Lu, A., and Sumanas, S. (2010). Cranial vasculature in zebrafish forms by angioblast cluster-derived angiogenesis. Dev Biol *348*, 34-46.

Ribatti, D. (2012). Chicken chorioallantoic membrane angiogenesis model. Methods Mol Biol *843*, 47-57.

Ribeiro, C., Neumann, M., and Affolter, M. (2004). Genetic control of cell intercalation during tracheal morphogenesis in Drosophila. Curr Biol *14*, 2197-2207.

Risau, W., and Flamme, I. (1995). Vasculogenesis. Annu Rev Cell Dev Biol *11*, 73-91.

Roostalu, U., and Strahle, U. (2012). In vivo imaging of molecular interactions at damaged sarcolemma. Developmental cell *22*, 515-529.

Samakovlis, C., Hacohen, N., Manning, G., Sutherland, D.C., Guillemin, K., and Krasnow, M.A. (1996a). Development of the Drosophila tracheal system occurs by a series of morphologically distinct but genetically coupled branching events. Development *122*, 1395-1407.

Samakovlis, C., Manning, G., Steneberg, P., Hacohen, N., Cantera, R., and Krasnow, M.A. (1996b). Genetic control of epithelial tube fusion during Drosophila tracheal development. Development *122*, 3531-3536.

Sehnert, A.J., Huq, A., Weinstein, B.M., Walker, C., Fishman, M., and Stainier, D.Y. (2002). Cardiac troponin T is essential in sarcomere assembly and cardiac contractility. Nature genetics *31*, 106-110.

Shalaby, F., Rossant, J., Yamaguchi, T.P., Gertsenstein, M., Wu, X.F., Breitman, M.L., and Schuh, A.C. (1995). Failure of blood-island formation and vasculogenesis in Flk-1-deficient mice. Nature *376*, 62-66.

Siekmann, A.F., and Lawson, N.D. (2007). Notch signalling limits angiogenic cell behaviour in developing zebrafish arteries. Nature *445*, 781-784.

Stainier, D.Y., Fouquet, B., Chen, J.N., Warren, K.S., Weinstein, B.M., Meiler, S.E., Mohideen, M.A., Neuhauss, S.C., Solnica-Krezel, L., Schier, A.F*., et al.* (1996). Mutations affecting the formation and function of the cardiovascular system in the zebrafish embryo. Development *123*, 285-292.

Streisinger, G., Walker, C., Dower, N., Knauber, D., and Singer, F. (1981). Production of clones of homozygous diploid zebra fish (Brachydanio rerio). Nature *291*, 293-296.

Strilic, B., Eglinger, J., Krieg, M., Zeeb, M., Axnick, J., Babal, P., Muller, D.J., and Lammert, E. (2010). Electrostatic cell-surface repulsion initiates lumen formation in developing blood vessels. Curr Biol *20*, 2003-2009.

Strilic, B., Kucera, T., Eglinger, J., Hughes, M.R., McNagny, K.M., Tsukita, S., Dejana, E., Ferrara, N., and Lammert, E. (2009). The molecular basis of vascular lumen formation in the developing mouse aorta. Dev Cell *17*, 505-515.

Suchting, S., Freitas, C., le Noble, F., Benedito, R., Breant, C., Duarte, A., and Eichmann, A. (2007). The Notch ligand Delta-like 4 negatively regulates endothelial tip cell formation and vessel branching. Proc Natl Acad Sci U S A *104*, 3225-3230.

Sutherland, D., Samakovlis, C., and Krasnow, M.A. (1996). branchless encodes a Drosophila FGF homolog that controls tracheal cell migration and the pattern of branching. Cell *87*, 1091-1101.

References

Taddei, A., Giampietro, C., Conti, A., Orsenigo, F., Breviario, F., Pirazzoli, V., Potente, M., Daly, C., Dimmeler, S., and Dejana, E. (2008). Endothelial adherens junctions control tight junctions by VE-cadherin-mediated upregulation of claudin-5. Nat Cell Biol *10*, 923-934.

Tamagnone, L., and Comoglio, P.M. (2000). Signalling by semaphorin receptors: cell guidance and beyond. Trends in cell biology *10*, 377-383.

Tammela, T., Zarkada, G., Nurmi, H., Jakobsson, L., Heinolainen, K., Tvorogov, D., Zheng, W., Franco, C.A., Murtomaki, A., Aranda, E.*, et al.* (2011). VEGFR-3 controls tip to stalk conversion at vessel fusion sites by reinforcing Notch signalling. Nature cell biology *13*, 1202-1213.

Tammela, T., Zarkada, G., Wallgard, E., Murtomaki, A., Suchting, S., Wirzenius, M., Waltari, M., Hellstrom, M., Schomber, T., Peltonen, R.*, et al.* (2008). Blocking VEGFR-3 suppresses angiogenic sprouting and vascular network formation. Nature *454*, 656-660.

Tanaka-Matakatsu, M., Uemura, T., Oda, H., Takeichi, M., and Hayashi, S. (1996). Cadherin-mediated cell adhesion and cell motility in Drosophila trachea regulated by the transcription factor Escargot. Development *122*, 3697-3705.

Torres-Vazquez, J., Gitler, A.D., Fraser, S.D., Berk, J.D., Van, N.P., Fishman, M.C., Childs, S., Epstein, J.A., and Weinstein, B.M. (2004). Semaphorin-plexin signaling guides patterning of the developing vasculature. Dev Cell *7*, 117-123.

Torres-Vazquez, J., Kamei, M., and Weinstein, B.M. (2003). Molecular distinction between arteries and veins. Cell and tissue research *314*, 43-59.

Totong, R., Schell, T., Lescroart, F., Ryckebusch, L., Lin, Y.F., Zygmunt, T., Herwig, L., Krudewig, A., Gershoony, D., Belting, H.G.*, et al.* (2011). The novel transmembrane protein Tmem2 is essential for coordination of myocardial and endocardial morphogenesis. Development *138*, 4199-4205.

Tzima, E., Irani-Tehrani, M., Kiosses, W.B., Dejana, E., Schultz, D.A., Engelhardt, B., Cao, G., DeLisser, H., and Schwartz, M.A. (2005). A mechanosensory complex that mediates the endothelial cell response to fluid shear stress. Nature *437*, 426-431.

Uemura, A., Kusuhara, S., Katsuta, H., and Nishikawa, S. (2006). Angiogenesis in the mouse retina: a model system for experimental manipulation. Experimental cell research *312*, 676-683.

Uemura, T., Oda, H., Kraut, R., Hayashi, S., Kotaoka, Y., and Takeichi, M. (1996). Zygotic Drosophila E-cadherin expression is required for processes of dynamic epithelial cell rearrangement in the Drosophila embryo. Genes Dev *10*, 659-671.

Ulrich, F., Ma, L.H., Baker, R.G., and Torres-Vazquez, J. (2011). Neurovascular development in the embryonic zebrafish hindbrain. Dev Biol *357*, 134-151.

Uv, A., Cantera, R., and Samakovlis, C. (2003). Drosophila tracheal morphogenesis: intricate cellular solutions to basic plumbing problems. Trends in cell biology *13*, 301-309.

van Groningen, J.P., Wenink, A.C., and Testers, L.H. (1991). Myocardial capillaries: increase in number by splitting of existing vessels. Anat Embryol (Berl) *184*, 65-70.

Vestweber, D. (2008). VE-cadherin: the major endothelial adhesion molecule controlling cellular junctions and blood vessel formation. Arterioscler Thromb Vasc Biol *28*, 223-232.

Vogeli, K.M., Jin, S.W., Martin, G.R., and Stainier, D.Y. (2006). A common progenitor for haematopoietic and endothelial lineages in the zebrafish gastrula. Nature *443*, 337-339.

Wang, H.U., Chen, Z.F., and Anderson, D.J. (1998). Molecular distinction and angiogenic interaction between embryonic arteries and veins revealed by ephrin-B2 and its receptor Eph-B4. Cell *93*, 741-753.

Wang, Y., Kaiser, M.S., Larson, J.D., Nasevicius, A., Clark, K.J., Wadman, S.A., Roberg-Perez, S.E., Ekker, S.C., Hackett, P.B., McGrail, M*., et al.* (2010). Moesin1 and Ve-cadherin are required in endothelial cells during in vivo tubulogenesis. Development *137*, 3119-3128.

Warga, R.M., Kane, D.A., and Ho, R.K. (2009). Fate mapping embryonic blood in zebrafish: multi- and unipotential lineages are segregated at gastrulation. Dev Cell *16*, 744-755.

Warming, S., Costantino, N., Court, D.L., Jenkins, N.A., and Copeland, N.G. (2005). Simple and highly efficient BAC recombineering using galK selection. Nucleic Acids Res *33*, e36.

Weinstein, B.M., Stemple, D.L., Driever, W., and Fishman, M.C. (1995). Gridlock, a localized heritable vascular patterning defect in the zebrafish. Nat Med *1*, 1143-1147.

Westerfield, M. (1993). The Zebrafish Book; A Guide for the Laboratory Use of Zebrafish (Brachydanio rerio). 2nd edition edn (University of Oregon Press, Eugene,).

Westerfield, M. (2000). The zebrafish book. A guide for the laboratory use of zebrafish Danio rerio (Univ. of Oregon Press, Eugene).

Xu, K., and Cleaver, O. (2011). Tubulogenesis during blood vessel formation. Seminars in cell & developmental biology *22*, 993-1004.

Xu, K., Sacharidou, A., Fu, S., Chong, D.C., Skaug, B., Chen, Z.J., Davis, G.E., and Cleaver, O. (2011). Blood vessel tubulogenesis requires Rasip1 regulation of GTPase signaling. Developmental cell *20*, 526-539.

You, L.R., Lin, F.J., Lee, C.T., DeMayo, F.J., Tsai, M.J., and Tsai, S.Y. (2005). Suppression of Notch signalling by the COUP-TFII transcription factor regulates vein identity. Nature *435*, 98-104.

Zeeb, M., Strilic, B., and Lammert, E. (2010). Resolving cell-cell junctions: lumen formation in blood vessels. Current opinion in cell biology *22*, 626-632.

Zhou, A., Egginton, S., Hudlicka, O., and Brown, M.D. (1998). Internal division of capillaries in rat skeletal muscle in response to chronic vasodilator treatment with alpha1-antagonist prazosin. Cell and tissue research *293*, 293-303.

Zhu, H., Traver, D., Davidson, A.J., Dibiase, A., Thisse, C., Thisse, B., Nimer, S., and Zon, L.I. (2005). Regulation of the lmo2 promoter during hematopoietic and vascular development in zebrafish. Dev Biol *281*, 256-269.

Zovein, A.C., Luque, A., Turlo, K.A., Hofmann, J.J., Yee, K.M., Becker, M.S., Fassler, R., Mellman, I., Lane, T.F., and Iruela-Arispe, M.L. (2010). Beta1 integrin establishes endothelial cell polarity and arteriolar lumen formation via a Par3-dependent mechanism. Developmental cell *18*, 39-51.

Zygmunt, T., Gay, C.M., Blondelle, J., Singh, M.K., Flaherty, K.M., Means, P.C., Herwig, L., Krudewig, A., Belting, H.G., Affolter, M*., et al.* (2011). Semaphorin-PlexinD1 signaling limits angiogenic potential via the VEGF decoy receptor sFlt1. Developmental cell *21*, 301-314.

CV

Curriculum vitae

Anna Lenard

Hebelstrasse 65

4056 Basel, Switzerland

+41 76 7270288

anna.lenard@uninbas.ch

Date of birth: 06.02.1984

Education

2008-currently	PhD student at the Biozentrum (Prof. Markus Affolter group), University of Basel, Switzerland
	PhD thesis "Dynamic Cell Rearrangements Shape the Cranial Vascular Network of Developing Zebrafish Embryos"
2003-2008	Master degree in Interdisciplinary Studies of Biotechnology, Warsaw University of Life Sciences, Warsaw, Poland
	Master thesis: " Analysis of TGF-beta 1 protein level in Syrian golden hamster during hookworm invasion using self-generated polyclonal chicken antibodies"

Additional experiences and activities

Project management activities

2011-currently	A member of the Career Development task group in the Young European Biotech Network, including organization of an international student conference on European Life Science Careers (12-13/10/2012) supported by EU Youth in Action initiative
2009-2012	A member of the PhD Representatives of the Biozentrum, co-organizer of the annual PhD Retreat and multiple student activities in the Biozentrum
11/2007-09/2008	Co-organizer of the International Life Sciences Students' Conference (Warsaw, 10-14/09/2008)
2004-2008	A member of the Association of Biotechnology Students (Warsaw University of Life Sciences) and of the of National Academic Students' Society of Biotechnology in Poland, co-organizer of multiple student activities focused on popularizing science

Teaching experience

2009-2012	A member of a team preparing and conducting practical course for final year undergraduate molecular biology students, Biozentrum, University of Basel, one week per year
2004-2008	A member of a team preparing and conducting workshops in molecular biology for high school students within the Polish Science Festival School

Awards and Conference Presentations

11.2008-03.2012	Werner Siemens-Foundation PhD Fellowship
7-9/09/2012	Oral presentation at the EMBO Conference on Morphogenesis and Dynamics of Multicellular Systems (Heidelberg, Germany)
2-5/06/2012	Oral presentation at the 17th International Vascular Biology Meeting (Wiesbaden, Germany)
13/04/2012	Oral presentation at the 5th Swiss Zebrafish meeting (Basel, Switzerland)
09/02/2012	Oral presentation at the annual Biozentrum Symposium (Basel, Switzerland)
20/09/2011	Poster Award, Biovalley Science Day (Basel, Switzerland)
2007-2008	Awarded a scholarship of the Minister for Science and Higher Education for prominent scientific achievements
2004-2008	Warsaw University of Life Sciences scholarship for outstanding scientific achievements

Other activities

2008-2009	A member of an editorial team of a "science news" column in the "Angora" weekly magazine (Poland)
07-09/2006	Participation in Ureka Supplement summer program for Life Sciences Students, National University of Ireland, Maynooth
09/2005	apprenticeship in the Departament of Cytogenetics of the Maria Skłodowska-Curie Memorial Cancer Center and Institute of Oncology (Warsaw, Poland)
09/2004	apprenticeship in the Department of Biophysics of the Institute of Biochemistry and Biophysics of Polish Academy of Sciences in Warsaw (Poland)

Languages

English	Proficient user
German	Independent user (B2)
French	Independent user (B1)
Polish	Native language

Computer skills:

Windows	Very good
Microsoft Office	Very good
Adobe Illustrator, Adobe Photoshop	Very good

Driving license: B

Other skills and competences

1991-2006	Music school diplomas in piano and flute (Warsaw, Poland)
2002-2003	Drawing course "Introduction to architecture"(Warsaw, Poland)

Other interests

Music, sketching, computer graphics, skiing, yoga.

List of publications

Ellertsdottir, E., **Lenard, A**., Blum, Y., Krudewig, A., Herwig, L., Affolter, M., and Belting, H.G. (2010). Vascular morphogenesis in the zebrafish embryo. Dev Biol 341, 56-65.

Herwig, L., Blum, Y., Krudewig, A., Ellertsdottir, E., **Lenard, A**., Belting, H.G., and Affolter, M. (2011). Distinct cellular mechanisms of blood vessel fusion in the zebrafish embryo. Curr Biol 21, 1942-1948.

Oggier, D.M., **Lenard, A**., Kury, M., Hoeger, B., Affolter, M., and Fent, K. (2011). Effects of the protein kinase inhibitor PKC412 on gene expression and link to physiological effects in zebrafish Danio rerio eleuthero-embryos. Toxicol Sci 119, 104-115.